TAL TECH

DOCTORAL THESIS

Wave-Driven Sediment Transport along Eastern Baltic Sea Shores

Mikolaj Zbigniew Jankowski

TALLINNA TEHNIKAÜLIKOOL
TALLINN UNIVERSITY OF TECHNOLOGY
TALLINN 2025

Wave-Driven Sediment Transport along Eastern Baltic Sea Shores

MIKOLAJ ZBIGNIEW JANKOWSKI

TAL
TECH
PRESS

TALLINN UNIVERSITY OF TECHNOLOGY
School of Engineering
Department of Cybernetics
This dissertation was accepted for the defence of the degree 27/08/2025

Supervisor: Prof. Dr. Tarmo Soomere
                                    Department of Cybernetics, School of Science
                                    Tallinn University of Technology
                                    Tallinn, Estonia

Co-supervisor: Prof. Kevin Ellis Parnell
                                    Department of Cybernetics, School of Science
                                    Tallinn University of Technology
                                    Tallinn, Estonia

Opponents: Prof. Dr. Joanna Dudzińska-Nowak
                                    Institute of Marine and Environmental Sciences
                                    University of Szczecin
                                    Szczecin, Poland

                                    Prof. Alar Rosentau
                                    Department of Geology
                                    Institute of Ecology and Earth Sciences
                                    University of Tartu
                                    Tartu, Estonia

Defence of the thesis: 29/09/2025, Tallinn

Declaration:
Hereby I declare that this doctoral thesis, my original investigation and achievement, submitted for the doctoral degree at Tallinn University of Technology has not been submitted for doctoral or equivalent academic degree.

Mikolaj Zbigniew Jankowski

                                    _____
                                                         signature

Läänemere idaranniku rannasetete lainepõhine transport

MIKOLAJ ZBIGNIEW JANKOWSKI

Contents

List of Publications

The list of author's publications, on the basis of which the thesis has been prepared:

I   Giudici, A., Jankowski, M.Z., Männikus, R., Najafzadeh, F., Suursaar, Ü., Soomere, T., 2023. A comparison of Baltic Sea wave properties simulated using two modelled wind data sets. Estuarine, Coastal and Shelf Science, 290, 108401. https://doi.org/10.1016/j.ecss.2023.108401

II   Najafzadeh, F., Jankowski, M.Z., Giudici, A., Männikus, R., Suursaar, Ü., Viška, M., Soomere, T. 2024. Spatiotemporal variability of wave climate in the Gulf of Riga. Oceanologia, 66, 56–77. https://doi.org/10.1016/j.oceano.2023.11.001

III Jankowski, M.Z., Soomere, T., Parnell, K.E., Eelsalu, M., 2024. Alongshore sediment transport in the eastern Baltic Sea. Journal of Coastal Research, Special Issue 113, 261–265. https://doi.org/10.2112/JCR-SI113-052.1

IV   Soomere, T., Jankowski, M.Z., Eelsalu, M., Parnell, K.E., Viška, M., 2025. Alongshore sediment transport analysis for a semi-enclosed basin: a case study of the Gulf of Riga, the Baltic Sea. Ocean Science, 21(2), 619–641. https://doi.org/10.5194/os-21-619-2025

V   Eelsalu, M., Soomere, T., Jankowski, M.Z., 2024. Climate change driven alongshore variations of directional forcing of sediment transport on the eastern Baltic Sea coast. Journal of Coastal Research, Special Issue 113, 190–194. https://doi.org/10.2112/JCR-SI113-038.1

Author's Contribution to the Publications

Contribution to the papers in this thesis are:

Paper I   Contributed to wave data processing and validation, highlighted and analysed identified differences between the two wave datasets contributed to and supervised the drafting, revision and review of the manuscript. Contributed to the results, discussion and conclusions.

Paper II   Supervised data processing activities, performing and assisting in special analysis of the data concerning the details of the wave climate in the Gulf of Riga. Contributed to the results and discussion sections.

Paper 3   Supervised production of the paper. Extended the methodology established in Paper IV to cover a larger area, performed data generation, calculation and most of analysis. Contributed to the writing of all sections as the primary author.

Paper 4   Performed calculation of sediment transport, contributed to their analysis and validation. Contributed to the formulation of the draft and assisted or acted directly in the generation of figures. Contributed in varying degrees to every section in the paper.

Paper 5   Supervised production of the paper. Provided data management assistance and contributed to writing the results and conclusion sections, as well as general assistance in the review of the prepared manuscript.

Introduction

Scientific Background and Motivation

The Baltic Sea is a semi-enclosed marginal sea in Northern Europe. It is an important resource for many countries, and is characterised by a complex and dynamic coastal environment, ranging from long sandy beaches to extensive bedrock shores and archipelagos (Leppäranta and Myrberg, 2009). Its low tidal range, brackish water, complex geometry, shallow bathymetry and the predominance of wind-seas (relatively young wind-driven waves) over swells distinguishes it significantly from typical open-ocean systems. It is also characterised by strong variation in coastal vulnerability (Bagdanavičiūtė et al., 2015), particularly in the eastern (Barzehkar et al., 2024) and southern Baltic Sea where the sandy-sediments dominated low lying shores are highly sensitive to variations in wave climate and associated wind forcing (Eelsalu et al., 2025). In those areas, even moderate changes to the hydrodynamic conditions can lead to significant morphodynamic changes, including shoreline retreat, sediment redistribution and alterations to the sediment transport pathways (Harff et al., 2017a, Weisse et al., 2021).

Over recent decades, increased awareness about coastal vulnerability has resulted in growth in interest to understand the conditions and behaviour of contemporary sedimentary coastlines in the Baltic Sea (Harff and Meyer, 2011). This is further highlighted by the climate change implications, including rising sea level (Cazenave et al., 2018), altered storm patterns (Rantanen et al., 2024) or shifts in dominant wind regimes, in both the wind direction and the frequency of extreme events (Soomere, 2024). Effective coastal zone management and hazard mitigation drive a need for developing accurate predictions of how these drivers affect the sediment transport patterns in the region, which in turn depend heavily on high-quality environmental data, which can be lacking in both quantity and quality at times (Pranzini and Williams, 2013).

Coastal Wave Dynamics and Modelling Framework

The scarcity of long-term *in situ* wave measurements, especially in coastal and nearshore zones of the eastern and south-eastern Baltic Sea (Suursaar, 2015), is a factor which contributed to numerical wave models becoming essential tools in Baltic coastal research (Soomere and Healy, 2011). Among these, SWAN (Simulating WAves Nearshore, Booij et al., 1999) and WAM (WAve Model, Komen et al., 1994) have proven to be particularly well-suited for applications in basins like the Baltic Sea (Tuomi et al., 2011; Björkqvist et al., 2018b). Both are third generation spectral wave models capable of simulating the generation, growth, propagation and wave-bottom interaction, including refraction, as well as dissipation of wind waves and nonlinear quadruplet energy exchange between wave components. SWAN added the capacity to account for the effect of triadic interactions of wave components in shallow waters (Booij et al., 1999). It also supports nested grid configurations, which makes it an effective tool for studying both large basins and high-resolution local dynamics. A short history of the Baltic Sea wave (climate) modelling studies that have employed SWAN or WAM is presented in Soomere (2023).

The reconstructed time series of wave properties have been used to assess nearshore energy fluxes (Soomere and Eelsalu, 2014) and to evaluate properties of wave-driven alongshore sediment transport (Viška and Soomere, 2013b) in the Baltic

Sea over almost one and half decades. The performance of these models is highly sensitive to the quality and resolution of the wind forcing (Räämet et al., 2009; Räämet and Soomere, 2021), especially in the nearshore regions (Paper I). The resolution of such models has only recently reached the level (about 500 m) that is necessary to adequately examine the main properties of alongshore wave-driven sediment flux for long segments of sedimentary shores.

The Eastern Baltic Wind and Wave Climate

The Baltic Sea wave climate is dominated by locally generated wind waves (Broman et al., 2006; Soomere et al., 2012). This feature reflects the small size of the Baltic proper and sub-basins of the Baltic Sea (Figure 1). Technically, swell systems are often present in the Baltic Sea (Björkqvist et al., 2021) but wave periods in such systems are much shorter than in the open ocean. The prevailing winds in the region vary seasonally. The most frequent are south-western winds. A specific feature of the northern Baltic proper is the presence of two systems of moderate and strong winds (Soomere and Keevallik, 2001; Soomere, 2003; Hünicke et al., 2015). The most frequent among such winds are south-western winds whereas north-north-western winds are less frequent but can be even stronger (Soomere, 2001). This feature gives rise to a bi-directional
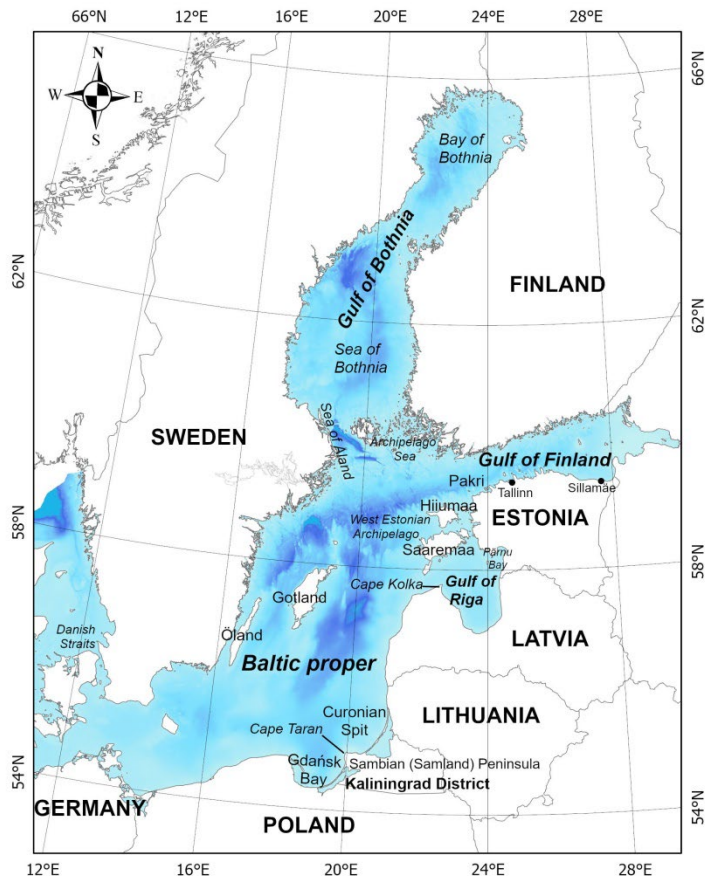

Figure 1. Location scheme of the Baltic Sea. Graphics by Maris Eelsalu. Modified from Paper II.

wave field (Soomere and Räämet, 2011) with significant implications for alongshore sediment transport (Soomere and Viška, 2014). The difference in the size of various basins of the Baltic Sea, equivalently, natural differences in the fetch length for wave generation, cause additional variations in typical and extreme wave properties between different sub-basins, such as the Gulf of Finland or Gulf of Riga (Figure 1). This in turn leads to significant spatial variability in coastal exposure with respect to the predominant wave approach directions and the associated wave energy flux (Soomere and Eelsalu, 2014). For example, wave properties in the Gulf of Finland with its narrow, elongated shape are especially sensitive to wind directionality (Pettersson et al., 2010; Männikus et al., 2024), while in the Gulf of Riga, a broader and more open geometry permits the development of directionally more varied wave fields (Paper II). A limited connection between the Gulf of Riga and the Baltic proper, and the geometrically sheltered nature of the Gulf of Finland with respect to waves excited by south-western winds, lead to strong gradients in wave-derived nearshore energy and sediment transport potentials in these basins.

Coastal Sediment Transport and Compartmentalisation

The described qualitative features of the Baltic Sea wave climate suggest that wave-driven alongshore sediment transport in the eastern Baltic Sea is driven primarily by the wind-seas. In the Baltic Sea conditions, intense wave-driven alongshore sediment transport often results in coastal erosion (Eberhards et al., 2009). Its counterpart – accumulation features – may occur at a large distance from the erosion areas (Tõnisson et al., 2016). This transport may reduce the performance of coastal defence structures (Bernatchez and Fraser, 2012), affect coastal infrastructure design rules and maintenance needs (Bulleri and Chapman, 2010), disturb the entire coastal landscape, and destabilise coastal socio-ecological systems (Villasante et al., 2023). Its magnitude and direction most crucially depend on the wave height, period and incident angle with respect to the coastline orientation. The actual transport is also governed by sediment properties and availability, and coastal morphology.

A useful conceptual framework for analysing systems that are shaped by intense alongshore transport involves the division of the coastline into sediment (transport) cells and compartments,[1] where sediment can exchange freely, while passing of sediment material between different cells or compartments is limited (Davies, 1974; Clayton, 1980; Thom et al., 2018). This framework greatly simplifies the analysis of dynamics of longer coastal segments by splitting the system into smaller units. It has been used only infrequently and in small sections in the eastern Baltic Sea such as the vicinity of Tallinn Bay (Soomere et al., 2007; Eelsalu et al., 2023), mostly in connection with numerical simulations of wave-driven sediment transport.

These compartments can be identified by analysis of local sediment divergence and convergence zones, which can often be associated with morphological features such as capes, headlands or bays (Viška and Soomere, 2013b). Sediment flux may also be greatly affected by various anthropogenic structures such as harbours, jetties and wave breakers (Soomere et al., 2007; Paper III) that may partially or fully block the transport. On top of that, divergence zones may appear as invisible barriers on almost straight

---

[1] Following the nomenclature defined in Paper III, in this thesis the term "cell" is used to denote relatively small, clearly identifiable elementary sedimentary units while the term "compartment" denotes clusters of cells that usually exchange sediment.

sections of the coast where they reflect changes in the predominant wave approach direction along the shore (Eelsalu et al., 2023). Sets of such locations often split sedimentary systems into cells and compartments. This feature simplifies the analysis of large coastal systems (Kinsela et al., 2017), makes it possible to better understand the functioning of its single parts, and optimises the consideration of various structures and beach management actions (such as beach nourishment) (Cappucci et al., 2020; Susilowati et al., 2022). Such locations also often serve as natural limits for the alongshore propagation of pollution. The identification and analysis of these compartments requires detailed modelling of wave conditions and associated transport rates, as will be discussed in Chapter 3.

Impacts of Climate Variability on Sediment Dynamics

Observed and projected changes in the Baltic Sea wind and wave conditions, including changes in wind and wave directions (Bierstedt et al., 2015; Soomere et al., 2015; Kudryavtseva and Soomere, 2017) are expected to modify the sediment transport regimes in the eastern Baltic Sea. These changes can significantly alter the sediment budget and coastal vulnerability of certain areas of the coast, leading to the emergence and intensification of erosion hotspots, or their relocation through changes in sediment compartments (Eelsalu et al., 2024). Such variations become evident at greatly different time scales, from single storms to decades.

A specific feature of the eastern Baltic Sea is that winds from the above-described two predominant directions generate waves that bring to the coasts the majority of annual wave energy flux (Eelsalu et al., 2022). Such waves generate oppositely directed alongshore sediment transport at many locations of this coastal stretch. Variations of their balance may lead to greatly different directional properties of sediment transport in differently oriented coastal sectors as highlighted in Paper IV.

The presence of such bi-directional wind and wave patterns leads to a delicate balance of wave-driven transport on some parts of the eastern Baltic Sea coast (Soomere and Viška, 2014). Any change to this balance can significantly modify the alongshore sediment transport (Flor-Blanco et al., 2021) and may lead to drastic consequences, e.g., to the loss of stability of even major landforms, such as the Curonian Spit (Figure 1) (Viška and Soomere, 2012). The existing balance can be altered, e.g., by an increase in the frequency of south-western winds that has been observed in wintertime in the Baltic Sea basin (Jaagus and Kull, 2011, Bierstedt et al., 2015). As wind wave heights have not significantly increased in the eastern Baltic Sea (Sokolov and Chubarenko, 2024), it is likely that several observed phenomena, such as an increase in the long-term mean rate of coastal retreat on some segments of Latvian shores since the 1990s (Eberhards and Lapinskis, 2008), rapid shoreline changes at some locations in the West Estonian Archipelago (Figure 1) (Suursaar et al., 2015) or changes in the potential net alongshore sediment transport along the Baltic proper coasts of Lithuania and Latvia 1970–2007 (Soomere et al., 2015), may be attributed to changes in the directional structure of winds. Paper V makes an attempt to highlight more exactly the nature of these changes on the eastern shore of the Baltic proper.

The material elaborated in Chapter 3 is crucial for the understanding and recognition of such changes, and carries implications for coastal stability, infrastructure vulnerability (Barzehkar et al., 2024) and overall sediment management activities (Šakurova et al., 2025), particularly with the scenarios of regionally effective increases in sea level extremes (Viigand et al., 2025) and changes in storm activity (Lorenz et al., 2025).

Scope and Objectives of the Thesis

This thesis aims to advance the current understanding of alongshore wave-driven sediment transport in the eastern Baltic Sea, by employing high resolution wave modelling and systemic analysis.

The primary objectives are to:

- provide a properly calibrated and validated wave modelling basis of suitable quality in order to perform systemic calculations of alongshore sediment transport properties;
- characterise performance of contemporary global and local wind datasets for wave climate simulations in the entire Baltic Sea and in the nearshore of Estonia;
- create a detailed description of the Gulf of Riga wave climate for engineering purposes;
- evaluate the main properties of alongshore net and bulk sediment transport for the sedimentary system of the eastern Baltic Sea;
- identify the main sediment compartments, to provide boundaries, and to assess the potential influence of climate-driven changes on sediment transport.

The thesis is organised into three main chapters. Chapter 1 presents the SWAN model setup and evaluates its performance using two different wind datasets, particularly focusing on the Baltic proper and Gulf of Riga. An important outcome is a set of time series of wave properties for the entire Baltic Sea at a moderate resolution that is used as boundary information for subsequent higher-resolution simulations of nearshore wave properties for a longer segment of the eastern Baltic Sea, from the Gulf of Riga to the Sambian (Samland) peninsula (Figure 1). Chapter 2 explores spatio-temporal variability of the wave climate in the Gulf of Riga, combining the outcome of Chapter 1 with high-resolution model simulations and observational data. Chapter 3 focuses on the sediment transport patterns along the sedimentary shores of the eastern Baltic proper from Cape Taran in Kaliningrad District to Pärnu Bay (Figure 1) in the Gulf of Riga, driven by the data from simulations presented in Chapter 1 and Chapter 2, and providing a detailed description of alongshore sediment transport rates, their spatio-temporal variations, and the natural and engineered barriers to sediment fluxes, developing compartmentalisation of the study area and exploring recent changes in the directional structure of wave forcing. The conclusions, serve to synthesise the key findings, discuss the methods used, and highlight the achievements of this research, also outlining the direction for possible future research.

Presentations to the Scientific Community

The basic results presented in this thesis have been presented by the author at the following scientific events:

Oral presentations

Giudici, A., Männikus, R., Najafzadeh, F., Jankowski, M.Z., Soomere, T., Suursaar, Ü., 2022. High resolution wave model for coastal management and engineering. Science Days for the Gulf of Finland and the eastern Baltic Sea (30 November–01 December 2022, Helsinki, Finland).

Jankowski, M.Z., Eelsalu, M., Parnell, K.E., Soomere, T., Viska, M., 2023. Modelled rates of potential bulk and net sediment transport along the Gulf of Riga coastlines. The Gulf of Finland and Eastern Baltic Sea Science Days 2023 (16–17 November 2023, Tallinn, Estonia).

Jankowski, M.Z., Parnell, K.E., Soomere, T., Eelsalu, M. 2023. Longshore sediment transport analysis for the Gulf of Riga based on high-resolution wave model results. 13th International Workshop on Modeling the Ocean (IWMO) (27–30 June 2023, Hamburg, Germany).

Jankowski, M.Z. Parnell, K.E., Soomere, T., 2024. Decomposing alongshore sediment transport into cells and compartments: A case study in the Gulf of Riga, the Baltic Sea. 8th IAHR Europe Congress "Water – Across boundaries" (4–7 June 2024, Lisbon, Portugal).

Soomere, T., Jankowski, M.Z., Parnell, K.E., 2024. Intriguing variations of sediment transport in the Gulf of Riga. 5th Baltic Earth Conference "New Challenges for the Baltic Sea Earth System Research" (13–17 May 2024, Jūrmala, Latvia).

Jankowski, M.Z., Soomere, T., Parnell, K.E., Eelsalu, M., 2024. Sediment transport along the eastern coast of the Baltic Sea. 4th Scientific Conference of Polish Marine Researchers "The State and Trends of Changes in the Marine Environment" (16–18 September 2024, Szczecin, Poland).

Jankowski, M.Z., Soomere, T., Eelsalu, M., Parnell, K.E., 2025. Temporal variability of alongshore sediment transport in the eastern Baltic Sea. Baltic Sea Science Congress 2025 (26–30 May 2025, Sopot, Poland).

Poster presentations

Giudici, A., Männikus, R., Najafzadeh, F., Jankowski, M.Z., Soomere, T. Suursaar, Ü., 2022. High-resolution wave model for coastal management and engineering in the eastern Baltic Sea. 4th Baltic Earth Conference "Assessing the Baltic Sea Earth System" (30 May–03 June 2022, Jastarnia, Poland).

Jankowski, M.Z., Parnell, K.P., Soomere, T., Eelsalu, M., Viska, M., 2023. Analysis of longshore sediment transport for the Gulf of Riga using high-resolution wave model results. Baltic Sea Science Congress 2023 (21–25 August 2023, Helsinki, Finland).

Oral presentations by co-authors

Viška, M. (presenter), Tõnisson, H., Männikus, R., Jankowski, M.Z., 2024. Coastal dynamics of the Daugavgriva Island beach in the Gulf of Riga, Latvia. 5th Baltic Earth Conference "New Challenges for the Baltic Sea Earth System Research" (13–17 May 2024, Jūrmala, Latvia).

Jankowski, M.Z., Soomere, T. (presenter), Parnell, K.P, Eelsalu, M., 2024. Alongshore sediment transport in the Eastern Baltic Sea. 17th International Coastal Symposium (ICS2024) "Coastlines Under Global Change" (24–27 September 2024, Doha, Qatar).

Eelsalu, M. (presenter), Soomere, T., Jankowski, M.Z., 2024. Climate change driven alongshore variations of directional forcing of sediment transport on the eastern Baltic Sea coast. 17th International Coastal Symposium (ICS2024) "Coastlines Under Global Change" (24–27 September 2024, Doha, Qatar).

Poster presentations by co-authors

Najafzadeh, F. (presenter), Jankowski, M., Giudici, A., Männikus, R., Suursaar Ü., Soomere, T., Viska, M., 2023. Wave climate and its variability in the Gulf of Riga. Baltic Sea Science Congress 2023 (21–25 August 2023, Helsinki, Finland).

Giudici, A. (presenter), Männikus, R., Najafzadeh, F., Jankowski, M.Z., Soomere, T., 2023. High-resolution Baltic Sea wave climatology obtained from two modelled wind data sets: a comparison. Baltic Sea Science Congress 2023 (21–25 August 2023, Helsinki, Finland).

Giudici, A. (presenter), Jankowski, M.Z., Männikus, R., Najafzadeh, F., Soomere, T., 2023. Baltic Sea Wave Climatology Dataset: high-resolution validation and comparison of the wave properties calculated using two input winds for the period 1979–2022. The Gulf of Finland and Eastern Baltic Sea Science Days 2023 (16–17 November 2023, Tallinn, Estonia).

Giudici, A. (presenter), Männikus, R., Jankowski, M.Z., Soomere, T., 2024. Analysis of wave properties in the Baltic Sea: integrating findings from the Gulf of Finland, Gulf of Riga and Western Baltic Coasts. 5th Baltic Earth Conference "New Challenges for the Baltic Sea Earth System Research" (13–17 May 2024, Jūrmala, Latvia).

Abbreviations

BaltAn65+	Baltic regional reanalysis atmospheric dataset (Luhamaa et al., 2011)
CERC	Coastal Engineering Research Centre
COSMO	COnsortium for Small-scale MOdeling
ECMWF	European Centre for Medium-Range Weather Forecasts
EMI	Estonian Marine Institute
ERA5	ECMWF Reanalysis v5
ERA-40	An earlier version of ECMWF reanalysis
ERA-Interim	An earlier version of ECMWF reanalysis
FMI	Finnish Meteorological Institute
H_s	Significant wave height
rmsd	root mean square difference
HIRLAM	High Resolution Limited Area Model
R	Pearson correlation coefficient
ADCP	Recording Acoustic Doppler Current Profiler
SWAN	Wave model Simulating WAves Nearshore (Booij et al., 1999)
SMHI	Swedish Meteorological and Hydrological Institute
T_p	Peak wave period
T_{m02}	Mean wave period
WAM	WAve Model (Komen et al., 1994)
USACE	United States Army Corps of Engineers

1 Wave modelling of the Baltic Sea

1.1 Introduction

Wave fields in the Baltic Sea are characterised by high spatial and temporal variability (Björkqvist et al., 2018b), governed by a combination of unique drivers and properties of this semi-enclosed sea. Those properties include highly irregular coastline geometry, a complex local wind regime and a much smaller size than the open ocean basins (Leppäranta and Myrberg, 2009). As the fetch is commonly only a few hundred or even a few tens of kilometres, wave fields are usually fetch-limited and classic regular long-period swell is a rare phenomenon (Broman et al., 2006). It is thus essential for various applications, to accurately replicate the time series of properties of wind driven waves of the Baltic Sea. Such simulations are often complicated by a scarcity of observational data that can be utilised for calibration and validation of wave models. As a result, the consequences of, for example, changes to wind forcing, remain uncertain.

This chapter follows Paper I and focuses on the configuration, validation and comparison of the performance of two long-term wave hindcasts using the third-generation spectral model SWAN (Booij et al., 1999). The model is applied across the entire Baltic Sea using a triple-nested grid as described in Section 1.2.1. This approach makes it possible to replicate wave properties in the entire sea with a resolution of 3 nautical miles (nmi; 1 nmi = 1852 m) down to 560 or 280 m in selected coastal areas (Figure 2). The simulations were performed for the time period 1991–2021, aligning with the most recent climatological normal, 1990–2020. Most of the model calibration and validation is performed for the 3 nmi implementation, encompassing the entire Baltic Sea as most long-term instrumental wave measurements are made in open parts of the sea. A particular focus of Paper I and Chapter 1 is the Gulf of Finland, which is an oceanographically and meteorologically complex sub-basin of the Baltic Sea (Figure 1, Figure 2), while Paper II and Chapter 2 concentrate on the Gulf of Riga that has a more regular shape and has less wave impact from the Baltic proper.

The novelty of this study stems from the use of two high-quality atmospheric reanalysis products: the global initiative ERA5 (Hersbach et al., 2020) and a local reanalysis BaltAn65+ (Luhamaa et al., 2011). The idea is to not only reconstruct the wave climate and build time series of wave properties for subsequent work but also to evaluate the sensitivity of modelled wave parameters with respect to differences in the wind data resolution and underlying physics, while taking the differences in temporal coverage into account. The results highlight clear spatial differences in the modelled wave climate and depict where the two wave datasets differ most significantly.

The chapter starts from a discussion of the model setup, the nested grid system and the bathymetric data, followed by a description of the calibration and validation steps and results. A comparison between modelled and recorded[2] wave parameters focuses on significant wave height (H_S) and peak wave period (T_p) and is conducted in the open sea, and in coastal and nearshore locations. The chapter discusses statistical characteristics of the simulated wave climate and assesses the differences introduced

---

[2] Instrumental wave measurements do not directly measure statistical properties of wave fields, such as significant wave height or peak period. These properties are calculated from measurable quantities. The relevant procedures vary depending on the particular device and approach. For this reason, the term "recorded" is used in this thesis to denote statistical properties of wave fields retrieved using *in situ* instrumental measurements or satellites.

by using the two wind products, both for long-term averages as well as higher quantiles suitable for the analysis of extremes. The final section reflects on the broader implications of these findings for Baltic Sea wave modelling practice.
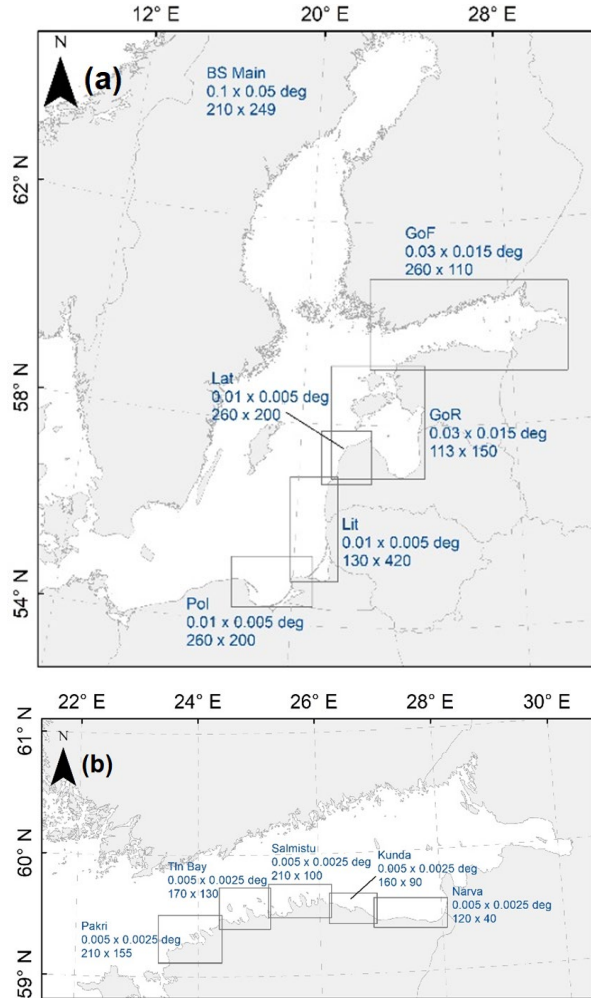

Figure 2. a) First level (BSMain, the entire Baltic Sea) and second level grids (boxes) and their spatial resolution used in various simulations with the SWAN model. See Section 1.2.1 for their description. b) Location and spatial resolution of the third level (the innermost) grids for the southern shore of the Gulf of Finland. The numbers below the name of the grid show resolution in degrees and number of grid cells in both directions. From Paper I.

1.2 SWAN Model Setup

In order to replicate wave properties of the Baltic Sea, the SWAN model version 41.32A was configured using a triple-nested grid architecture optimised for both computational efficiency and spatial resolution in the areas of interest for long-term (multi-decadal) hindcast simulations. As the outcome of simulations was further used to evaluate the properties of alongshore transport, it was necessary to accurately represent not only wave properties in the offshore (that are relatively well known; Björkqvist et al., 2018b;

Sokolov and Chubarenko, 2020, 2024) but even more importantly, also adequately replicate nearshore bathymetry and coastal geometry that substantially impact the quality of wave simulations in some parts of the Baltic Sea (Björkqvist et al., 2018a). These features are critical, especially for reliable replication of wave propagation and dissipation in the nearshore zones (Alari and Raudsepp, 2010), specifically as wave properties at the breaker line govern the properties of alongshore transport (USACE, 2002).

The waves are described by a two-dimensional (2D) wave action density spectrum N. Its evolution is governed by the wave action balance equation, which, in Cartesian coordinates without ambient currents, takes the form:

$$\frac{\partial N}{\partial t} + \frac{\partial c_x N}{\partial x} + \frac{\partial c_y N}{\partial y} + \frac{\partial c_\sigma N}{\partial \sigma} + \frac{\partial c_\theta N}{\partial \theta} = \frac{S_{tot}}{\sigma}. \tag{1}$$

The terms on the left-hand side of this equation represent the rate of change and propagation of wave energy in a two-dimensional geographical space, as well as the modification in group speed and wave propagation direction caused by variations in depth and depth-induced refraction. The x- and y- components of the group velocity are denoted as c_x and c_y. The spectral space is defined with angular frequency σ and the direction of propagation θ. The propagation velocities in the spectral space are expressed with respective quantities c_σ and c_θ. The quantity S_{tot} on the right-hand side stands for the the sum of all processes that represent generation, dissipation or redistribution of wave energy in SWAN. Further expressions for spectral velocities were used as explained in the SWAN technical manual (The SWAN team, 2019).

The model was validated mostly against instrumental wave measurements in the region covered by the coarse grid, while a few such locations were also employed in areas covered by the medium-resolution grid (Figure 2). Model validation for several locations in the higher-resolution grid is discussed in Chapter 2. This accurately validated wave information was used as input information for nearshore higher-resolution simulations in Chapter 2 that accounted for the geometric and bathymetric features of the area, which govern wave transformation processes like refraction, shoaling, other wave-bottom interactions, and breaking.

Wave fields naturally interact with sea ice, currents, and varying water level. The impact of sea ice on wave fields is substantial in the northern parts of the Baltic Sea (Tuomi et al., 2019) while the impact of currents and varying sea level may be significant in strong storms (Viitak et al., 2016).

As information about surface currents is not available and the presence of currents usually only insignificantly modifies the properties of wave fields in water bodies of similar size (Causio et al., 2021; Kanarik et al., 2021), the contribution of currents into the development of wave fields is ignored. Ignoring sea ice may result in an underestimate of the total annual wave energy flux in the nearshore of the Gulf of Riga by up to 15% (Najafzadeh et al., 2024), while this impact is clearly smaller for the coastal stretch from Cape Kolka to Cape Taran (Figure 1), addressed in Chapter 3. This level of uncertainty was considered acceptable for the analysis in Paper III, Paper IV, and Paper V. High water levels and strong waves are often synchronised in the eastern Baltic Sea (Soomere et al., 2017; Kudryavtseva et al., 2020; Johansson et al., 2022). The resulting actual impact of waves on shore sediment greatly depends on the instantaneous water level. However, the quantities evaluated in Paper III, Paper IV, and

Paper V are invariant with respect to the water level. Based on the listed arguments, the presence of sea ice and currents as well as the possibility of varying water level were ignored in the simulations in Paper I and Paper II.

1.2.1 Bathymetric Data

The grid system incorporated three levels of spatial nesting:

- Level 1 – BSMain (Baltic Sea Main) grid (Figure 2a), which encompasses the entire Baltic Sea (Figure 3) at a resolution of about 3 nmi (~5.5 km). This grid is used to capture large-scale wave dynamics, including basin-scale swell and wind-sea evolution.
- Level 2 – sub-basin grids for the Gulf of Finland, Gulf of Riga, Lithuanian and Latvian coasts, and Gdańsk Bay (Figure 1) with a resolution of about 1 nmi (~1.8 km). This allows for sufficient resolution of wave properties that govern coastal processes in regions with longer, almost straight segments of shoreline.
- Level 3 – high resolution local coastal grids, varying in resolution between 260 m and 560 m, selected in key nearshore environments of each sub-basin. In particular they were used along the northern coast of Estonia (Figure 2b) within the Gulf of Finland, where the typical size of almost straight coastal segments is <500 m and a resolution of a few 100s of metres is necessary for accurately resolving nearshore waves.
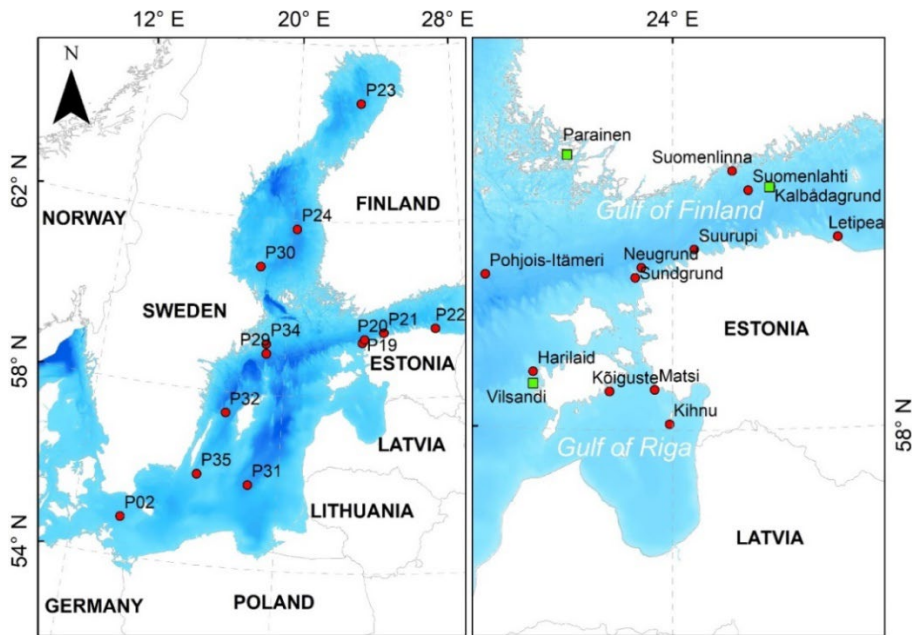

Figure 3. Wave (red) and wind (green) measurement locations in the Baltic proper, Sea of Bothnia, Bay of Bothnia (Figure 1), Gulf of Finland and Gulf of Riga employed in this thesis. Site P02 – Warnemünde represents the south of the Baltic Sea. Sites P19 – Neugrund, P20 – Sundgrund, P21 – Suurupi, P22 – Letipea represent the southern nearshore of the Gulf of Finland. P23 – Perämeri represents the Bay of Bothnia, P24 – Selkämeri and P30 – Finngrundet represent the Sea of Bothnia, and sites P29 – Huvudskär, P31 – Södra Östersjön, P32 – Knolls grund, P34 – Almagrundet, P35 – Ölands södra grund and Pohjois-Itämeri (also known as the northern Baltic proper, Tuomi et al., 2011) represent the Baltic proper. Graphics by Maris Eelsalu. From Paper I.

The bathymetric data (see a visualisation in Figure 3) was retrieved from the Baltic Sea Bathymetry Database[3] (Baltic Sea Hydrographic Commission, 2013) for the entire basin. This data set was combined with higher-resolution data held by national agencies, such as the Estonian Transport Administration and the Latvian Institute of Aquatic Ecology, to construct bathymetry and geometry for Level 3 grids in nearshore regions. The datasets were bi-linearly interpolated to match the input grid formats of SWAN, and smoothed where necessary to suppress numerical instabilities arising from sharp depth gradients. The coastline was generated using this bathymetric information separately for each level of grid.

The resolution of 280 m is still insufficient in some parts of the Baltic Sea archipelagic areas, like the northern Gulf of Finland or the Archipelago Sea between Finnish mainland and the Åland Archipelago (Figure 1), where resolution in the order of 100 m is needed to resolve island-induced diffraction and wave shadowing effects (Björkqvist et al., 2018a). These effects are acknowledged as a source of residual model error in the nearshore spectral structure (Björkqvist et al., 2019). However, these issues do not become evident on the southern nearshore of the Gulf of Finland and along the sedimentary shores from Pärnu to Cape Taran.

1.2.2 Wind Data

Wind is the principal forcing for wave generation, and therefore is the largest source of uncertainty in wave modelling (Nikolkina et al., 2014; Soomere, 2023). In the past, wind data quality and quantity significantly affected most wave simulations in the eastern Baltic proper, while the nearshore of some other locations, e.g., Sweden, was covered by adequate wind information (Räämet et al., 2009). In Paper I, two different contemporary high-quality reanalysis datasets were used to force wave simulations:

1) ERA5 (Hersbach et al., 2020) is the fifth generation ECMWF (European Centre for Medium-Range Weather Forecasts) product that provides *inter alia* hourly surface wind fields at a horizontal resolution of 0.25° (~30 km). The ERA5 product incorporates extensive data assimilation (including scatterometry and altimetry), modern physics parameterisations, variable roughness length and partial ice coverage.

2) BaltAn65+ (Luhamaa et al., 2011) is a regional atmospheric reanalysis created by dynamically downscaling earlier versions of ERA5, namely ERA-40 (Uppala et al., 2005) and ERA-Interim (Dee et al., 2011) data, using the HIRLAM-B mesoscale model (Unden et al., 2002; Eerola, 2013). It operates at an 11 km spatial resolution with 6-hourly timesteps, covering the period 1965–2005. Unlike ERA5, it uses a fixed roughness length over ice (0.03 m) and assimilates ice data without feedback mechanisms. Its core advantage is finer spatial resolution that is expected to better reproduce wind properties near the shoreline, especially in narrow basins such as the Gulf of Finland.

For wave simulations, wind input is extracted as 10 m above sea level u- and v-components and interpolated onto the wave model via tri-linear (bi-linear spatial and linear temporal) interpolation. The wind fields are used as provided in the relevant data

---

[3] The link used to retrieve bathymetric information for simulations in Paper I and Paper II no longer works. The new link to the Baltic Sea Bathymetry portal page is www.bshc.pro.

sets, allowing consistent assessment of differences of wave climates reconstructed using different wind data sets and the performance of each data sets in terms of the resulting wave properties.

1.2.3 Input Data Validation

To validate the wind forcing, wind speed and direction from both reanalysis datasets were compared to measured data from three meteorological stations (Figure 3):

- **Kalbådagrund** in the middle of the Gulf of Finland is an offshore station with minimal coastal influence, often used as a benchmark for wave reconstruction in the region (Soomere, 2005). Wind properties are recorded 32 m above sea level. Wind speed was reduced to the 10 m level using a correction factor 0.85 (Launianen and Laurila, 1984; Soomere, 2005).
- **Vilsandi** meteorological station on a small island 6 m above the mean water level located in the western periphery of the West Estonian Archipelago is exposed to predominant westerly winds. The data are often used for estimating parameters of wind climate and for validating extreme wind events. Wind properties were collected at 10 m height and used without correction.
- **Parainen Fagerholm** weather station is located at the Gulf of Finland entrance in southwest Finland, 6 m above the mean water level and is expected to represent well marine wind properties. The recordings are to some extent sensitive to wind direction and coastal convergence effects. Wind properties were collected at 10 m height and used without correction.

Comparison of monthly mean modelled and recorded wind speeds (Figure 4) revealed that the ERA5 wind product performed better during the summer months (June–August), closely matching observed means at all stations, while the winds in the BaltAn65+ data set overall presented a lower bias. Both datasets show high correlation with measured data, with the relevant correlation coefficients (R) generally exceeding 0.95. However, ERA5 wind data consistently underestimated strong wind events, with BaltAN65+ data capturing these better (Paper I), apparently due to its finer resolution and regional tuning. These discrepancies directly influence the wave generation potential, particularly in storm conditions in fetch limited regions, where short-lived directional changes can govern the development of peak wave heights.

1.3 Model Calibration and Validation

The SWAN model allows the selection of user-defined values for a number of parameters: whitecapping coefficient, bottom friction-induced energy dissipation, depth-induced wave breaking, nonlinear transfer of wave energy through three-wave interacttions, and the wind drag coefficient. An aim in Paper I was to identify an optimum set of these parameters that would provide adequate results in the entire Baltic Sea, first of all in the Baltic proper, Gulf of Finland and Gulf of Riga. This task was crucial to provide high-quality information about wave properties for high-resolution simulation of wave time series in the eastern nearshore of the Baltic Sea for use in Paper III and Paper IV. The parameters were iteratively adjusted to maximise first of all the accuracy of the model in strong storms that generate particularly intense alongshore transport.

The following options were selected (Paper I): the whitecapping coefficient $\delta = 1$ as suggested in Pallares et al. (2014) and Rogers et al. (2003), the bottom friction coefficient 0.038 m^2/s^3 following Zijlema et al. (2012); the parameters for the depth-induced wave breaking source term $\alpha = 1$ and $\gamma = 0.73$. As suggested by Björkqvist et al. (2018a), wind drag parameterisation was taken from Wu (2012) and the default parameters for whitecapping were selected from Komen et al. (1984).

Modelled wave parameters were compared in Paper I with a suite of *in situ* wave measurements from across the Baltic Sea (Figure 3). The validation targeted two main wave parameters, significant wave height (H_S) and peak wave period (T_p). Significant wave height is the most stable and reliable wave parameter and is directly comparable between models and observations. It is defined as $H_S = 4\sqrt{m_0}$, where m_0 is the zeroth moment of the wave spectrum. Peak wave period represents the inverse of the spectral peak frequency (the frequency at which the wave energy reaches its maximum). This period thus normally is the period of the highest waves in the field. This quantity is often used to assess energy propagation and storm maturity. However, T_p is sensitive to spectral noise and limited measurement duration, particularly in short records
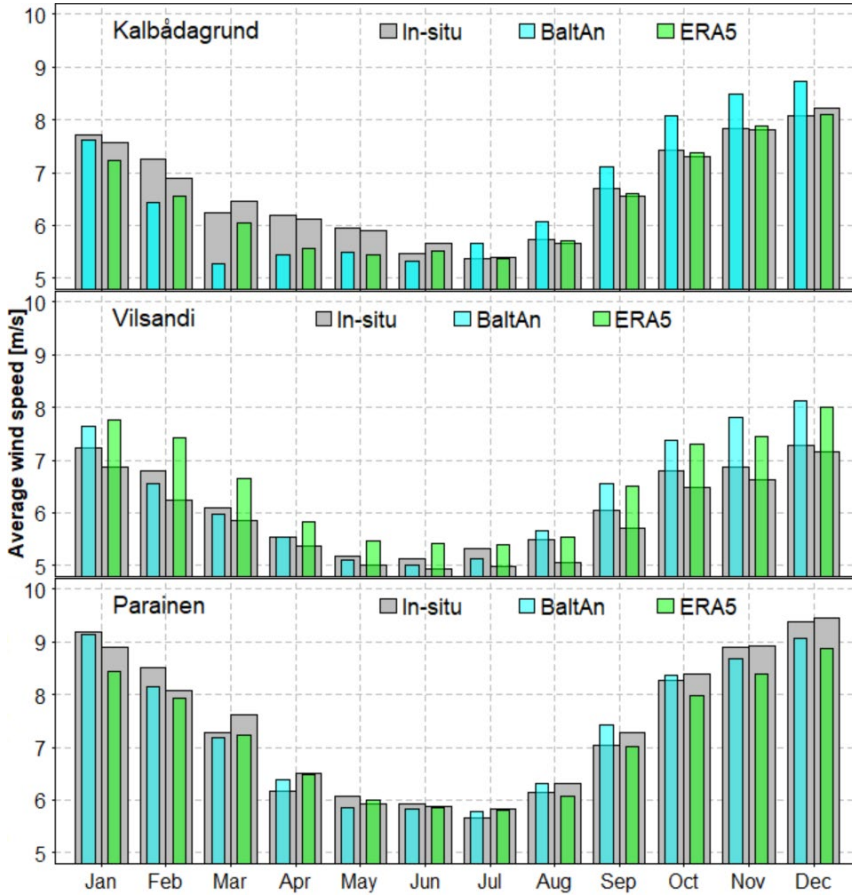

Figure 4. Seasonal distribution of the average measured and modelled wind speeds from the two wind datasets at Kalbådagrund, Vilsandi, and Parainen (Fagerholm) (Figure 3). Two bars of the in situ data correspond to time periods 1991–2021 for a comparison with ERA5 data and 1985–2005 for a comparison with BaltAn65+ data, respectively. Adjusted from Paper I.

and/or during mixed multi-modal sea states (e.g., Ahn, 2021; Muraleedharan et al., 2023). For validation, only data with $H_S > 0.5$ m was included, following Björkqvist et al. (2018b), to reduce the influence of poorly resolved small waves. Together with wave propagation direction, H_S and T_p govern the properties of wave energy flux in the nearshore and wave-driven alongshore sediment transport, addressed in Papers III–V.

In situ recorded data were drawn from long-term deployments of directional waveriders operated by the Finnish Meteorological Institute (FMI) and the Swedish Meteorological and Hydrological Institute (SMHI). These data sets provide information about wave properties in the offshore of the Baltic Sea, in one location of the Gulf of Finland and in three locations of the Gulf of Bothnia[4] (Figure 1). These data sets were complemented with recordings made during several shorter measurement campaigns by the Estonian Maritime Institute (EMI) in the nearshore of the Gulf of Finland and on the western coast of Saaremaa (Figure 1) using a recording acoustic Doppler current profiler (ADCP) (Suursaar, 2015). Collectively these datasets provide information over several decades and cover a large variety of conditions.

Comparisons of modelled and measured wave properties were made at the model grid points nearest to each measurement site, with temporal interpolation made to match the measurement time slots. The recorded wave properties were typically available either hourly or every 30 minutes. Validation statistics were calculated for each wind forcing separately and in overlapping periods where applicable, including metrics such as bias, root mean square difference (rmsd) and Pearson correlation coefficient (R).

1.3.1 Significant Wave Height

The validation of data modelled using BaltAn65+ is performed in Paper I only for the time period 1985–2005 because of the lack of earlier instrumental wave measurements. The ERA5 wind dataset also covers a more recent time period, 1991–2021, for which numerous measured data sets are available. The validation dataset comprises over a dozen locations across the Baltic Sea (Figure 3).

The focus in Paper I is on three open-sea locations in radically different domains of the sea where wave properties have been recorded over at least 15 years: at Ölands södra grund, Almagrundet and near Warnemünde (Figure 3). The bias and rmsd between modelled and recorded H_S are in the range from 0.09 to 0.29 m and from 0.20 to 0.41 m, respectively, for the two model runs. Thus, the models slightly overestimate wave height while the run forced by BaltAn65+ often shows smaller bias and rmsd. Only the run forced by BaltAn65+ slightly underestimates wave heights at Pohjois-Itämeri (also known as northern Baltic proper, Figure 3). The bias is thus fairly small for both modelled data sets at Ölands södra grund and near Warnemünde while the correlation coefficient varies from 0.88 to 0.97, being the highest at Pohjois-Itämeri (Paper I). These values are almost the same for simulations for southern regions of the Baltic Sea using COSMO (COnsortium for Small-scale MOdeling, www.cosmo-model.org) winds (Sapiega et al., 2023) and for simulations for the entire Baltic Sea that used ERA5 wind data and took sea ice into account (Björkqvist et al., 2018b).

---

[4] This thesis uses the notion from Leppäranta and Myrberg (2009) that the Gulf of Bothnia denotes the entire sea area to north of the Sea of Åland and the Archipelago Sea (Figure 1), and is divided into Sea of Bothnia in the south and Bay of Bothnia in the north.

The level of scatter of H_S is also fairly small for all locations with contemporary measurements in the Baltic proper, such as Pohjois-Itämeri (Figure 5) but is clearly larger for the historical Almagrundet data that had certain quality issues (Broman et al., 2006) even though the correlation coefficients for time series of modelled and recorded H_S were fairly large, 0.92 and 0.91, for the ERA5 and BaltAn65+ forcing, respectively.

The run forced with ERA5 data also replicated H_S well in the Sea of Bothnia where the run forced with BaltAn65+ data had almost no matching recorded data. The correlation coefficient was 0.6 in both measurement locations while bias was 0.15/0.17 m and rmsd was 0.25/0.28 m. As the measurement devices were deployed only during the ice-free season in this domain, these comparisons cover only a part of the time. The match was even better for both runs and wave data from Suomenlahti (Figure 3) in the Gulf of Finland. The bias, rmsd and correlation coefficient were 0.01/0.1 m, 0.20/0.21 m, and 0.94/0.94 for the runs forced with the BaltAn65+ and ERA5 data, respectively (Paper I). Similar values were obtained for a run that used the ERA5 forcing and took ice cover into account (Björkqvist et al., 2018b).

The match of recorded and modelled wave properties in the nearshore can only be evaluated for the run forced by ERA5 wind data as there are no earlier measured data available. This match, evaluated using wave properties in the innermost high-resolution grids (Figure 2, Figure 3), is highly variable for four locations in the southern nearshore of the Gulf of Finland (Paper I). The bias varies from 0.21 to 0.51 m, rmsd from 0.24 to 0.58 m, and correlation coefficient from 0.76 to 0.93 in these locations. The match is better for sites located near straighter coastline segments with smoother bathymetry (Sillamäe, Figure 1, and Letipea, Figure 3). These measurements only reflect ice-free periods and thus the match is not affected by ignoring sea ice in the model.

Therefore, both runs described in Paper I provide high-quality reproduction of wave height time series for offshore locations of the Baltic proper, Gulf of Bothnia and Gulf of Finland. The statistical quantities characterising the match of modelled and measured wave properties differ insignificantly. They are slightly better for the run forced with BaltAn65+ wind data. This advantage cannot be realised for the current situation as this run only covers years 1965–2005. However, the match of modelled and measured nearshore wave height is acceptable only in places with relatively smooth bathymetry and simple geometry of the coast.
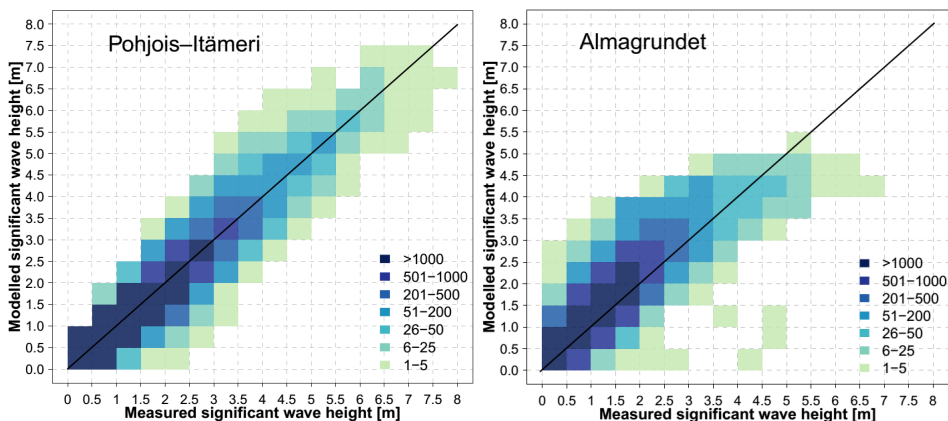

Figure 5. Comparison of H_S reconstructed using BaltAn65+ wind data with values retrieved from measurements at Pohjois-Itämeri and Almagrundet (Figure 3). From Paper I.

The use of even a very fine grid does not lead to good match in areas with complicated bathymetry, such as Neugrund (Figure 3) near the entrance of the Gulf of Finland. The bias approaches half a meter in areas with sharply changing topography or complex geometry that partially shelters the measurement location against predominant winds. The grid resolution of 280–560 m thus may still be insufficient to fully capture local features of the wave field in such locations. Notably, the run that uses the BaltAn65+ forcing seem to perform slightly better in the Baltic proper and in the offshore of the Gulf of Finland; most probably due to its finer spatial wind resolution, although this varies by site and becomes evident based on a few examples only. Moreover, the model tends to overestimate wave heights in the immediate nearshore.

1.3.2 Peak Period

The accuracy of estimates of peak period T_p is poor for low wave conditions of the Baltic Sea (Björkqvist et al., 2018b) when very low remote swell may create a multi-peak spectrum and the peak period is poorly defined. For this reason, the modelled values of T_p are only validated in Paper I for reasonably energetic wave conditions with $H_S > 0.5$ m (Figure 6).

The hindcast of T_p using ERA5 and BaltAn65+ wind data demonstrate a very good match with instrumentally recorded values in the Baltic proper and in the south of the Baltic Sea. The bias varies from –0.28 s at Pohjois-Itämeri (Figure 6) up to 0.39 s at Warnemünde in the south of the sea for the run forced by BaltAn65+ wind data. The range was even smaller, from –0.08 s to 0.36 s, at the same locations for the run forced by ERA5 wind data. The rmsd varies from 1.18 s to 1.62 s and from 0.65 s to 1.06 s, respectively. However, the correlation coefficient R is much smaller than for H_S. It is 0.45 at Warnemünde and 0.8 at Pohjois-Itämeri for the run forced by BaltAn65+ wind data. Its values are in the range from 0.47 at Warnemünde to 0.83 at Pohjois-Itämeri for the run forced by ERA5 wind data (Paper I). Therefore, modelled peak periods have almost no bias in the Baltic proper but the match of single values is much worse than the match of the values of H_S.

The situation is basically the same in the Gulf of Finland where only one location (Suomenlahti, Figure 6) can be used to characterise the match of the outcome of both models. Both models slightly underestimate T_p while the run forced with ERA5 wind data offers slightly smaller rmsd (1.39 s versus 1.62 s) and slightly larger correlation coefficient (0.59 versus 0.50; Paper I). This imperfect match suggests that both models have issues with the replication of wave properties in smaller sub-basins of the Baltic Sea. In this context, the situation in the Gulf of Finland is probably the most complicated because predominant winds blow obliquely across this gulf and may excite specific long-period wave components (Pettersson et al., 2010). The recorded values of T_p are reproduced with the largest accuracy for wave fields in the Gulf of Bothnia where bias is 0.07–0.28 s, rmsd is 0.65–0.84 s and the correlation coefficient is 0.81–0.89 (Paper I).

Peak periods are replicated in the run forced with ERA5 wind data much less accurately in the nearshore locations of the Gulf of Finland where wave properties were evaluated with a spatial resolution of about 280 m. The match is acceptable (correlation coefficient 0.4–0.47) near the entrance of the gulf at Sundgrund and Suurupi (Figure 3), but poor (correlation coefficient –0.06 or 0.18, bias –1.35 s or –0.78 s) at Sillamäe (Figure 1) and Letipea (Figure 3). This poor match may reflect specific wave conditions during relatively short *in situ* measurements at these locations.
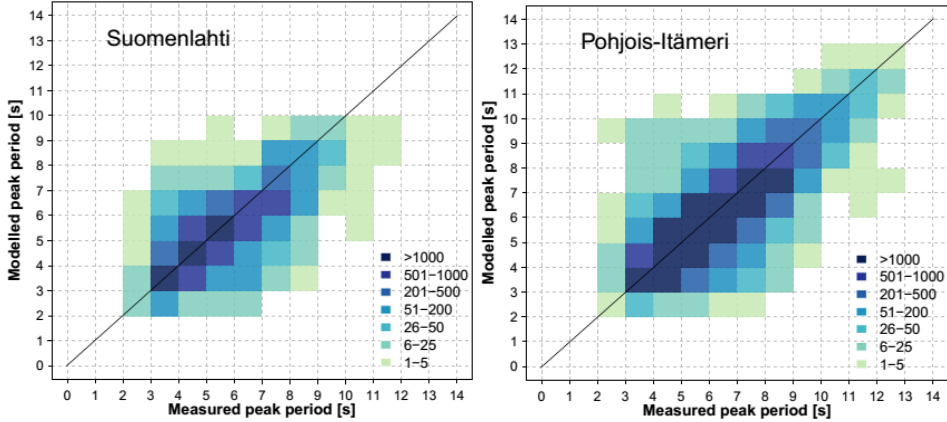
Figure 6. Comparison of T_p reconstructed using BaltAn65+ wind data with recorded values for waves with $H_S > 0.5$ m at Suomenlahti in the Gulf of Finland and Pohjois-Itämeri (Figure 3) in the Baltic proper. The colour indicates the total count of values within each square. From Paper I.

In general, the accuracy of the replication of T_p by both model runs is reasonable for offshore areas of the Baltic proper, the Gulf of Bothnia and the Gulf of Finland, however it is lower than the accuracy of reproduction of H_S. The quality of reproduction of T_p by the model forced with ERA5 wind data, estimated based on the presented statistical characteristics, is slightly better than by the model that uses BaltAn65+ wind data, possibly due to the higher (hourly) temporal resolution of ERA5 data.

The validation exercise in Paper I demonstrates that the SWAN model performs reliably across the entire offshore domain of the Baltic Sea, including its two largest sub-basin Gulf of Bothnia and Gulf of Finland. In particular, H_S is accurately reproduced in both open-sea and nearshore domains while the accuracy of replication of T_p is much worse in the coastal zone. The latter feature probably signals that wave modelling in nearshore locations is more challenging due to unresolved small-scale bathymetry and geometry of the basin, and uncertainties in the description of wave-bottom interaction (Alari and Raudsepp, 2010; Björkqvist et al., 2018a). For T_p, limitations are more systemic, and although the outcome of the run that uses ERA5 wind data is better, neither dataset allows perfect reconstruction of spectral peak behaviour. Nearshore T_p is especially difficult to resolve, as local depth, sheltering effects, wave refraction, and possibly multi-peak spectra are not always captured even by high-resolution models.

1.4 Wave heights in the Baltic Sea Wave Climate

The properties of simulated wave climate of the Baltic Sea reflect the interplay between regional wind patterns, bathymetry and the unique geometry of semi-enclosed sub-regions of the sea. The modelled fields of H_S enable the exploration of the core long-term statistical properties of H_S, focusing on spatial patterns of the long-term average wave height, higher (90th, 95th, 99th) percentiles and maxima of H_S (Figure 7) in the Baltic Sea. In particular, the resulting data set made it possible to highlight spatially varying differences in these characteristics of wave height for the common hindcast period of the two models 1991–2005.

1.4.1 Spatial Distribution of Wave Heights in the Baltic Proper

The Baltic Sea region is frequently exposed to westerly winds. In particular, south-western and north to north-western winds have the longest fetches in the Baltic proper. It is therefore natural that the highest wave energy levels are found in the south-eastern, eastern and north-eastern domains of the Baltic proper (Figure 7). This pattern becomes evident in both idealised ice-free simulations (Soomere and Räämet, 2011) and more realistic runs that take sea ice into account (Tuomi et al., 2011; Björkqvist et al., 2018b). As expected, in both our simulations, the spatial patterns of different characteristics of wave height are generally smooth and match this almost intuitive spatial pattern. All measures of wave height increase from the western part of the basin towards the central, south-eastern and north-eastern domains that have the longest unobstructed fetch (Figure 7).

In the simulation driven by ERA5 wind data, the long-term average H_S across the central and eastern side of the Baltic proper is typically slightly over 1 m, with a wide area of maximum values around 1.1 m, and with peak values located southeast of Gotland (Figure 1) and relatively high values extending to the sea area to the west of Saaremaa (Figure 1). These areas have typical fetch length over 300 km for some of the predominant moderate and strong wind directions.
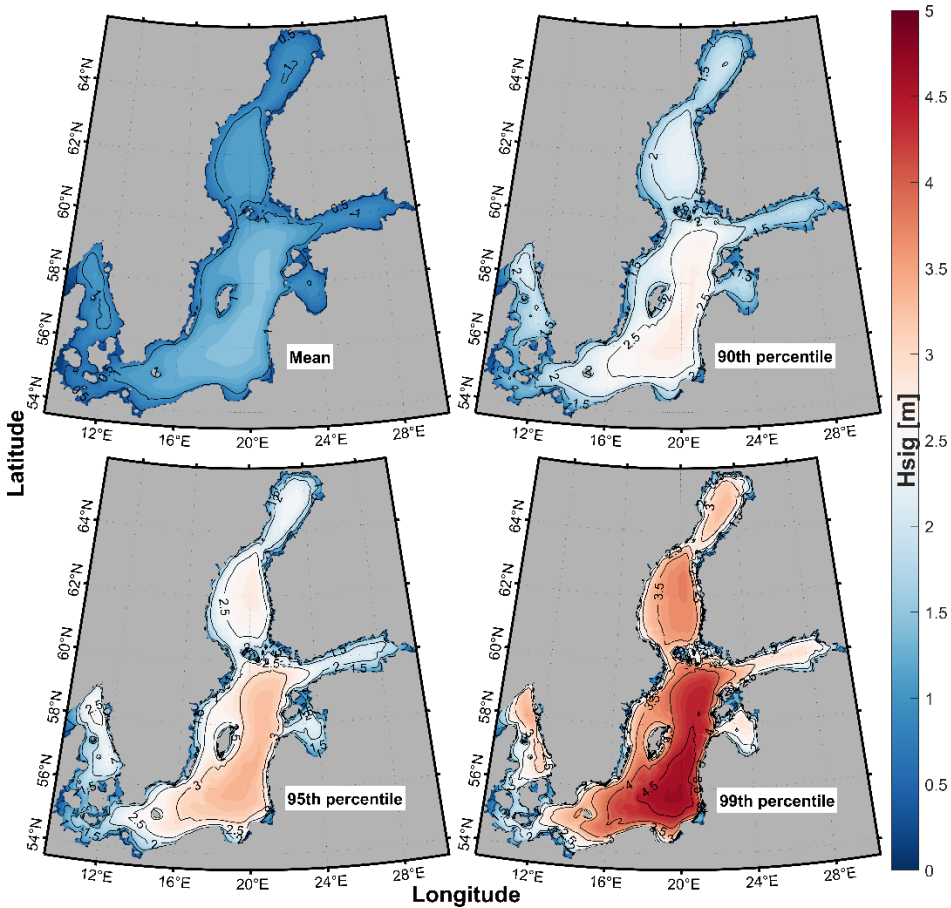

Figure 7. Spatial distribution of statistical properties of H_S simulated using ERA5 wind data 1991–2021: mean H_S, 90th, 95th, and 99th percentile of H_S. Combined from Figures 8 and 9 from Paper I.

Properties of H_S from the run forced by BaltAn65+ wind data show a similar spatial pattern, but with long-term average values of H_S about 0.1–0.15 m lower. This pattern holds true across all addressed percentiles of H_S (Paper I).

The difference between estimates of higher percentiles of H_S from the two runs is larger than the difference in mean H_S. For example, the 99th percentile of H_S from the run using ERA5 wind data peaks above 4.0 m in the eastern Baltic proper while similar peaks of H_S, from the run with BaltAn65+ wind data remains in the range of 3.7–3.9 m. This difference is likely attributable to a higher temporal resolution of the ERA5 dataset which captures short-lived wind maxima more effectively, and avoids smoothing over these events, different from the 6-hourly BaltAn65+ wind dataset.

Despite these differences, the properties of simulated H_S from the two runs are in excellent agreement in terms of spatial orientation and zonation of wave energy in the Baltic proper. The distinct east-west gradient and the local maxima are aligned, and the sheltering effects behind islands are reproduced accurately. The ability of both datasets to yield such spatially consistent results, while slightly differing in amplitude, underscores the robustness of the model.

1.4.2 Gulf of Finland Wave Climate

Different from the Baltic proper, the Gulf of Finland is a narrow, elongated basin that is oriented obliquely with respect to predominant moderate and strong winds. These features suggest that wave properties in this gulf are sensitive with respect to even small changes in storm wind directions (Männikus et al., 2024) and may have strong gradients in wave properties. The orientation of the gulf is approximately from the west to the east, which makes it responsive to long duration south-western and particularly western winds. For example, during the 2005 January storm, very high waves were recorded in the gulf (Soomere et al., 2008) even though the wind was not aligned with the gulf. Additionally, its complex bathymetry and coastal morphology locally modulate wave growth and transformation at scales comparable to the major bathymetric features.

In both simulations described in Paper I, the largest wave heights in the gulf are found in its central and western sectors (Figure 8). The mean H_S in the area typically reaches ~1 m in the simulation forced with ERA5 wind data or ~0.9 m in the run forced with BaltAn65+ wind data. This slight difference mirrors the similar difference in the Baltic proper. The 95th and 99th percentiles of H_S exhibit more substantial differences. The simulations using ERA5 wind data suggest that the 99th percentile of H_S values in the central Gulf of Finland exceeds 2.7 m over quite a large area, with local maxima east of Helsinki even 2.9 m (Figure 8). The simulation forced by BaltAn65+ wind data yields values closer to ~2.5 m in the same area. It is likely that this difference reflects the better ability of ERA5 wind data with higher temporal resolution to replicate wind speed maxima in this directionally sensitive sub-basin. The area where wave heights are larger in simulations using ERA5 wind data than in runs forced with BaltAn65+ wind data form a broad band elongated along the basin (Paper I).

The pattern of differences is opposite near the coastline (Figure 8), particularly along the southern shores of the gulf. The simulation using BaltAn65+ wind data produces slightly higher H_S values in this nearshore area than the run forced with ERA5 wind data. This difference is particularly pronounced for the 90th and 95th percentiles of H_S. For example, the run using BaltAn65+ wind data produces slightly higher (by ~0.1–0.2 m) 95th percentile of H_S in the nearshore of Finland and Estonia. This kind

of difference in the nearshore wave height is attributed to the spatial resolution difference of wind forcing discussed in Paper I. Specifically, the finer spatial resolution of BaltAn65+ wind data (~11 km) apparently allows a better representation of the local coastal wind features than the more moderate resolution of ERA5 wind data (~30 km) even though the ERA5 data set represents more enhanced physics and global optimised assimilation (Hersbach et al., 2020).

Overall, the Gulf of Finland is a useful case study of the sensitivity of wave modelling to the spatial and temporal structure of wind forcing (Pettersson et al., 2010; Suursaar, 2015; Männikus et al., 2024). As the match of the outcome of the two runs with recorded data has basically the same quality in both the Baltic proper and the Gulf of Finland, it was not possible to determine (in Paper I) which wind forcing leads to more adequate representation of the wave climate.

It can be speculated that the advantage of the use of ERA5 wind data lies offshore, its higher temporal resolution possibly more adequate for tracking storm events in the open sea because of improved data assimilation and enhanced representation of
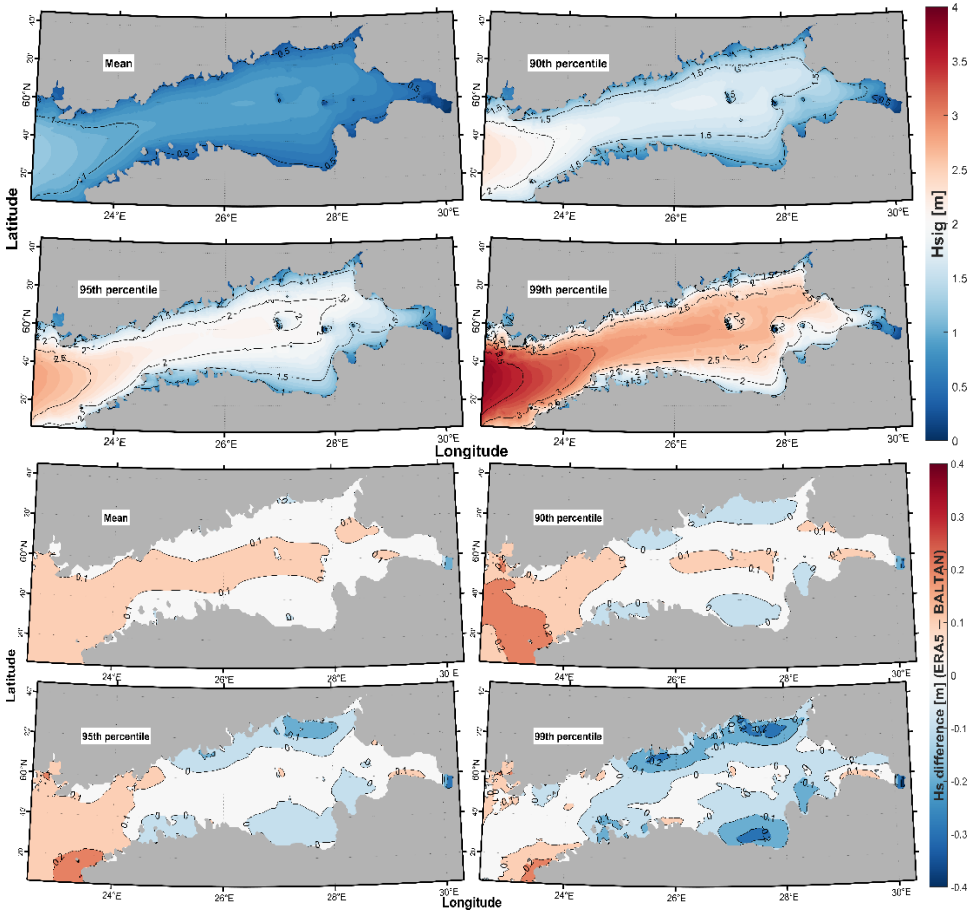

Figure 8. Four upper panels: H_S quantiles in the Gulf of Finland according to simulations using ERA5 winds: mean H_S, 90th, 95th, and 99th percentile of H_S. Four lower panels: Difference in the H_S quantiles estimated using ERA5 and BaltAn65+ wind data 1991–2005: mean H_S, 95th, 99th, and 99.5th percentile. Red means that simulations using ERA5 wind data result in higher H_S values than simulations using BaltAn65+ wind data. Modified from Paper I.

physics than in the ERA-40 and ERA-Interim products. The core advantage of the BaltAn65+ wind data is its higher spatial resolution. Most likely this feature allows for more adequate replication of wave properties in the nearshore areas. The contrasts between spatial patterns of different characteristics of wave heights are particularly sharp in the Gulf of Finland. However, similar tendencies of providing higher estimates of wave heights in the offshore in the runs forced by ERA5 wind data are evident in the Baltic proper as well.

1.5 Differences Between the Two Realisations of Wave Climate

The use of two wind forcing datasets in the long-term wave hindcast exemplifies how differences in atmospheric input translate into the wave model outputs. The presented comparison has revealed both overall spatial consistency and substantial regional variability in wave statistics. The key differences include temporal resolution, spatial resolution and differences in replication in some physical processes, such as ice representation and wind-ice interactions (Paper I). These differences are present only in wind datasets as our simulations considered only an idealised ice-free sea surface. The common hindcast period is 1991–2005. The comparison is only performed in Paper I in terms of selected time series and different statistical properties of H_S.

1.5.1 Spatial Patterns in Wave Height Differences

The differences in wave climate estimates using the two wind forcing datasets are small in terms of the mean values of H_S across the entire Baltic Sea, but substantial in terms of higher quantiles of H_S in some locations, first of all in the Sea of Bothnia (Figure 9). The differences vary by statistical quantile and to some extent they also depend on the exposure of the particular location to storm tracks.

As described in Section 1.4.1, in most of the central and southern Baltic proper, the model run using ERA5 wind data yields mean H_S values by 0.05–0.15 m higher than simulations using BaltAn65+ wind data (Figure 9). The differences are mostly uniform and have a moderate and wide peak in the area to the west and north-west of Gotland. A largely uniform difference of about 0.2 m characterises the spatial distributions of the 90th percentiles. The differences are larger, up to 0.3–0.5 m and concentrated in smaller locations in terms of the 95th percentiles. The differences of the 99th percentile are much smaller in most of the Baltic proper. They are only substantial between the island of Gotland (Figure 1) and the Swedish mainland.

The largest deviations between the mean value and higher quantiles of H_S are detected in the Gulf of Bothnia (Figure 9). The estimates of average H_S using ERA5 wind data exceed those evaluated using BaltAn65+ systematically by more than 0.2 m, that is, >20% of the typical value. The difference in 90th, 95th and 99th percentiles is systematically in the range of 0.3–0.4 m in the entire Gulf of Bothnia and exceeds 0.5 m for the 95th percentile and 0.6 m in the very north of the Bay of Bothnia. As simulations in Paper I ignore the presence of sea ice (that is only reflected to some extent in the physics of atmospheric models as discussed above), it is likely that these deviations mirror substantial differences in wind properties in the Gulf of Bothnia (Paper I).

1.6 Wave hindcast during selected storm events

The fastest wave-driven sediment transport occurs during very strong storms that bring massive amounts of wave energy to the shore. It is therefore crucial that the wave model used for sediment transport analysis adequately replicates the strongest storms in the areas of interest.

To estimate the ability of the two model runs in this context, Paper I provides insight into the accuracy of representation of time series of wave properties against instrumental recordings in a selection of severe storms where the simulated H_S exceeded 7 m in the Baltic proper and 5 m in the Gulf of Finland (Figure 10). Such events are considered as the harshest in the Baltic Sea as $H_S > 7$ m has been instrumentally recorded only five times up to 2017 (Björkqvist et al., 2017).
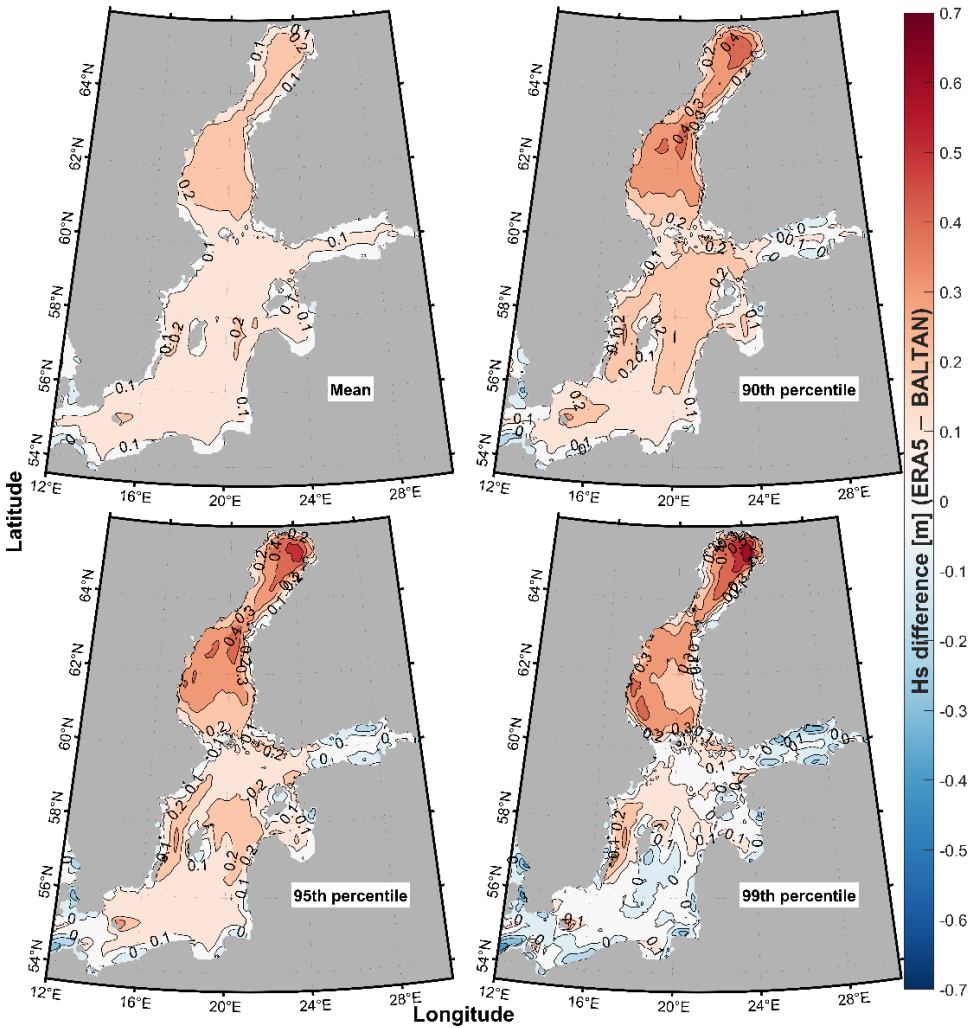
Figure 9. Difference of wave heights in simulations forced with ERA5 and BaltAn65+ wind data 1991–2005 in terms of mean H_S, 90th, 95th, and 99th percentile of H_S. Positive values indicate areas where the use of ERA5 wind data leads to larger values of H_S. Modified from Paper I.

Figure 10 shows that both models capture the magnitude and timing of H_S adequately in such storms. This is true for both sequences of multiple storm peaks on 16–19 December 1999, captured by the Pohjois-Itämeri wave buoy. The outcomes of both runs follow the general pattern of wave growth and decay well, with high correlation coefficients. The run forced with ERA5 wind data slightly overestimates the observed highest peak by ~1 m (blue above black), while the simulation forced by BaltAn65+ wind data replicates values of H_S closer to the maximum observed value. The rmsd values are nearly identical for both runs. Simulations with both wind forcings hindcast the peak to occur marginally earlier compared to measurements. Therefore, the better match of the recorded statistical properties with the outcome of wave simulations forced with ERA5 wind data does not mean that this model always better captures wave heights in all locations. Interestingly, the recorded wave heights tend to fall in between the projections from the two models.

The situation is similar in the case of a single, well defined wave storm peak in December 1999 in the Baltic proper (Figure 10b). Both simulations successfully reproduce the overall shape of the course of H_S, with the timing and the rate of increase and decrease in this quantity corresponding well to the recorded storm passage. On this
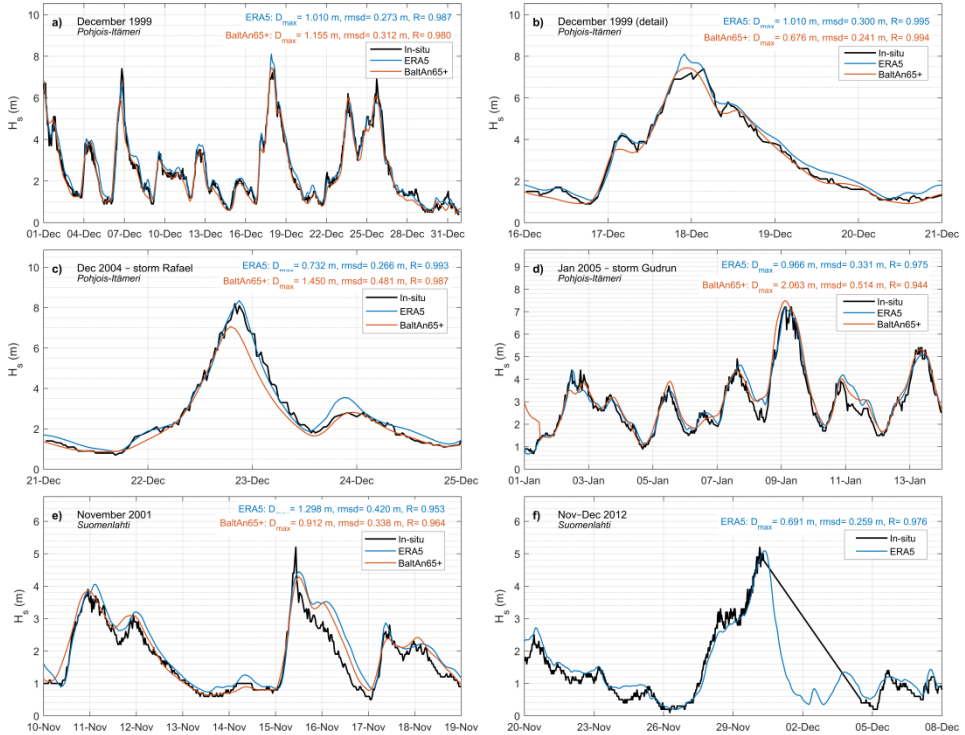

Figure 10. Comparison of H_S reconstructed using the ERA5 and BaltAn65+ wind data during storms that created $H_S > 7$ m. a) Pohjois-Itämeri (Figure 3), December 1999, b) Pohjois-Itämeri, December 1999 (detail), c) Pohjois-Itämeri, storm Rafael in December 2004, d) Pohjois-Itämeri, storm Gudrun in January 2005, e) Suomenlahti (Figure 3), November 2001, f) Suomenlahti, storm Antti in November 2012. Black: measured data, blue: simulations using ERA5, red: simulations using BaltAn65+ wind data, D_{max} is the maximum difference between the modelled and recorded H_S within the shown time interval and R is the correlation coefficient Recorded data are from the SMHI database. Modified from Paper I, with small changes in the represented time periods and associated changes in statistical properties.

occasion the simulation using ERA5 wind data shows a closer alignment with the properties of the peak, underestimating the maximum H_S by 0.71 m compared to 1.46 m in the simulation using BaltAn65+ wind data. The time series of H_S replicated using ERA5 wind data also has a lower rmsd deviation from the recorded values and a slightly higher correlation coefficient with these values. Moreover, the simulation with the BaltAn65+ forcing appears to smooth the storm peak to some extent.

1.7 Concluding remarks

The dual-forcing simulations performed in Paper I provide interesting insights into how even small differences in the atmospheric input data can affect the wave hindcasts in the Baltic Sea. While the use of ERA5 wind data tends to yield slightly higher estimates for average and extreme wave heights (in terms of higher percentiles) in offshore locations, the use of BaltAn65+ wind data produces larger wave heights in nearshore regions, most notably in the Gulf of Finland. It is hypothesised in Paper I that these aspects reflect the better ability of the ERA5 wind data to capture storm evolution in the offshore, with the higher spatial resolution of the BaltAn65+ wind data set having a better ability in complex coastal settings. Also, both sets of wind data perform equally well in reproducing the timing and magnitude of the most severe storms even though simulations using ERA5 seem to provide a slightly better match with recorded data.

The most intriguing outcome is that all addressed statistical properties of H_S differ considerably in the entire Gulf of Bothnia between the two models. Paper I only describes this feature and does not explore its reasons.

The most important feature for this thesis is that the outputs of performed simulations have only minor differences in the nearshore of the Gulf of Riga and along the sedimentary eastern Baltic Sea coast from Cape Kolka to Cape Taran (Figure 9, see Figure 1 for locations). Even though there are almost no instrumentally recorded wave data from these coastal segments, the match of the outputs of the two simulations that have been quality controlled in many other locations, can be interpreted as showing that both are reliable in the nearshore of these coastal segments. This conjecture suggests that results of simulations in Papers III–V based on time series of wave properties hindcast using the ERA5 forcing adequately reflect reality.

2 Wave Climate of the Gulf of Riga

2.1 Introduction and Physical Setting

The Gulf of Riga is a semi-enclosed basin in the eastern Baltic Sea (Figure 11). It is much smaller than the Gulf of Bothnia or Gulf of Finland, covering an area of approximately 17,913 km² between Estonia and Latvia, and having a generally regular, oval-like shape. With the average water depth of 21 m and maximum depth of 52 m (Seifert et al., 2001; Suursaar et al., 2002; Feistel et al., 2005) it has mostly relatively smooth bathymetry, except for the northern part.

The gulf is connected to the Baltic proper via the Irbe Strait (Figure 11). Even though this waterway is *ca* 27 km wide, it inhibits the propagation of most Baltic proper wave systems, including long-period swell from most directions, into the gulf. The much narrower Suur Strait allows very limited wave propagation from the Moonsund (Väinameri Sea, Figure 11). All this reinforces the dominance of locally generated wind-sea conditions in the gulf (Eelsalu et al., 2014). Thus, the wave climate in this basin can differ substantially from that in the Baltic proper or in the previously discussed Gulf of Finland that is widely open to the northern Baltic proper.

The prevailing wind directions in the gulf region, similar to the northern Baltic proper are from the south-west and north-north-west (Soomere and Keevallik, 2001). They both have relatively long fetch in the gulf. South-west winds are more frequent but north-north-west winds, although less frequent, tend to produce the highest individual wave events in the area (Davidan and Lopatukhin, 1982; cited in Eelsalu et al., 2014). Waves excited by south-west winds in the Baltic proper may enter the gulf and
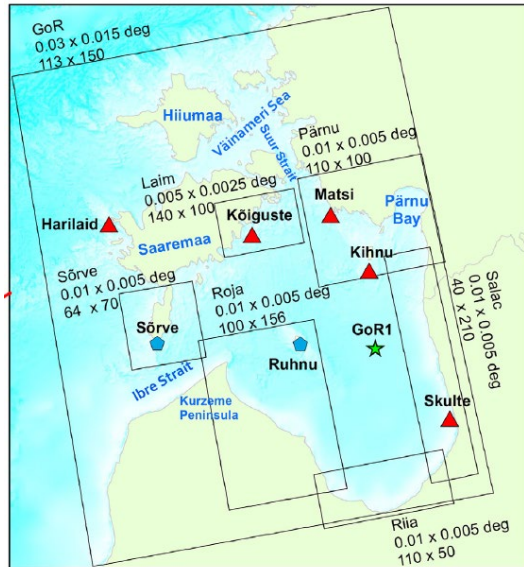

Figure 11. Map of the study area and the location of visual wave observation (blue pentagons) and instrumental measurement (red triangles) sites in the Gulf of Riga and near its entrance (Harilaid). The green pentagram GoR1 denotes an open location of the Gulf of Riga at 23.87°E, 57.7°N that is used as a reference point for modelled data (no measurements are from this location). The boxes indicate nested grid areas used in the model. The numbers below the names of the grids show the resolution in degrees and the number of grid cells in the West-East and North-South directions. Graphics by Maris Eelsalu. Modified from Paper II.

contribute to the formation of the local wave climate in the north of the gulf. The combined effect of the anisotropic wind climate and small size gives rise to rapidly varying wave conditions that have a memory of only a few hours. Some areas, such as Pärnu Bay (Figure 11), are sheltered from waves from most directions and generally experience mild wave conditions. These features complicate calibration and validation of wave models in this region.

While wave properties and wave climate changes in the offshore of the Baltic Sea can be quantified using satellite altimetry (Kudryavtseva and Soomere, 2016, 2017), the small size of the Gulf of Riga does not allow this. The limitation is that satellite altimetry can provide reliable wave heights only at a distance of >0.2° from the land (Queffeulou, 2004). This limits the applicability of satellite altimetry to a narrow portion of the central basin far from the mainland and islands, such as Ruhnu or Kihnu (Figure 11).

This chapter follows Paper II. It provides first a short insight into the outcome of the analysis of historical visual wave observations. The existing instrumental measurements are used to validate high-resolution wave hindcasts performed using the SWAN model described in Chapter 1. The central purpose is to create a thorough description of the wave climate (including its extremes) in the Gulf of Riga in the period 1990–2021 and to provide input data for the analysis of wave-driven sediment transport along the shores of the gulf (Paper III, Paper IV and Paper V).

2.2 Data Sources and Methodology

2.2.1 Visual Wave Observations

Visual wave observations have been an important source of information about the core properties of wave climate (Gulev and Hasse, 1998, 1999) even though they suffer from significant limitations (Guedes Soares, 1986). In particular, wave observations from the shore are complicated when used to compare with instrumentally measured or modelled data because of low temporal resolution, gaps in records due to poor visibility, observer subjectivity, systematic underestimation of wave heights, etc. (Soomere, 2013). For the listed reasons, visual wave observations should be used with care but they may still be a valuable tool to derive a first-order estimate of the most robust properties of the wave climate.

Long-term visual wave observations have been performed in the Gulf of Riga at two locations: the island of Ruhnu and the Sõrve Peninsula (Figure 11) in accordance with the Soviet maritime meteorological protocols (Guidelines, 1985, cited by Soomere and Zaitseva, 2007). Wave properties, usually certain measures of wave height, period and direction, were typically recorded 1–4 times a day 1954–2011 at Ruhnu and 1957–1992 at Sõrve.

The main outcome of these observations (Paper II) was consistent with the above qualitative description of wave fields in the Gulf of Riga. The wave climate in this gulf is milder than in the nearshore of the Baltic proper at the shores of Latvia and West Estonian Archipelago. Wave periods in the gulf are shorter than in the Baltic proper. Seasonal variation of typical wave heights has the same magnitude as in the Baltic proper. Finally, wave climate in different parts of the gulf is remarkably different: the long-term observed wave height at Ruhnu is about twice as high as at Sõrve. The latter feature is consistent with asymmetry of the local wind climate: as winds predominantly blow from the south-west or north-north-west, high waves often reach Ruhnu but infrequently the observation location at Sõrve.

2.2.2 Instrumental Wave Recordings

The performed wave simulations were validated against the output of four short-term instrumental wave measurement campaigns conducted between 2006 and 2021 at Kõiguste, Kihnu, and Matsi by Estonian Marine Institute (EMI) using an ADCP (Suursaar, 2013, 2015) and near Skulte by the Latvian Institute of Aquatic Ecology (LHEI) using a so-called SmartBuoy (Figure 11). For comparison of wave properties, in the eastern Baltic proper, wave data recorded using an ADCP near Harilaid (Figure 11) were also used. The devices collected H_S and T_p at hourly intervals. The number of single recordings used in comparisons varied from 1941 at Matsi to 6736 near Skulte (see Table 1 in Paper II). As simulations in Paper II ignore the presence of sea ice, comparisons of simulated and recorded wave properties are performed only for ice-free times and thus against a somewhat smaller set of recordings at Kõiguste and Kihnu.

2.2.3 Wave Model Configuration

Wave conditions were simulated using the third-generation SWAN model (Booij et al., 1999), applied in a nested grid system introduced in Chapter 1 and Paper I. Information about the full spectrum of waves from the outer grid covering the entire Baltic Sea at ~5.5 km (3 nmi) resolution (Figure 2a) was used as boundary conditions for the intermediate grid that covers the Gulf of Riga and its vicinity at ~1.85 km (1 nmi) resolution (the largest box named GoR in Figure 11). The same technique was employed to generate boundary conditions for the nearshore grids with a resolution of ~560 m or finer (e.g., 280 m of the grid named Laim around Kõiguste in the north of the Gulf of Riga in Figure 11).

As described in Chapter 1, this model forced with ERA5 and BaltAn65+ wind data led to almost coinciding results in the Gulf of Riga and its vicinity (Figure 9). For this reason wave simulations in Paper II were performed using the ERA5 data set only. While generally robust, the ERA5 product may underrepresent small-scale features such as convective gusts, which can be locally important in semi-enclosed seas. As in Paper I, simulations assumed constant sea level and neglected sea ice and marine currents. While consistent with observational records (which exclude ice periods), this practice likely results in overestimation of winter wave energy (Najafzadeh and Soomere, 2024). The model covered the period 1990–2021, producing hourly outputs of H_S and mean and peak wave periods (T_{m02}, T_p) as well as directional spectra.

2.3 Wave Model Validation

2.3.1 Instrumental Wave Recordings

To evaluate the quality wave information hindcast using the SWAN model, the modelled H_S and T_p were compared in Paper II with the recordings of the described instrumental measurements from five sites using wave data from the 1 nmi grid and for some locations also from the local 560 m grid. The main statistical properties of wave climate were also compared against similar properties retrieved from visual observations. The analysis focused on both the temporal and spatial performance of the model.

The simulations reasonably replicated time series of recorded H_S at all locations. The timing of individual storm events was captured adequately. The model tended to overestimate the peaks at Harilaid, which is a relatively exposed offshore location in the Baltic proper near the entrance to the Gulf of Riga, but underestimate the peaks near Skulte in the interior of the gulf (Figure 12; see locations in Figure 11). The bias varied from 0.02 m at Skulte up to 0.35 m at Harilaid 2006–2007, the rmsd from 0.19 m at Skulte up to 0.41 m at Harilaid 2006–2007, and the Pearson correlation coefficient varied from 0.89 at Kõiguste up to 0.92 at Kihnu, Matsi and Skulte, and 0.93 at Harilaid 2006–2007 (see Table 2 of Paper II).

The model performs best at open or semi-exposed locations such as Kihnu and Matsi, where the correlation coefficient exceeds ~0.9 and rmsd stays below 0.35 m. A less perfect match of recorded and modelled data is evident at shallow, nearshore stations like Kõiguste and Skulte. The probable reasons for this feature are insufficient resolution of bathymetry, local sheltering and unresolved fine-scale wave processes (Paper II). The match of recorded and modelled wave periods is basically the same as in the Baltic proper and Gulf of Finland (Paper I), where the period data provided a reasonable, but worse match with the measurements than H_S. Therefore, the presented statistical quantities also signal that the simulations adequately replicate the course of the main wave properties.
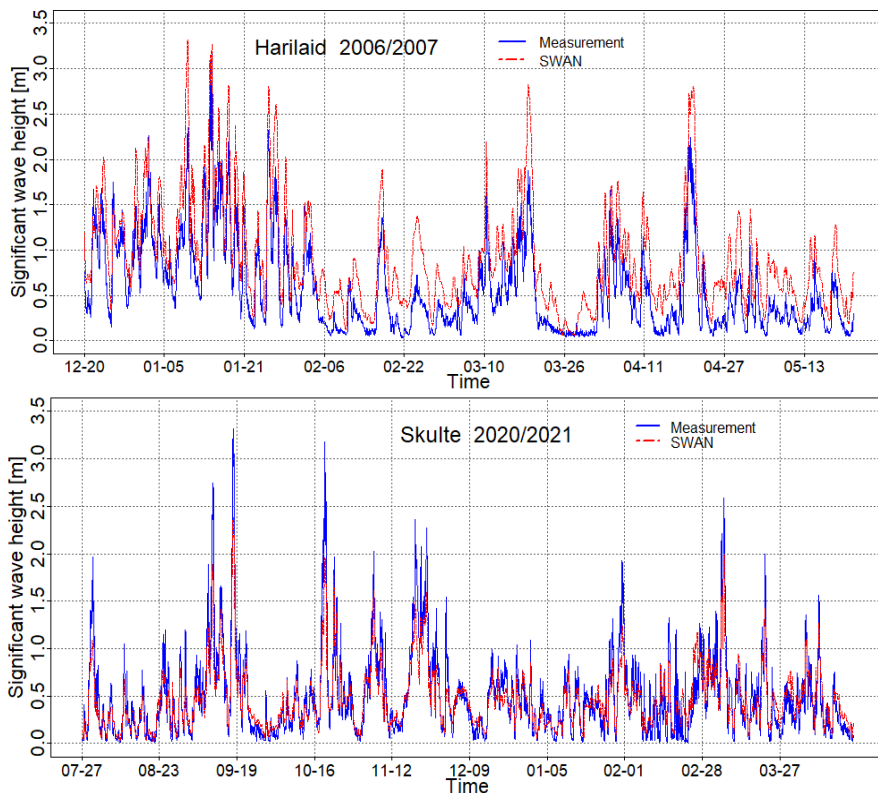

Figure 12. Time series of recorded (blue) and modelled (red) H_S at Harilaid 2006–2007 (upper panel) and near Skulte 2020–2021. From Paper II.
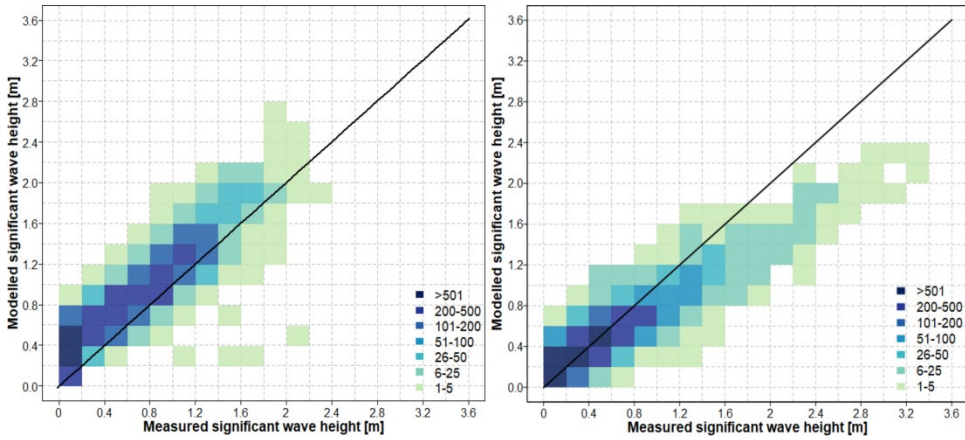
Figure 13. Comparison of the recorded and modelled H_S at Kihnu (left) and Skulte (right). The colour indicates the total count of values within each square. From Paper II.

A selection of scatter plot diagrams of recorded and modelled H_S for two locations (Figure 13) confirm that the match of these quantities in the nearshore of the Gulf of Riga is basically of the same quality as in offshore locations (Chapter 1; Paper I). While most of the pairs of wave conditions lie reasonably close to the diagonal of the plot at Kihnu (Figure 13), there are a few single time instants when the model did not reproduce recorded H_S values in the range of 1.0–2.2 m.

In a similar manner, a few modelled H_S values in the range of 2.4–2.8 m were overestimated by more than 0.5 m in recordings. Such deviations between recorded and modelled wave properties are characteristic in regions of the Baltic Sea with complex geometry and bathymetry (Björkqvist et al., 2018a).

The match is clearly worse for the Skulte data. As demonstrated above, the model tends to systematically overestimate H_S in this location. While usually the match is better for reasonably high waves ($H_S > 0.5$ m, Paper II), heights of larger waves are even more overestimated by the model at this location (Figure 13).

This observation is further demonstrated by the histograms of H_S (equivalently, empirical distributions of the occurrence of different wave heights) at these two locations (Figure 14). It is natural that very low waves are about 1/4 of all recorded
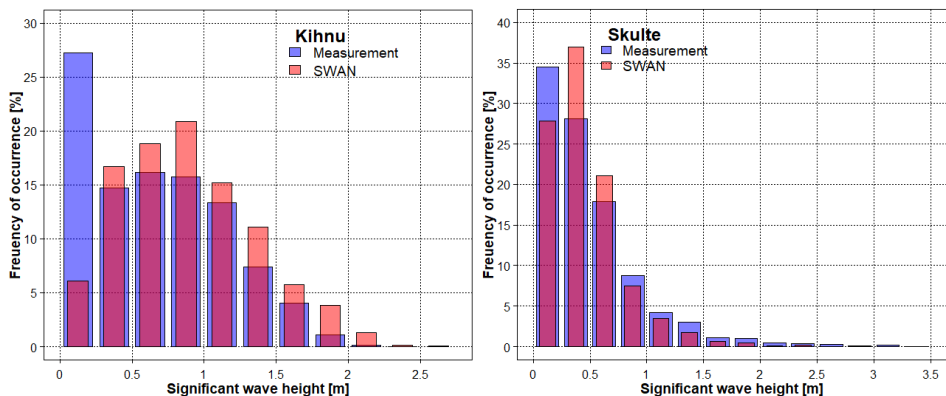

Figure 14. The empirical probability of occurrence of recorded (blue) and modelled (red) H_S at Kihnu and Skulte. The modelled data sets only represent the time interval covered by observations. From Paper II.

wave conditions at Kihnu where the measurement site close to the shore is sheltered from waves from some directions. In other words, the model fails to replicate the correct frequency of the lowest wave heights. It is thus natural that the model projects larger frequencies of more energetic wave conditions while the rate of this "overperforming" is more or less constant in other parts of the wave height record.

The situation is different at Skulte where the model similarly underpredicts very low waves and overpredicts the frequency of waves with H_S 0.25–0.5 m and 0.5–0.75 m. The reason(s) for this mismatch remained unknown in the analysis provided in Paper II where it was hypothesised that it may mirror ERA5's smoothed wind fields and insufficient accuracy of the nearshore bathymetry at this location.

The match of recorded and simulated wave periods is also different at Kihnu and Sõrve. Different from the above, the match is almost perfect at Skulte and poor at Kihnu in terms of the empirical probability distribution of peak periods (Figure 15). Part of the difference at Kihnu may stem from the technical limitations of the ADCP device: its pressure sensor does not recognise shorter waves when deployed at greater depths. For this reason, wave periods below 3 s are not represented in the instrument output at Kihnu (Paper II).
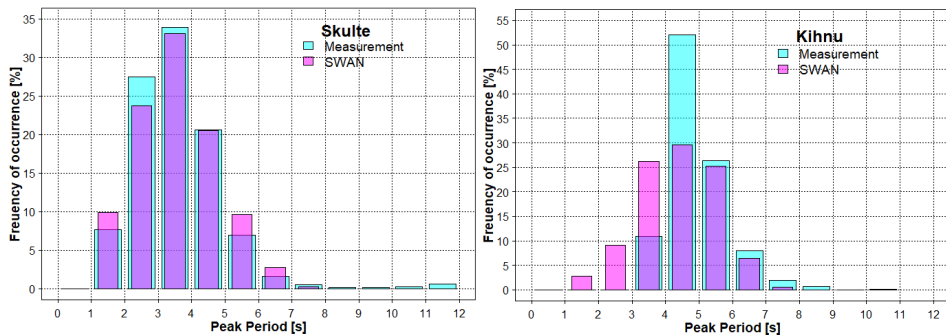

Figure 15. Empirical probability distributions of recorded (blue) and modelled (pink) peak periods at Kihnu and Skulte. The modelled data sets only represent the time interval covered by observations. From Paper II.

However, Figures 12–14, notwithstanding the mismatch, reveal that the wave climate in the Gulf of Riga is primarily dominated by short-period (2–5 s) wind-seas with moderate H_S. This feature once more confirms that the wave climate in this gulf is mostly shaped by local wind forcing. Long-period waves are rare across all stations but they still may occasionally occur in this basin, whether in sheltered areas like Skulte or in more exposed locations like Kihnu.

2.3.2 Qualitative Comparison with Visual Observations

As explained above, a comparison of visually observed wave properties and modelled data is not straightforward for several reasons. Interestingly, the match of some modelled and visually observed wave properties is not much worse than the match of instrumentally recorded and modelled quantities. This applies to wave periods (Figure 16) that often do not differ much between offshore and nearshore locations while the wave height is usually much smaller near the shore (e.g., Kudryavtseva et al., 2019).

The outcome of visual observations (Figure 16) reproduces the general shape and mode of the relevant distribution generated using modelled data (Paper II). It is expected that the match is better at Ruhnu where the observation location is more exposed to
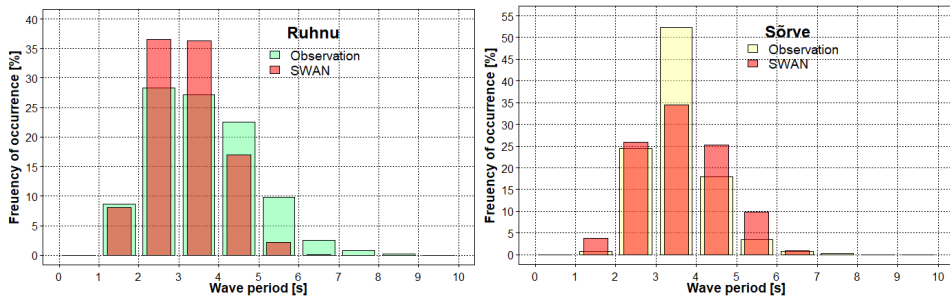
Figure 16. Empirical probability distribution of the frequency of occurrence of modelled and visually observed wave periods at Ruhnu and Sõrve (Figure 11). From Paper II.

predominant wind and wave directions, but the basic shape of this distribution is also captured by visual observations at Sõrve (Figure 11).

The match of empirical probability distribution of observed and modelled wave heights is less perfect (Figure 17), most importantly because visually observed wave heights contain a very high proportion (33–40%) of very low waves with heights <0.25 m.

This feature apparently reflects underestimation of storm heights in the visual observations. The difference in the frequency of very low modelled and observed wave heights is smaller at Ruhnu than at Sõrve, but even the overall shape of this distribution for modelled H_S is not equalled by the distribution of observed wave heights. The mismatch is larger at Sõrve, which is situated in a more sheltered location. A near absence of higher waves in the observed data signals that this location is fairly sheltered.

The presented material suggests that while visual wave observations may provide quite important information about some properties of the local wave climate, their use for different applications is limited. This conjecture is supported in Paper II by a comparison of long-term wave heights in terms of annual mean values.

While the modelled H_S show coherent courses, with clearly smaller values at the sheltered Sõrve location, similar estimates from observations show a fairly limited match (Figure 18). However, the difference between the long-term average visually observed and modelled wave heights at these two locations is the same.

To summarise, the presented 32-year SWAN hindcast accurately reproduces wave conditions in the open and moderately exposed areas of the Gulf of Riga, with some limitations in shallow, bathymetrically complex areas.
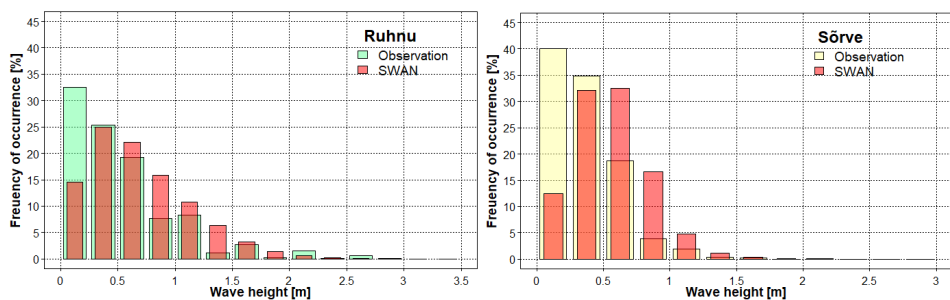

Figure 17. Empirical probability distribution of the frequency of occurrence of all modelled significant wave heights and visually observed wave heights at Ruhnu and Sõrve. Bars in the distributions of visually observed wave properties show the simple arithmetic mean of all observations in a single day (Eelsalu et al., 2014). From Paper II.
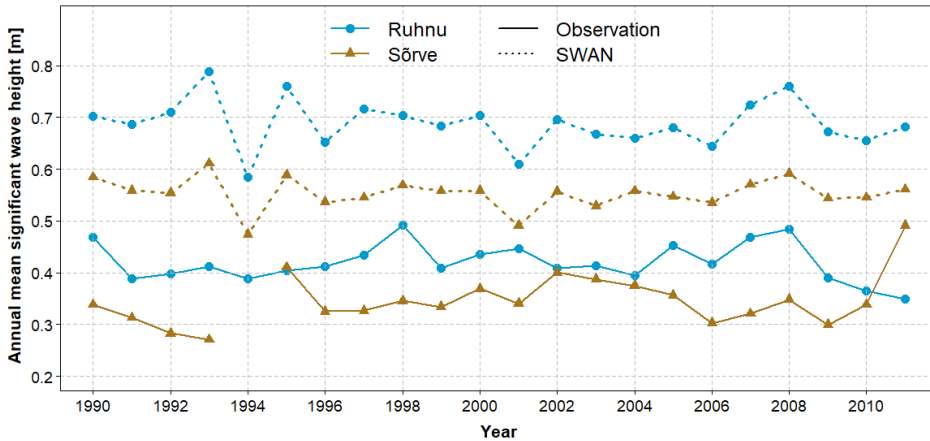
41

Figure 18. Annual average of visually observed wave height and modelled H_S at Ruhnu and Sõrve (Figure 11). From Paper II.

Its overall performance supports its application for long-term wave climate and coastal studies in this gulf. The strong agreement between data and observations supports the model results' suitability in both areas for reconstructing long-term wave statistics.

2.4 Properties of the Wave Climate in the Gulf of Riga

Maps of spatial patterns of the average H_S, its higher quantiles and the distribution of H_S maxima (Figure 19) all show a clear gradient in the Irbe Strait (Figure 11). The difference between typical values of average H_S in the eastern Baltic proper (~1.1 m) and in the interior of the Gulf of Riga (~0.7–0.8 m) is about 0.3–0.4 m, that is, up to half the typical values in the gulf. The typical difference is about 1 m for the 95th percentile, 1.5 m for the 99th percentile, and 2–2.5 m for the H_S maxima. Therefore, the wave climate in the Gulf of Riga is much milder than in the eastern Baltic proper and also milder than in the Gulf of Finland.

Figure 19 also signals that the highest waves generated in the Baltic proper usually do not enter the Gulf of Riga even though the Irbe Strait is about 25 km wide and that the contribution of wave fields in the gulf from the Suur Strait (Figure 11) is minor. Therefore, most of the internal variability in the wave fields in the gulf is created locally, by winds over this water body. Only wind-seas and swell waves may to some extent enter the northern part of the gulf via the Irbe Strait, In other words, the wave climate in the Gulf of Riga is largely decoupled from that in the rest of the Baltic Sea.

Spatial distributions of the average H_S, its higher quantiles and H_S maxima are all asymmetric in the south-west–north-east direction, with maximum values concentrated in the eastern and north-eastern part of the gulf (Figure 19). The higher the quantile, the closer to the eastern shore are located the maximum values. This feature apparently reflects the predominance of south-western winds among moderate and strong winds during the simulation period 1991–2021. The largest average H_S values slightly exceed 0.8 m.

The southern nearshore and the relatively sheltered Pärnu Bay (Figure 11, Figure 19) are much calmer with mean H_S below 0.4–0.5 m. The maxima of the 95th percentile more clearly mimic the directional pattern of storm winds in the gulf, with maxima in

the north-east exceeding 1.7 m and remaining below 1.25 m in the south-west of the gulf and in the interior of Pärnu Bay. The higher quantiles and the maxima of H_S have a similar spatial distribution. The maximum value of the 99th percentile is >2.25 m in a large sea area between Ruhnu and Kihnu (see the locations in Figure 11), while the maxima of H_S reach 4.5 m near Kihnu.

Together, the basic appearance of these spatial distributions illustrates how the fetch length and predominant directions of moderate and strong winds shape the wave properties in the gulf: the pattern of locations of maxima is consistent with the main features of the wind regime. The distribution of the 99th percentile of H_S, with relatively small values in the entire southern part of the gulf, suggests that the simulation period did not contain any exceptional north-north-west storms.
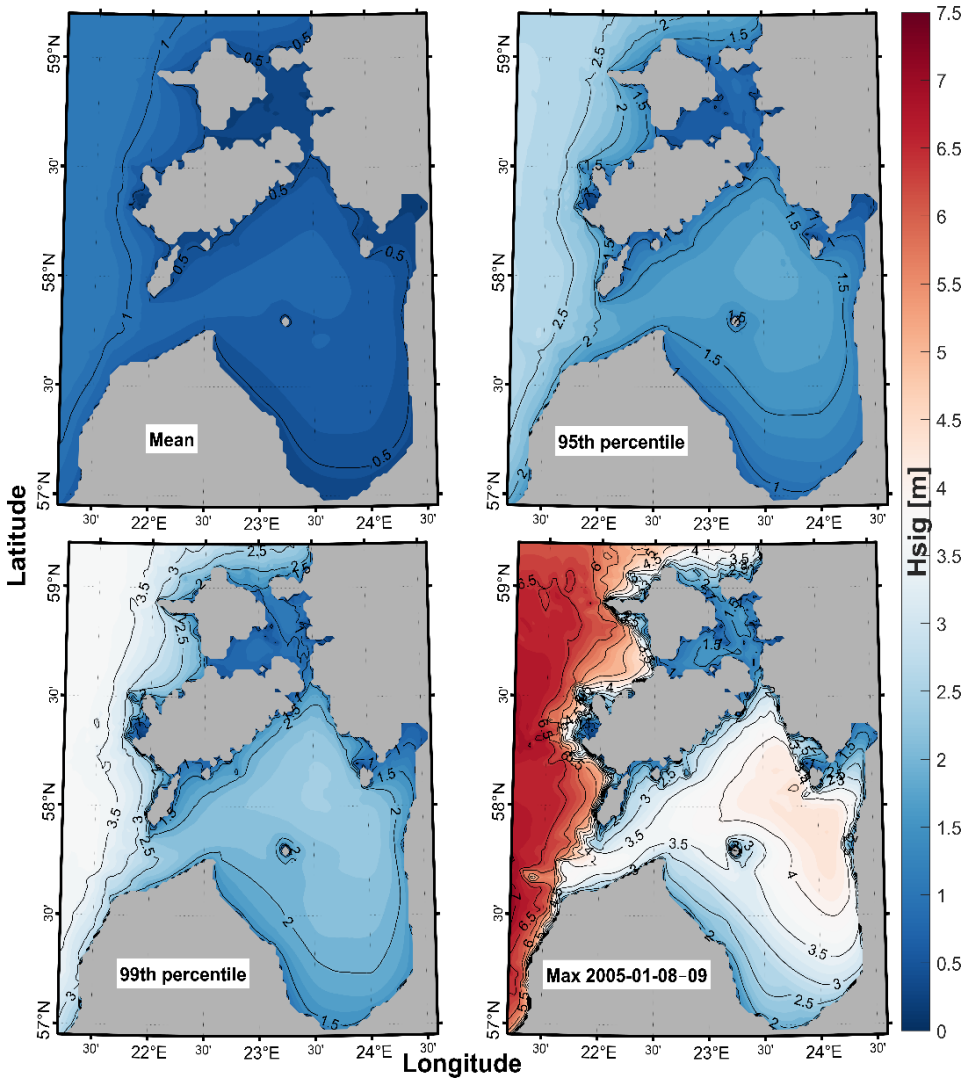
Figure 19. Spatial distribution of modelled wave properties in the Gulf of Riga 1990–2021, showcasing the mean (top left), 95th percentile (top right), 99th percentile (bottom left) and maximum during storm event on 8–9 January 2005 (bottom right) values of H_S. The figures reflect simulations at a resolution of 1 nmi. From Paper II.
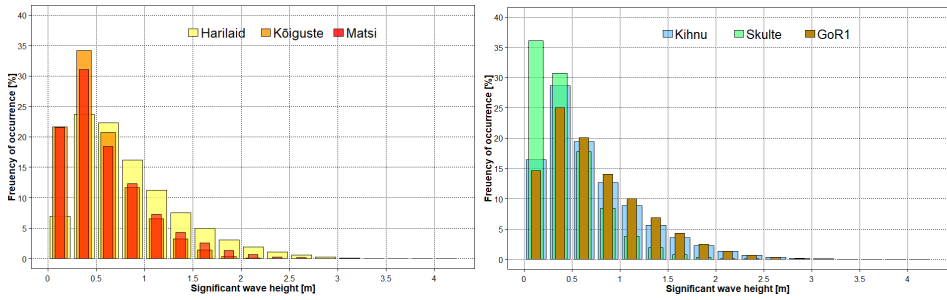
Figure 20. Empirical probability distribution of modelled H_S at six locations 1990–2021. From Paper II.

Empirical distributions of the frequency of occurrence of modelled H_S (Figure 20) in different locations are qualitatively similar to each other, with clear maximum for waves with H_S between 0.5 m and 1 m, and a rapidly decreasing frequency of occurrence for higher waves. Based on the above arguments, it is expected that higher waves occur much more frequently at Harilaid (Figure 11, Figure 20) in the nearshore of the western Baltic proper than in the interior of the Gulf of Finland. Only at Skulte is the distribution much narrower than at more exposed locations like Harilaid or Ruhnu (Figure 11, Figure 20), and very low waves ($H_S < 0.5$ m) predominate at this location similar to the situation in semi-sheltered bays (Soomere, 2005). These contrasts reflect the above-discussed spatial differences in wave fields, but also indicate how all the sites are influenced by the same wind climate.

The empirical probability distributions of modelled wave periods (Figure 21) are also qualitatively and quantitatively similar across the six selected sites in different regions of the gulf. The most frequent periods range between 2 and 5 s while periods >7 s are rare even though longer swell waves may occasionally enter the gulf from the Baltic proper. This feature clearly distinguishes the wave climate in the interior of the gulf from that at stations exposed to the Baltic proper like Harilaid where typical periods are 3–7 s and periods up to 10 s occur quite frequently.

The joint distribution of the Baltic Sea wave heights and periods generally has two branches. The wave heights and periods of the majority of wave conditions roughly match those characteristic of so-called fully developed wave systems with a Pierson-Moskowitz spectrum (Broman et al., 2006). Another branch of this distribution reflects longer and lower waves that are usually interpreted as remote swells. The distribution at Harilaid (Figure 22) closely follows the described shape, with the two branches clearly present.
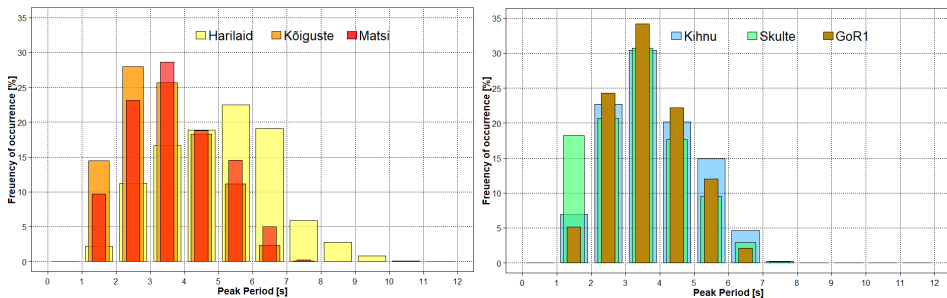

Figure 21. Empirical probability distribution of modelled wave periods at six locations (Figure 11) 1990–2021. From Paper II.

44

The branch that reflects swells is less clearly present at sheltered locations, such as Kõiguste (Figure 22) where relatively short but steep waves, represented by combinations of mean period and H_S (green dots) located above the curve that represent wave systems with a Pierson-Moskowitz spectrum, are much more frequent than at offshore locations. The presence of steeper waves than is typical in fully developed seas is also relatively frequent at the location GoR1 (Figure 11) where the proportion of long and low waves is smaller than at other locations (Figure 22). This feature suggests that this location usually hosts young wind-seas. The nearshore location Skulte also has a relatively large proportion of comparatively steep waves (apparently wind-seas) and long-period waves with H_S mostly below 0.5 m. As their periods are usually less than 4 s, it is likely that they reflect waves created within the Gulf of Riga (Paper II).

The diagrams in Figure 22 make it possible to roughly evaluate the wave heights and periods in the most severe wave conditions. These combinations are reflected by the dots that mark the upper right ends of the distributions in Figure 22. These situations roughly correspond with the properties of fully developed wave systems with a Pierson-Moskowitz spectrum at the particular locations. The relevant parameters are heights close to 4 m and period about 7 s at Harilaid, but wave height of ~2.5 m and period about 5.5 s at Kõiguste (Figure 11).

This analysis confirms that the Gulf of Riga is predominantly a short-period wind-sea environment, with limited swell influence. Most notably, the periods of swell-type waves are smaller than the typical periods in strong wave storms (Figure 22). Nonetheless, the presence of long-period waves in certain locations underscores the importance of monitoring impactful events for hazard assessment and coastal planning decision making, rare as such events may be.
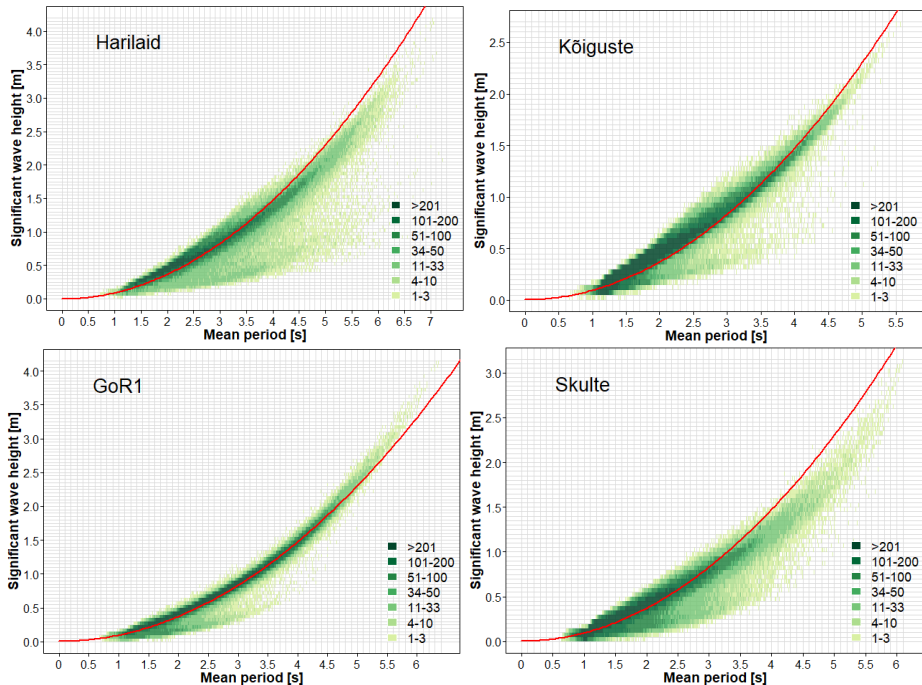

Figure 22. Joint distribution of modelled H_S and mean period T_{02}. The width of classes of H_S and T_{02} is 0.05 and 0.01 s, respectively. The red line shows the H_S of wave systems with a Pierson-Moskowitz spectrum for the given T_{02}. See locations of sites in Figure 11. From Paper II.

2.5 Interannual and Decadal Variability

The 32-year wave hindcast offers insights into the long-term variability of the Gulf of Riga wave climate. The presented material has demonstrated strong spatial contrasts in wave properties, most significantly in wave heights, across the basin. This contrast persists in a coherent manner over time with respect to wave heights across the selected sites (Figure 23). This coherence becomes clearly evident in terms of the annual mean modelled H_S over the years 1990–2021. The typical level of interannual variability in this quantity is within about ±10% of the multi-year average, with higher values in stormy years such as 2008, 2011 and 2020.

Paper II stresses two important features of interannual variability of annual average values of H_S. First, temporal patterns are consistent across stations, regardless of their exposure, while the amplitude of interannual changes is smaller for more sheltered locations, such as Skulte (Figure 11, Figure 23). This feature is interpreted in Paper II as indicating that atmospheric forcing is often spatially coherent across the entire gulf. Second, the annual average values of H_S do not show any significant (upward or downward trend) at any location. These findings support earlier conclusions that the Baltic Sea wind climate has remained stationary over the last decades (Rutgersson et al., 2014). The simulations described in Paper II are consistent with this conjecture and show that the wave climate in the Gulf of Riga has been stable over the past three decades even though it contains spatially consistent interannual fluctuations driven by regional weather patterns.

2.6 Concluding Remarks: Wave Simulations for Estimates of Transport

This chapter has presented a detailed assessment of wave climate characteristics in the Gulf of Riga using a 32-year hindcast of wave time series at medium (1 nmi) and high (280–560 m) resolution performed with the SWAN model forced by ERA5 wind data and published in Paper II. The model was meticulously calibrated against instrumental wave recordings in the Baltic proper, Gulf of Finland and Gulf of Bothnia (Figure 3) in Paper I (Chapter 1) to capture basin-wide dynamics and methodically validated for the Gulf of Riga in this chapter, in order to make clear how it performs in this smaller basin and specifically in its nearshore zone.
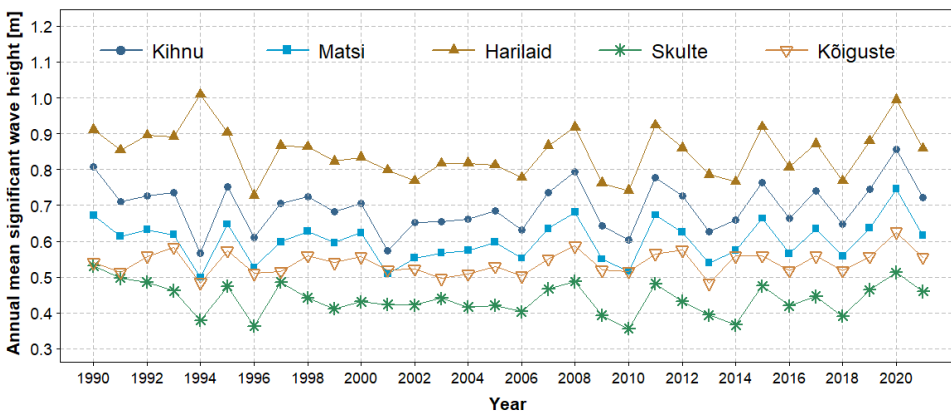

Figure 23. Time series of annual mean modelled H_S at Harilaid and at four sites in the Gulf of Riga. From Paper II.

The model does not account for extensive water level variability in this gulf (up to +2.75/–1.2 m) due to local storm surges, seiches and a specific mechanism of filling the gulf (Jaagus and Suursaar, 2013; Männikus et al., 2019), and ignores the seasonal presence of sea ice. The year-round open water assumption causes an overestimation of winter wave energy, particularly in the northern and eastern areas of the gulf (Najafzadeh and Soomere, 2024).

The outcome of the model has a good match with instrumentally recorded wave properties compared to other wave modelling efforts in the Baltic Sea (Björkqvist et al., 2018b). While the model performed well in the offshore and at exposed sites, the match was worse at some nearshore locations. Wave properties in these areas are sensitive to the accuracy of representation of the local bathymetry that cannot be fully resolved even at ~560 m grid resolution. As a result, local refraction, shoaling or wave breaking is not always well captured. As expected, historical visual observations, though useful for some qualitative comparisons, e.g., in terms of trends or spatial variations in the wave climate, underreport storm events, underestimate wave heights and lack the necessary temporal resolution for a more efficient analysis of the wave climate.

This study confirms an earlier conjecture concerning the spatial asymmetry of the Gulf of Riga wave climate, showing that the highest wave activity consistently occurs in the north-eastern and eastern parts of the gulf owing to the relatively longer fetch of the predominant south-western winds. In contrast, southern and eastern sectors of the gulf as well as the interior of Pärnu Bay (Figure 11) are relatively sheltered.

The typical wave periods in the gulf are shorter than in the Baltic proper, with peak periods usually 2–5 s. The model showed no significant trend in wave height across the 1990–2021 period, although interannual variability of ±10% was observed. This supports earlier statements of wind field stationarity in the region and suggests that the wave climate in the Gulf of Riga has not undergone (yet) any major climate change driven alteration.

Based on the presented comparisons and analysis in Paper I and Paper II, it is reasonable to conclude that the validated set of hindcast wave properties in the Gulf of Riga and its vicinity, including the Baltic proper shores of Latvia, Lithuania and the Sambian Peninsula, provides a valuable foundation for coastal studies, including sediment transport modelling in Paper III, Paper IV and Paper V, and vulnerability assessment and coastal infrastructure design (Barzehkar et al., 2024). It also contributes to further exploration of wave-driven morphodynamic processes of the Baltic Sea, and showcases the Gulf of Riga wave climate as spatially variable and relatively complex, despite being moderate. Together, these comparisons demonstrate how local exposure conditions, shaped by basin geometry and wind alignment, govern the wave conditions at each site. They also reflect the broader pattern in the eastern Baltic Sea, where wave energy is modulated by both atmospheric drivers and the local fetch geometry.

3 Alongshore Sediment Transport in the Eastern Baltic Sea

3.1 Introduction and Context

Wave-driven alongshore sediment transport is one of the fundamental processes that shape the coastal environment. Its contribution particularly impacts the redistribution of coastal sediment in microtidal systems like the Baltic Sea where substantial changes to the local water level are rare and often synchronised with high waves (Soomere et al., 2017; Kudryavtseva et al., 2020; Johansson et al., 2022). This influence covers a wide nearshore belt, from the depths where wave-driven near-bed velocity or turbulence impacts sediment (Aagaard et al., 2021) up to at the location of the maximum reach of waves, affecting erosion, sediment accumulation and the formation of morphological features such as beach cusps or spits (e.g., Žaromskis and Gulbinskas, 2010, Ryabchuk et al., 2011). On an open coast with clearly predominant wave directions, this transport is often unidirectional and modulated by large-scale features like headlands. In contrast, sediment dynamics in semi-enclosed basins is shaped by wave fields that are generated under shorter fetch and directionally highly variable wind fields acting upon irregular shoreline geometry, often resulting in the formation of complex and discontinuous transport patterns (Suursaar et al., 2014).

The Baltic Sea is a classic example of this type of wave-driven impact (Harff et al., 2017). Previous studies (Viška and Soomere, 2013b; Soomere and Viška, 2014) have provided valuable conceptual and regional insights into sediment dynamics on the eastern Baltic Sea shores. However, their spatial resolution of 3 nmi (~5.5 km) was insufficient to capture the influence of minor headlands, local changes in shoreline orientation, or the presence of coastal engineering structures all of which can act as barriers to sediment transport. They were therefore unable to resolve the fine structure of sediment transport and to identify single sedimentary cells and larger compartments. *In situ* observations and estimates (Ulsts, 1998) have to some extent updated the results of historic surveys (e.g., Knaps, 1966) but have rarely captured smaller-scale transport variability.

The Gulf of Riga (Figure 11), located in the eastern Baltic Sea, can serve as an example of these complexities. An indication of the unusual properties of sediment transport in this gulf came from the observation that changes to the wave-driven alongshore transport were different from changes on the open Baltic Sea shores (Viška and Soomere, 2013a). A possible reason could be the specific bi-directional wind regime described in Chapter 2 that produces the wave climate that is dominated by wind-seas. These winds often produce waves that approach some coastline sections at a very high angle, generating strong, intermittently reversing alongshore sediment flux. The core hypothesis in Paper III, Paper IV, Paper V and Chapter 3 is that despite the low mean wave energy in some parts of the region (Chapter 2), these conditions may result in strong, but spatially and temporally variable, sediment transport, particularly during storms events.

The main objective of this Chapter is to dissect and analyse the patterns of alongshore sediment transport along the eastern Baltic Sea shores. The outcome of the high resolution (~560 m) wave modelling framework presented in Chapter 1 and Chapter 2 is used to develop a detailed insight into wave-driven alongshore sediment transport along the shores of Latvia, Lithuania and the Kaliningrad District, from Cape Taran to Cape Kolka (Figure 24) in Paper III, then along the western, southern, and eastern shores of the Gulf of Riga from Cape Kolka to the Estonian township of

Häädemeeste (Figure 24) in Paper IV, and finally to understand changes in the directional distribution of wind and wave fields in Paper V.

The main tools are the calculation of bulk and net potential sediment transport rates, evaluated numerically using the Coastal Engineering Research Center (CERC) approach (USACE, 2002). These quantities characterise transport in idealised conditions of abundance of non-cohesive sediment with fixed constant grain size along the entire study area. These assumptions are usually not satisfied, and the actual transport is often several times (or even tens of times) smaller than the potential transport. However, qualitative features of the actual transport are usually well reproduced by the potential transport. The spatial scale that is used allows for the identification of most local transport discontinuities and the mapping of sediment convergence and divergence zones. The core result is a new framework for understanding the shorelines as a series of disconnected or partially connected sedimentary compartments and cells.
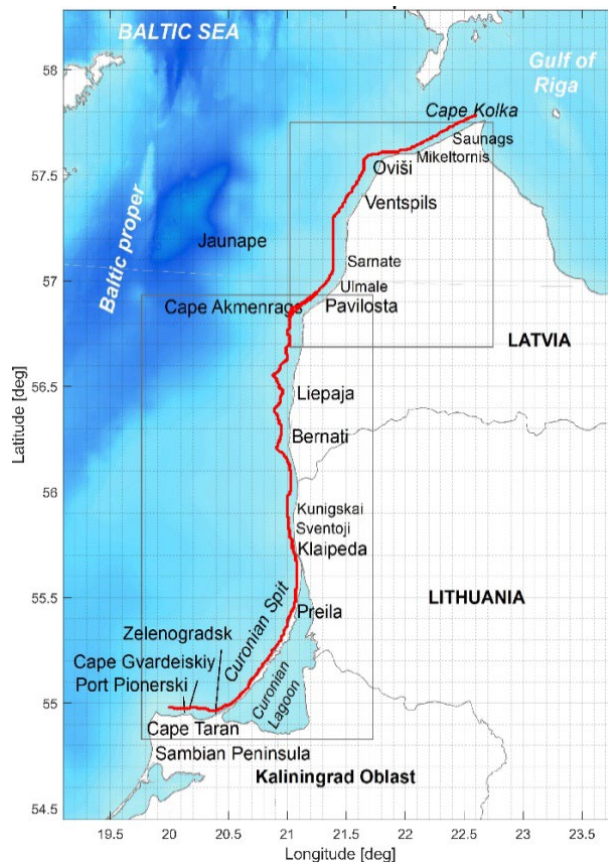
Figure 24. Study area addressed in Paper III encompasses several SWAN modelling domains at varying resolution (Figure 2). The area from Cape Taran to Cape Kolka is covered by two higher resolutions grids with spacing of ~560 m. The red line displays grid points extracted for the study presented in Paper III. Boundary information for these grids was extracted from simulations at 1 nmi or 3 nmi resolution described in Chapter 1. Graphics by Maris Eelsalu. From Paper III.

3.2 Methodology

The modelling framework for the analysis of wave-driven potential alongshore sediment transport in the Gulf of Riga used in Paper III and Paper IV builds upon high-resolution simulations of nearshore wave conditions discussed in Chapter 1 and Chapter 2, respectively. Wave simulations were performed using a nested version of the SWAN model forced by ERA5 wind data to simulate wave conditions across the Baltic Sea. Wave properties in the nearshore of the study area were evaluated with a spatial resolution of ~560 m. This enables adequate representation of coastal wave properties in the selected study areas, critical for estimating sediment transport. The outcome of these simulations is converted into hourly estimates of sediment transport using wave conditions at the breaker line and the CERC approach that assumes that transport is basically proportional to the rate of beaching of wave energy flux. While simplified, this method captures the primary dynamics of directional alongshore transport. Along with mapping bulk and net transport, emphasis is placed on estimates of alongshore variations in the transport rates and identification of divergence zones of net transport that decompose the coast into separated units. Different from Chapter 1 and Chapter 2, the analysis in Paper III and Paper IV and this Chapter is performed over the 33-year period from 1990 to 2022.

One of the main tools explained in Paper III and employed systematically in Paper IV is the analysis of alongshore variations in the net potential sediment flux (Figure 25). These variations mirror the changing volume of sediment transported along the shore. A reduction of flux in the transport direction for whatever reason (e.g., a decrease in the wave height), reflects a kind of block in this transport (Dette and Asce, 2001). This means that part of the sediment arriving at such a location must be deposited on the shore, creating an accumulation feature, or diverted offshore.

In a similar manner, convergence zones of this transport (zero-downcrossings of the black line in Figure 25), are the likely intense accumulation areas. In contrast, divergence zones (zero-upcrossings of the black line in Figure 25) are stretches of coast where net
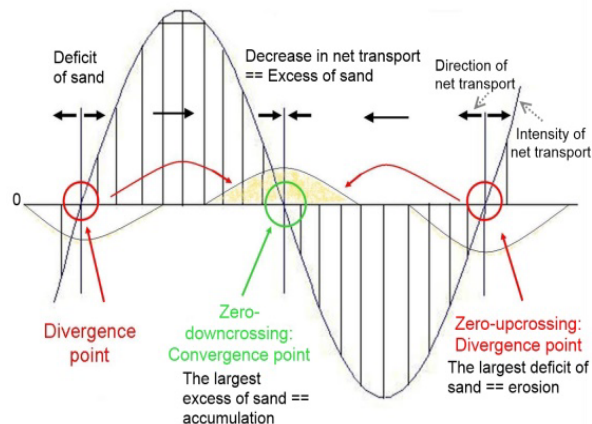

Figure 25. Interpretation of alongshore variations in the alongshore net transport in terms of increase and decrease in its intensity and divergence and convergence points of sediment flux and likely accumulation and erosion areas. The black curve shows the intensity of transport and arrows indicate its direction. Graphics by Maija Viška (Soomere and Viška, 2014). Reproduced from Paper III.

transport systematically carries sediment away. This process leads to chronic sediment deficit and usually to coastal erosion. Such divergence points are usually associated with capes or headlands (e.g., Cape Akmenrags (Figure 24) on the western shore of Latvia, Viška and Soomere, 2013) but may also exist on almost straight coastline segment that exhibits variations in the predominant wave approach direction (Eelsalu et al., 2023).

3.2.1 Study Area

The eastern coast of the Baltic Sea is a complex and climatically responsive sedimentary environment (Figure 24). Its sedimentary shores from Kaliningrad District (Oblast in Russian maps) to Pärnu Bay (Figure 26) are the longest interconnected system of sedimentary shores in the Baltic Sea. Coastal evolution in this region is dominated by wave-induced sediment transport, that depends on the local wave conditions, both height and direction, and the associated coastal orientation.

As the wave forcing and sediment transport properties are greatly different on the shores of the Baltic proper and in semi-sheltered sub-basins of this sea (Knaps, 1966; Ulsts, 1998; Viška and Soomere, 2013b; Soomere and Viška, 2014), these shores are addressed separately. The analysis in Paper III focuses on the Baltic proper shores from Cape Taran to Cape Kolka (Figure 24), while Paper IV addresses the interior of the Gulf of Riga. This gulf (Figure 26) is at the end of a >700 km long interconnected sedimentary system along the eastern Baltic Sea coast. This system stretches from the Sambian (Samland) Peninsula in the Kaliningrad District, Russian Federation, to Pärnu Bay in Estonia (Figure 26) (Knaps, 1966). Wind waves drive massive amounts of fine sediment, estimated at ~700,000–800,000 m³/yr (Knaps, 1966), along the north-western Baltic proper shore of the Courland (Kurzeme) Peninsula (Figure 26) towards the gulf. This flux discharges into the vicinity of Cape Kolka. Most of it is deposited on the shores of this peninsula or in a shallow area to the north of Cape Kolka while only ~50,000 m³ continues into the gulf itself (Knaps, 1966; Ulsts, 1998). In this context, the northern tip
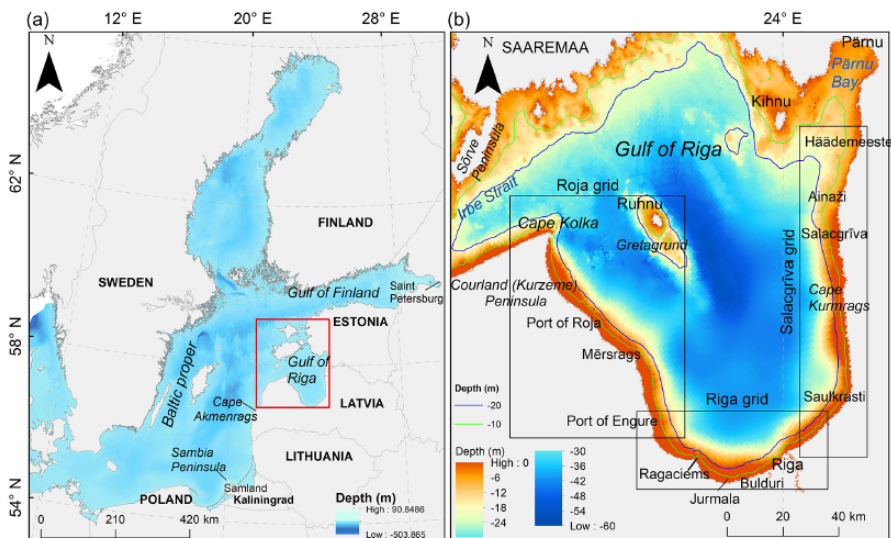

Figure 26. Left: Map of the wave modelling domain of the Baltic Sea and the 2ⁿᵈ level Gulf of Riga grid (red). Right: Bathymetry of the Gulf of Riga and the location of three 3ʳᵈ level grids in the gulf. Graphics by Maris Eelsalu. From Paper IV.

of Latvia is a one-way gateway of sediment into the Gulf of Riga. The existing estimates (Knaps, 1966; Ulsts, 1998) and simulations (Viška and Soomere, 2013b, Soomere and Viška, 2014) suggest that this sediment is locked in the Gulf of Riga between Cape Kolka and Pärnu Bay (Figure 26). Even though there is no exit for sediment, the gulf is much more than a simple accumulation zone. Both *in situ* estimates and numerical simulations signal that sediment transport in this gulf has complicated internal dynamics, with several fully or partially disconnected sediment cells or compartments (Knaps, 1966; Ulsts, 1998; Soomere and Viška, 2014).

The location and main features of geometry, bathymetry, and wind and wave climates of the Gulf of Riga (Figure 26) are presented in Chapter 2. Different parts of its shores have greatly different appearance, and geological and geometric features (Viška and Soomere, 2013b). The western (south of Cape Kolka), southern and most of the eastern shores (from Riga until Pärnu Bay) have an almost straight or gently curving coastline, and in most locations, isobaths to 10–20 m water depth, largely parallel to the shoreline. Even though the geological setting varies along the coastal stretch from Cape Kolka to Pärnu Bay, these shores have an almost continuous sandy strip and favourable conditions for wave-driven alongshore sediment transport.

In contrast, the shores of Saaremaa and the coastal section to the west and north of Pärnu Bay are usually either muddy (in the east) or rocky (shores of Saaremaa, Figure 26), with very limited amounts of mobile sediment. This part of the shoreline has complex geometry, the bathymetry exhibits many underwater features with sharp gradients, and the nearshore contains numerous islets and islands (Tsyrulnikov et al., 2008). For the listed reasons, the northern and north-eastern parts of the gulf are excluded from the analysis in Paper IV that focuses on the western, southern, and eastern coasts, which are predominantly sandy and morphodynamically active.

These shorelines have experienced varying erosion and accretion patterns over the past century. Increased erosion has been observed since the 1990s, particularly near Roja, Engure, Ragaciems, Saulkrasti, and Cape Kurmrags (Eberhards and Lapinskis, 2008; Tõnisson et al., 2013), while accumulation predominates near Jurmala (Figure 26).

Paper IV explores the wave-driven relocation of mobile sediment along the coasts of the Gulf of Riga in terms of net and bulk potential transport. For modelling purposes, the coastal stretch from Cape Kolka and Pärnu Bay is divided into three sectors. To make the presentation clearer, these sectors are named as follows. The western shore from Cape Kolka to Engure is represented by Roja grid, the southern shore from Engure to the Gauja River near Saulkrasti mouth by Riga grid, and the eastern shore from the Gauja River mouth to Häädemeeste by Salacgrīva grid (Figure 26).

3.2.2 Wind and Wave Climate Characteristics

While the general properties of the wind and wave climate in the study area have already been discussed in Chapter 1 and Chapter 2, a few regional aspects must be noted here. Wind forcing in the eastern Baltic Sea plays a central role in shaping the wave conditions that mobilise and redistribute sediment alongshore. The entire region, including the Gulf of Riga and West Estonian Archipelago, is primarily influenced by two systems of moderate and strong winds that blow predominantly from the south-west or north-north-west (Soomere and Keevallik, 2001; Soomere, 2003) (Chapter 1). The resulting wave system also has a two-peaked structure with the relative importance of north-north-west (or north) winds decreasing from the north to the south (Soomere et al., 2024). It is likely that this forcing governs not only wave-driven sediment transport

intensity but also its reversals, the location of divergence and convergence zones (Viška and Soomere, 2013b; Soomere and Viška, 2014), and thus the formation of sedimentary compartments and cells. However, the frequency and intensity of winds from different directions has extensive variability, with notable shifts during single seasons, especially during winter on the Estonian mainland (Jaagus and Kull, 2011).

The wave climate in the Baltic proper and even more in the interior of the Gulf of Riga is relatively mild but highly intermittent (Chapter 1, Chapter 2). Regionally, long-term wind and wave statistics confirm strong interannual variability in wave energy delivery (Björkqvist et al., 2018b). Approximately one-third of the annual wave energy flux is concentrated in just the 3–4 stormiest days of the year (Soomere and Eelsalu, 2014). The entire Gulf of Riga is characterised by the predominance of relatively short, locally generated, fetch-limited waves (Chapter 2) that may approach the coast at large incident angles.

While south-western winds are more frequent, the strongest wave events may be linked to north-north-west storms, which, though rare, likely generate the most energetic sea states in the Gulf of Riga (Davidan and Lopatukhin, 1982, cited in Eelsalu et al., 2014). These features give rise to a complicated pattern of variations in the most frequently occurring wave directions in this gulf (Figure 27). The variability of potential wind (and thus wave approach) directions is particularly large in the interior of the Gulf of Riga (Figure 27). The combination of these factors makes the wave approach during storm events a disproportionally important determinant of sediment transport and makes the eastern Baltic Sea a region that is highly sensitive to directional changes in wave forcing (Soomere et al., 2015).
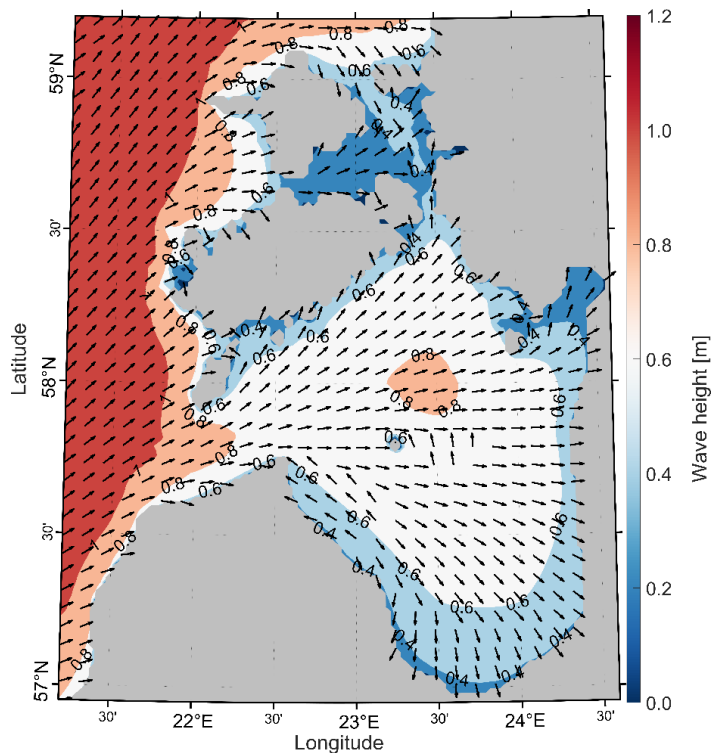

Figure 27. Mean H_S 1990–2022 (color scale) with the most often occurring wave direction, defined by count with 10° bins (arrows showing only the direction).

3.2.3 Selection of Suitable Grid Cells of the Wave Model

Estimates of alongshore sediment transport build on time series of wave properties simulated using the triple-nested implementation of the wave model SWAN forced by ERA5 wind data (Chapter 1, Chapter 2). The two nearshore grids in Paper III (Figure 24) and the three innermost grids used for sediment transport estimates in the Gulf of Riga (Roja, Riga, and Salacgrīva, Figure 26) have a resolution of ~560 m (0.32 nmi) that captures the main features of shoreline variability and nearshore bathymetry. The outcome of comparisons of modelled and recorded data, especially for the Gulf of Riga (Chapter 2) suggests that, despite uncertainties in modelling shallow wave transformation processes, the reconstructed time series of wave height, period, and direction are robust enough for adequate potential transport estimates.

The shoreline of the study area was divided into about 600–800 m long sectors depending on the mutual orientation of the shoreline and grid cells (Figure 28). The CERC formula relies on the wave height at the breaking line (USACE, 2002). To extract representative wave forcing for sediment transport estimates, wave properties were sampled from the most nearshore model grid points in which waves were not yet breaking even in strongest wave storms that affected the relevant coastal sector (Figure 28). A natural criterion for the associated minimum water depth is that the selected grid cells should be located beyond the local closure depth – that is, at depths where wave motion no longer affects a fixed-shape bottom profile (see, e.g., Soomere et al., 2017). The 95th percentile wave height was used to define a proxy of closure depth for each coastal segment. The final selection of points (see details in Paper IV) ensures that (i) wave properties in this cell can be used to provide adequate estimates of the input values for transport calculations including during severe storm conditions and that (ii) the selected cells are located at a more or less constant distance from the shoreline (Figure 29). The orientation of the isobaths in these cells was chosen to match the orientation of the shoreline in the associated sectors of the coast along the shoreline normal.
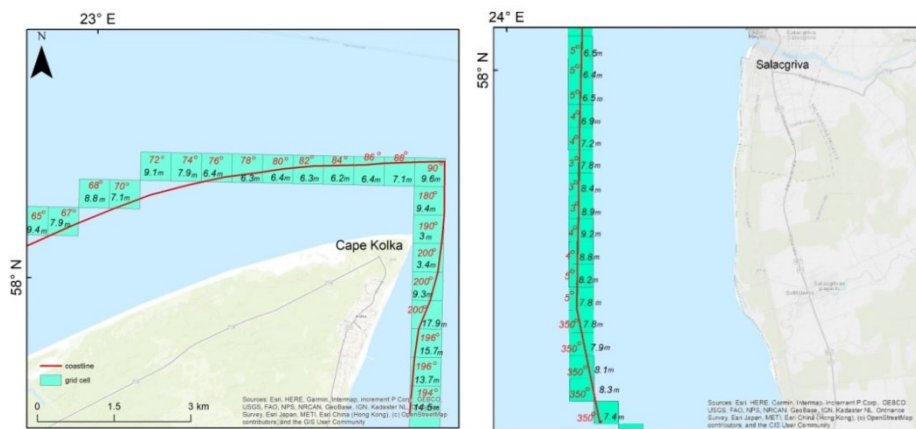

Figure 28. Examples of wave model grid cells used in the analysis, water depth in these cells and the associated orientation of the coastline (bold red line in the cells) near Cape Kolka (left) and Salacgrīva (right). The red line indicates the orientation of isobaths in single cells. From Paper IV.

Changes in coastal orientation that naturally occur, e.g., at headlands or capes (Figure 24), obviously impact the sediment transport. Also, engineering obstacles, such as groynes or harbour breakwaters affect sediment transport and may induce erosion or deposition, or partially or fully block the alongshore sediment flux. Large-scale infrastructure, such as the jetties of the Klaipėda Strait (Figure 24) (Paper III) and the River Daugava mouth near Riga (Figure 26) (Paper IV), were replicated by the wave model. However, most such structures in the study area were too small to be properly resolved by the wave model (Figure 29). These cases were treated similarly to natural headlands, by means of defining them as sharp changes in the orientation of isobaths in the relevant grid cells. These changes were chosen to roughly match the size and orientation of the harbour or jetty (Figure 29).

Even though the model has not necessarily resolved the details of sediment flux at such locations, it usually provides information about compartmentalisation effects in terms of clear convergence or divergence of sediment flux. Namely, the application of the CERC approach in the cells that followed sharp changes in shoreline and isobath orientation triggered by the presence of jetties or breakwaters, usually led to systematic changes in the transport direction compared to the neighbouring cells. Such situations at natural capes or headlands signal that the cape serves as a strict barrier to alongshore sediment flux. This is also the case with harbours and breakwaters that protrude into water that is deeper than closure depth. Therefore, even though the particular values of transport in such locations were unrealistic, the presence of a pair of local systematic divergence and convergence areas in such cells correctly indicates a major obstacle to sediment transport. Some such locations are removed from the depictions of alongshore transport below. It was also concluded in Paper IV that structures extending deeper than the closure depth naturally serve as almost complete barriers to sediment flux, except during the most extreme conditions where some transport may occur.
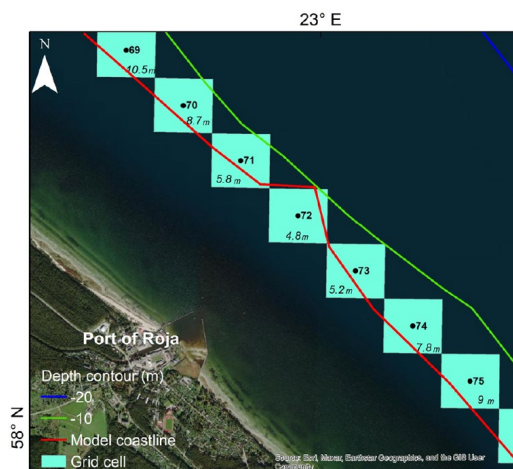

Figure 29. Example from the vicinity of the Port of Roja (Figure 26), showing how harbour breakwaters are mirrored in the model, creating sharp changes in the orientation of isobaths. Cyan boxes represent the selected cells from the model grid, while the red line indicates the reflection of the shoreline in the orientation of isobaths. The green contour shows the 10 m isobath, and the blue the 20 m isobath. From Paper IV.

3.2.4 Sediment transport modelling

Potential alongshore sediment transport is calculated in Paper III and Paper IV using the well-established CERC formula (USACE, 2002). The CERC approach relates the wave energy flux approaching the coast at the breaker line to potential sediment transport generated by these waves. It remains one of the most widely applied empirical formulations for engineering-scale transport estimation in wave-dominated coastal zones (Shaeri et al., 2020).

The general form of the CERC equation used in this study is:

$$I_t = KEc_{gb} \sin\theta_b \cos\theta_b, \tag{2}$$

where:

- $I_t = (\rho_s - \rho)(1 - p)Q_t$ is the potential immersed weight transport rate that is proportional to the central evaluated quantity – instantaneous potential alongshore sediment transport rate Q_t (m³/s)
- K is the so-called CERC coefficient; essentially a nondimensional empirical coefficient that is typically ~0.77 for medium sand in standard units
- ρ_s is the density of non-cohesive sediment (kg/m³)
- water density ρ = 1004 kg/m³
- p is the (nondimensional) porosity coefficient
- $E = \frac{1}{16}\rho g H_b^2$ is wave energy density at the breaker line in terms of significant wave height (J/m²)
- $g = 9.81$ is acceleration due to gravity (m/s²)
- H_b is significant wave height at breaking (at the breaker line, m)
- c_{gb} is group speed of waves at the breaker line (m/s)
- θ_b is the angle between the wave vector and shore normal at the breaker line relative to the shoreline (radians).

Equation (2) signals that wave-driven potential transport is particularly sensitive to the angle of wave approach: it increases linearly if the approach angle increases. Therefore, obliquely arriving waves with large approach angle θ_b may generate very strong alongshore transport compared to waves that approach at a small angle.

The analysis in Paper III and Paper IV uses constant values for porosity coefficient $p = 0.4$ and water density $\rho = 1004$ kg/m³. These values roughly correspond to the typical material of beach sand (quartz) and to the typical surface salinity of 4.90–5.38 g/kg in the Gulf of Riga (Skudra and Lips, 2017). Even though salinity is higher in most of the study area, its particular value enters as a linear coefficient into Eq. (2) and small variations of its values do not impact the results. For the empirical coefficient K the following direction dependent formulation was used (USACE, 2002) to mirror regional characteristics of the Gulf of Riga where large approach angles are usual:

$$K = 0.05 + 2.6\sin^2 2\theta_b + 0.007u_{mb}/w_f, \tag{3}$$

where:

- $u_{mb} = (H_b/2)\sqrt{g/d_b}$ is the maximum orbital velocity in linear waves (m/s)
- $w_f = 1.6\sqrt{gd_{50}(\rho_s - \rho)/\rho}$ is the fall velocity (m/s)
- $d_{50} = 0.17$ is the typical grain size (mm)
- $\rho_s = 2650$ is the density of sand (kg/m³)

Wave models provide time series of wave properties at some distance from the shore (Figure 28, Figure 29), ideally in locations close to the breaker line. Modelled wave heights and propagation directions were linked to breaker-line conditions using the method developed by Soomere et al. (2013). This method makes it possible to systematically evaluate shoaling and refraction of waves as they propagate from a model grid cell to the breaker line, without knowing beforehand the location or depth of the breaker line. This method assumes that the seabed is locally flat, isobaths are parallel to the shoreline, the wave field is monochromatic and unidirectional, and that breaking waves are long waves. Application of this method is essential for properly (at least to a first approximation) estimating the breaking wave properties at relatively large approach angles, generalising the results of Larson et al. (2010) for larger angles.

The method relates the modelled wave height H_0, with its phase and group speed and propagation angle c_{f0}, c_{g0}, θ_0, respectively, with the wave height H_b at the breaker line via an algebraic equation of 6th degree:

$$H_b^5 g \left(1 - \frac{H_b g}{\gamma_b} \frac{\sin^2 \theta_0}{c_{f0}^2}\right) = H_0^4 \gamma_b c_{g0}^2 (1 - \sin^2 \theta_0). \tag{4}$$

Equation (4) has two real solutions and the smaller solution gives the breaking wave height. The angle θ_b is evaluated using Snell's law $\sin \theta / c_f = \text{const}$. This pair of equations is closed by assuming that the breaking index $\gamma_b = H_b/d_b = 0.8$ is constant (where d_b is the water depth at the breaker line) and that breaking waves are long waves. The latter assumption means that phase speed c_{fb} and group speed c_{gb} are equal: $c_{gb} = c_{fb} = \sqrt{gd_b}$ at the breaker line. Paper IV stresses that these approximations are not perfect as the breaking index may substantially vary and breaking waves are often not ideal long waves.

The potential transport was evaluated in terms of its hourly values. This transport can be either negative or positive. The positive direction means transport to the right (counter-clockwise) for the observer looking at the sea.

Two key transport metrics were derived for each shoreline segment:

- **Net transport**: the sum of hourly transport values with sign over some time period, indicating the net direction of movement of sediment during this time period.
- **Bulk transport**: the sum of the absolute values of hourly transport magnitudes over some time period, representing the total volume of sediment moved by waves in any direction during this period.

Hourly estimates were computed across the full 33-year wave hindcast, and these values were aggregated monthly, seasonally and annually to analyse both the intensity and directionality of transport. Most of the analysis was performed to obtain monthly values of net and bulk transport in each selected coastal sector. To further interpret transport stability and directionality, the net-to-bulk transport ratio was evaluated for each segment in Paper IV. This dimensionless indicator ranges from −1 to 1, where values near ±1 reflect strongly unidirectional transport, and values near 0 indicate frequent reversals and unstable alongshore flux. It serves as a descriptive measure of how coherent or fragmented the sediment transport is across different seasons and locations.

3.3 Transport Patterns on the Eastern Baltic Proper Shore

3.3.1 Almost equilibrium segments from Curonian Spit to Cape Akmenrags

Alongshore sediment transport along the eastern Baltic Sea coast from Cape Taran (Paper III) is broadly counter-clockwise (Knaps, 1966; Ulsts, 1998; Viška and Soomere, 2013b) (Figure 30). It is likely that Cape Taran serves as an almost impassable location for wave-driven sediment motion with transport almost entirely to the east along the northern shore of the Sambian Peninsula (Ryabchuk et al., 2020) (Figure 30). In reality, sediment transport is strongly modulated by numerous coastal protection structures (Ryabchuk et al., 2020) and by changes in the orientation of the shoreline (Figure 30).

Sediment transport reduces along the Curonian Spit. The net transport is systematically almost zero along this spit and also between Klaipėda and Palanga (Figure 30) (Paper III). This outcome is consistent with the general perception that the Curonian Spit is in an equilibrium state with respect to wave-driven transport in the current climate (Viška and Soomere, 2012). As expected, breakwaters of the Port of Klaipėda (Figure 24) fully stop wave-driven sediment transport (Figure 30).
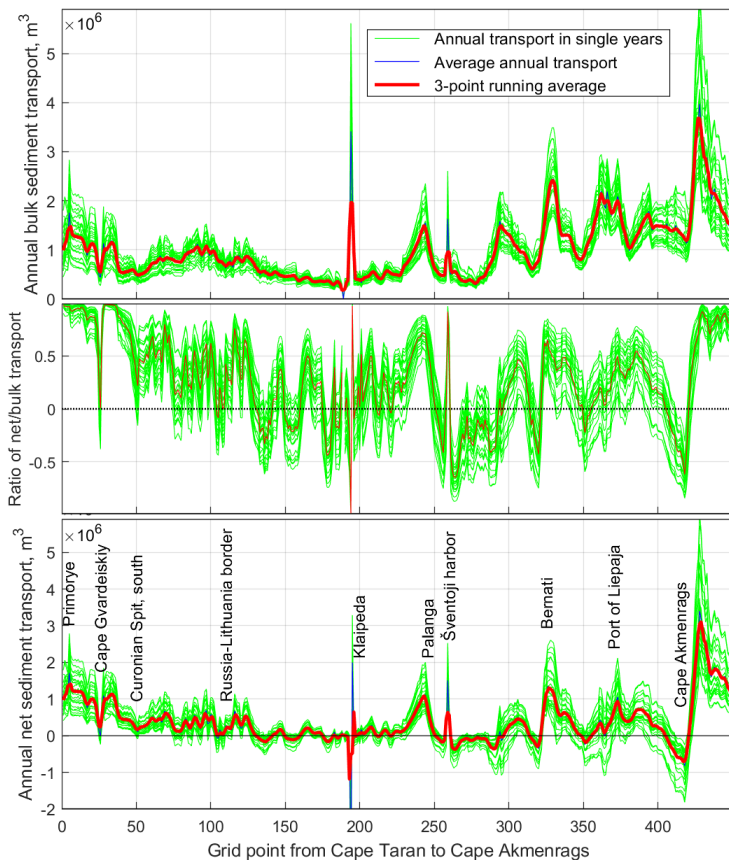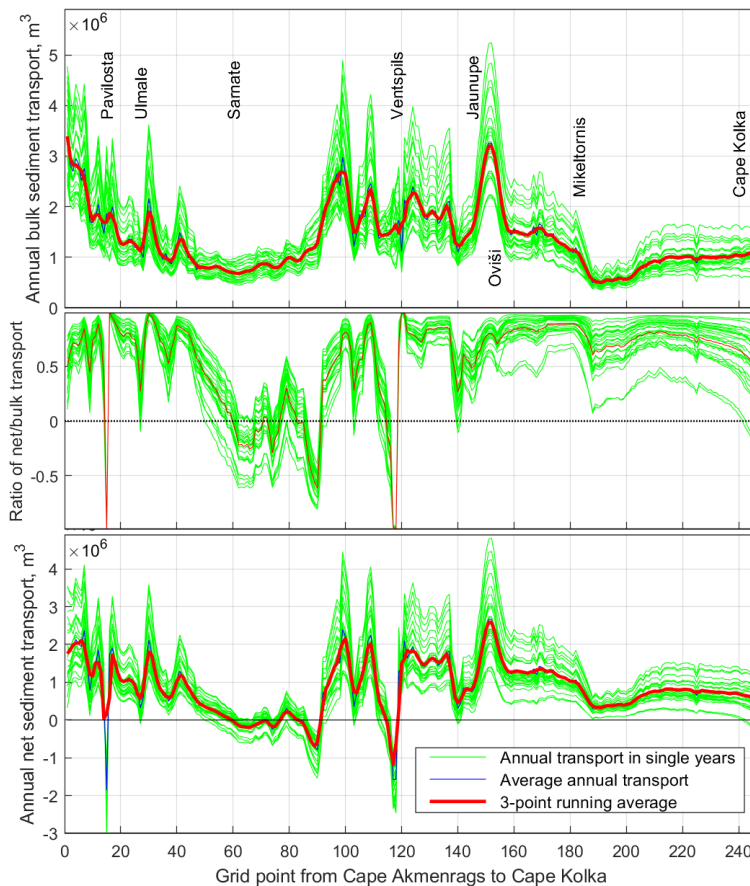

Figure 30. Annual wave-driven potential bulk transport (upper panel), ratio of annual net and bulk transport (middle panel), and annual net transport (lower panel) along the coastal stretch from Cape Taran in Kaliningrad District, Russia, to Cape Akmenrags in Latvia. The positive transport direction is counter-clockwise to the east, north-east, and north. See locations in Figure 24. From Paper III.

By contrast, the rest of the Lithuanian coast, from the vicinity of Palanga and along the southern part of the Latvian nearshore to Cape Akmenrags, exhibits more intense and directionally variable transport patterns (Figure 30). While bulk transport increases by about a factor of two from Palanga (Figure 30) to Cape Akmenrags, frequent reversals caused by natural features and the breakwaters of the Port of Šventoji (Figure 30) split this coastal segment into several only weakly connected sedimentary cells. It is likely that alongshore changes in net transport direction are observed due to bi-directional forcing and complex shoreline geometry.

3.3.2 Intense Transport from Cape Akmenrags to Cape Kolka

Potential bulk transport is exceptionally intense, with bulk volumes frequently exceeding 1–2 million m³/yr, on the rest of the Baltic proper shore of Latvia to the north of Cape Akmenrags (Figure 30) to Cape Kolka (Figure 31). Net transport along much of the Latvian coast is to the north-east, that is, mostly counter-clockwise but with two clearly evident natural divergence points and reversals (that is, clockwise transport to the south-west) to the south of these points, The intensity of bulk transport

Figure 31. Annual wave-driven potential bulk transport (upper panel), ratio of annual net and bulk transport (middle panel), and annual net transport along the north-western shore of Latvia from Cape Akmenrags to Cape Kolka. See locations in Figure 24. From Paper III.

decreases in the northern part of the Courland Peninsula (Figure 26) evidently because this coastal segment is sheltered from waves from northern directions by the Sõrve Peninsula. However, the intensity of net transport remains very large, on average 600,000–800,000 m³/yr almost to Cape Kolka, where sediment accumulates before entering the Gulf of Riga. These estimates closely match the outcomes of historical observations (Knaps, 1966; Ulsts, 1998).

An important finding in Paper III is the presence of several reversals of the mostly unidirectional counter-clockwise transport systems, notably in the vicinity of the Port of Šventoji, to the south of Bernati and to the south of Cape Akmenrags (Figure 24). These reversals apparently reflect a delicate balance of waves from the two predominant directions (Paper V). As the reversals are relatively short, it is likely that even small shifts in wind direction can disrupt this balance, leading to the formation of other divergence points and/or reversals, and possibly to localised sediment deficit.

3.3.3 Sediment Compartments

The presented results highlight several natural and engineered barriers to wave-driven sediment transport on the eastern Baltic proper shore. Natural barriers are due to persistent divergence zones of wave-driven transport (net transport zero-upcrossings in Figure 30 and Figure 31) associated with natural headlands. They are complemented by engineered barriers like jetties or breakwaters. Together they separate the study area into several fully or partially isolated sediment cells and compartments – coastal segments where sediment circulates internally but exchanges with neighbouring areas are small.

The engineered key boundaries are the breakwaters of the Port of Klaipėda, the Port of Šventoji, jetties at Pavilosta and the Port of Ventspils (Figure 24). Even though the Port of Liepaja is not highlighted as a barrier for net sediment transport, strong erosion of the coast to the north of this port (Eelsalu et al., 2025) confirms its impact. The natural barriers are persistent divergence points: a headland to the south of Bernāti (Figure 24), Cape Akmenrags and a zero-upcrossing of net transport in grid point 90 in Figure 31. Persistent local reversals (areas of clockwise transport) are highlighted to the south of all three major net sediment transport divergence points. Among those, only the divergence point at Cape Akmenrags was identified in earlier simulations (Viška and Soomere, 2013b, Soomere and Viška, 2014).

The Curonian Spit stands out as a near-equilibrium coastal segment. Low and locally variable net transport suggests a self-contained re-circulation system with minimal sediment exchange – consistent with its morphological persistence despite storm exposure (Viška and Soomere, 2012; Šakurova et al., 2023). The vicinity of Cape Kolka acts as a terminal sediment sink for sediment transport along the Baltic proper shore of the Courland Peninsula, where intense transport from the south accumulates due to shoreline curvature and only a small fraction of sand moves further into the Gulf of Riga.

3.4 Spatial Patterns of Alongshore Transport in the Gulf of Riga

The spatial structure of wave-driven alongshore sediment transport within the Gulf of Riga (Paper IV) is highly non-uniform and defined by a large number of factors, including shoreline orientation, wave directionality from anisotropic winds, sediment availability and presence of natural and artificial boundaries.

3.4.1 Western Shore: Almost Unidirectional Transport

The western shore from the vicinity of Cape Kolka to the Port of Engure is covered by the Roja grid (Figure 26). The coastline is mostly gently curving, with only one relatively prominent headland at Mersrags. Earlier simulations (Viška and Soomere, 2013b) and *in situ* estimates (Knaps, 1966) suggest largely straightforward nearly continuous counter-clockwise sediment transport predominantly directed to the south-east, from Cape Kolka towards Riga. Most of the sediment input to Cape Kolka (up to 800,000 m³/yr, Paper III) is deposited at Cape Kolka and only ~50,000 m³/yr enters the gulf (Knaps, 1966; Ulsts, 1998; Viška and Soomere, 2013b).

   Estimates derived in Paper IV confirm this pattern. The simulated massive net and bulk transport along the north-western shore of Cape Kolka (Figure 32) drops significantly after passing the cape. The net transport is predominantly counter-clockwise, with localised variations due to headlands and bathymetric anomalies described in Paper IV.
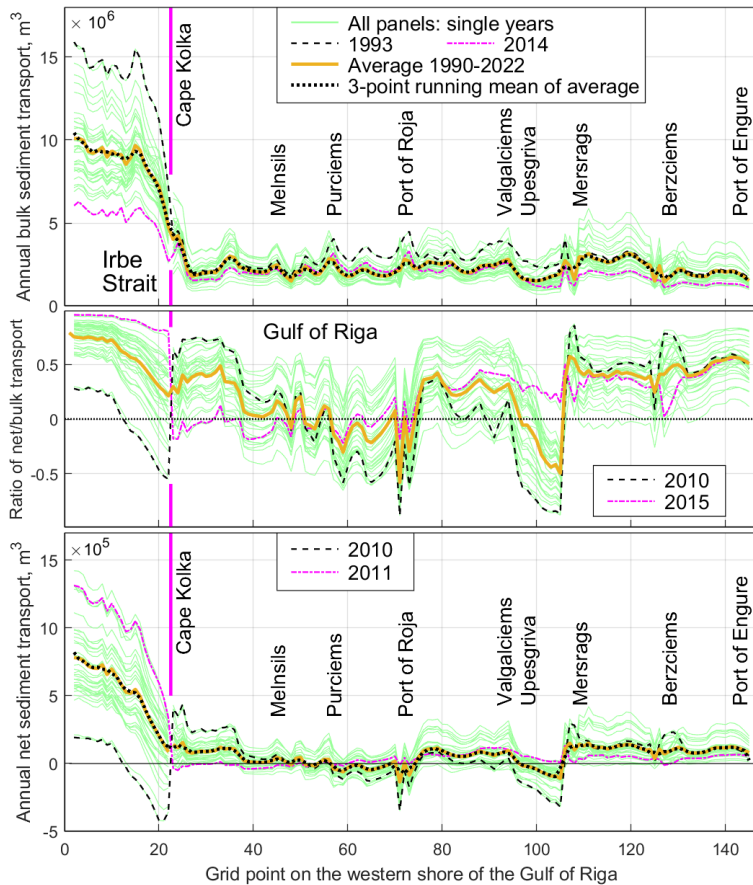
Figure 32. Simulated annual wave-driven potential bulk sediment transport (upper panel), ratio of net to bulk transport (middle panel) and net potential sediment transport (lower panel) along the western shore of the Gulf of Riga. Individual years are shown in green, with selected examples highlighted according to the legend. The orange line (average transport 1990–2022) is almost wholly masked by the black dotted line (3-grid point running mean of the average transport 1990–2022) in the upper and lower panels. The data for grid points that follow the orientation of breakwaters of the Port of Engure are omitted. See locations in Figure 26. From Paper IV.

The area is also characterised with three transport reversals of various frequency of occurrence, unresolved in the earlier coarser resolution studies (Viška and Soomere, 2013b). They occur between Purciems and Roja in several years, systematically between Upesgrīva and Mērsrags, and occasionally along the eastern face of Cape Kolka (Figure 32). The presence of the two occasional reversals apparently reflects the sensitivity of wave-driven transport to subtle variations in shoreline orientation and typical wave approach angle in single years (Paper IV).

The headland near Mērsrags, however, acts as a key sediment divergence point, sharply altering the direction and intensity of transport. It forms a natural almost impassable barrier between the sediment compartments to the west and south of this headland at an annual scale (Figure 32). The breakwaters at the Port of Roja and the Port of Engure have a similar effect on simulated sediment transport. Model grid cells adjacent to these features display spikes that indicate discontinuities in transport.

As explained in Section 3.2.3, the numerical estimates of transport at such locations are incorrect; however, systematic changes in the sign (direction) of the transport adequately indicate major changes in the sediment flux. Most of these values were removed from the analysis of total transport and its annual variations in Paper IV and in the rest of this Chapter. As breakwaters of both ports extend beyond the estimated closure depth of ~4 m, they act as almost impassable barriers, blocking alongshore transport.

3.4.2 Southern Shore: Variable Transport and Accumulation

The southern shore (Riga grid, Figure 26, Figure 33), spans from the Port of Engure to the Gauja River mouth near Saulkrasti. It is characterised by a gently curving coastline with several headlands and massive engineering structures at the Daugava River mouth near Riga (Figure 26).

In contrast to the western shore, sediment transport here is less intense, but more directionally consistent, with average bulk transport between 50,000 and 300,000 m³/yr. The net transport is mostly counter-clockwise, with no almost impermeable divergence locations. Thus, different parts of this shore are connected with each other by unidirectional transport. The transport direction varies considerably in single years in the area to the north of Ragaciems. A headland at Ragaciems functions as a semi-permeable boundary where transport is counter-clockwise in 13 out of 33 analysed years (Figure 33).

Sediment transport is high to the south of Engure, to the south-east of Ragaciems and in the vicinity of the Daugava River and Gauja River mouths (Figure 26, Figure 33). The relatively low transport on the rest of the shore is apparently associated with a short fetch for south-western winds and with smaller approach angle for waves arriving from northern directions (Paper IV). Significant accumulation zones are located near Klapkalnciems, Jūrmala, and at the mouth of the Daugava River. Thus, the gently curving shoreline gives rise to a natural division of the southern shore into several interconnected segments while the Daugava River mouth divides this shore into two almost totally separated compartments.
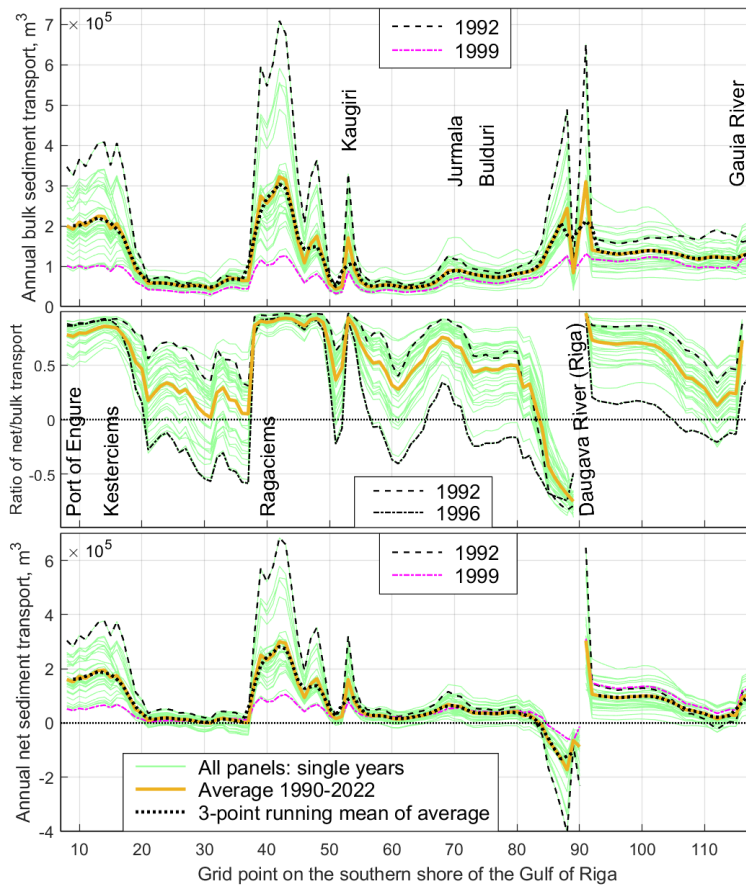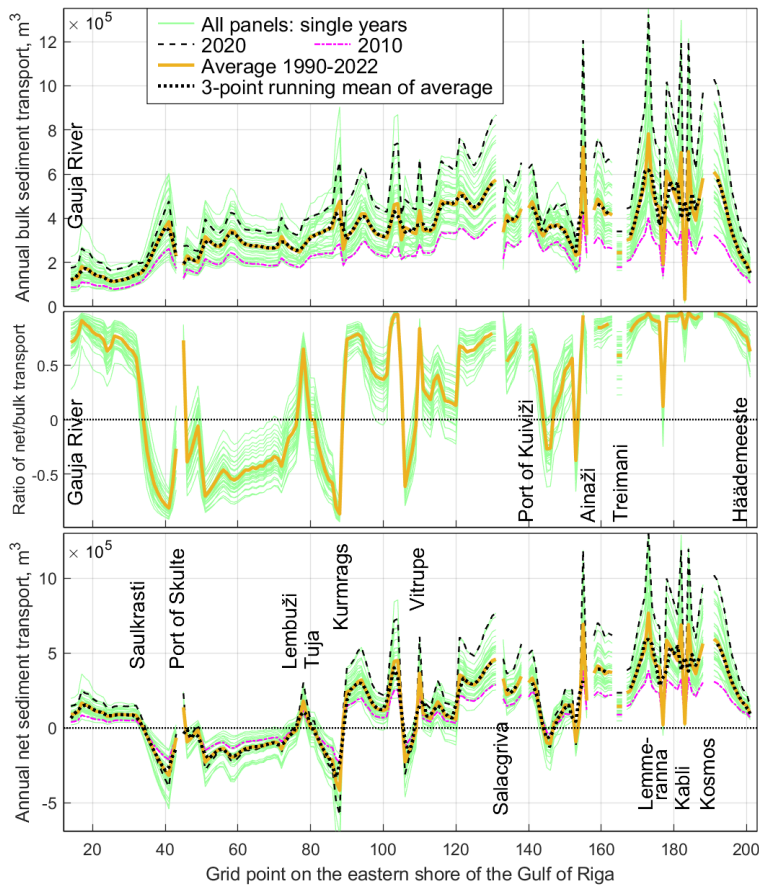
Figure 33. Simulated wave-driven potential bulk potential sediment transport (upper panel), ratio of net to bulk transport (middle panel) and net potential sediment transport (lower panel) along the southern shore of the Gulf of Riga. Note the different vertical scales of the upper and lower panels compared to Figure 32. The data for grid points that follow the orientation of breakwaters of the port of Engure and for the cells between jetties of the Daugava River mouth are omitted. See locations in Figure 26. From Paper IV.

3.4.3 Eastern Shore: Fragmented and Complex

The eastern shore of the gulf, from the Gauja River mouth to Häädemeeste (Figure 26, Figure 34) is covered by the Salacgrīva grid. Despite appearing almost straight on large-scale maps, this coastline is the most structurally fragmented sedimentary system in the study area, with numerous interruptions to the wave-driven alongshore flux.

The simulated potential bulk transport increases from ~150,000 m³/yr in the south to ~400,000 m³/yr in the north. The actual transport is much smaller because of low availability of mobile sediment. The net transport has several reversals, most noticeably between Saulkrasti and Cape Kurmrags (Figure 34), aligning with earlier observations of sediment flux divergence in this area (Knaps, 1966; Soomere and Viška, 2014). The transport pattern also indicates high interannual variability.

Figure 34. Simulated wave-driven potential bulk sediment transport (upper panel), ratio of net to bulk transport (middle panel) and potential net sediment transport (lower panel) along the eastern shore of the Gulf of Riga. Note the different scales in the upper and lower panels compared to Figure 32. The data for grid points that follow the orientation of breakwaters of ports of Skulte, Salacgrīva, Kuiviži, Treimani and Kosmos are omitted. See locations in Figure 26. From Paper IV.

Cape Kurmrags most likely functions as a natural barrier to wave-driven sediment transport. Minor headlands at Lembuzi and Vitrupe, as well as infrastructure of ports of Skulte, Salacgrīva, Kuiviži, Ainaži, and Treimani (Figure 26, Figure 34), further dissect the coast into several distinct sedimentary cells. This pattern suggests weak sediment connectivity, with cells and compartments remaining largely separated at annual timescales.

3.5 Compartmentalisation and Connectivity

The presented analysis demonstrates that the sedimentary system of the eastern Baltic Sea shores (Figure 35) is divided into a few large compartments and several smaller sedimentary cells. Overall, this compartmentalisation reflects both natural and anthropogenic controls, and is further shaped by directional wave forcing. The boundaries between such units are critical for coastal planning, as changes or interventions in one cell may have limited unintended effects beyond its limits.

Not all sediment compartments along the eastern Baltic Sea coast are equally isolated. Their degree of connectivity depends on the combination of wave directions and shoreline orientation as well as on the scale of engineered barriers. It is well known that the vicinity of Cape Kolka is as one-way gateway to the Gulf of Riga (Knaps, 1966; Ulsts, 1998) and thus divides the system into two parts with one-way impact: while sediment is transported from the Baltic proper shores into this gulf, there is no reverse transport at any longer time scale. It is also obvious that the massive breakwaters at the Daugava River mouth near Riga (Figure 26) and the Klaipėda Strait (Figure 24) almost entirely block wave-driven nearshore sediment transport. These barriers have been constructed in industrial time and there has evidently been some transport of coastal sediment across these rivers in the more remote past. An almost impermeable natural barrier has been identified at Cape Akmenrags (Figure 26) in earlier simulations. A substantial amount of sediment was transported along this cape in one year of 40 simulated in Viška and Soomere (2013b) and Soomere and Viška (2014). These four locations, that were basically known from previous research, separate the system into five compartments.

Simulations performed in Paper III and Paper IV have highlighted several additional obstacles to sediment transport on both the Baltic proper and Gulf of Riga shores. Most of them are likely partially permeable and the identified sedimentary cells are thus not
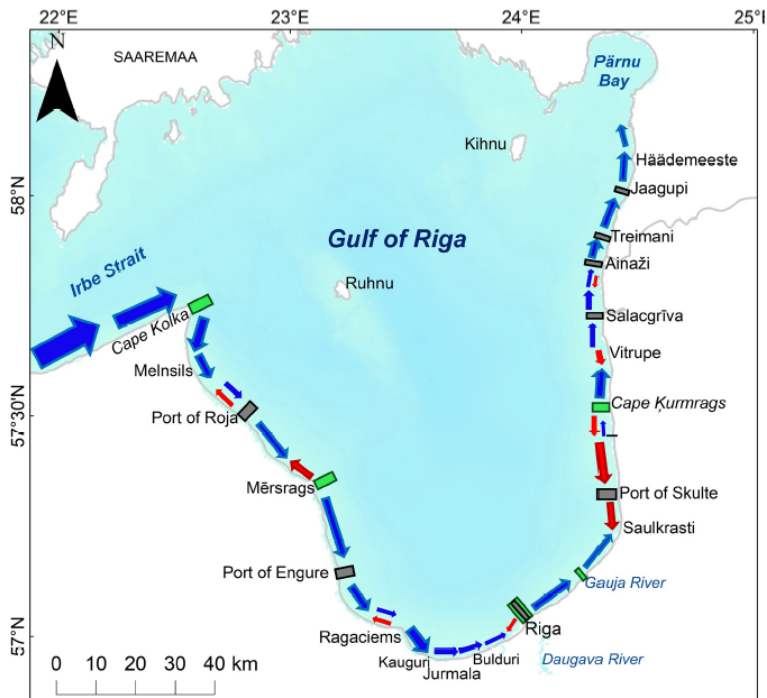
Figure 35. Transport directions (arrow widths correspond to the rate of potential net transport), major interconnected sedimentary compartments separated by major natural divergence points of net sediment transport (green rectangles), and large harbours and jetties (black rectangles) that split the sedimentary compartments into almost separated cells. Blue arrows indicate counter-clockwise transport and red arrows show clockwise transport. Parallel narrow blue and red arrows denote a variable transport regime in different years. Graphics by Maris Eelsalu. From Paper IV.

fully separated from each other. The list includes the breakwaters of the Port of Šventoji, Cape Bernati, the jetty at Pavilosta, a small headland to the south of Ventspils, and most probably the Port of Ventspils (even though simulations in Paper III do not resolve this feature) (Figure 24). It is thus likely that most of the sediment between these locations has been trapped during industrial times.

The analysis performed in Paper IV signals that the studied part of the Gulf of Riga coastline can also be divided into several sediment (transport) compartments that are almost fully separated either by persistent divergence zones, major river mouths, or large artificial structures (Figure 35). The western shore includes two broad compartments with largely unidirectional transport and few major interruptions. One of them is divided into two by the breakwaters of the Port of Roja. The southern shore is more connected but still split into two independent compartments by the River Daugava mouth. In contrast, the eastern coast is fragmented, composed of several smaller compartments separated by transport reversals and engineering structures. The degree of morphodynamical dependence varies: western and southern compartments tend to function as continuous transport corridors, while the eastern compartments behave as semi-isolated cells.

3.6 Temporal Dynamics of Sediment Transport

3.6.1 Temporal Variability in the Gulf of Riga

The presented results reflect the situation in a stationary wind and wave climate. However, wind and wave properties exhibit clear changes in the study area at different time scales (Kelpšaitė et al., 2011; Zaitseva-Pärnaste et al., 2011; Bierstedt et al., 2015; Soomere et al., 2015). These changes, either in wave height or direction, naturally translate into variability of wave-driven sediment transport (Soomere et al., 2015). Paper IV demonstrates that a complex interplay between the wind regime and shoreline orientation leads to several interesting features in the Gulf of Riga in terms of
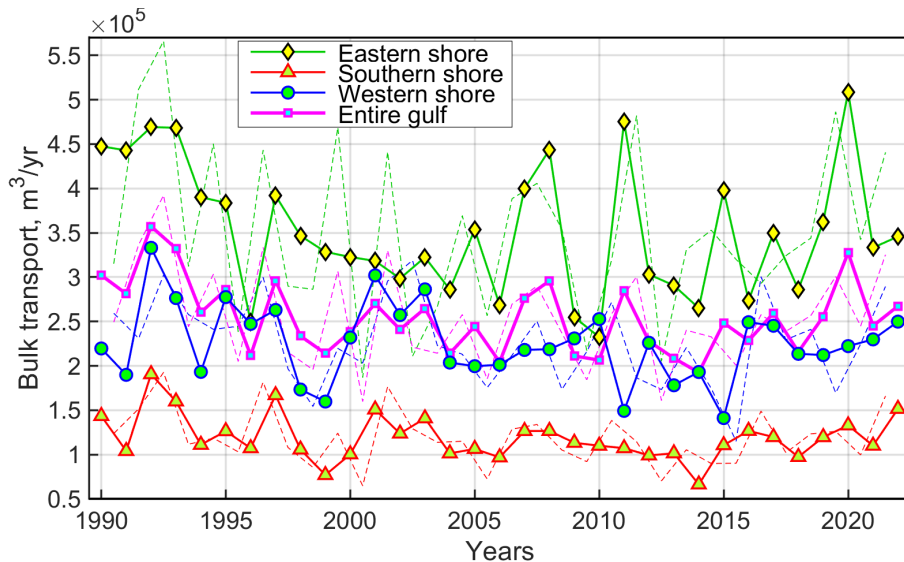

Figure 36. Average annual (solid lines with markers) and storm season (thin dashed lines) potential bulk sediment transport 1990–2022 for each coastal sector and the Gulf of Riga as a whole. From Paper IV.

interannual variations and decadal-scale trends in bulk and net potential transport rates 1990–2022 in the three addressed coastal segments.

Both bulk and net sediment transport along the entire studied part of the Gulf of Riga coastline showed pronounced year-to-year variability without any consistent long-term trend (Figure 36). This variability apparently reflects the episodic nature of changes to the wave forcing. A statistically significant decrease in bulk transport across the entire domain occurred during the period 1990–2005, with an average decline of −5,590 m³/yr ($p = 0.018$). Much of this decrease was driven by an even steeper statistically significant decrease on the eastern shore (−10,600 m³/yr, $p = 0.0008$). The decrease on the southern and western shores was smaller and not statistically significant. This decrease was followed by a non-significant upward trend in the entire domain 2005–2022.

The eastern shore exhibited the highest bulk transport ~352,000 m³/yr on average per grid cell. In several years, particularly in the early 1990s and mid-2010s, estimated bulk transport peaks exceeded 450,000 m³/yr. Interannual variations in so-called storm season transport (from July to June of the subsequent year, Figure 36) are particularly large on the eastern shore. The western shore showed smaller average values (~226,000 m³/yr) of bulk transport, with no statistically significant trend, with moderate interannual variation and no systematic directional evolution over the study period.

The southern shore had the lowest average bulk transport (~119,000 m³/yr) and the least interannual variation. No statistically significant trend was detected here either. The much lower values of transport suggest that the southern coast experiences relatively steady and lower-intensity wave-driven transport even though the intensity of wave forcing is not necessarily smaller compared to the western segment of the shore.

Net sediment transport, representing the directional balance of alongshore fluxes, showed more pronounced variability than bulk transport across all three coastal segments (Figure 37). This variability was especially strong during storm seasons, which often enhanced or even reversed the dominant annual transport.

On the eastern shore, net transport was consistently positive in terms of both annual and storm season estimates, except for 2001 when the annual transport had a very small negative value. Single annual and storm season values strongly varied, mostly coherently with each other. Net transport along the western shore exhibits basically the same features: mostly positive with a few exceptions and strong interannual variability. Different from the situation on the eastern shore, estimates of transport for storm seasons frequently fluctuated around zero, most likely reflecting the varying balance of south-western and north-north-western winds. Also, estimates for storm seasons often differed significantly from similar estimates of annual net transport, apparently underlining the sensitivity of this segment to wind direction in single autumns and winters. In contrast, the southern shore maintained low transport volumes and with smaller interannual variability but consistently eastward net transport, with average values close to the similar average values over the entire study area and with no significant trends.

Therefore, while the transport along the southern coast remains directionally stable and less intense, sedimentary systems on the eastern and western shores are far more reactive to interannual and possibly seasonal changes in wind properties.

A highly interesting feature of the temporal course of wave-driven net sediment transport in the Gulf of Riga is that intense counter-clockwise transport over storm seasons along the eastern shore is accompanied by low transport on the western shore

and vice versa (Figure 37). This pattern of interannual variations is much weaker but still evident in bulk transport (Figure 36). The possible explanation of these features is that while bulk transport correlates positively with storm activity across the entire region, the sign of net transport on the eastern and western coasts may be different under the action of the predominant moderate and strong wind events. South-western winds drive clockwise transport (to the north) along the western shore and counter-clockwise movement (also to the north) on the eastern shore. North-north-western winds excite waves that carry sediment to the south on both these coasts but the resulting transport is counter-clockwise on the western shore and clockwise on the eastern shore. This pattern does not extend to the southern shore, where waves excited by south-western winds are weak and waves from the northern directions approach at a small angle.

The described feature highlights how coastal orientation and anisotropy of the wind regime may shape both the magnitude and direction of regional sediment fluxes so that taking the average over longer coastal segments smooths out these regionally crucial variations. The interplay of orientation of the coasts and regional wind asymmetry is thus critical in explaining the observed spatial and temporal contrasts in the reaction of large coastal systems to variations in wind forcing (Viška and Soomere, 2013a).
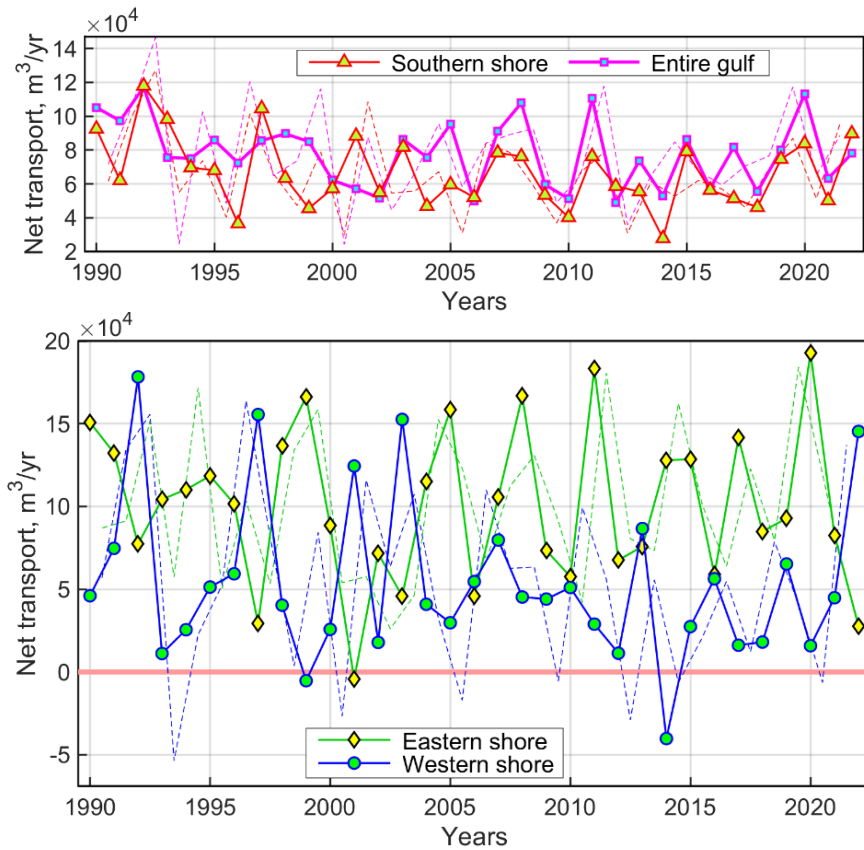
Figure 37. Average annual (solid lines) and storm season (thin dashed lines) potential net transport per wave model grid cell along the entire study area and southern coast (upper panel) and eastern and western shores (lower panel) of the Gulf of Riga in single years 1990–2022. Note the different scales in the upper and lower panel. From Paper IV.

3.6.2 Contribution and Balance of Directional Forcing

While the described variations in the net transport are created because of the different orientation of coastal segments under the specific anisotropic wind and wave climate, Paper V addresses changes in the directional structure of wave-driven forcing and attempts to locate where these changes may lead to substantial alterations to alongshore transport. The study area is the entire eastern Baltic Sea shore from Cape Taran to the entrance of the Gulf of Finland (Figure 38), including the study areas in Paper III and Paper IV.

The entire coastal stretch is divided into 261 sectors with a spatial resolution of 1 nmi in the Gulf of Riga and along the northern part of the study area and 3 nmi in the southern part. The grid cells representing these coastal sectors were chosen using the principles described in Section 3.2.3. Time series of wave properties in these cells were extracted from simulations using the SWAN model forced with ERA5 wind data over a 31-year period 1990–2021 and described in Chapter 1 and Chapter 2. The rates of net and bulk potential transport were evaluated using the CERC formula, with parameters and approximations as described in Section 3.2.4.
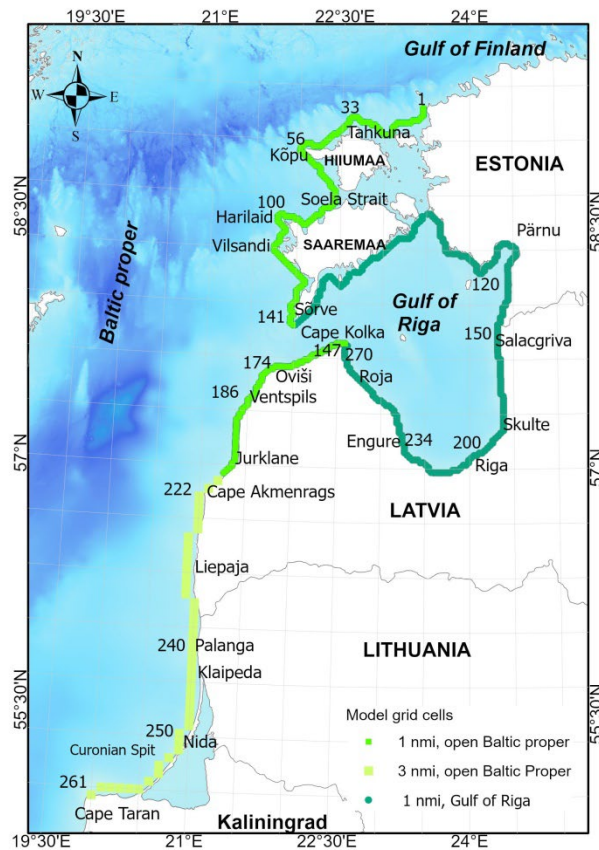
Figure 38. Coastal sections considered in Paper V. Green squares: nearshore grid cells in the Baltic proper from a wave model with a resolution of 1 nmi. Light green squares: nearshore model grid cells of the Baltic proper with a resolution of 3 nmi. Dark green squares: grid cells in the nearshore of the interior of the Gulf of Riga with 1 nmi resolution. The nearshore of southern Saaremaa is not considered in Paper V. Graphics by Maris Eelsalu. From Paper V.

The directions of waves that drive the majority of alongshore transport in each coastal section are described with a resolution of 30° in Paper V. The changes to the predominant direction of wave energy flux are thus also resolved with this resolution. As the predominant wind directions differ by >100°, this resolution is expected to be fine enough to identify coastal areas where a bi-directional sediment transport pattern is the predominant feature and to highlight alterations of its directional structure. The statistical significance of identified changes – particularly declines in transport driven by waves that approach from north-west – was estimated utilizing the Mann-Kendall test at a 95% level.

The core conjecture of Paper V is that the majority of annual alongshore sediment transport is driven by almost unidirectional waves approaching from one or two directions (that is, from a range of ±15° of one or two main directions). These waves usually contribute >60% and often 80–90% of the entire transport (Figure 39).

The contribution of such wave fields and whether there are one or two wave systems that drive the transport highly varies along the study area. Almost unidirectional forcing of alongshore transport is common along the northern coasts of the West Estonian Archipelago. Its western shores are subject to bi-directional forcing by wave fields that approach from the south-west and north-west. Depending on the coastline orientation, single sectors may have either counter-clockwise or clockwise
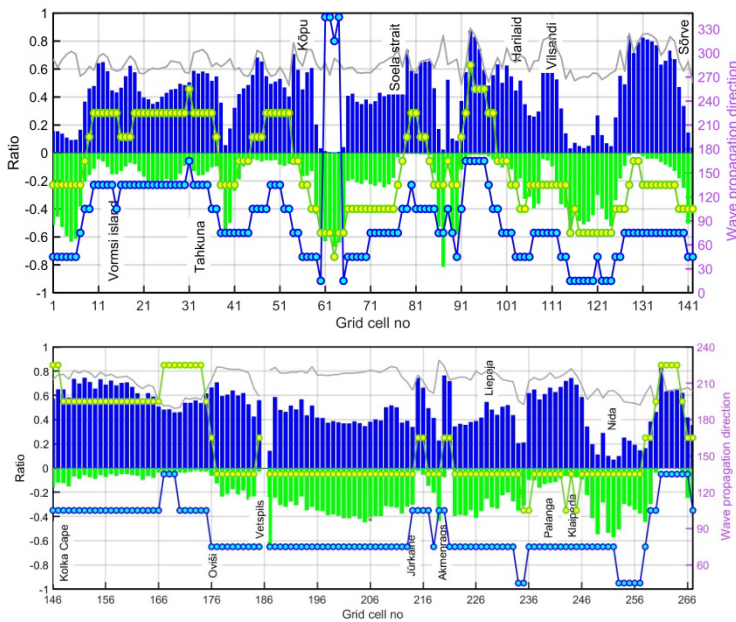
Figure 39. Ratio of net transport for storm seasons (from July to June of subsequent year 1990–2021) driven by waves from a narrow directional range to the bulk wave-driven transport near the West Estonian Archipelago (upper panel) and in the nearshore of Latvia and Lithuania (lower panel). Blue and green bars: counter-clockwise/clockwise transport, respectively, driven by waves within a 30° range. Cyan circles on blue line and yellow circles on green line: prevailing counter-clockwise/clockwise transport wave direction (±15°), respectively. Vertical scale: wave propagation direction (180±15° opposite to the approach direction). Horizontal scale: grid cell number in Figure 38. Gray line: sum of contributions of two prevailing wave directions to the average annual bulk transport. Spatial resolution of lower panel starting from Jurkalne is 3 nmi. For geographical locations see Figure 38. From Paper V.

transport. Some sectors (e.g., the Sõrve Peninsula on the western coast of Saaremaa, Figure 38) have strong unidirectional sediment transport. Even though Paper V did not explore the details of alongshore variations in net transport, the described features suggest that the western shores of the West Estonian Archipelago contain numerous local convergence and divergence areas.

Consistent with the above, sediment transport along both shores of the Courland Peninsula (Figure 26) is unidirectional and counter-clockwise (Figure 39), driven primarily by waves that approach from directions 270°–300°. On the contrary, on the coastal stretch from the entrance to the Irbe Strait to Palanga (Figure 24, Figure 38), ~80% of the sediment transport is almost evenly driven by two wave systems that arrive from the directions 255°±15° and 315°±15°. Therefore, the complicated spatial patterns of net transport described in Section 3.3 reflect the balance of the impact of these two wave systems.

The same wave systems are predominant from Palanga to the latitude of Nida (Figure 38, Figure 39) but their impact varies as the orientation of the shore turns. The north of this segment is dominated by western-southern-western winds while the shores of the Curonian Spit are more dominated by north-western winds. Waves approaching from the north-west generate counter-clockwise transport along the northern shore of the Sambian Peninsula (Figure 24).

Consistent with the above, primarily waves from the west drive counter-clockwise sediment transport along most of the eastern shore of the Gulf of Riga. In contrast, sediment transport along the western shore is predominantly driven by northerly waves that also induce counter-clockwise transport towards Riga. The southern shore is developing under joint impact of the two systems of waves.

3.6.3 Changing Forcing Directions

Another important outcome of Paper V is the identification of statistically significant changes (at a >95% level) in the directional forcing of alongshore sediment transport in terms of storm seasons 1990–2021 (Figure 40). These changes have a different nature in different coastal segments. On the coast of the West Estonian Archipelago they reflect alterations in wave properties arriving from the directions 315±15°° or 345±15°. Changes in transport driven by waves that arrive from the range of directions 315±15° are most pronounced in the Baltic proper nearshore of Latvia and Lithuania from Oviši to Palanga (Figure 40) where two wave systems create a largely balanced alongshore sediment system (Section 3.3). Changes in sediment transport in the interior of the Gulf of Riga are also mainly driven by alteration of properties of waves from the north-east and/or north-west (Figure 40).

Even though the described changes are somewhat different in different coastal segments, they all signify changes in properties of waves from the north-west, north-north-west or north (and also from the north-east in the Gulf of Riga) while the properties of waves arriving from the other western directions have not changed. As these alterations affect the balance of bi-directional sediment transport, it is likely that they may lead to significant changes in coastal processes. The reasons for this change were not addressed in Paper V.

No equivalent alteration in transport by waves arriving from other directions offsets this decline, leading to growing directional asymmetry. If this process continues, formerly balanced sectors – such as the Latvian coast south of Cape Kolka, the Klaipėda

region, and parts of the Kaliningrad District – will be dominated by more asymmetric transport, heightening erosion risks in previously stable zones.

The slopes of trends in transport rates vary greatly (Figure 40), being steeper on the Baltic proper shores than in the interior of the Gulf of Riga. They are generally larger for larger values of transport.

Importantly, the established changes and trends do not signal a rotation of predominant wind and wave directions (Figure 41). The analysis in Paper V confirms the wave directions that create most of the counterclockwise and clockwise alongshore transport have not changed 1990–2021 (Figure 41). However, the number of days with waves from the northern directions has decreased while the number of waves from the southwest has not increased at a comparable pace. This observation confirms that the described changes in transport result from changes in the speed or frequency of winds and waves from one of the predominant directions, specifically, wave energy brought to the study area by waves approaching from the north-west, north-north-west or north. In other words, this feature highlights directional frequency imbalance, rather than directional shift, as the main driver of changes to the transport.

Paper V also offers an explanation as to why the changes to these (northern) wind directions are easier to recognise. Namely, the usual frequency of occurrence of waves from these directions is approximately three times less than the frequency of occurrence of waves from the south-west and adjacent directions. This difference means that any missing or weaker wave events from northern directions have stronger relative importance.
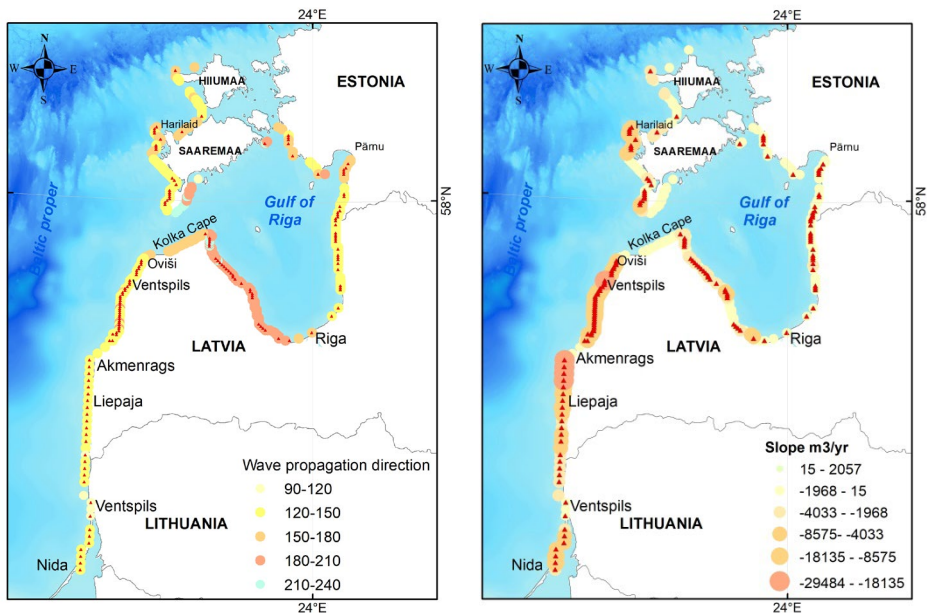
Figure 40. Left: Locations (red markers) in the study area where changes at a ≥95% level of statistical significance have occurred 1990–2021 in the alongshore sediment transport driven by waves from a particular direction range (colour scale). Right: The slope of trends in net transport driven by waves approaching at angles ±15° from directions indicated on the left panel. The trend slope is nonzero at a ≥95% significance level at 38 grid points and at a ≥90% level at 82 grid points out of 551 points. From Paper V.

3.7 Concluding Remarks

Even though the wave hindcasts in Chapter 1 and Chapter 2 have been shown to adequately reflect the reality, it is necessary to interpret the outcome of the presented studies with some care. No model is perfect and the conjectures about alongshore transport presented above are based on the use of a series of models. The output of an atmospheric model is used to force a wave model, simulated wave properties are traced until the breaker line and then feed to a sediment transport model. On top of that, the presence of sea ice is ignored and the sediment transport model omits cross-shore sediment exchange and riverine inputs, focusing strictly on potential alongshore fluxes driven by wave forcing, assuming unlimited availability of sediment with constant properties. This means that the estimated transport rates can be several times larger than actual sediment transport, in particular in coastal segments where the supply is limited.
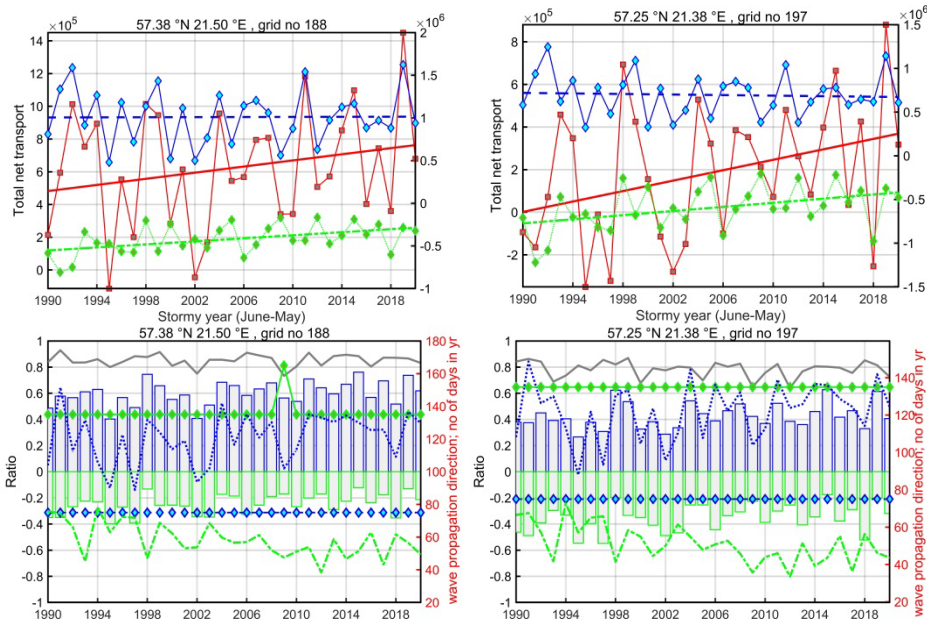
Figure 41. Changes in two selected coastal sectors in the eastern Baltic proper presented in Figure 38 over storm seasons 1990–2021. Upper panels: Blue: counter-clockwise (CCW) transport driven by waves from a 30° direction range, green: clockwise (CW) transport from a 30° wave range. Transport rates (m³/yr) correspond to the right vertical scale. Red line: average net transport 1990–2021, left vertical scale. Lower panels: Bars indicate the annual contribution driven by waves creating CCW (blue) and CW (green) transport. Gray line: total contribution by two wave systems; blue and green line: total number of days with waves creating CCW and CW transport, respectively. Green and blue markers: wave direction leading to CCW or CW transport direction, respectively, in each storm season. Scale left: ratio; scale right: wave propagation direction and number of days. From Paper V.

Nevertheless, many presented results and interpretations present an adequate picture of sediment transport for many purposes. First of all, many aspects of the functioning of coasts and other sedimentary systems are properly represented by means of the analysis of changes in the potential sediment flux. Thus, the direction and spatial patterns of net transport and flux divergence and convergence zones are realistic as they are invariant with respect to the availability and properties of sediment. These aspects thus serve as robust indicators of regional sediment transport properties in the existing wave climate. In a similar manner, estimates of changes in some components of sediment transport or its drivers provide a clear signal of environmental changes that may not yet be visible in the functioning of the coasts. This conceptual framework provides a useful lens for interpreting both spatial variability and long-term stability in transport behaviour. It also highlights where shoreline evolution is likely to be locally driven as opposed to where it is more influenced by large-scale transport conditions. This information is critical for effective coastal zone planning.

Conclusions

Summary of results

This thesis presents a detailed investigation into the wave properties of the Baltic Sea from the viewpoint of wave-induced sediment transport and with focus on the Gulf of Finland, the Gulf of Riga and the eastern Baltic proper. The analysis combines high-resolution numerical wave modelling for 30+ years, 1990–2021/2022, with potential wave-driven alongshore sediment transport estimation, systematically exploring its properties and spatio-temporal variations for the last three decades.

The analysis in Paper I confirms, not unexpectedly, that properly calibrated and validated contemporary spectral wave models, such as SWAN, forced by either ERA5 or BaltAn65+ reanalysis wind datasets, can effectively reproduce the known spatial and temporal features of the Baltic Sea wave climate. The hindcast properties of this wave climate at a moderate resolution of 3 nautical miles (about 5.5 km) almost match each other in the Baltic proper and Gulf of Riga. The use of ERA5 wind data tends to project slightly larger significant wave heights and its higher quantiles in the open parts of the Baltic proper and the Gulf of Finland. The difference between the outcomes of these two models is substantial in the Gulf of Bothnia where the simulation forced by ERA5 wind data leads to clearly larger wave heights than the model run forced by BaltAn65+ wind data.

The pattern of differences is more complicated in the Gulf of Finland, where the model run forced with ERA5 wind data yields higher waves in the offshore areas while the simulation that used BaltAn65+ wind data produces higher values in the nearshore, most significantly near the Estonian coasts. Importantly for the analysis of wave-driven sediment transport, the two simulations resulted in nearly identical estimates of the main properties of the wave climate along the eastern shores of the Baltic proper from Cape Taran to the entrance of the Gulf of Finland as well as in the Gulf of Riga.

More detailed insight into the wave climate of the Gulf of Riga is developed using higher-resolution simulations with the same calibrated and validated SWAN model forced with ERA winds 1990–2021 performed with a resolution of 1 nautical mile (about 1.85 km) for the entire gulf and down to 280 m in single coastal areas. The wave model was additionally validated against existing short-term instrumental measurements. The output of this simulation confirms and details the main properties of the wave climate of this gulf and its single coastal segments. Even though some of the established features were qualitatively known from historical visual wave observations and heuristic considerations, the wave climate in this gulf is now quantified in detail in terms of spatial patterns of averages and higher quantiles of significant wave heights, empirical distributions of the frequency of occurrence of wave heights and wave periods, joint distributions of properties of different wave conditions, and long-term variations in wave heights.

The Gulf of Riga wave climate 1990–2021 is clearly milder than in the eastern Baltic proper and is largely detached from waves in the Baltic proper. It comprises mostly fetch-limited relatively short-period waves with the level of interannual variability of ±10% from the long-term significant wave height throughout the modelled period. In spite of various manifestations of climate change in the region, there has been no statistically significant trend in annual significant wave height over the 32-year period in the Gulf of Riga.

The simulated time series of wave properties with a resolution of about 560 m 1990–2022 were used to evaluate spatio-temporal variations in the potential alongshore sediment transport along the eastern Baltic proper from the Sambian Peninsula to Cape Kolka, and from Cape Kolka along the western, southern and eastern shores of the Gulf of Riga to Pärnu Bay. This analysis revealed that coastal segments with seemingly similar appearance, orientation and level of forcing have remarkably different properties in terms of sediment transport. While the Curonian Spit and a segment to the north of the Klaipėda Strait are in a near-equilibrium state or have moderately variable, generally northward transport, the coastal stretch to the north of Cape Akmenrags to Cape Kolka hosts massive, mostly unidirectional transport to the north. Cape Kolka is an endpoint to this sediment pathway and a one-way entrance to the Gulf of Riga.

The Gulf of Riga, however, is not simply an end station of this transport even though there is no exit for sediment at an annual scale. Its different coastal segments have greatly different properties. The transport along the western coast from Cape Kolka to the Port of Engure is essentially counter-clockwise (viewed from the shore looking towards the sea) to the south, with a discontinuity at Mersrags, a natural headland, acting as a barrier. The southern part of the gulf to the River Daugava mouth is a largely interconnected sedimentary system. The eastern shore of the Gulf of Riga is highly fragmented into numerous relatively small sediment cells. This natural large-scale pattern is further fragmented into smaller, almost isolated cells by engineered infrastructure, such as breakwaters or jetties. This system has extensive interannual variations, with statistically significant decline in bulk transport 1990–2005, but no evident trend since. The asymmetric wind climate causes a specific pattern in net transport on the western and eastern shores: when the predominant winds force counter-clockwise transport on the western shore, the same winds drive clockwise transport on the eastern shore.

These regional differences highlight the strong influence of coastal orientation and predominant wave directions. The presence of a bi-directional wind climate in the region, with primary components from the south-west and north-north-west, also becomes evident in terms of wave-driven transport that is dominated by a similar bi-directional wave climate. From the entire annual potential wave-driven sediment transport along the eastern Baltic Sea coast, including, the Gulf of Riga, usually 60–80% is driven by waves arriving from two narrow directional sectors (approximately 255°±15° and 315°±15°). While no rotation in the prevailing wind or wave directions was observed across the hindcast period, a statistically significant decrease in energy input of north-north-western waves was detected at 15–20% of nearshore locations. This process alters the directional balance of sediment transport.

The main message for practical applications is that in the eastern Baltic Sea, sediment transport is not continuous along the coast. Instead, it is highly variable in space and time. It is organised into a sequence of discrete compartments and cells, some of which are almost isolated, some one-way connected, and with some apparently frequently exchanging sediment. These cells and compartments are shaped by local bathymetry (that affects wave propagation direction in the nearshore), shoreline geometry and the angular structure of the approaching waves. The eastern Baltic proper coast thus displays significant spatial variability and also most likely, sensitivity to changes in the balance of local forcing. The Gulf of Riga is a self-contained

system with respect to sediment transport. Collectively, the presented results establish a consistent framework for understanding the wave climate and potential sediment transport in the eastern Baltic Sea.

Main conclusions proposed to defend

1. The properly calibrated triple-nested SWAN wave model forced with ERA5 or BaltAn65+ wind data produces an adequate representation of the Baltic Sea wave climate, with higher waves in the eastern Baltic proper and milder local wave climates in smaller sub-basins.

2. The wave climates replicated using these winds exhibit significant differences that are most pronounced in the Gulf of Bothnia. While simulations driven by ERA5 wind data project larger wave heights in the offshore of the Baltic proper and the Gulf of Finland, the use of BaltAn65+ wind data projects larger wave heights in the nearshore of the Gulf of Finland.

3. Wave simulations driven by ERA5 and BaltAn65+ wind datasets provide nearly identical estimates of the main properties of the wave climate in the eastern nearshore of the Baltic proper and in the Gulf of Riga. This consistency makes it possible to use only one of the wind-forcing datasets in later studies.

4. The ERA5-wind data forced high-resolution SWAN model results, through careful validation against existing instrumental wave measurements is a suitable tool to reproduce the main properties of the Gulf of Riga wave climate.

5. The Gulf of Riga is largely detached from wave fields in the Baltic proper. Its wave climate is substantially milder than in the Baltic proper, mainly wind-sea dominated and with a low proportion of swells. Wave periods (usually 2–5 s) are shorter and average and extreme wave heights lower than in the Baltic proper. Spatial distributions of average and higher quantiles of wave heights are strongly asymmetric.

6. There is no long-term trend in wave energy in the Gulf of Riga. The interannual variability remains within ±10% of the long-term average wave height 1990–2021.

7. The coastal stretch from Cape Taran to Cape Kolka consists of two different parts in terms of wave-driven potential alongshore sediment transport. While the coastal segment from the Curonian Spit to Cape Akmenrags is either in a near equilibrium state or exhibits relatively modest net northward (counter-clockwise) transport with minor reversals in some years, the segment to the north of Cape Akmenrags hosts massive essentially unidirectional transport towards Cape Kolka. Cape Kolka is a deposition endpoint with only limited sediment supply into the Gulf of Riga.

8. The Gulf of Riga is a distinct sedimentary system, with limited one-way connection to the eastern Baltic Sea and with essentially different dynamics. It is divided into several large almost isolated sedimentary compartments by large river mouths, headlands and engineering structures.

9. The western shore of the Gulf of Riga is split into two compartments by a headland at Mersrags. Sediment transport is relatively intense and mainly counter-clockwise. The southern shore of the gulf is an interconnected system with lower and less directionally constrained counter-clockwise sediment transport that is fully interrupted by breakwaters at the Daugava River mouth. The sedimentary system of the eastern shore is highly fragmented, with mainly counter-clockwise transport but with reversals.

10. Waves approaching the nearshore from one or two narrow directional bands (255±15° and 315°±15°) account for 60–80% of wave-driven potential alongshore

sediment flux in the entire eastern Baltic Sea from Cape Taran to the entrance of the Gulf of Finland. The directional bands have been constant over three decades 1990–2022. Wave energy flux arriving from the north-west has significantly decreased in about 20% of the eastern Baltic Sea shores. The change stems from weakening of north-western winds rather than a rotation of the entire wind-wave forcing.

Potential implications and further research

The results described in this thesis demonstrate two aspects that may have substantial implications for the planning and management of the coastal zone in the eastern Baltic Sea and eastern sub-basins of this water body. First, projections of wave climate (and thus also wave properties) reconstructed using different high-quality wind data sets may markedly differ in the coastal area even when they match in the offshore. Second, the eastern shores of the Baltic Sea have extremely complicated structure in terms of alongshore sediment transport patterns, that require serious consideration for planning and management. The comprehensive characterisation of the Gulf of Riga wave climate supports practical applications ranging from erosion risk monitoring and infrastructure planning to sediment budget closure and climate resilience strategies.

While the difference in projections of wave properties eventually can be resolved by means of further improvement of atmospheric models and refinement of bathymetric information, the spatial segmentation of the eastern Baltic Sea shores most probably reflects the essential structural features that are jointly created by enhanced directionality of their forcing mechanisms, the specific geometry of the coastline and the many large-scale engineering structures. As a result, the coastline is divided into several sediment compartments and cells with distinct characteristics stemming from the coastal orientation and the local properties of directional wind wave forcing.

The refined understanding of wave-driven alongshore transport patterns along the eastern Baltic Sea and the Gulf of Riga has clear implications for projections of the future of coastal morphology, erosion risk, and regional shoreline management. The findings underscore the value of a compartment-based framework to support sediment budget monitoring and adaptive coastal planning. On the one hand, this fragmentation considerably simplifies the analysis of sediment transport, erosion and accumulation processes as alongshore excursion rates are in most cases fairly limited. Decomposing the coastline into sedimentary cells and compartments provides a powerful basis for spatial planning. On the other hand, this perspective has implications for shoreline management in areas where these compartments intersect, particularly at partially crossable divergence zones such as Cape Akmenrags or one-way gateways such as Cape Kolka. The presented results suggest that management strategies that assume consistent directionality of sediment transport may require revision to account for the compartmentalised nature of the sedimentary system of the eastern Baltic Sea.

While it has been known for some time that moderate and strong winds in the study area blow from a few predominant directions, it is still instructive as to how consistent is directional wave forcing. The situation where 60–80% of all alongshore sediment transport is driven by waves from one or two narrow sets of directions highlights the vulnerability of several locations of the study area to even moderate shifts in the directional wave energy distribution, be it a rotation of the entire wind system or a change in the balance of wave energy approaching from different directions.

Simulations presented in the thesis show that no systemic rotation of wind or wave directions occurred over the study period. However, the reduction in the amount of

wave energy approaching from the north-west most probably has implications for long-term local sediment budgets and potential shifts in the zones of erosion and accumulation of sediments. The consequences of this process most likely become first evident in the Gulf of Riga, where the compartmental structure of alongshore sediment transport forms a challenge in applying a uniform sediment budget approach. In a similar manner, it is likely that this process has reduced the clockwise component of sediment flux along Baltic proper shores of Latvia and Lithuania. Given the data limitations and complexity of possible changes in the pattern of local divergence and convergence zones, a compartment-based framework would appear better suited in the region. Future studies would benefit from an effort to quantify sediment budgets at the level of individual cells and compartments, with specific studies aimed at each of them for the purpose of providing measurements of actual, rather than only potential, sediment transport.

While this study has thoroughly described the spatial structure of alongshore sediment transport fluxes under typical and basically stationary forcing conditions, the compartment behaviour is not yet properly analysed for extreme events. Some barriers to transport and identified patterns may be considered as semi-permeable. While the 32 year long hindcast provided insight into averaged, long-term conditions, the potential of transport during individual high water level events still needs to be resolved.

While this thesis has focused on specific areas of the eastern Baltic Sea, the broader implication of the outcome lies in further application of high-resolution wave modelling to study compartmentalisation of large sedimentary systems in terms of alongshore variations in the potential sediment transport. This method has proven effective in identifying spatial patterns and structuring long coastal segments into smaller units that may not be visible from large-scale regional assessments alone. While quantitative calculations of potential sediment transport do not necessarily directly reflect on reality, qualitative analysis of alongshore patterns of net transport often leads to new and enhanced understanding. Future work should therefore prioritise refining the knowledge of sediment transport budgets within known compartments and across their boundaries.

The presented analysis signals that sediment cell connectivity may be dynamic and highly climate-sensitive. Importantly, this process occurs despite relatively stable total wave energy levels. Recognising possibly shifting boundaries or their permeability, e.g., because of climate driven changes in the directional structure of wave forcing even with unchanged energy levels, is vital for understanding coastal responses and ensuring effective, compartment-aware management. The complementary use of high-resolution modelling and long-term directional trend analysis offers one more option for transitioning from reactive coastal management to a proactive, process-based planning paradigm.

These findings indicate that directional imbalances, rather than changes in the wave energy magnitude, may play a central role in shaping the sediment transport regimes in the eastern Baltic Sea. This highlights the limitations of static sediment budget models and their assumptions of stable and consistent transport pathways. In addition, the increasing frequency of storm events and high wave energy conditions that is projected to happen in changing climate may further amplify sediment mobility and complicate budget estimations. Future studies and management strategies should shift towards being more adaptive in response, in order to enable a better identification of necessary coastal protection, recovery or mitigation measures across study areas, allowing the coastlines to evolve naturally in a sustainable manner.

List of Figures

References

Ahn, S., 2021. Modelling mean relation between peak period and energy period of ocean surface wave systems. Ocean Engineering, 228, 108937. https://doi.org/10.1016/j.oceaneng.2021.108937

Alari, V., Raudsepp, U., 2010. Depth induced breaking of wind generated surface gravity waves in Estonian coastal waters. Boreal Environment Research, 15(3), 295–300. https://www.borenv.net/BER/archive/pdfs/ber15/ber15-295.pdf

Aagaard, T., Brinkkemper, J., Christensen, D.F., Hughes, M.G., Ruessink, G., 2021. Surf zone turbulence and suspended sediment dynamics – A review. Journal of Marine Science and Engineering, 9(11), 1300. https://doi.org/10.3390/jmse9111300

Bagdanavičiūtė, I., Kelpšaitė, L., Soomere, T., 2015. Multi-criteria evaluation approach to coastal vulnerability index development in micro-tidal low-lying areas. Ocean & Coastal Management, 104, 124–135. https://doi.org/10.1016/j.ocecoaman.2014.12.011

Baltic Sea Hydrographic Commission, 2013. Baltic Sea Bathymetry Database Version 0.9.3. Downloaded from http://data.bshc.pro/on 15.02.2020. New link: www.bshc.pro

Barzehkar, M., Parnell, K., Soomere, T., 2024. Extending multi-criteria coastal vulnerability assessment to low-lying inland areas: examples from Estonia, eastern Baltic Sea. Estuarine, Coastal and Shelf Science, 311, 109014. https://doi.org/10.1016/j.ecss.2024.109014

Bernatchez, P., Fraser, C., 2012. Evolution of coastal defence structures and consequences for beach width trends, Quebec, Canada. Journal of Coastal Research, 28(6), 1550–1566. https://doi.org/10.2112/JCOASTRES-D-10-00189.1

Bierstedt, S.E., Hünicke, B., Zorita, E., 2015. Variability of wind direction statistics of mean and extreme wind events over the Baltic Sea region. Tellus A, 67, 29073. https://doi.org/10.3402/tellusa.v67.29073

Björkqvist, J.-V., Tuomi, L., Tollman, N., Kangas, A., Pettersson, H., Marjamaa, R., Jokinen, H., Fortelius, C., 2017b. Brief communication: Characteristic properties of extreme wave events observed in the northern Baltic Proper, Baltic Sea. Natural Hazards and Earth Systems Sciences, 17(9), 1653–1658. https://doi.org/10.5194/nhess-17-1653-2017

Björkqvist, J.-V., Kanarik, H., Johansson, M.M., Tuomi, L., 2018a. A wave forecast for the Helsinki archipelago in the Gulf of Finland. In: 2018 IEEE/OES Baltic International Symposium (BALTIC), June 12–15, 2018, Klaipėda, Lithuania. IEEE OES. https://doi.org/10.1109/BALTIC.2018.8634863

Björkqvist, J.-V., Lukas, I., Alari, V., van Vledder, P.G., Hulst, S., Pettersson, H., Behrens, A., Männik A., 2018b. Comparing a 41-year model hindcast with decades of wave measurements from the Baltic Sea. Ocean Engineering, 152, 57–71. https://doi.org/10.1016/j.oceaneng.2018.01.048

Björkqvist, J.-V., Pettersson, H., Kahma, K.K., 2019. The wave spectrum in archipelagos. Ocean Science, 15(6), 1469–1487. https://doi.org/10.5194/os-15-1469-2019

Björkqvist, J.-V., Pärt, S., Alari, V., Rikka, S., Lindgren, E., Tuomi, L., 2021. Swell hindcast statistics for the Baltic Sea. Ocean Science, 17(6), 1815–1829. https://doi.org/10.5194/os-17-1815-2021

Booij, N., Ris, R., Holthuijsen, L., 1999. A third generation wave model for coastal regions, 1: model description and validation. Journal of Geophysical Research-Oceans, 104(C4), 7649–7666. https://doi.org/10.1029/98JC02622

Broman, B., Hammarklint, T., Rannat, K., Soomere, T., Valdmann, A., 2006. Trends and extremes of wave fields in the north–eastern part of the Baltic Proper. Oceanologia, 48(S), 165–184

Bulleri, F., Chapman, M.G., 2010. The introduction of coastal infrastructure as a driver of change in marine environments. Journal of Applied Ecology, 47(1), 26–35. https://doi.org/10.1111/j.1365-2664.2009.01751.x

Cappucci, S., Bertoni, D., Cipriani, L. E., Boninsegni, G., Sarti, G., 2020. Assessment of the anthropogenic sediment budget of a littoral cell system (Northern Tuscany, Italy). Water, 12(11), 3240. https://doi.org/10.3390/w12113240

Causio, S., Ciliberti, S.A., Clementi, E., Coppini, G., Lionello, P., 2021. A modelling approach for the assessment of wave-currents interaction in the Black Sea. Journal of Marine Science and Engineering, 9(8), 893. https://doi.org/10.3390/jmse9080893

Cazenave, A., WCRP Global Sea Level Budget Group, 2018. Global sea-level budget 1993–present. Earth System Science Data, 10(3), 1551–1590. https://doi.org/10.5194/essd-10-1551-2018

Clayton, K.M., 1980. Beach sediment budgets and coastal modification. Progress in Physical Geography: Earth and Environment, 4(4), 471–486. https://doi.org/10.1177/030913338000400401

Davidan, I.N., Lopatukhin, L.I., 1982. Facing the Storms. Leningrad, Gidrometeoizdat, 136 pp. (in Russian).

Davies, J.L., 1974. The coastal sediment compartment. Australian Geographical Studies, 12(2), 139–151. https://doi.org/10.1111/j.1467-8470.1974.tb00270.x

Dee, D.P., Uppala, S.M., Simmons, A.J., Berrisford, P., Poli, P., Kobayashi, S., Andrae, U., Balmaseda, M.A., Balsamo, G., Bauer, P., Bechtold, P., Beljaars, A.C.M, van de Berg, L., Bidlot, J., Bormann, N., Delsol, C., Dragani, R., Fuentes, M., Geer, A.J., Haimberger, L., Healy, S.B., Hersbach, H., Hólm, E.V., Isaksen, L., Kållberg, P., Köhler, M. Matricardi, M., McNally, A.P., Monge-Sanz, B.M., Morcrette, J.-J., Park, B.-K., Peubey, C., de Rosnay, P., Tavolato, C., Thépaut, J.-N., Vitart, F., 2011. The ERA-Interim reanalysis: configuration and performance of the data assimilation system. Quarterly Journal of Royal Meteorological Society 137(656), 553–597, https://doi.org/10.1002/qj.828

Dette, H.H., Asce, M., 2001. Influence of shoreline alignment on offshore sediment transport. In: Hanson, H., Larson, M. (eds.), Coastal Dynamics '01: Proceedings. 4th International Conference on Coastal Dynamics, Lund, Sweden, June 11–15, 2001. American Society of Civil Engineers, Coasts, Oceans, Ports & Rivers Institute, 938–947.

Eberhards, G., Lapinskis, J., 2008. Processes on the Latvian coast of the Baltic Sea. Atlas. Riga, University of Latvia. ISBN 9789984450209, 2008.

Eberhards, G., Grine, I., Lapinskis, J., Purgalis, I., Saltupe, B., Torklere, A., 2009. Changes in Latvia's seacoast (1935–2007). Baltica, 22(1), 11–22, 2009.

Eelsalu, M., Org, M., Soomere, T., 2014. Visually observed wave climate in the Gulf of Riga. In: The 6th IEEE/OES Baltic Symposium Measuring and Modeling of Multi-Scale Interactions in the Marine Environment, May 26–29, Tallinn, Estonia. IEEE Conference Publications, 6887829, 10 pp. https://doi.org/10.1109/BALTIC.2014.6887829

Eelsalu, M., Parnell, K.E., Soomere, T., 2022. Sandy beach evolution in the low-energy microtidal Baltic Sea: attribution of changes to hydrometeorological forcing. Geomorphology, 414, 108383. https://doi.org/10.1016/j.geomorph.2022.108383

Eelsalu, M., Viigand, K., Soomere, T., 2023. Quantification of sediment budget in extensively developed urban areas: a case study of Tallinn Bay, the Baltic Sea. Regional Studies in Marine Science, 67, 103199. https://doi.org/10.1016/j.rsma.2023.103199

Eelsalu, M., Soomere, T., Parnell, K.E., Viška, M., 2025. Attribution of alterations in coastal processes in the southern and eastern Baltic Sea to climate change driven modifications of coastal drivers. Oceanologia, 67(1), 67103, https://doi.org/10.5697/LXTZ5389

Eerola, K., 2013. Twenty-one years of verification from the HIRLAM NWP system. Weather and Forecasting, 28(1), 270–285. https://doi.org/10.1175/WAF-D-12-00068.1

Feistel, R., Nausch, G., Wasmund, N., 2005. State and evolution of the Baltic Sea, 1952–2005. Wiley-VCH, Weinheim, 728 pp. https://doi.org/10.1002/9780470283134

Flor-Blanco, G., Alcántara-Carrió, J., Jackson, D.W.T., Flor, G., Flores-Soriano, C., 2021. Coastal erosion in NW Spain: Recent patterns under extreme storm wave events. Geomorphology, 387. https://doi.org/10.1016/j.geomorph.2021.10776

Guedes Soares, C., 1986. Assessment of the uncertainty in visual observations of wave height. Ocean Engineering, 13(1), 37–56. https://doi.org/10.1016/0029-8018(86)90003-X

Guidelines, 1985. Guidelines for Hydrometeorological Stations and Posts. Meteorological observations at stations. Leningrad, Gidrometeoizdat, 3(1), 300 pp. (in Russian).

Gulev, S.K., Hasse, L., 1998. North Atlantic wind waves and wind stress fields from voluntary observing ship data. Journal of Physical Oceanography, 28(6), 1107–1130, https://doi.org/10.1175/1520-0485(1998)028<1107:NAWWAW>2.0.CO;2

Gulev, S.K., Hasse, L., 1999. Changes of wind waves in the North Atlantic over the last 30 years. International Journal of Climatology, 19(10), 1091–1117. https://doi.org/10.1002/(SICI)1097-0088(199908)19:10<1091::AID-JOC403>3.0.CO;2-U

Harff, J., Meyer, M. 2011. Coastlines of the Baltic Sea – zones of competition between geological processes and a changing climate: Examples from the southern Baltic In: Harff, J., Björck, S., Hoth, P. (eds.), The Baltic Sea Basin. Central and Eastern European Development Studies, 5, Springer, Berlin, Heidelberg, pp. 149–164, https://doi.org/10.1007/978-3-642-17220-5_7

Harff, J., Deng, J.J., Dudzinska-Nowak, J., Fröhle, P., Groh, A., Hünicke, B., Soomere, T., Zhang, W.Y., 2017. What Determines the Change of Coastlines in the Baltic Sea?. In: Harff, J., Furmańczyk, K., von Storch, H. (eds.), Coastline Changes of the Baltic Sea from South to East: Past and Future Projection. Coastal Research Library 19, pp. 15–35. https://doi.org/10.1007/978-3-319-49894-2_2

Hersbach, H., Bell, B., Berrisford, P., Hirahara, S., Horanyi, A., Munoz-Sabater, J., Nicolas, J., Peubey, C., Radu, R., Schepers, D., Simmons, A., Soci, C., Abdalla, S., Abellan, X., Balsamo, G., Bechtold, P., Biavati, G., Bidlot, J., Bonavita, M., De Chiara, G., Dahlgren, P., Dee, D., Diamantakis, M., Dragani, R., Flemming, J., Forbes, R., Fuentes, M., Geer, A., Haimberger, L., Healy, S., Hogan, R.J., Holm, E., Janiskova, M., Keeley, S., Laloyaux, P., Lopez, P., Lupu, C., Radnoti, G., de Rosnay, P., Rozum, I., Vamborg, F., Villaume, S., Thepaut, J.N., 2020. The ERA5 global reanalysis. Quarterly Journal of the Royal Meteorological Society, 146(730), 730, 1999–2049. https://doi.org/10.1002/qj.3803

Hünicke, B., Zorita, E., Soomere, T., Skovgaard Madsen, K., Johansson, M., Suursaar, Ü., 2015. Recent change – sea level and wind waves. In: The BACC II Author Team, Second Assessment of Climate Change for the Baltic Sea Basin, Regional Climate Studies, Springer, Cham, 155–185. https://doi.org/10.1007/978-3-319-16006-1_9

Jaagus, J., Kull, A., 2011. Changes in surface wind directions in Estonia during 1966–2008 and their relationships with large-scale atmospheric circulation. Estonian Journal of Earth Sciences, 60(4), 220–231, https://doi.org/10.3176/earth.2011.4.03

Jaagus, J., Suursaar, Ü., 2013. Long-term storminess and sea level variations on the Estonian coast of the Baltic Sea in relation to large-scale atmospheric circulation. Estonian Journal of Earth Sciences, 62(2), 73—92. https://doi.org/10.3176/earth.2013.07

Johansson, M.M., Björkqvist, J.V., Särkkä, J., Leijala, U., Kahma, K.K., 2022. Natural Hazards and Earth System Sciences, 22(3), 813–829. https://doi.org/10.5194/nhess-22-813-2022

Kanarik, H., Tuomi, L., Björkqvist, J.-V., Kärnä, T., 2021. Improving Baltic Sea wave forecasts using modelled surface currents. Ocean Dynamics, 71(6–7), 635–653. https://doi.org/10.1007/s10236-021-01455-y

Kelpšaitė, L., Dailidienė, I., Soomere, T., 2011. Changes in wave dynamics at the south-eastern coast of the Baltic Proper during 1993–2008. Boreal Environment Research, 16 (Supplement A), 220–232.

Kinsela, M.A., Morris, B.D., Linklater, M., Hanslow, D.J., 2017. Second-pass assessment of potential exposure to shoreline change in New South Wales, Australia, using sediment compartments framework. Journal of Marine Science and Engineering, 5(4), 61. https://doi.org/10.3390/jmse5040061

Knaps, R.J., 1966. Sediment transport near the coasts of the Eastern Baltic. In: Development of sea shores under the conditions of oscillations of the Earth's crust. Valgus, Tallinn, pp. 21–29 (in Russian).

Komen, G.J., Hasselmann, S., Hasselmann, K., 1984. On the existence of a fully developed wind-sea spectrum. Journal of Physical Oceanography, 14(8), 1271–1285. https://doi. org/10.1175/1520-0485(1984)014<1271:oteoaf>2.0.co

Komen, G.J., Cavaleri, L., Donelan, M., Hasselmann, K., Hasselmann, S., Janssen, P.A.E.M., 1994. Dynamics and Modelling of Ocean Waves. Cambridge University Press, Cambridge, 532 pp.

Kudryavtseva, N.A., Soomere, T., 2016. Validation of the multi-mission altimeter wave height data for the Baltic Sea region. Estonian Journal of Earth Sciences, 65(3), 161–175. https://doi.org/10.3176/earth.2016.13

Kudryavtseva, N., Soomere, T., 2017. Satellite altimetry reveals spatial patterns of variations in the Baltic Sea wave climate. Earth System Dynamics, 8(3), 697–706. https://doi.org/10.5194/esd-8-697-2017

Kudryavtseva, N., Kussembayeva, K., Rakisheva, Z.B., Soomere, T. 2019. Spatial variations in the Caspian Sea wave climate in 2002–2013. Estonian Journal of Earth Sciences, 68(4), 225–240. https://doi.org/10.3176/earth.2019.16

Kudryavtseva, N., Räämet, A., Soomere, T., 2020. Coastal flooding: Joint probability of extreme water levels and waves along the Baltic Sea coast. Journal of Coastal Research, Special Issue 95, 1146–1151. https://doi.org/10.2112/SI95-222.1

Larson, M., Hoan, L. X., Hanson, H., 2010. Direct formula to compute wave height and angle at incipient breaking. Journal of Waterway, Port, Coastal, and Ocean Engineering, 136(2), 119–122. https://doi.org/10.1061/(ASCE)WW.1943-5460.0000030

Launiainen, J., Laurila, T., 1984. Marine wind characteristics in the northern Baltic Sea. Finnish Marine Research, 250, 52–86.

Leppäranta, M., Myrberg, K., 2009. Physical Oceanography of the Baltic Sea. Springer, Berlin, 378 pp. https://doi.org/10.1007/978-3-540-79703-6

Lorenz, M., Viigand, K., Gräwe, U., 2025. Untangling the waves: decomposing extreme sea levels in a non-tidal basin, the Baltic Sea. Natural Hazards and Earth System Sciences, 25(4), 1439–1458. https://doi.org/10.5194/nhess-25-1439-2025

Luhamaa, A., Kimmel, K., Männik, A., Rõõm, R., 2011. High resolution re-analysis for the Baltic Sea region during 1965–2005 period. Climate Dynamics, 36, 727–738. https://doi.org/10.1007/s00382-010-0842-y

Männikus, R., Soomere, T., Kudryavtseva, N., 2019. Identification of mechanisms that drive water level extremes from in situ mea- surements in the Gulf of Riga during 1961–2017. Continental Shelf Research, 182, 22–36. https://doi.org/10.1016/j.csr.2019.05.014

Männikus, R., Soomere, T., Suursaar, Ü., 2024. How do simple wave models perform compared with sophisticated models and measurements in the Gulf of Finland? Estonian Journal of Earth Sciences, 73(2), 98–111, https://doi.org/10.3176/earth.2024.10

Muraleedharan, G., Lucas, L., Guedes Soares, C., 2023. Spectral wave energy period and peak period statistics concomitant with maximum significant wave heights. Coastal Engineering, 183, 104260. https://doi.org/10.1016/j.coastaleng.2022.104260

Najafzadeh, F., Soomere, T., 2024. Impact of changes in sea ice cover on wave climate of semi-enclosed seasonally ice-covered water bodies on temperate latitudes: a case study in the Gulf of Riga. Estonian Journal of Earth Sciences, 73(1), 26–36. https://doi.org/10.3176/earth.2024.03

Nikolkina, I., Soomere, T., Räämet, A., 2014. Multidecadal ensemble hindcast of wave fields in the Baltic Sea. In: 6th IEEE/OES Baltic International Symposium (BALTIC) Measuring and Modeling of Multi-Scale Interactions in the Marine Environment, May 26–29, Tallinn Estonia. IEEE EOS, 6887854. https://doi.org/10.1109/BALTIC.2014.6887854

Pallares, E., Sánchez-Arcilla, A., Espino, M., 2014. Wave energy balance in wave models (SWAN) for semi-enclosed domains–Application to the Catalan coast. Continental Shelf Research, 87, 41–53. https://doi.org/https://doi.org/10.1016/j.csr.2014.03.008

Pettersson, H., Kahma, K.K., Tuomi, L., 2010. Wave directions in a narrow bay. Journal of Physical Oceanography, 40(1), 155–169. https://doi.org/10.1175/2009JPO4220.1

Pranzini, E., Williams, A., 2013. Coastal Erosion and Protection in Europe. Routledge, London, 488 pp. https://doi.org/10.4324/9780203128558

Queffeulou, P., 2004. Long-term validation of wave height measurements from altimeters. Marine Geodesy, 27(3–4), 495–510. https://doi.org/10.1080/01490410490883478

Räämet, A., Soomere, T., 2021. Spatial pattern of quality of historical wave climate reconstructions for the Baltic Sea. Boreal Environment Research, 26, 29–41. https://www.borenv.net/BER/archive/pdfs/ber26/ber26-029-041.pdf

Räämet, A., Suursaar, Ü., Kullas, T., Soomere, T., 2009. Reconsidering uncertainties of wave conditions in the coastal areas of the northern Baltic Sea. Journal of Coastal Research, Special Issue 56, 257–261. https://www.jstor.org/stable/25737577

Rantanen, M., van den Broek, D., Cornér, J., Sinclair, V.A., Johansson, M.M., Särkkä, J., Laurila, T.K., Jylhä, K., 2024. The impact of serial cyclone clustering on extremely high sea levels in the Baltic Sea. Geophysical Research Letters, 51(6), e2023GL107203. https://doi.org/10.1029/2023GL107203

Rogers, W.E., Hwang, P.A., Wang, D.W., 2003. Investigation of wave growth and decay in the SWAN model: Three regional-scale applications. Journal of Physical Oceanography, 33(2), 366–389. https://doi.org/10.1175/1520-0485(2003)033<0366:IOWGAD>2.0.CO;2

Rutgersson, A., Jaagus, J., Schenk, F., Stendel, M., Bärring, L., Briede, A., Claremar, B., Hanssen-Bauer, I., Holopainen, J., Moberg, A., Nordli, Ø., Rimkus, E., Wibig, J., 2015. Recent Change–Atmosphere. In: The BACC II Author Team, Second Assessment of Climate Change for the Baltic Sea Basin, Regional Climate Studies, Springer, Cham, 69–97. https://doi.org/10.1007/978-3-319-16006-1_4

Ryabchuk, D., Leontyev, I., Sergeev, A., Nesterova, E., Sukhacheva, L., Zhamoida, V., 2011. The morphology of sand spits and the genesis of longshore sand waves on the coast of the eastern Gulf of Finland. Baltica, 24(1), 13–24.

Ryabchuk, D., Sergeev, A., Burnashev, E., Khorikov, V., Neevin, I., Kovaleva, O., Budanov, L., Zhamoida, V., Danchenkov, A., 2020. Coastal processes in the Russian Baltic (eastern Gulf of Finland and Kaliningrad area). Quarterly Journal of Engineering Geology and Hydrogeology, 54(1), qjegh2020-036. https://doi.org/10.1144/qjegh2020-036

Šakurova, I., Kondrat, V., Baltranaitė, E., Vasiliauskienė, E., Kelpšaitė-Rimkienė, L., 2023. Assessment of coastal morphology on the south-eastern Baltic Sea coast: The case of Lithuania. Water, 15(1), 79. https://doi.org/10.3390/w15010079

Šakurova, I., Kondrat, V., Baltranaitė, E., Gardauskė, V., Kelpšaitė-Rimkienė, L., Soomere, T., Parnell, K.E., 2025. Initial adjustment of underwater profiles after nourishment in a mild wave climate: a case study near Klaipėda, the Baltic Sea. Estonian Journal of Earth Sciences, 74(1), 22–33. https://doi.org/10.3176/earth.2025.02

Sapiega, P., Zalewska, T., Struzik, P., 2023. Application of SWAN model for wave forecasting in the southern Baltic Sea supplemented with measurement and satellite data. Environmental Modelling & Software, 163, 105624. https://doi.org/10.1016/j.envsoft.2023.105624.

Seifert, T, Tauber, F., Kayser B., 2001. A high resolution spherical grid topography of the Baltic Sea–revised edition. In: Baltic Sea Science Congress 2001, Nov 25–29.

Shaeri, S., Etemad-Shahidi, A., Tomlinson, R., 2020 Revisiting longshore sediment transport formulas. Journal of Waterway, Port, Coastal, and Ocean Engineering, 146(4), 04020009. https://doi.org/10.1061/(ASCE)WW.1943-5460.0000557

Skudra, M., Lips, U., 2017. Characteristics and inter-annual changes in temperature, salinity and density distribution in the Gulf of Riga. Oceanologia, 59(1), 37–48. https://doi.org/10.1016/j.oceano.2016.07.001

Sokolov, A.N., Chubarenko, B.V., 2020. Temporal variability of the wind wave parameters in the Baltic Sea in 1979–2018 based on the numerical modeling results. Physical Oceanography, 27(4), 352–363. https://doi.org/10.22449/1573-160X-2020-4-352-363

Sokolov, A., Chubarenko, B., 2024. Baltic Sea wave climate in 1979–2018: Numerical modelling results. Ocean Engineering, 297, 117088. https://doi.org/10.1016/j.oceaneng.2024.117088

Soomere, T., 2001. Extreme wind speeds and spatially uniform wind events in the Baltic Proper. Proceedings of the Estonian Academy of Sciences. Engineering, 7(3), 195–211. https://doi.org/10.3176/eng.2001.3.01

Soomere, T., 2003. Anisotropy of wind and wave regimes in the Baltic Proper. Journal of Sea Research, 49(4), 305–316. https://doi.org/10.1016/S1385-1101(03)00034-0)

Soomere, T., 2005. Wind wave statistics in Tallinn Bay, Boreal Environment Research, 10(2), 103–118. http://www.borenv.net/BER/archive/pdfs/ber10/ber10-103.pdf

Soomere, T., 2013. Extending the observed Baltic Sea wave climate back to the 1940s. Journal of Coastal Research, Special Issue 65, 1969–1974, https://doi.org/10.2112/SI65-333.1

Soomere, T., 2023. Numerical simulations of wave climate in the Baltic Sea: a review. Oceanologia, 65(1), 117–140. https://doi.org/10.1016/j.oceano.2022.01.004

Soomere, T., 2024. Climate change and coastal processes in the Baltic Sea, Oxford Encyclopedia of Climate Science, https://doi.org/10.1093/acrefore/9780190228620.013.897

Soomere, T., Keevallik, S., 2001. Anisotropy of moderate and strong winds in the Baltic Proper. Proceedings of the Estonian Academy of Sciences. Engineering 7(1), 35–49. https://doi.org/10.3176/eng.2001.1.04

Soomere, T., Zaitseva, I., 2007. Estimates of wave climate in the northern Baltic Proper derived from visual wave observations at Vilsandi. Proceedings of the Estonian Academy of Sciences. Enginering, 13(1), 48–64. https://doi.org/10.3176/eng.2007.1.02

Soomere, T., Healy, T., 2011. On the dynamics of "almost equilibrium" beaches in semi-sheltered bays along the southern coast of the Gulf of Finland. In: Harff, J., Björck, S., Hoth, P. (eds.), The Baltic Sea Basin. Central and Eastern European Development Studies, 5, Springer, Berlin, Heidelberg, pp. 255–279. https://doi.org/10.1007/978-3-642-17220-5_13

Soomere, T., Räämet, A., 2011. Spatial patterns of the wave climate in the Baltic Proper and the Gulf of Finland. Oceanologia 53(1), 335–371. https://doi.org/10.5697/oc.53-1-TI.335

Soomere, T., Eelsalu, M., 2014. On the wave energy potential along the eastern Baltic Sea coast. Renewable Energy, 71, 221–233. https://doi.org/10.1016/j.renene.2014.05.025

Soomere, T., Viška, M., 2014. Simulated sediment transport along the eastern coast of the Baltic Sea. Journal of Marine Systems, 129, 96–105. https://doi.org/10.1016/j.jmarsys.2013.02.001

Soomere, T., Kask, A., Kask, J., Nerman, R., 2007. Transport and distribution of bottom sediments at Pirita Beach. Estonian Journal of Earth Sciences, 56(4), 233–254. https://doi.org/10.3176/earth.2007.04

Soomere, T., Behrens, A.., Tuomi, L., Nielsen, J.W., 2008. Wave conditions in the Baltic Proper and in the Gulf of Finland during windstorm Gudrun. Natural Hazards and Earth System Sciences, 8(1), 37–46. https://doi.org/10.5194/nhess-8-37-2008

Soomere, T., Weisse, R., Behrens, A., 2012. Wave climate in the Arkona Basin, the Baltic Sea. Ocean Science, 8(2), 287–300. https://doi.org/10.5194/os-8-287-2012

Soomere, T., Pindsoo, K., Bishop, S.R., Käärd, A., Valdmann, A., 2013. Mapping wave set-up near a complex geometric urban coastline. Natural Hazards and Earth System Sciences, 13(11), 3049–3061. https://doi.org/10.5194/nhess-13-3049-2013

Soomere, T., Bishop, S.R., Viška, M., Räämet, A., 2015. An abrupt change in winds that may radically affect the coasts and deep sections of the Baltic Sea. Climate Research, 62(2), 163–171. https://doi.org/10.3354/cr01269

Soomere, T., Männikus, R., Pindsoo, K., Kudryavtseva, N., Eelsalu, M., 2017. Modification of closure depths by synchronisation of severe seas and high water levels. Geo-Marine Letters, 37(1), 35–46. https://doi.org/10.1007/s00367-016-0471-5

Soomere, T., Eelsalu, M., Viigand, K., Giudici, A. 2024. Linking changes in the directional distribution of moderate and strong winds with changes in wave properties in the eastern Baltic proper. Journal of Coastal Research, Special Issue 113, 190–194. https://doi.org/10.2112/JCR-SI113-038.1

Susilowati, Y., Nur, W.H., Sulaiman, A., Kumoro, Y., Yunarto, 2022. Study of dynamics of coastal sediment cell boundary in Cirebon coastal area based on integrated shoreline Montecarlo model and remote sensing data. Regional Studies in Marine Science, 52, 102268. https://doi.org/10.1016/j.rsma.2022.102268

Suursaar, Ü., 2013. Locally calibrated wave hindcasts in the Estonian coastal sea in 1966–2011. Estonian Journal of Earth Sciences, 62(1), 42–56. https://doi.org/10.3176/earth.2013.05

Suursaar, Ü., 2015. Analysis of wave time series in the Estonian coastal sea in 2003–2014. Estonian Journal of Earth Sciences, 64(4), 289–304. https://doi.org/10.3176/earth.2015.35

Suursaar, Ü., Kullas, T., Otsmann, M., 2002. A model study of the sea level variations in the Gulf of Riga and the Väinameri Sea. Continental Shelf Research, 22(14), 2001–2019. https://doi.org/10.1016/S0278-4343(02)00046-8

Suursaar, Ü., Alari, V., Tõnisson, H., 2014. Multi-scale analysis of wave conditions and coastal changes in the north-eastern Baltic Sea. Journal of Coastal Research, Special Issue 70, 223–228. https://www.jstor.org/stable/43290956

Suursaar, Ü., Jaagus, J., Tõnisson, H., 2015. How to quantify long-term changes in coastal sea storminess? Estuarine, Coastal and Shelf Science, 156, 31–41. https://doi.org/10.1016/j.ecss.2014.08.001

The SWAN team, 2019. SWAN Scientific and Technical Documentation. Delft University of Technology version 41.31. Technical Report. http://swanmodel.sourceforge.net/download/zip/.swantech.pdf. Downloaded on 10.10.2019.

Thom, B.G., Eliot, I., Eliot, M., Harvey, N., Rissik, D., Sharples, C., Short, A.D., Woodroffe, C.D., 2018. National sediment compartment framework for Australian coastal management. Ocean & Coastal Management, 154, 103–120. https://doi.org/10.1016/j.ocecoaman.2018.01.001

Tsyrulnikov, A., Tuuling, I., Hang, T., 2008. Streamlined topographical features in and around the Gulf of Riga as evidence of Late Weichselian glacial dynamics. Geological Quarterly, 52(1), 81–89. https://doi.org/10.7306/gq.v52i1

Tõnisson, H., Orviku, K., Lapinskis, J., Gulbinskas, S., Zaromskis, R., 2013. The Baltic States – Estonia, Latvia and Lithuania. In: Pranzini, E., Williams, A. (eds.), Coastal Erosion and Protection in Europe. Routledge, London, pp. 47–80. https://doi.org/10.4324/9780203128558

Tõnisson, H., Suursaar, Ü., Alari, V., Muru, M., Rivis, R., Kont, A., Viitak, M., 2016, Measurement and model simulations of hydrodynamic parameters, observations of coastal changes and experiments with indicator sediments to analyse the impact of storm St. Jude in October, 2013. Journal of Coastal Research, Special Issue 75, 1257–1261. https://doi.org/10.2112/SI75-25

Tuomi, L., Kahma, K.K., Pettersson, H., 2011. Wave hindcast statistics in the seasonally ice-covered Baltic Sea. Boreal Environment Research, 16(6), 451–472. http://www.borenv.net/BER/archive/pdfs/ber16/ber16-451.pdf

Tuomi, L., Kanarik, H., Björkqvist, J.-V., Marjamaa, R., Vainio, J., Hordoir, R., Höglund, A., Kahma, K.K., 2019. Impact of ice data quality and treatment on wave hindcast statistics in seasonally ice-covered seas. Frontiers in Earth Science, 7, 166. https://doi.org/10.3389/feart.2019.00166

Ulsts, V., 1998. Latvian coastal zone of the Baltic Sea. Atlas. State Geological Survey of Latvia. ISBN 9789984929903.

Unden, P., Rontu, L., Jarvinen, H., Lynch, P., Calvo, J., Cats, G., Cuxart, J., Eerola, K., Fortelius, C., Garcia-Moya, J.A., Jones, C., Lenderlink, G., McDonald, A., McGrath, R., Navascues, B., Nielsen, N.W., deGaard, V., Rodriguez, E., Rummukainen, M., Rõõm, R., Sattler, K., Sass, B.H., Savijärvi, H., Schreur, B.W., Sigg, R., The, H., Tijm, A., 2002. HIRLAM-5 Scientific Documentation. Swedish Meteorological and Hydrological Institute, 144 pp. [Available online at http://hirlam.org.]

USACE, 2002. Coastal Engineering Manual. Manual No. 1110-2-1100. Department of the Army, US Army Corps of Engineers. https://www.publications.usace.army.mil/USACE-Publications/Engineer-Manuals/u43544q/636F617374616C20656E67696E656572696E67206D616E75616C/ (last access: 16 January 2025).

Uppala, S.M., Kållberg, P.W., Simmons, A.J., Andrae, U., Bechtold, V.D.C., Fiorino, M., Gibson, J.K., Haseler, J., Hernandez, A., Kelly, G.A., Li, X., Onogi, K., Saarinen, S., Sokka, N., Allan, R.P., Andersson, E., Arpe, K., Balmaseda, M.A., Beljaars, A.C.M., Berg, L.V.D., Bidlot, J., Bormann, N., Caires, S., Chevallier, F., Dethof, A., Dragosavac, M., Fisher, M., Fuentes, M., Hagemann, S., Holm, E., Hoskins, B.J., Isaksen, L., Janssen, P.A.E.M., Jenne, R., Mcnally, A.P., Mahfouf, J.-F., Morcrette, J.-J., Rayner, N.A., Saunders, R.W., Simon, P., Sterl, A., Trenberth, K.E., Untch, A., Vasiljevic, D., Viterbo, P., Woollen, J., 2005 The ERA-40 re-analysis. Quarterly Journal of Royal Meteorological Society, 131(612), 2961–3012. https://doi.org/10.1256/qj.04.176

Viigand, K., Eelsalu, M., Soomere, T., 2025. Quantifying exposedness of the eastern Baltic Sea shores with respect to extremely high and low water levels. Estuarine. Coastal and Shelf Science, 319, 109267. https://doi.org/10.1016/j.ecss.2025.109267

Viitak, M., Maljutenko, I., Alari, V., Suursaar, Ü., Rikka, S., Lagemaa, P., 2016. The impact of surface currents and sea level on the wave field evolution during St. Jude storm in the eastern Baltic Sea. Oceanologia, 58(3), 176–186. https://doi.org/10.1016/j.oceano.2016.01.004

Villasante, S., Richter, K., Bailey, J., Blenckner, T., Farrell, E., Mongruel, R., Timmermann, K., Bouma, T., Melaku Canu, D., Chen, M., Lachs, L., Payo, A., Sousa Pinto, I., 2023. Building Coastal Resilience in Europe. Position Paper 27 of the European Marine Board, edited by: Alexander, B., Muñiz Piniella, A., Kellett, P., Rodriguez Perez, A., Van Elslander, J., Bayo Ruiz, F., Heymans, J.J. Ostend, Belgium. https://doi.org/10.5281/zenodo.8224055

Viška, M., Soomere, T., 2012. Hindcast of sediment flow along the Curonian Spit under different wave climates. In: Proceedings of the IEEE/OES Baltic 2012 International Symposium "Ocean: Past, Present and Future. Climate Change Research, Ocean Observation & Advanced Technologies for Regional Sustainability," May 8–11, Klaipėda, Lithuania. IEEE Conference Publications. https://doi.org/10.1109/BALTIC.2012.6249195

Viška, M., Soomere, T., 2013a. Long-term variations of simulated sediment transport along the eastern Baltic Sea coast as a possible indicator of climate change. In: Reckermann, M., Köppen, S. (eds.), 7th Study Conference on BALTEX, 10–14 June 2013, Borgholm, Island of Öland, Sweden, Conference Proceedings, International BALTEX Secretariat, Publication No. 53, pp. 99–100. https://www.baltex-research.eu/oland2013/material/Proceedings_Final_web.pdf

Viška, M., Soomere, T., 2013b. Simulated and observed reversals of wave-driven alongshore sediment transport at the eastern Baltic Sea coast. Baltica, 26(2), 145–156. https://doi.org/10.5200/baltica.2013.26.15

Weisse, R., Dailidienė, I., Hünicke, B., Kahma, K., Madsen, K., Omstedt, A., Parnell, K., Schöne, T., Soomere, T., Zhang, W., Zorita, E. 2021. Sea level dynamics and coastal erosion in the Baltic Sea region. Earth Systems Dynamics, 12, 871–898. https://doi.org/10.5194/esd-12-871-2021

Wu, J., 2012. Wind-stress coefficients over sea surface from breeze to hurricane. Journal of Geophysical Research-Oceans, 87(C12), 9704–9706. https://doi.org/10.1029/JC087iC12p09704

Zaitseva-Pärnaste, I., Soomere, T., Tribštok O., 2011. Spatial variations in the wave climate change in the eastern part of the Baltic Sea, Journal of Coastal Research, Special Issue 64, vol. I, 195–199.

Žaromskis, R., Gulbinskas, S., 2010. Main patterns of coastal zone development of the Curonian Spit, Lithuania. Baltica, 23(2), 149–156.

Zijlema, M., van Vledder, G.P., Holthuijsen, L.H., 2012. Bottom friction and wind drag for wave models. Coastal Engineering, 65, 19–26. https://doi.org/10.1016/j.coastaleng.2012.03.002.

Acknowledgements

I would like to express my deepest gratitude to my supervisor, Prof. Tarmo Soomere, whose vast knowledge and experience have been a constant source of inspiration throughout my doctoral journey. His guidance and example have greatly shaped my approach to research, and I have benefitted enormously from the depth and breadth of his understanding of ocean sciences.

I am equally indebted to my co-supervisor, Prof. Kevin Parnell, who has been a steady mentor, always available with constructive criticism and practical advice that kept my work on track and moving forward. His encouragement and careful attention to detail have played a crucial role in developing both my academic skills and confidence as a researcher.

My heartfelt thanks go to Maris Eelsalu, whose guidance was essential in developing my modelling skills and in producing clear and effective figures. I also thank Dr. Andrea Giudici for many insightful discussions and Dr. Rain Männikus for his inspiring perspective. Further thanks are due to my colleagues at TalTech, including Dr. Fatemeh Najafzadeh, Dr. Katri Pindsoo, Dr. Nicole Delpeche-Ellmann, Dr. Mojtaba Barzerkhar, Dr. Andrus Räimmet, Dr. Dmitri Kartofelev, and Dr. Heiko Jens Herrmann, for their collaboration and support.

I am especially grateful to my parents, family, and friends, whose encouragement has been vital throughout this journey. Their support, along with that of colleagues and professional contacts met at conferences and beyond, has helped me maintain motivation and balance along the way.

Abstract

Wave-Driven Sediment Transport along Eastern Baltic Sea Shores

This thesis addresses structural properties of wave-driven alongshore sediment transport along the sedimentary coasts of the eastern Baltic Sea and the Gulf of Riga. The main tool is the use of potential sediment transport, that is proportional to wave energy flux and is evaluated using the Coastal Engineering Research Centre (CERC) approach. For this task, the wave climate of the Baltic Sea and its larger sub-basins is reconstructed for the period 1991–2021 using carefully calibrated and validated wave model SWAN forced with two wind data sets. The model grid is triple-nested, with a spatial resolution of 5.5 km for the entire sea, 1.8 km for the Gulf of Finland and Gulf of Riga, and 560 m for the study area from the Sambian Peninsula to Pärnu Bay.

The main properties of the wave climate reconstructed with ERA5 and BaltAn65+ winds match well in the open part of the Baltic Sea and in the nearshore for sediment transport simulations. Waves hindcast using ERA5 forcing are clearly higher than those reconstructed using BaltAn65+ winds in the Gulf of Bothnia and in the offshore of the Gulf of Finland but lower in the nearshore of the Gulf of Finland. The likely reason for differences is the different spatial resolution of wind data. The wave climate of the Gulf of Riga is milder than in the Baltic proper or Gulf of Finland. Wave fields in the Guf of Riga are predominantly fetch-limited, with a small proportion of swell, have shorter periods (2–5 s) than in the Baltic proper and are often even steeper than so-called fully developed wave systems.

The >700 km long sedimentary system of the eastern Baltic Sea coast from the Kaliningrad District to Pärnu Bay in Estonia has mostly counter-clockwise transport with several shorter segments of clockwise transport. This system is split into almost separated compartments by two natural features (Cape Kolka and Cape Akmenrags) and three engineering structures (breakwaters of the Port of Klaipėda, Port of Ventspils and at the River Daugava mouth). These compartments are split into several smaller sedimentary cells by several natural headlands and breakwaters of smaller ports.

While the Baltic proper shores of Lithuania and southern Latvia have low net wave-driven transport, the north-western shore of Latvia hosts massive transport towards Cape Kolka which serves as a one-way gateway for sediment transport into the Gulf of Riga. The western and eastern shores of the Gulf of Riga exhibit more intense transport than the southern shore. The western and southern shores have a few smaller sedimentary cells that host mostly clockwise transport while the sedimentary system of the eastern shore is heavily fragmented. Wave-driven transport in the Gulf of Riga exhibits extensive interannual variations in bulk and net transport but no statistically significant trend 1991–2022.

At least 60% and often >80% of wave-driven alongshore transport in the entire eastern Baltic Sea, from the entrance of the Gulf of Finland to Cape Taran, including the Gulf of Riga, is generated by waves approaching from one or two narrow ($\pm 15°$) ranges of directions: south-west and/or (north-)north-west. These directions have been constant 1991–2022, whereas the amount of energy from the north has statistically significantly decreased in large segments of the study area. The established structural features of wave-driven transport and identified changes in forcing provide crucial input for understanding and managing these sedimentary shores.

Lühikokkuvõte

Läänemere idaranniku rannasetete lainepõhine transport

Töös analüüsitakse piki Läänemere idarannikut ja Liivi lahe rannikutel toimuva lainepõhise settetranspordi struktuurseid omadusi. Keskne tööriist on nn potentsiaalne transport, mis on võrdeline randa saabuva laineenergia vooga. Seda hinnatakse klassikalise CERC (Coastal Engineering Research Centre) meetodiga lainete kõrguse, pikkuse ja levikusuuna alusel. Nende lainetuse parameetrite ja Läänemere ning selle suuremate osade lainekliima arvutamiseks aastatel 1991–2021 rakendati hoolikalt kalibreeritud ja valideeritud lainemudelit SWAN ja kaht kvaliteetset tuuleandmestikku, ERA5 ja BaltAn65+. Kolmeastmeline mudel kirjeldas Läänemere avaosa lahutusvõimega 5,5 km, Soome lahe ja Liivi lahe laineid lahutusvõimega 1,8 km ning Liivi lahe lõunaosa ja Läti ja Leedu randasid lahutusvõimega 560 m.

Eri tuultega rekonstrueeritud lainekliima peamised omadused kattusid hästi Läänemere ja Soome lahe avaosas, aga ka Liivi lahes ja Läänemere idaranniku neis piirkondades, kus arvutati settetranspordi omadused. ERA5 tuultega hinnatud lainekõrgused olid Botnia lahes ja Soome lahe keskosas märksa kõrgemad kui need, mis olid arvutatud BaltAn65+ tuulte abil, kuid samas märksa väiksemad Soome lahe rannavööndis. Erinevuse tõenäoline põhjus on tuuleandmestike erinev lahutusvõime. Liivi lahe lainekliima on märksa mahedam, kui Läänemere avaosa või Soome lahe lääneosa lainekliima. Lainetus Liivi lahel on põhiosas värske tuulelainetus. Ummiklaine osakaal on väike. Lained on märksa lühemad (perioodid 2–5 s) kui Läänemere avaosas ja sageli isegi järsemad kui nn küllastunud lainesüsteemid.

Näidati et Läänemere idaranniku >700 km pikkuses setterandade süsteemis Kaliningradi oblastist Pärnu laheni domineerib setete liikumine vastu kellaosuti liikumise suunda. Vaid üksikutes lühikestes lõikudes liiguvad setted kellaosuti suunas. Süsteemi jagavad peaaegu sõltumatuteks setteüksusteks Kolka neem ja Akmenragsi neem Lätis ning lainemurdjad Klaipėda ja Ventspilsi sadamates ja Daugava jõe suudmes. Mitmed looduslikud neemed ja väiksemate sadamate lainemurdjad jagavad need üksused omakorda väiksemateks osadeks.

Setete netotransport Leedu rannikul ja Läti ranniku lõunaosas on tagasihoidlik ja Kura säär on praktiliselt tasakaalus. Seevastu Läti looderannikul tekitavad lained väga intensiivse transpordi Kolka neeme poole. Seal suurem osa liikuvast liivast settib ja vaid väike osa transporditakse ühesuunaliselt Liivi lahte. Transport lõunasse piki Liivi lahe lääne- ja idarannikut on vilkam kui lahe lõunarannikul. Lääne- ja lõunaranniku setteüksused on suured ja enamasti omavahel ühendatud; transport on peamiselt vastu kellaosuti suunda. Seevastu on idaranniku setete süsteem jagunenud paljudeks peaaegu sõltumatuteks osadeks, millest mõnedes käib transport kellaosuti suunas. Aastate lõikes varieerus transport oluliselt ja brutotransport vähenes 1991–2005, kuid kogu arvutuste perioodi 1991–2022 vältel olulisi muutusi ei tuvastatud.

Lõviosa (vähemalt 60%; sageli üle >80%) lainepõhisest settetranspordist kogu Läänemere idarannikul Soome lahe suudmest Kaliningradi oblastini käivitavad lained, mis saabuvad ühest või kahest kitsast ($\pm15°$) suunast – edelast ja loodest. Need suunad aastatel 1991–2022 ei muutunud. Küll aga vähenes paljudes Läänemere idaranniku lõikudes oluliselt loodest saabuvate lainete energia voog. Lainete käivitatud settetranspordi struktuursed omadused ja selged muutused ühest suunast saabuvate lainete omadustes on olulised uued aspektid Läänemere idaranniku funktsioneerimise mõistmisel ja selle ranniku eri osade haldamisel.

Appendix: Publications constituting the thesis

Publication I

Giudici, A., Jankowski, M.Z., Männikus, R., Najafzadeh, F., Suursaar, Ü., Soomere, T., 2023. A comparison of Baltic Sea wave properties simulated using two modelled wind data sets. Estuarine, Coastal and Shelf Science, 290, 108401. https://doi.org/10.1016/j.ecss.2023.108401

A comparison of Baltic Sea wave properties simulated using two modelled wind data sets

Andrea Giudici [a], Mikolaj Zbigniew Jankowski [a,*], Rain Männikus [a], Fatemeh Najafzadeh [a], Ülo Suursaar [c], Tarmo Soomere [a,b]

[a] Wave Engineering Laboratory, Department of Cybernetics, School of Science, Tallinn University of Technology, Estonia
[b] Estonian Academy of Sciences, Tallinn, Estonia
[c] Estonian Marine Institute, Faculty of Science and Technology, University of Tartu, Tallinn, Estonia

ARTICLE INFO

ABSTRACT

We calculated two sets of idealised ice-free wave hindcast data on a high-resolution, three-layer nested grid covering the Baltic Sea, using two different wind datasets (ERA5 and BaltAn65+), to evaluate the performance of the model in the open and sheltered parts of the sea. The highest resolution of the grids is 260 m. The outcome of simulations is compared against the available in-situ measurements. The main statistical properties of the Baltic Sea wave climate as well as the timing and maximum values of extreme significant wave heights are well replicated in the Baltic proper using the 3 nautical mile (nmi) grid. Simulations using BaltAn65+ have a better match with recorded average wave properties while the ERA5 forcing better replicates wave extremes. The largest differences between the two simulations occur in the Sea of Bothnia, Bay of Bothnia and to the east of large islands. Wave climate in the Gulf of Finland is replicated with a resolution of 1 nmi in the open part of the gulf a down to a resolution of 260 m in selected coastal areas. The wave intensity is the largest in the central part of the gulf and decreases towards the coast and from the West to the East. The use of ERA5 winds yields higher wave heights at the entrance of the gulf and in the central part of the gulf along its axis. Simulations using BaltAn65+ winds show higher waves in the nearshore regions.

1. Introduction

Successful coastal management and engineering require comprehensive understanding of the properties of waves and their extremes at various spatio-temporal scales and especially in semi-sheltered regions (Monbaliu et al., 2014). The knowledge of long-term information on wave fields is of paramount importance to ensure safe and sustainable practices in marine and coastal environments (Cooper and McKenna, 2008). Nevertheless, the ever-growing need for this knowledge is still often met with scarce availability of in situ wave measurements both in time and in space in some (remote) regions (e.g., Derkani et al., 2021) and with insufficient temporal and spatial resolution of satellite estimated wave properties in regions with complex shape (Kudryavtseva and Soomere, 2017; Kudryavtseva et al., 2019; Wiese et al., 2018). This situation calls for the use of numerical wave modelling tools as an important component to gather insight to long-term wave information in such areas.

Similar to other parts of the World Ocean, wave measurements are scarce in terms of spatial (and often, temporal) coverage in the Baltic Sea region (Björkqvist et al., 2018b). Numerical modelling is used to provide information about the core wave parameters also in the areas of the Baltic Sea where direct measurements are not broadly available (Siewert et al., 2015; Soomere, 2023). However, numerical modelling comes with certain limitations and risks. These are particularly pronounced in seasonally ice-covered semi-enclosed seas under highly variable atmospheric forcing, such as the Baltic Sea (Tuomi et al., 2011, 2019; Najafzadeh et al., 2021). Complex topography and bathymetry of the Baltic Sea is one of the reasons why the local wave climate is very inhomogeneous (Soomere and Räämet, 2011). Another reason is the specific bi-directional structure of moderate and strong winds (Soomere, 2003).

Wave models, which are run using a grid with resolution of up to 1 nautical miles (nmi) for the entire sea (Björkqvist et al., 2018b; Nilsson et al., 2019), are not always able to account for the irregular shorelines and complex bathymetry in local studies of the northern and north-eastern Baltic, and to resolve wave transformations in specific

areas (Männikus et al., 2022). The largest challenge is the modelling of waves in archipelagos (Tuomi et al., 2014; Björkqvist et al., 2017a, 2018a) where even the wave spectrum has an unusual shape (Björkqvist et al., 2019). The accuracy of the outcome of wave modelling largely depends on the wind fields used. In the Baltic Sea, an extensive mismatch between wave properties estimated using different

high-quality wind forcings has been noted (e.g., Nikolkina et al., 2014).

The purpose of this research is twofold. Firstly, we quantify the differences between the main statistical properties of wave climate evaluated using the same wave model set-up and two sets of contemporary wind information. Secondly, we explore how these differences propagate into relatively sheltered coastal areas. These tasks are
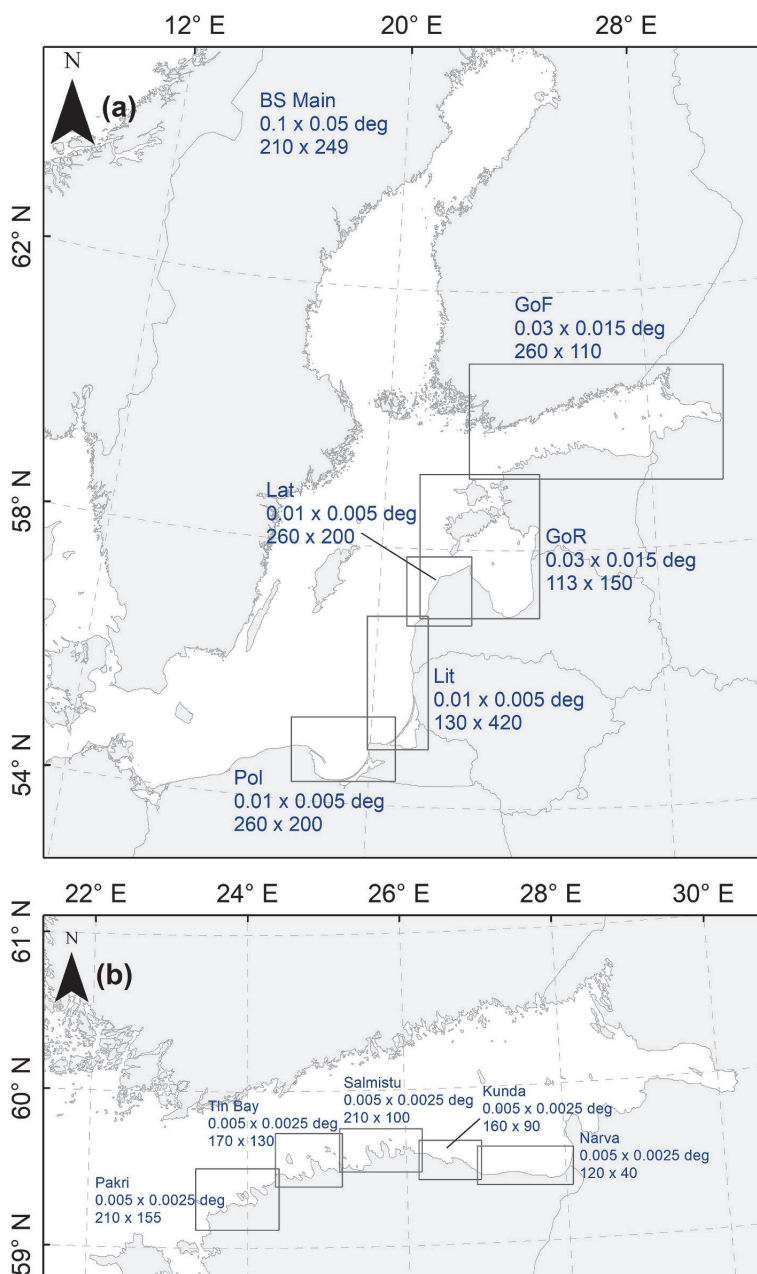
Fig. 1. a) The first and second level grids (boxes) used in the model. The domain BSMain covers the entire Baltic Sea, GoF – Gulf of Finland, GoR – Gulf of Riga, Lat – western Latvia, Lit – Lithuania, Pol – Gdańsk Bay. b) The innermost grids near the southern shore of the Gulf of Finland. The numbers below the name of the grid show resolution in degrees and the number of grid cells in both directions.

addressed by developing a triple-nested wave model using grids with increasing resolution along the nearshore of Estonia, Latvia, Lithuania and Gdańsk Bay (Fig. 1).

As we are specifically interested in the differences in wave properties driven by the two wind fields, we perform calculations for a hypothetical ice-free climate. Therefore, the evaluated properties of wave statistics reflect so-called Type N statistics (Tuomi et al., 2011) that correspond to idealised ice-free conditions during the entire year. While wave properties estimated in this manner reflect reality well in the southern Baltic Sea, they severely (often by a factor of 2) overestimate the impact of waves in the northern part of the sea in terms of annual wave energy flux (Najafzadeh et al., 2022). A side outcome of the analysis is a set of high-resolution time series of wave properties in the nearshore of sedimentary coasts of the eastern Baltic Sea.

Along with addressing similarities and differences in statistics of wave heights in the entire sea, we focus on the open part and southern coast of the Gulf of Finland. On the one hand, this water body has a particularly complex shape and is oriented obliquely with respect to predominant winds. The latter feature leads to the frequent presence of wave fields that are generated in slanted fetch conditions (Pettersson et al., 2010). On the other hand, severe waves excited by strong winds in the Baltic proper often substantially contribute to wave conditions in this gulf. It is therefore likely that differences between wave properties evaluated using two different wind fields and the possible mismatch with in situ measured wave properties are the largest in the coastal area of this gulf. The situation on the coasts of Latvia, Lithuania, Gdańsk Bay and Gulf of Riga will be analysed and reported elsewhere.

The wave properties in the interior of the Gulf of Finland are evaluated in the classic manner. Firstly, wave parameters are calculated for the entire Baltic Sea with a resolution of about 3 nmi ($0.1 \times 0.05°$). The wave properties at the border of the computational area of the Gulf of Finland are used as the boundary conditions for this computational grid. This process is repeated to calculate propagation of waves in the nearshore computational areas.

The wave parameters analysed in this study are calculated for the time frame 1991–2021. This 30-year period is chosen to match the time interval used for the recent WMO climatological normal 1991–2020. It is fully covered by ERA-5 data but involves only 15 years of BaltAn65+ data. The earlier years have very limited in situ wave data. The analysis is concentrated on wave heights and periods, for which it is possible to have validation data whereas more advanced properties, such as wave propagation direction, wave age or cumulative properties of wave fields are not addressed.

We start our paper by describing the wave model and the two wind datasets (Section 2). Section 3 presents validation of the wave model. The main statistical properties of the wave climate in selected areas are covered in Section 4. The results are discussed and main conclusions are formulated in Section 5.

2. Methods

2.1. The wave model SWAN

The wave parameters are calculated using the SWAN wave model, cycle III, version 41.31A. We employ the OpenMP 2.0-compliant version to take advantage of a 24-core processing unit used for this study. The wave model SWAN (Booij et al., 1999) is a third-generation phase-averaged spectral wave model developed at Delft University of Technology. The waves are described via the two-dimensional (2D) wave action density spectrum N, the evolution of which is governed by the wave action balance equation. This equation, in Cartesian coordinates without ambient currents, takes the following form:

$$\frac{\partial N}{\partial t} + \frac{\partial c_x N}{\partial x} + \frac{\partial c_y N}{\partial y} + \frac{\partial c_\sigma N}{\partial \sigma} + \frac{\partial c_\theta N}{\partial \theta} = \frac{S_{tot}}{\sigma}.$$

The terms on the left of this equation represent the rate of change and the propagation of wave energy in 2D geographical space, as well as the modifications in group speed and wave propagation direction caused by variations in depth and depth-induced refraction. The x- and y-components of the group velocity are denoted by c_x and c_y. The propagation velocities in the spectral space, which is defined by the angular frequency σ and the propagation direction θ, are c_σ and c_θ, respectively. Expressions for the spectral velocities can be found in the SWAN technical manual (The SWAN team, 2019).

The core quantity on the right-hand side S_{tot} denotes the sum of all physical processes that represent generation, dissipation or redistribution of wave energy in SWAN. The deep water source terms are the energy input by wind (Komen et al., 1984), the dissipation of waves by whitecapping (Komen et al., 1984), and the nonlinear transfer of wave energy due to four-wave interactions using the Discrete Interaction Approximation (Hasselmann and Hasselmann, 1985).

The model options were set as follows. The whitecapping coefficient δ was set at $\delta = 1$ following Rogers et al. (2003) and Pallares et al. (2014). The shallow-water source terms are the energy dissipation through bottom friction (Hasselmann et al., 1973), dissipation due to depth-induced wave breaking (Battjes and Janssen, 1978) and the nonlinear transfer of wave energy through three-wave interactions using the Lumped Triad Approximation (LTA, Eldeberky et al., 1996). The bottom friction coefficient was set at 0.038 m^2/s^3, as suggested by Zijlema et al. (2012). The parameters α and γ for the depth-induced wave breaking source term were set at $\alpha = 1$ and $\gamma = 0.73$. Following the recommendation of Björkqvist et al. (2018b), we used wind drag parameterisation suggested by Wu (2012), since the default drag description in SWAN Zijlema et al. (2012) led to considerable underestimation of wave heights in Baltic Sea conditions (Björkqvist et al., 2018b). The important limitations of this study are: (i) the model is run without ice information and (ii) it does not include currents and varying water levels. A similar configuration of the SWAN model has shown excellent results in calculations of Baltic Sea wave fields using BaltAn65+ winds, adequate ice information and a flat grid system (Björkqvist et al., 2018b).

We used a three-level nested scheme of rectangular model grids. The first level grid (BSMain, Fig. 1a) covers the entire Baltic Sea at the resolution of 3 nmi (approximately 5500 m). The results are used as boundary conditions for finer second level grids. These cover the Gulf of Finland and Gulf of Riga with a resolution of about 1700 m and part of Latvia and Lithuanian waters, and Gdańsk Bay with a resolution down to about 500 m.

In the Gulf of Finland (Fig. 1b), we used five sub-grids with a resolution from 260 to 560 m to account for varying properties of the coastline and the presence of multiple peninsulas and bays deeply cut into the mainland. The replication of wave properties in the archipelago areas of the northern and north-eastern Gulf of Finland remains challenging even for very high-resolution models with a grid size less than 200 m (Björkqvist et al., 2017a), partially because the wave spectrum has a specific shape in the archipelago (Björkqvist et al., 2019). The bathymetry and geometry of the central, eastern and southern parts of this gulf are much more regular. It is thus likely that a resolution down to 260 m is generally sufficient for an adequate estimation of spatio-temporal variations of waves and coastal processes in this region. The wave spectrum is computed with a resolution of 10° (thus, over 36 directions) and over 32 logarithmically distributed frequencies, in the range 0.05–1 Hz (periods from 1 to 20 s) in all nesting levels of the model.

The bathymetry was taken from the databases of the Estonian Transport Administration and Latvian Institute of Aquatic Ecology, and from the Baltic Sea Bathymetry Database (Baltic Sea Hydrographic Commission, 2013) (http://data.bshc.pro/legal/).

2.2. Forcing wind data

We implement two modelled wind datasets defined on a partially

overlapping time period, to explore the influence of wind forcing on wave properties and statistics. The first dataset, ERA5 reanalysis, is the fifth-generation global atmospheric reanalysis produced by the European Centre for Medium-Range Weather Forecasts (ECMWF) from 1979 to present, with trimestral updates. In this paper, we use the data for the latest WMO climatological standard normals 1991–2020 and extend that to 2021. Compared to its predecessors, ERA5 uses a more recent version of the ECMWF Integrated Forecast System model (IFS 41r2, ECMWF, 2006), with increased temporal output, horizontal and vertical resolutions (1 h, 0.25° and 137 vertical levels, respectively), and several improvements to different parameterisations (e.g., convection and microphysics) and to the data assimilation scheme (Hersbach et al., 2018).

The second wind dataset originates from the ERA-40 and ERA Interim (1979–2005) datasets. Their regionalisation BaltAn65+ for the Baltic Sea, with a spatial resolution of 11 km (Luhamaa et al., 2011), has been made through the atmospheric model HIRLAM-B with a 6 h resolution.

The hourly near-surface *u*- and *v*-components of wind velocity at 10 m are used to compute the wind speed and direction fed into the model. The SWAN model employs tri-linear interpolation of the user-provided information on the given input grid and time instants/windows (The SWAN team, 2019) to develop the necessary information for its spatial grid and internal time step (10 min in this study). To verify the modelled wind data and to remove inconsistencies in the wind data sets, we used wind data from the Finnish Meteorological Institute (FMI). Instantaneous weather observations are available from 2010, and daily and monthly data from the 1960s on the FMI website.

The accuracy of wind reconstruction over partially ice-covered seas crucially depends on the adequacy of the treatment of the presence of sea ice. Both models that were used to produce ERA5 and BaltAn65+ datasets include ice information. While production of ERA5 used an ice information assimilation procedure, the HIRLAM model that was used to produce the BaltAn65+ data set (Luhamaa et al., 2011) basically took ice information "as is" (A. Männik, personal communication, 07.02.2023). Both models employ roughness length that depends on the presence of ice. The roughness length for ice in HIRLAM is taken as constant. The particular value 0.03 m is meant to account for irregularities of natural ice fields (Unden et al., 2002). The roughness length for momentum in ERA5 is assumed to depend on the sea ice

concentration. This is meant to reflect that when the sea has partial ice cover, ice is more likely to be broken up resulting in increased form drag (ECMWF, 2006).

2.3. Wave measurements

The model runs were validated by comparing significant wave heights H_S and peak periods T_p calculated from the wave spectrum at different locations of the Baltic Sea (Fig. 2) with the outcome of in situ measurements. Significant wave height is the most commonly used wave parameter calculated based on the energy spectrum. It coincides almost exactly with the average height of the 1/3 highest waves for Rayleigh-distributed wave fields and matches well the visually observed (average) wave height (Wiegel, 1964, p. 198; Massel, 1989).

Some of the available measurements originate from local campaigns, and only cover a few months while others originate from semi-permanent measurement stations which provide time series spanning several years. The earliest data are from Almagrundet. The longest available measured datasets are those of Pohjois-Itämeri (northern Baltic proper, NBP in the research literature, from 1996) and Suomenlahti (from 2000) and Suomenlinna (from 2016) in the Gulf of Finland.

The data samples retrieved from an echosounder at Almagrundet operated by the Swedish Meteorological and Hydrological Institute (SMHI) and waverider buoys at the listed measurement sites (Tables 1 and 2) are available once in every 0.5–2 h. These devices also provide an estimate of H_S and T_p for certain time intervals as described below. When performing comparisons, modelled wave data were down-sampled in order to match the sampling rate of the measurements.

2.3.1. FMI and SMHI

During the 1970s and 1980s, the FMI wave measurements were generally made once every 3 h with Datawell Waveriders using a 15 min time series with a sampling time of 0.4 s. The wave buoy at Bogskär used a 10 min time series once an hour. Starting from the 1990s, the measurements were made with Datawell Directional Waveriders using a 1600 s time series with a sampling time of 0.78 s. The data were transmitted to the FMI and made public almost instantaneously. One exception was the storm of December 2004, when the data from the operational buoy in the northern Baltic proper was retrieved from the
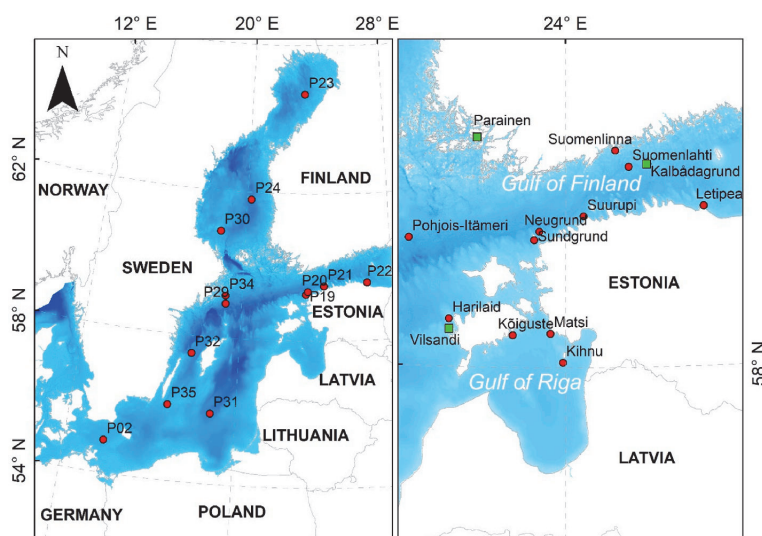
Fig. 2. Wave (red) and wind (green) measurement locations in the Baltic proper and Sea of Bothnia (left) and in the northern Baltic proper (Pohjois-Itämeri) Gulf of Finland and Estonian coastal waters (right). See the description of locations on the left panel in Tables 1 and 2 All stations on the map have been used as calibration data to optimise local performance of the model. However, only selected wave measurement points with good temporal coverage are included in these tables. Graphics by Maris Eelsalu. (For interpretation of the references to colour in this figure legend, the reader is referred to the Web version of this article.)

Table 1

Bias, root mean square difference (rmsd) and correlation coefficient R of the modelled H_S and T_p based on ERA5 winds compared against all the available wave measurements for varied time ranges between 1990 and 2021. The label "C" in column "Nested grid, Panel" corresponds to the innermost high-resolution grids in the southern nearshore of the Gulf of Finland, label "B" to the grid that covers the entire Gulf of Finland and label "A" to the grid that covers the entire Baltic Sea.

Site	H_S (m)			T_p (s)			Nested grid; Panel	Number of data points	Years
	Bias (m)	rmsd (m)	R	Bias (s)	rmsd (s)	R			
Letipea (P22)	0.27	0.32	0.92	−0.78	1.55	0.18	C, Kunda	7,406	2006,2008, 2009,2014
Neugrund (P19)	0.51	0.58	0.76	–	–	–	C, Pakri	3,070	2010
Sillamäe	0.21	0.24	0.87	−1.35	2.23	−0.06	C, Narva	1,033	2009
Sundgrund (P20)	0.35	0.41	0.93	−0.34	1.50	0.40	C, Pakri	1,275	2011
Suurupi (P21)	0.14	0.23	0.94	−0.01	1.48	0.47	C, Pakri	1,274	2011
Suomenlahti	0.10	0.21	0.95	−0.39	1.39	0.59	B, GoF	115,859	2000–2021
Suomenlinna (Helsinki)	0.31	0.38	0.90	−0.17	1.97	0.21	B, GoF	30,558	2016–2021
Pohjois-Itämeri	0.14	0.26	0.97	−0.08	0.94	0.83	A, BSMain	176,019	1996–2021
Perämeri (P23)	0.15	0.25	0.96	0.07	0.65	0.88	A, BSMain	36,403	2012–2021
Selkämeri (P24)	0.17	0.28	0.96	0.09	0.65	0.89	A, BSMain	71,953	2011–2021
Finngrundet (P30)	0.20	0.28	0.95	0.28	0.84	0.81	A, BSMain	93,166	2006–2021
Almagrundet (P34)	0.39	0.51	0.92	–	–	–	A, BSMain	18,526	1990–1995
Huvudskär (P29)	0.25	0.34	0.95	0.28	0.91	0.78	A, BSMain	39,383	2010–2021
Knolls grund (P32)	0.23	0.33	0.95	0.21	1.06	0.73	A, BSMain	67,362	2011–2021
Södra Östersjön (P31)	0.17	0.29	0.97	–	–	–	A, BSMain	33,947	2005–2011
Ölands södra grund (P35)	0.29	0.41	0.94	–	–	–	A, BSMain	70,737	1990–2004
Warnemünde (P2)	0.09	0.20	0.90	0.36	1.06	0.47	A, BSMain	21,454	1998–2002

Table 2

Bias, rmsd, and correlation coefficient R between the measured and modelled H_S and T_p based on BaltAn65+ wind data at selected measurement sites.

Site	H_S (m)			T_p (s)			Nested grid; Panel	Number of data points	Years
	Bias (m)	rmsd (m)	R	Bias (s)	rmsd (s)	R			
Suomenlahti	0.01	0.20	0.94	−0.64	1.62	0.50	B, GoF	20,621	2000–2005
Pohjois-Itämeri	−0.04	0.26	0.96	−0.28	1.04	0.80	A, BSMain	59,360	1996–2005
Almagrundet (P34)	0.22	0.38	0.91	–	–	–	A, BSMain	54,731	1985–1995
Ölands södra grund (P35)	0.15	0.36	0.92	–	–	–	A, BSMain	110,622	1985–2004
Warnemünde (P2)	0.12	0.25	0.88	0.39	1.18	0.45	A, BSMain	21,454	1998–2002

on-board data logger and reported later. The data logger uses a 1320 s time series to calculate the spectrum (Björkqvist et al., 2018b).

SMHI data from various locations (Fig. 2) was retrieved from the SMHI open data portal. One of the longest available measured time series of wave height in the Baltic Sea was from near a lighthouse located at Almagrundet ranges, 1978 to 2003; however, only data from the Simrad device up until 1995 are reliable (Broman et al., 2006). The data is gathered by means of echo-sounders positioned at a depth of 30 m. The measured signal is filtered and the evaluated wave properties are stored with a time resolution of 1 h. This dataset does not include T_p. Instead of H_S, it reports the mean value of the highest one-third of waves, evaluated under the assumption that wave heights are Rayleigh distributed (Broman et al., 2006). Even though this data set has some quality problems, it provides one of the very few options to validate numerically simulated wave parameters against measurements in the 1980s and 1990s.

2.3.2. Estonian Marine Institute

Numerous shorter measurement campaigns using an Acoustic Doppler Current Profiler (ADCP) were carried out in Estonian coastal waters in 2003–2013 (Fig. 2). Some of them are located in the area of the innermost high-resolution grids in the south of the Gulf of Finland (Fig. 1). The instrument evaluates and stores H_S, and also maximum wave height (which usually is approximately 1.5–1.8 times H_S depending on the wave period and the length of the measurement segment), and produces several estimations for wave periods, including T_p. The self-contained upward-looking instrument was deployed at the seabed by divers. The mooring depth varied between 10 and 20 m. More information is given in Suursaar (2013, 2015).

3. Model validation

3.1. Wind validation

Wind measurements at three weather stations, Kalbådagrund, Vilsandi, and Parainen were used to quantify the match of the modelled values in the ERA5 and BaltAn65+ datasets with local wind data. Kalbådagrund is the only measurement location in the Gulf of Finland where the marine wind properties are almost not impacted by the presence of the mainland. For this reason wind information from this site is often used to reconstruct wave properties in the entire Gulf of Finland (e.g., Soomere, 2005). The site at Vilsandi is open to the predominant wind directions and the data from this site are often used as ground truth for the region (e.g., Suursaar and Kullas, 2009). The site at Parainen adds information from the area to the north of the entrance of the Gulf of Finland.

For ERA5, the period of comparison starts in 1991 and ends in 2021. BaltAn65+ wind data is available from 1968 to 2005, however for wind comparison only the period of modelled wave data (1985–2005) is taken into account. The wind properties at Kalbådagrund, Vilsandi, and Parainen are measured at the height of 32 m, 5.5 m and 6 m above sea level, respectively. The suitable height correction factors to reduce the recorded wind speed at Kalbådagrund to the reference height of 10 m are 0.91 for neutral, 0.94 for unstable and 0.71 for stable stratifications (Launiainen and Laurila, 1984). As the atmospheric stability data were not available, to the first approximation, to estimate the speed of wind data at the height of 10 m, the Kalbådagrund wind data is multiplied by a correction factor of 0.85 as suggested in Soomere (2005). The data at Vilsandi and Parainen are used as is.

The match of the basic measured wind properties with simulated data at these locations is almost perfect in terms of monthly means in summer months June and July (Fig. 3). The monthly averages of in-situ
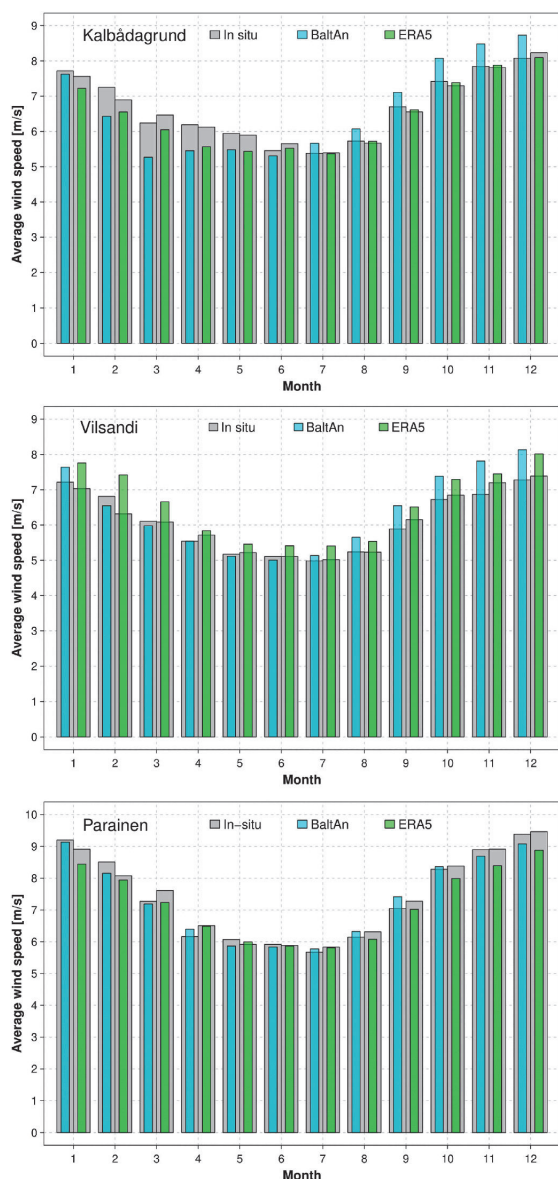
Fig. 3. Seasonal distribution of the average modelled and measured wind speed at Kalbådagrund, Vilsandi, and Parainen. BaltAn stands for BaltAn65+.

data are slightly different due to the various time periods of comparison with ERA5 and BaltAn65+ datasets. For the ERA5 wind data the correlation coefficients for modelled and measured values at Kalbådagrund, Vilsandi, and Parainen have slightly higher values (0.97, 0.97, 1.0, respectively) than BaltAn65+ (0.90, 0.95, 0.99). The difference between the in-situ and the model wind speeds (bias) is on average 0.18, −0.45, 0.24 m/s (for ERA5) and 0.02, −0.30, −0.03 m/s (for BaltAn65+). Positive values indicate that the in situ recorded wind speed (reduced to the height of 10 m at Kalbådagrund) is larger than the modelled counterpart. Overall the BaltAn65+ wind data has lower bias than the ERA5 for all the studied locations.

The modelled data in ERA5 tend to underestimate wind speed throughout the year, most notably at Kalbådagrund and Parainen from January to May (Fig. 3). On the contrary, this data systematically overestimates wind speed at Vilsandi. Similar to the above, wind data in BaltAn65+ also tend to underestimate wind speed at Parainen but overestimate wind speed at Kalbådagrund and Parainen during most of the windy season from August to January. This reconstruction also systematically overestimates wind speed at Vilsandi. Part of this difference may reflect the tuning of data originating from satellite observations for open ocean conditions (Abdalla, 2012) while another part apparently stems from local features at Vilsandi and Parainen.

3.2. Validation of wave properties

The wave properties calculated using the SWAN model were compared with the outcome of measurements at all the available measurement points. The comparison focuses on H_S and T_p. For some locations, the comparison with T_p is omitted as measurements were not available. Table 1 summarizes the comparisons made and shows the average bias, root mean square difference (rmsd) and correlation coefficient for each property, as well as the temporal coverage and resolution of measurements at each location. This comparison is usually insensitive with respect to the representation of sea ice in the wave models because measurement devices (except for the one at Almagrundet) are removed well before the ice season starts.

3.2.1. Significant wave height H_S

For the validation of wave model, the H_S hindcasts are compared with the in-situ measurements in different parts of the Baltic Sea. We only performed the validation of modelled data hindcast using BaltAn65+ (Table 2) for the time period 1985–2005 because of the low number of earlier measurements. The results of validation for both wind forcings represent well the measured H_S in different sub-basins.

The temporal coverage of the ERA5 wind dataset (1991–2021) allows for more extensive data validation especially along the southern coast of the Gulf of Finland (Table 1). The wave hindcasts are compared with in situ measurements at Sundgrund, Letipea, and Suomenlahti in the Gulf of Finland. The locations Sundgrund and Letipea are in the areas covered by the innermost high-resolution grid (C in Table 1) and modelled data from this grid are used for validation. All the comparisons exhibit relatively high correlation coefficients (>0.92). Among these stations Suomenlahti has lower bias (0.10 m) and root mean square difference (0.21 cm), and higher correlation coefficient (0.95). A positive bias means that the wave height or period is overestimated by the wave model. The bias (and rmsd) for Letipea and Sundgrund are 0.27 m (0.32 m) and 0.35 m (0.41 m), respectively. These measurements are for the ice-free time only and thus ignoring sea ice does not impact the results.

The measurements at Suomenlahti cover a longer period of time (2000–2021) with approximately 116,000 data points. This good coverage might be the reason behind the lower bias and rmsd for this location. The model also represents H_S well in the Sea of Bothnia. A comparison of the data from Selkämeri (71,000 measurements) with the ERA5 hindcast resulted in a high correlation coefficient of 0.96, bias of 0.17 m and rmsd 0.28 m. The data for the other station in this basin, Perämeri, also showed similar results (correlation coefficient 0.96, bias 0.15 m) (Table 1). These comparisons may be to some extent affected by the presence of sea ice; however, the measurement devices are routinely removed before the ice season.

In the Baltic proper, the adequacy of H_S reproduction is estimated by means of comparison with the data from Ölands södra grund, with correlation coefficient of 0.97 (bias 0.17 m). This strength of correlation almost exactly matches the one established for the southern part of the Baltic Sea using SWAN model forced by COSMO winds (Sapiega et al., 2023). In the southernmost Baltic Sea, represented by the Warnemünde

station, the hindcast H_S values are compared with in situ data from 1998 to 2002 with ~21,450 measurements. The simulation driven by the ERA5 wind data led to a correlation coefficient of 0.90 and low bias of 0.09 m of the measured and modelled H_S (Table 1). The level of scatter of the modelled and observed H_S is fairly small (Fig. 4).

The bias of H_S hindcast driven by BaltAn65+ winds compared with wave measurements at Suomenlahti was 0.01 m, with a high correlation coefficient of 0.94 (Table 2). A similar very low bias was observed at this location by Björkqvist et al. (2018b). The hindcast using ERA5 resulted in marginally better agreement with the in situ measurements at this site in terms of a slightly higher correlation coefficient (0.97), while it drops to 0.92 for BaltAn65+ wind data at Ölands södra grund. The bias for hindcast forced by ERA5 winds (0.17 m) is slightly higher than for

BaltAn65+ winds (0.15 m), while the rmsd for ERA5 (0.29 m) is considerably lower than for BaltAn65+ (0.36 m). In the southern Baltic proper, at Warnemünde (Fig. 5), the correlation coefficient and bias for BaltAn65+ are 0.88 and 0.12 m, respectively (Table 1). The bias of simulated H_S using either of these wind datasets is positive, except for BaltAn65+ at Pohjois-Itämeri with an average bias of −0.04 m.

Among all the comparisons, the simulation results for Almagrundet in the north-western Baltic proper show the lowest agreement with in situ measurements. It is likely that the difference originates from the relatively low quality of measurements at this location and an alternative way of specification of the estimate of H_S (Broman et al., 2006) rather than from the ignoring of ice in our simulations. Similar results are found by Björkqvist et al. (2018b) who did include ice in their model.
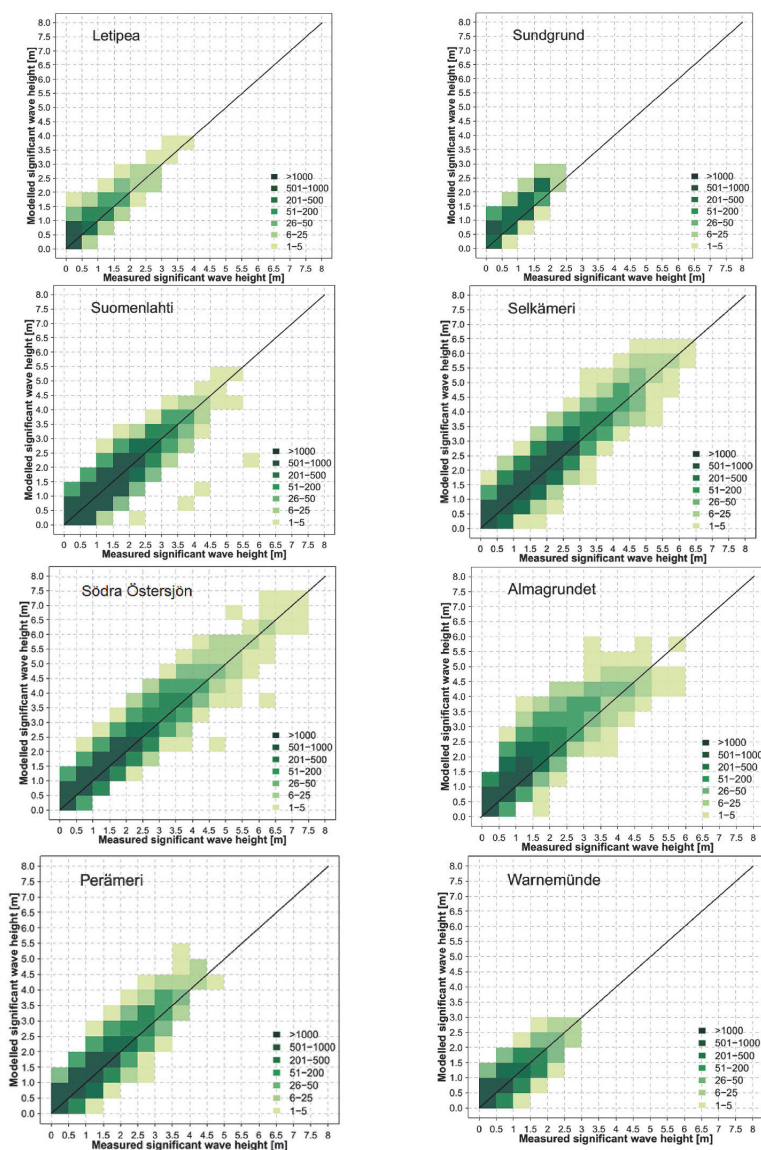
Fig. 4. Comparison of SWAN modelled H_S (forced with ERA5 winds) with measurements at eight locations.
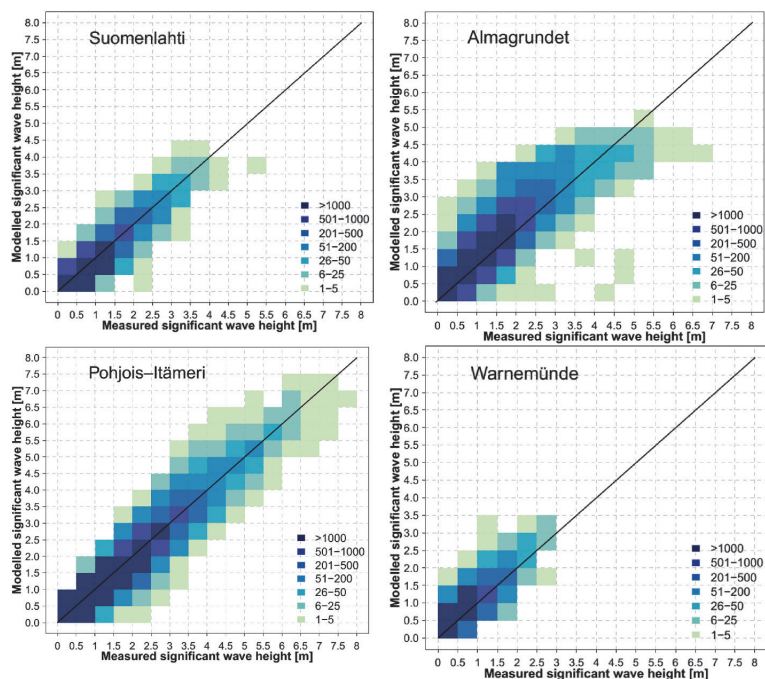
Fig. 5. Comparison of SWAN modelled H_S (forced with BaltAn65+ winds) with measurements at four locations.

There are about 58,000 recorded datapoints in the period 1990–2003. As recommended by Broman et al. (2006), for comparison with the simulated data sets (Figs. 4 and 5), only Simrad data up until mid-September 1995 are used. The modelled H_S values are systematically larger than the recorded values. The reasons for the difference are unclear. The hindcasts driven by ERA5 and BaltAn65+ have almost
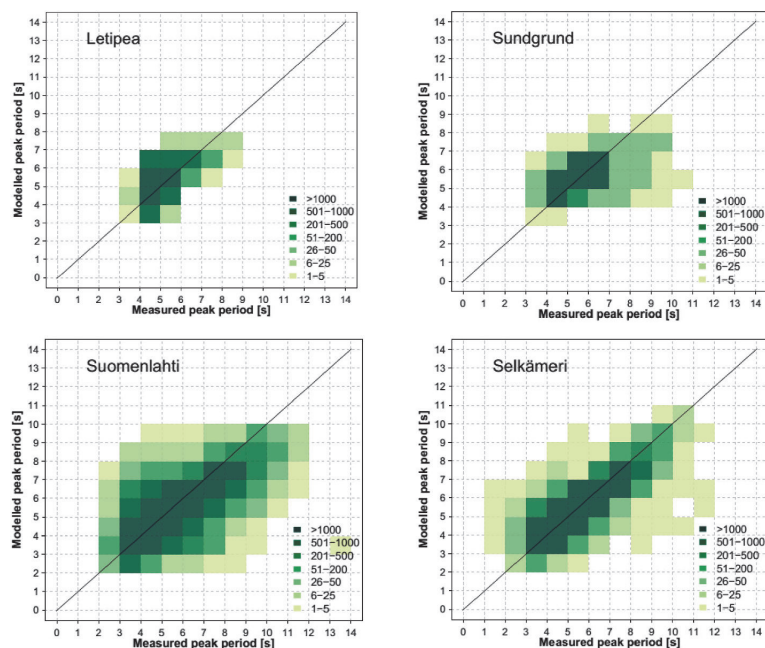
Fig. 6. Comparison of SWAN modelled T_p for the situations where $H_S > 0.5$ m (forced with ERA5 winds) with measurements at four locations.

equal correlation coefficients (0.92 and 0.91, respectively) with the measured data.

3.2.2. Peak period T_p

Although the wave models tend to replicate T_p less precisely than the wave height, the hindcast T_p using ERA5 and BaltAn65+ winds display an overall fair match with the values extracted from observations. The modelled T_p is slightly underestimated for both wind data sets (that is, the bias has negative values, Table 1). The T_p of higher H_S situations are reproduced better. Following Björkqvist et al. (2018b), we choose for validation of modelled T_p only wave situations where $H_S > 0.5$ m (Figs. 6 and 7).

For the ERA5 wind data, the validation of T_p in the Gulf of Finland is performed for three locations: Letipea and Sundgrund using modelled data from the innermost C grid, and Suomenlahti from the 1 nmi grid of the Gulf of Finland (Table 1). The hindcast values of T_p at these locations have a bias of -0.78, -0.34, and -0.39 s, respectively. The modelled T_p at Letipea have the lowest correlation with measured values and thus apparently a lower accuracy than in other locations in this basin. In the Sea of Bothnia, the hindcast T_p at Selkämeri exhibit a good match with the outcome of observations. On the majority of occasions, the T_p is predicted very well. The short data set from Sillamäe during summer with short waves shows larger differences. The bias and rmsd between modelled and recorded T_p reached up to 1.35 and 2.23 s, respectively. The scatter of estimates of T_p from observations and wave models is much larger than for the wave heights (Fig. 6).

The reproduction of T_p by the model forced with BaltAn65+ wind data is slightly less exact than using the ERA5 data. In the Gulf of Finland for Suomenlahti, the bias and rmsd are -0.64 and 1.62 s, respectively, while the overall range of scatter is smaller. In the northern and southern Baltic proper, T_p from observations and modelling are compared at Pohjois-Itämeri and Warnemünde. For Pohjois-Itämeri the majority of the modelled T_p in the range of 3–8 s are aligned well with those from measurements (Fig. 7). The bias and rmsd are -0.28 and 1.04 s,

respectively.

However, for Warnemünde, in most cases the modelled T_p are by about 1 s larger than the ones from in-situ measurements. The data sets from Almagrundet and Södra Östersjön contain estimates of the zero-crossing period and not the T_p. For this reason, the scatter plots are not representative and are not presented here. In general, the accuracy of replication of T_p is reasonable, however it is definitely lower than the accuracy of reproduction of H_S.

4. Statistics of wave heights

4.1. The Baltic proper

Wave field statistics were calculated for each nesting level of the grid system for the entire time period covered by the simulations, and for both wind datasets. Fig. 8 shows results for ERA5 winds 1991–2021. Consistently with the gamut of earlier research, the highest H_S over the entire Baltic proper occur in the Baltic proper in terms of both long-term average and higher quantiles. Lower H_S values occur in semi-enclosed basins (e.g., Gulf of Riga) and in coastal regions where the local features shelter some areas and interactions with the seabed redistribute and/or dissipate part of the wave energy. The results agree with Björkqvist et al. (2018b) who used a longer time interval of simulations.

The differences in local values of spatial distributions of mean H_S and its higher quantiles evaluated using two different models (ERA5 and BaltAn65+) are <0.1 m; however, this is almost 10% of the long-term average H_S in many locations. Only in one isolated location near the eastern boundary of the main grid in Skagerrak, the difference reached 0.9 m. This can be entirely attributed to the uncertainty of the replication of wave parameters at the open boundary of the main grid, and has no statistical relevance. However, the use of ERA5 winds tends to yield higher H_S than BaltAn65+ (Fig. 9), especially for the higher (95th and 99th) percentiles.

When considering the top 1% (99th percentile) of H_S time series,
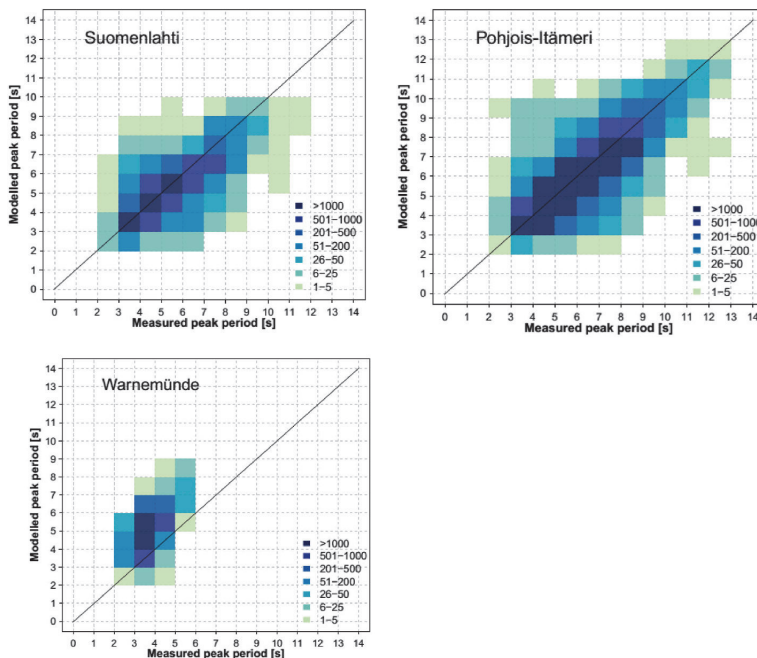
Fig. 7. Comparison of SWAN modelled (forced with BaltAn65+ winds) and measured T_p for the waves with $H_S > 0.5$ m at three locations.
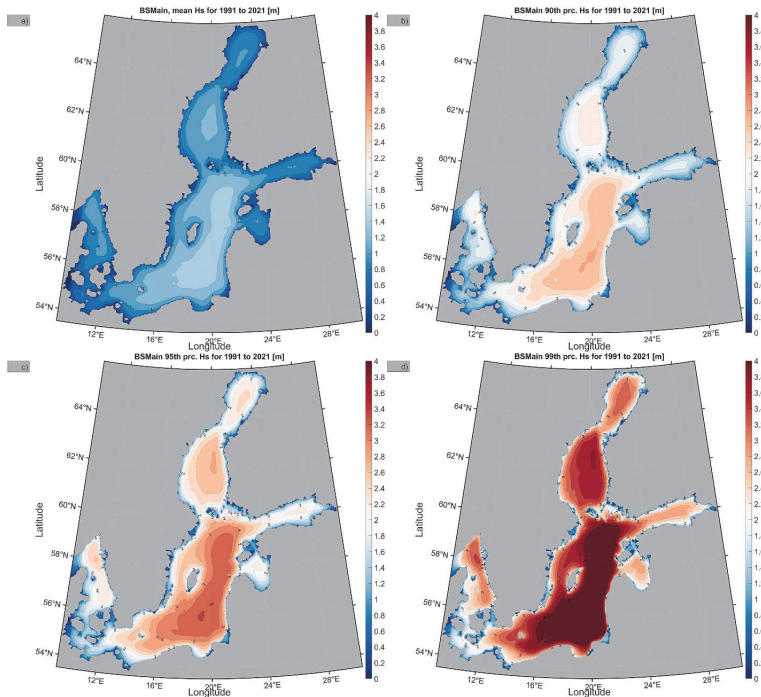
Fig. 8. Spatial distribution of statistical properties of H_S simulated using ERA5 winds for the period 1991–2021: a) mean H_S, b) 90th, c), 95th, d) 99th percentile of H_S. The results agree with Björkqvist et al. (2018b) who used a longer time interval of simulations.

simulations with ERA5 winds produce results which are up to 0.5 m higher in the Sea of Bothnia and Bay of Bothnia than those produced using BaltAn65+. This suggests that ERA5 wind speeds may be higher, or fetch positioned (oriented) so that the associated wind field causes higher waves. There is, however, no systematic difference in mean wind speeds for the two data sets. The above comparison of modelled wind data with measurements suggests that ERA5 has higher speeds in the first half of the year, whereas BaltAn65+ has higher speeds in the second half of the year. As the models replicate the presence of sea ice only in slightly different manners, it is likely that the differences reflect greatly different spatial resolution of wind data in the models rather than the impact of ice.

4.2. The Gulf of Finland

Our simulations produced much weaker North-South asymmetry in the wave properties in the Gulf of Finland than was detected by (Björkqvist et al., 2018b). This feature is not surprising because Björkqvist et al. (2018b) took into account the presence of ice. Ice occurs systematically more frequently and the ice season is longer in the northern part of the gulf compared to its southern part (SMHI, 1982). It is thus natural that the presence of seasonal ice cover amplifies this kind of asymmetry in wave statistics.

The values of average and higher quantiles of H_S are largest in the central part of the gulf and decrease gradually towards the coast and from the West to the East. The lowest values are at mouth of the Neva River where the Saint Petersburg flood protection facility protects the interior of Neva Bight against waves. The maximum of the average H_S occurs in regions where the geometry of the coast allows for maximum wind fetch. Its lower values are located in sheltered areas close to the coast (Fig. 10).

The results obtained using ERA5 and BaltAn65+ forcings have larger relative differences in the Gulf of Finland than in the Baltic proper (Fig. 11). On the one hand, the use of ERA5 winds yields larger wave heights at the entrance of the gulf and in the central part of the gulf along its axis. The highest differences are 0.1–0.15 m for the average H_S and up to 0.3 m for the higher percentiles. On the other hand, simulations using BaltAn65+ wind data show generally higher waves in the nearshore regions. This feature is less evident for the average H_S but the difference reaches about 0.3 m for higher quantiles. As discussed above, it is unlikely that such large differences stem from the differences in the use of ice information in the procedure of development of the two forcings in use. It is more likely that the greatly different spatial resolution of the models and ice information plays a role.

4.3. Replication of extreme events in the Baltic proper

The above analysis demonstrates that the model replicates well the average wave properties and the thresholds for severe wave conditions. From an engineering and management point of view it is crucial that the model is also able to reconstruct wave time series in extreme conditions. Such situations inter alia provide the largest part of wave energy flux to the nearshore (Soomere and Eelsalu, 2014).

Extreme events were selected as those where the H_S exceeds 7 m anywhere in the Baltic Sea. Such occasions occur in the measured data from Pohjois-Itämeri (NBP) once in about 4–5 years (Björkqvist et al., 2017b) but apparently much more frequently in the entire sea. This H_S coincides with the highest value of the 99.9th percentile of H_S.

We identified 28 such storms in the Baltic Sea in the period 1991–2021 within ERA5 coverage, and 15 storms within Balt-An65+ coverage, 1985–2005. The time interval for which both ERA5 and BaltAn65+ data are available (1991–2005) contained 13 such events. All these events took place between the end of September and first week of April. This time period is longer than the period from December to
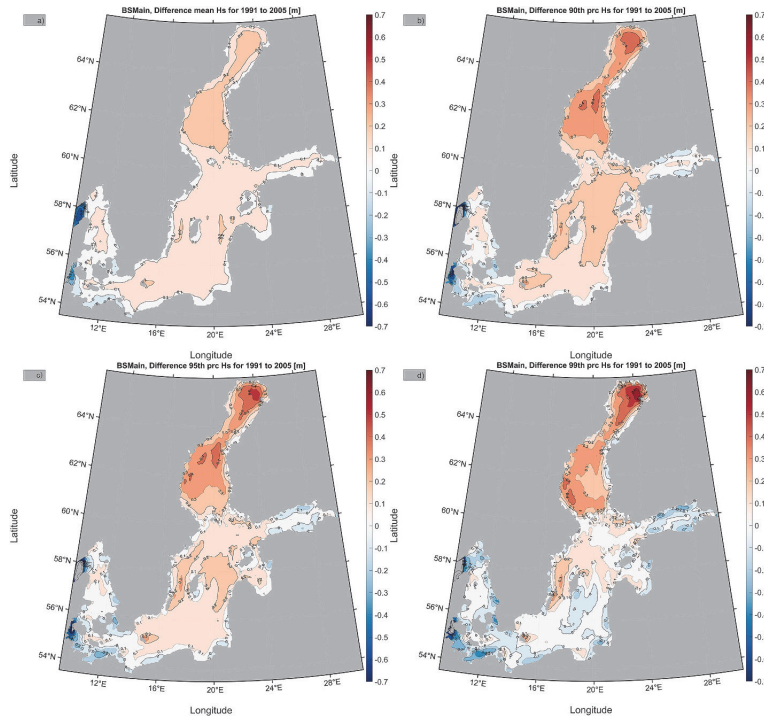
Fig. 9. Difference between H_S in simulations forced with ERA5 and BaltAn65+ in the Baltic Sea. Positive values indicate areas where the use of ERA5 leads to larger values of H_S. a) mean H_S, b) 90th, c) 95th, d) 99th percentile of H_S. Note different time period than that used for Fig. 8.

January that was considered by Björkqvist et al. (2017b) to accommodate most of the extreme events recorded in Pohjois-Itämeri but matches the storm period identified in (Björkqvist et al., 2018b). In simulations with ERA5 wind data, the modelled H_S exceeded 8 m in 10 cases, 9 m in two storms and never reached 10 m. With BaltAn65+ wind data, there as 5, 4 and 1 such instances, respectively.

The highest H_S in simulations with ERA5 and BaltAn65+ wind data were 9.6 m and 10.2 m, respectively, on 04 December 1999 in the southern Baltic Sea. This compares well with Björkqvist et al. (2018b) where a similar maximum of 10.2 m was identified using BaltAn65+ winds. To compare the modelled results with the buoy measurements, we used data from the Pohjois-Itämeri buoy where the highest measured H_S of 7.4 m was recorded twice during this storm (Björkqvist et al., 2017b). The corresponding modelled H_S values were 6.6 m and 7.9 m with ERA5 and 5.8 and 7.3 m with BaltAn65+ (Fig. 12a and b). The correlation coefficient and the rmsd (Fig. 12) show that the ERA5 wind data set provides a better match of H_S maxima for this event.

However, the all-time highest H_S values in the entire Baltic Sea were recorded in storm Rafael on 22 December 2004 (8.2 m, Fig. 12c) and storm Toini on 12 January 2017 (8.0 m). The corresponding modelled values with ERA5 winds are 8.3 m and 6.8 m. Simulations with BaltAn65+ winds showed 7.0 m in 2004. The presented results concerning extreme events agree well with the outcome of previous studies (Björkqvist et al., 2017b) that reflect the outcome of the FMI operational wave forecasts in 2004 and 2017, with grid size of 22 km and 7.4 km (4 nmi), respectively. This feature confirms the common perception of the Baltic Sea wave modelling community that the basic wave properties, including extremes, in the offshore Baltic proper can be adequately represented by relatively low-resolution simulations provided the wind information is adequate (see Soomere, 2023 for discussion and references).

During storm Gudrun (January 2005), the maximum H_S may have reached about 9.5 m (Soomere et al., 2008a). This was an exceptionally long storm in which $H_S > 7$ m was recorded for 17 consecutive hours. The H_S maxima were hindcast to occur in the area between Gotland and northern Lithuania. This estimate is in line with the results shown in Soomere et al. (2008a), Tuomi et al. (2011), and Björkqvist et al. (2018b). The recorded maximum SWH at the FMI NBP buoy was 7.2 m. The modelled maxima were 6.9 m and 7.2 m using ERA5 and Balt-An65+ data sets, respectively (Fig. 12d). For the storm Rafael (and to lesser extent, storm Gudrun), the highest waves obtained with ERA5 data were located in the northern part of the Baltic proper.

4.4. Extremes in the Gulf of Finland

The highest measured H_S in the Gulf of Finland, 5.2 m, was observed for the first time during a south-western storm on 15 November 2001 (https://en.ilmatieteenlaitos.fi/wave-height-records-in-the-baltic-sea). The modelled H_S were 4.2 m and 3.8 m with ERA5 and Balt-An65+, respectively. Although the peak of the storm is slightly underestimated, the rest of this event is modelled accurately (Fig. 12e). This value of H_S, 5.2 m, was also recorded under strong eastern winds in storm Antti in 2012. Here, in contrast, the maximum H_S values were overestimated by the models. Due to a four day long gap in the buoy measurements after the peak of the storm (Fig. 12f), further comparison is not possible. The highest measured H_S in the nearshore of Estonia was 5.11 m at Suurupi during a W-NW storm on 13 December 2013 (Suursaar, 2015).

The T_p were between 10.2 s and 12.3 s at the times when the H_S exceeded 7 m. The T_p at the exact time of the maximum H_S (10.1 m) was 12.3 s. In the Gulf of Finland and Tallinn Bay, the maximum T_p for wave events over 5 m were up to 10.2 s. Extreme waves in this water body thus can be longer than those in the Gulf of Riga or the Bay of Bothnia, where
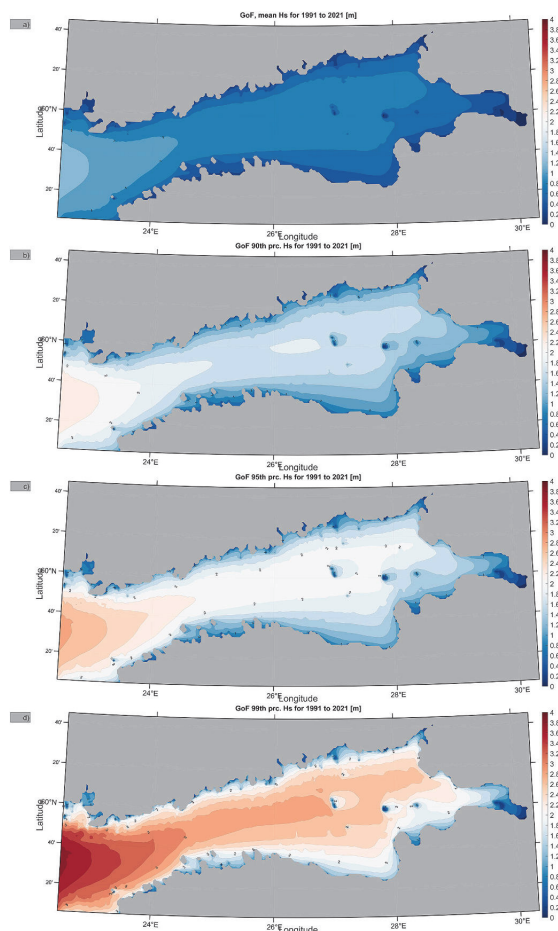
Fig. 10. H_S quantiles in the Gulf of Finland according to simulations using ERA5 winds: a) mean H_S, b) 90th, c) 95th, d) 99th percentile.

the maximum T_p did not exceed 9 s. This apparently occurs because of the propagation of wave energy from the Baltic proper into the Gulf of Finland. In the Sea of Bothnia, the highest T_p reached 11.2 s in the case of the highest waves.

5. Discussion and conclusions

The presented results from running a high-resolution wave model in parallel with two different sets of wind information, ERA5 and Balt-An65+, first of all confirms the well-known perception that contemporary wave models with a medium resolution adequately replicate the main properties of the Baltic Sea wave climate in terms of wave heights and periods, provided the wind information is appropriate. The timing and maximum values of extreme wave heights are also well replicated in the Baltic proper. It is thus expected that both simulations reconfirm the well-known spatial patterns and properties of the Baltic Sea wave fields. Simulations using BaltAn65+ tend to achieve a better match of average wave properties with measurements while the ERA5 forcing leads to better replication of wave height extremes. The match of recorded and simulated wave periods is less accurate than the match of wave heights.

Somewhat surprisingly, the two simulations led to considerable deviations in the mean wave heights, particularly in the higher quantiles of
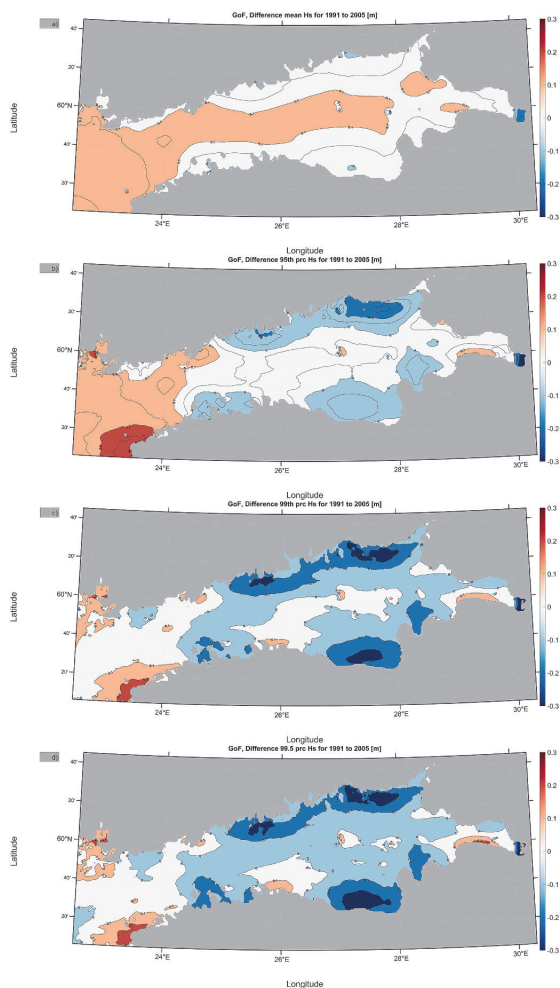
Fig. 11. Difference in the H_S quantiles in the Gulf of Finland estimated using ERA5 and BaltAn65+ for the period of 1991–2005: a) mean H_S, b) 95th, c) 99th, d) 99.5th percentile. Red means that simulations using ERA5 result in higher values than simulations using BaltAn65+. (For interpretation of the references to colour in this figure legend, the reader is referred to the Web version of this article.)

wave heights in some regions. The differences are noteworthy in areas shadowed from predominant westerly winds in regions to the east of large islands, such as Bornholm. This feature apparently stems from the difference in spatial resolution of ERA5 and BaltAn65+ data sets.

The largest differences between the outcomes of the simulations occur in the northernmost Baltic Sea (Sea of Bothnia and Bay of Bothnia). It is unlikely that these differences in fairly large sub-basins are caused by different spatial resolutions of the atmospheric models. As discussed above, the procedures of production of both wind data sets take sea ice into account in a realistic manner. Even though they treat ice somewhat differently, it is also unlikely that the noted differences could stem from differences in the models' way of treatment of ice. This conjecture suggests that there is still room for the improvement of atmospheric models in the northern part of the Baltic Sea.

The situation is different in the Gulf of Finland where wave fields are resolved in the entire gulf at a resolution of 1 nautical mile. The wave
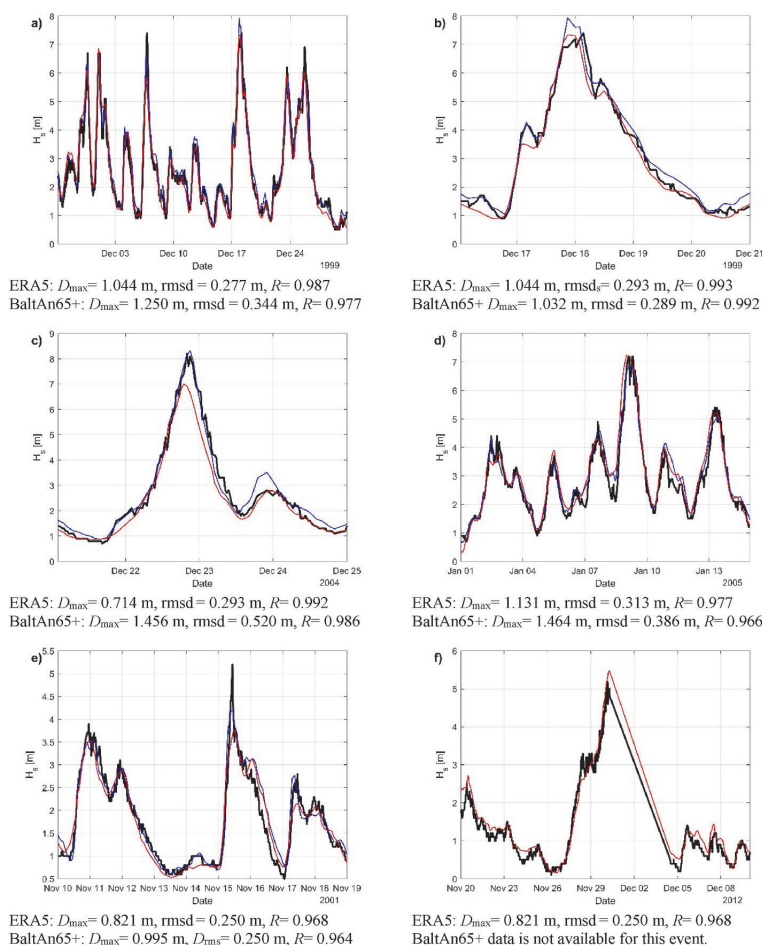
Fig. 12. Comparison of SWAN modelled H_S (forced with both ERA5 and BaltAn65+ winds, whenever available) during storms that created $H_S > 7$ m. a) Pohjois-Itämeri, December 1999, b) Pohjois-Itämeri, December 1999 (detail), c) Pohjois-Itämeri, storm Rafael in December 2004, d) Pohjois-Itämeri, storm Gudrun in January 2005, e) Suomenlahti, November 2001, f) Suomenlahti, storm Antti in November 2012. Black: measured data, blue: simulations using ERA5, red: simulations using BaltAn65+ winds, $D_{\max}$ is the maximum difference between the modelled and measured H_S within the shown time interval and R is the correlation coefficient. (For interpretation of the references to colour in this figure legend, the reader is referred to the Web version of this article.)

intensity in terms of all evaluated properties is the largest in the central part of the gulf and decreases towards the coast and from the West to the East. The North-South asymmetry of wave properties is less pronounced than noted in Björkqvist et al. (2018b).

The use of ERA5 winds yields larger wave heights at the entrance of the gulf and in the central part of the gulf along its axis. The largest differences are 0.1–0.15 m for the average significant wave height and up to 0.3 m for its higher percentiles. Simulations using BaltAn65+ winds show higher waves in the nearshore regions. The difference reaches about 0.3 m, that is, well over 10% for higher quantiles. The may be several reasons for such a difference. A possible explanation is the difference in replication of strong wind directions in this region, a feature that has been discussed for decades in the past (see Soomere et al., 2008b). However, an even stronger reason could be a combination of the asymmetry of properties of sea ice in the Gulf of Finland and the difference in spatial resolutions of the underlying atmospheric models. Large parts of this water body are so narrow (~70–80 km) that the resolution of 30 km at which ERA5 works is at times insufficient to replicate gradients across the gulf.

It is remarkable that the largest systematic difference in the modelled and measured wave heights occurs in nearshore locations, such as Neugrund or Sundgrund in the south of the Gulf of Finland (Table 1). This bias is almost equal to the average wave height during the

measurement period. These sites are located at the entrance to the Gulf of Finland in an area where even small differences in the replication of wind directions may lead to great differences in the observed wave heights because of local sheltering effects.

We also observe massive differences in wave periods in the nearshore of the eastern Gulf of Finland at Letipea and Sillamäe (Table 2). Sediment transport properties crucially depend on the approach angle and length of waves in the nearshore that together govern the impact of refraction on the wave fields. Therefore, large uncertainties in these wave parameters may lead to even larger errors in estimates of the course of coastal processes. This situation suggests that, for the needs of coastal engineering and design, it would be necessary to resolve the identified differences. A first step would be a comparison of modelling results at higher resolution with recorded wave heights at nearshore measurement points over longer time periods.

The major limitation of our study is the use of an idealised ice-free approach. This approach apparently does not affect the results of the validation exercises as most wave measurements used for this purpose were collected in ice-free times. This limitation obviously affects the estimates of climatological wave properties. As shown by Tuomi et al. (2019), ignoring ice (and also uncertainties in the representation of the ice-covered areas), may lead to major differences in spatial distributions of wave properties in strong storms and thus to large changes to such

distributions of higher quantiles of wave heights. Similar large differences are likely for estimates of cumulative wave energy and its flux (Najafzadeh et al., 2022). These quantities are not addressed in our study.

Even though the analysis of Najafzadeh et al. (2022) suggests that the average wave properties over longer time periods (e.g., annual average wave height) for actual and idealised ice-free wave climates for the Sea of Bothnia almost coincide, ignoring ice may lead to substantial differences between estimates at the latitudes of the Gulf of Finland. It is likely that ignoring ice is the main reason why the North-South asymmetry of the wave climate in the gulf is weaker compared to the estimates of Björkqvist et al. (2018b). It is however unlikely that this feature generates fairly large North-South differences between wave climates simulated using the ERA5 and BaltAn65+ wind fields in the Gulf of Finland.

A feasible way to identify the reasons for these differences is to employ more advanced properties of wave climate, such as (the inverse) wave age (e.g., Hanley et al., 2010). The Baltic Sea is relatively small and strong swells are infrequent (Broman et al., 2006) and have fairly short propagation distances in this water body (Björkqvist et al., 2021). It is thus likely that the loss of energy from "old" swells to the atmosphere (Smedman et al., 1999; Grachev and Fairall, 2001) usually insignificantly decreases the height of waves that reach the nearshore. However, an analysis of spatial distributions of wave age is eventually able to more exactly recognise the areas where wind is feeding waves with energy and/or areas where waves may lose considerable amounts of energy (Husain et al., 2022). In other words, systematic analysis of wave age might better quantify differences in the areas covered by strong winds according to different simulated wind data and thus highlight the reasons for reported differences.

There are two main messages from this research. On the one hand, contemporary wave models apparently replicate well wave properties in the open part of the Baltic Sea in ice-free conditions, provided that wind information is adequate and the model itself is properly set up. On the other hand, the situation is more complicated in the largest sub-basins of the Baltic Sea where the use of seemingly almost equivalent contemporary wind data sets leads to considerable differences in several statistical properties of the numerically evaluated wave climate. Consequently, there is room for improvement of the wave models or the wind information in order to adequately reconstruct wave properties in the nearshore and partially sheltered regions of sub-basins of this water body for local applications. A natural extension of our work is to systematically address the "climate" of other properties of waves in the Baltic Sea, such as wave directions, wave age, or the cumulative properties of wave-driven energy flux.

CRediT authorship contribution statement

Andrea Giudici: Software, Resources, Project administration, Methodology, Investigation, Formal analysis, Writing – original draft. **Mikolaj Zbigniew Jankowski:** Visualization, Validation, Software, Investigation, Data curation, Writing – original draft. **Rain Männikus:** Validation, Software, Resources, Methodology, Investigation, Formal analysis, Writing – original draft. **Fatemeh Najafzadeh:** Visualization, Validation, Software, Investigation, Formal analysis, Data curation, Writing – original draft. **Ülo Suursaar:** Resources. **Tarmo Soomere:** Supervision, Project administration, Conceptualization, Funding acquisition, Methodology, Writing – review & editing.

Declaration of competing interest

The authors declare that they have no known competing financial interests or personal relationships that could have appeared to influence the work reported in this paper

Data availability

Data will be made available on request.

References

Abdalla, S., 2012. Ku-Band radar altimeter surface wind speed algorithm. Mar. Geodesy 35 (Suppl. 1), 276–298. https://doi.org/10.1080/01490419.2012.718676.

Baltic Sea Hydrographic Commission, 2013. Baltic Sea Bathymetry Database Version 0.9.3. Downloaded from. http://data.bshc.pro/on 15.02.2020.

Battjes, J.A., Janssen, J.P.F.M., 1978. Energy loss and set-up due to breaking of random waves. Coastal Engineering Proceedings 1 (16), 569–587. https://doi.org/10.9753/icce.v16.32.

Bjorkqvist, J.-V., Tuomi, L., Fortelius, C., Pettersson, H., Tikka, K., Kahma, K.K., 2017a. Improved estimates of nearshore wave conditions in the Gulf of Finland. J. Mar. Syst. 171, 43–53. https://doi.org/10.1016/j.jmarsys.2016.07.005.

Bjorkqvist, J.-V., Tuomi, L., Tollman, N., Kangas, A., Pettersson, H., Marjamaa, R., Jokinen, H., Fortelius, C., 2017b. Brief communication: characteristic properties of extreme wave events observed in the northern Baltic Proper, Baltic Sea. Nat. Hazards Earth Syst. Sci. 17 (9), 1653–1658. https://doi.org/10.5194/nhess-17-1653-2017.

Bjorkqvist, J.-V., Kanarik, H., Johansson, M.M., Tuomi, L., 2018a. A wave forecast for the Helsinki archipelago in the Gulf of Finland. In: 2018 IEEE/OES Baltic International Symposium (BALTIC), June 12–15, 2018, Klaipėda, Lithuania. IEEE OES. https://doi.org/10.1109/BALTIC.2018.8634863.

Bjorkqvist, J.-V., Lukas, I., Alari, V., van Vledder, G.P., Hulst, S., Pettersson, H., Behrens, A., Mannik, A., 2018b. Comparing a 41-year model hindcast with decades of wave measurements from the Baltic Sea. Ocean Eng. 152, 57–71. https://doi.org/10.1016/j.oceaneng.2018.01.048.

Bjorkqvist, J.-V., Pettersson, H., Kahma, K.K., 2019. The wave spectrum in archipelagos. Ocean Sci. 15 (6), 1469–1487. https://doi.org/10.5194/os-15-1469-2019.

Bjorkqvist, J.-V., Part, S., Alari, V., Rikka, S., Lindgren, E., Tuomi, L., 2021. Swell hindcast statistics for the Baltic Sea. Ocean Sci. 17, 1815–1829. https://doi.org/10.5194/os-17-1815-2021.

Booij, N., Ris, R.C., Holthuijsen, L.H., 1999. A third-generation wave model for coastal regions: 1. Model description and validation. J. Geophys. Res. 104 (C4), 7649–7666. doi:10.1029/98JC02622.

Broman, B., Hammarklint, T., Rannat, K., Soomere, T., Valdmann, A., 2006. Trends and extremes of wave fields in the north-eastern part of the Baltic Proper. Oceanologia 48 (S), 165–184.

Cooper, J.A.G., McKenna, J., 2008. Working with natural processes: the challenge for coastal protection strategies. Geogr. J. 174 (4), 315–331. https://doi.org/10.1111/j.1475-4959.2008.00302.x.

Derkani, M.H., Alberello, A., Nelli, F., Bennetts, L.G., Hessner, K.G., MacHutchon, K., Reichert, K., Aouf, L., Khan, S., Toffoli, A., 2021. Wind, waves, and surface currents in the southern ocean: observations from the Antarctic circumnavigation expedition. Earth Syst. Sci. Data 13 (3), 1189–1209. https://doi.org/10.5194/essd-13-1189-2021.

ECMWF, 2006. IFS Documentation – Cy41r2. Operational Implementation 8 March 2016. Part IV: Physical Processes. In: https://www.ecmwf.int/en/elibrary/79697-ifs-documentation-cy41r2-part-iv-physical-processes. accessed 07 February 2023.

Eldeberky, Y., Polnikov, V., Battjes, J.A., 1996. A statistical approach for modelling triad interactions in dispersive waves. Coastal Engineering Proceedings 1 (25). https://doi.org/10.1061/9780784402429.085.

Grachev, A.A., Fairall, C.W., 2001. Upward momentum transfer in the marine boundary layer. J. Phys. Oceanogr. 31 (7), 1698–1711. https://doi.org/10.1175/1520-0485(2001)031<1698:UMTITM>2.0.CO.

Hanley, K.E., Belcher, S.E., Sullivan, P.P., 2010. A global climatology of wind-wave interaction. J. Phys. Oceanogr. 40 (6), 1263–1282. https://doi.org/10.1175/2010JPO43.

Hasselmann, S., Hasselmann, K., 1985. Computations and parameterizations of the nonlinear energy transfer in a gravity-wave spectrum. Part I: A new method for efficient computations of the exact nonlinear transfer integral. J. Phys. Oceanogr. 15 (11), 1369–1377. https://doi.org/10.1175/1520-0485(1985)015<1369:CAPOTN>2.0.CO.

Hasselmann, K., Barnett, T., Bouws, E., Carlson, H., Cartwright, D., Enke, K., Ewing, J., Gienapp, H., Hasselmann, D., Kruseman, P., Meerburg, A., Muller, P., Olbers, D., Richter, K., Sell, W., Walden, H., 1973. Measurements of Wind-Wave Growth and

Swell Decay during the Joint North Sea Wave Project (JONSWAP), vol. 12. Ergänzungsheft zur Deutsche Hydrographischen Zeitschrift, Reihe A.

Hersbach, H., Bell, B., Berrisford, P., Biavati, G., Horanyi, A., Munoz Sabater, J., Nicolas, J., Peubey, C., Radu, R., Rozum, I., Schepers, D., Simmons, A., Soci, C., Dee, D., Thepaut, J.-N., 2018. ERA5 hourly data on pressure levels from 1979 to present. Copernicus Climate Change Service (C3S) Climate Data Store (CDS). https://doi.org/10.24381/cds.bd0915c6.

Husain, N., Hara, T., Sullivan, P.P., 2022. Wind turbulence over misaligned surface waves and air-sea momentum flux. Part I: Waves following and opposing wind. J. Phys. Oceanogr. 52 (1), 119–139. https://doi.org/10.1175/JPO-D-21-0043.1.

Komen, G.J., Hasselmann, S., Hasselmann, K., 1984. On the existence of a fully developed wind-sea spectrum. J. Phys. Oceanogr. 14 (8), 1271–1285. https://doi.org/10.1175/1520-0485(1984)014<1271:oteoaf>2.0.co.

Kudryavtseva, N., Soomere, T., 2017. Satellite altimetry reveals spatial patterns of variations in the Baltic Sea wave climate. Earth Syst. Dyn. 8 (3), 697–706. https://doi.org/10.5194/esd-8-697-2017.

Kudryavtseva, N., Kussembayeva, K., Rakisheva, Z.B., Soomere, T., 2019. Spatial variations in the Caspian Sea wave climate in 2002–2013 from satellite altimetry. Est. J. Earth Sci. 68 (4), 225–240. https://doi.org/10.3176/earth.2019.16.

Launiainen, J., Laurila, T., 1984. Marine wind characteristics in the northern Baltic Sea. Fin. Mar. Res. 250, 52–86.

Luhamaa, A., Kimmel, K., Männik, A., Rõõm, R., 2011. High resolution re-analysis for the Baltic Sea region during 1965-2005 period. Clim. Dynam. 36, 727–738. https://doi.org/10.1007/s00382-010-0842-y.

Männikus, R., Soomere, T., Najafzadeh, F., 2022. Refraction may redirect waves from multiple directions into a harbour: a case study in the Gulf of Riga, eastern Baltic Sea. Est. J. Earth Sci. https://doi.org/10.3176/earth.2022.06.

Massel, S.R., 1989. Hydrodynamics of Coastal Zones. Elsevier, Amsterdam.

Monbaliu, J., Chen, Z.Y., Felts, D., Ge, J.Z., Hissel, F., Kappenberg, J., Narayan, S., Nicholls, R.J., Ohle, N., Schuster, D., Sothmann, J., Willems, P., 2014. Risk assessment of estuaries under climate change: lessons from Western Europe. Coast. Eng. 87, 32–49. https://doi.org/10.1016/j.coastaleng.2014.01.001.

Najafzadeh, F., Kudryavtseva, N., Soomere, T., 2021. Effects of large-scale atmospheric circulation on the Baltic Sea wave climate: application of the EOF method on multi-mission satellite altimetry data. Clim. Dynam. 57 (11), 3465–3478. https://doi.org/10.1007/s00382-021-05874-x.

Najafzadeh, F., Kudryavtseva, N., Soomere, T., Giudici, A., 2022. Effect of ice cover on wave statistics and wave-driven processes in the northern Baltic Sea. Boreal Environ. Res. 27, 97–116. http://www.borenv.net/BER/archive/pdfs/ber27/ber27-097-116.pdf.

Nikolkina, I., Soomere, T., Räämet, A., 2014. Multidecadal ensemble hindcast of wave fields in the Baltic Sea. In: The 6th IEEE/OES Baltic Symposium Measuring and Modeling of Multi-Scale Interactions in the Marine Environment, May 26–29, 2014. IEEE Conference Publications, Tallinn Estonia. https://doi.org/10.1109/BALTIC.2014.6887854.

Nilsson, E., Rutgersson, A., Dingwell, A., Björkqvist, J.-V., Pettersson, H., Axell, L., Nyberg, J., Stromstedt, E., 2019. Characterization of wave energy potential for the Baltic Sea with focus on the Swedish exclusive economic zone. Energies 12 (5), 793. https://doi.org/10.3390/en12050793.

Pallares, E., Sanchez-Arcilla, A., Espino, M., 2014. Wave energy balance in wave models (SWAN) for semi-enclosed domains–Application to the Catalan coast. Cont. Shelf Res. 87, 41–53. https://doi.org/10.1016/j.csr.2014.03.008.

Pettersson, H., Kahma, K.K., Tuomi, L., 2010. Wave directions in a narrow bay. J. Phys. Oceanogr. 40 (1), 155–169. https://doi.org/10.1175/2009JPO4220.

Rogers, W.E., Hwang, P.A., Wang, D.W., 2003. Investigation of wave growth and decay in the SWAN model: three regional-scale applications. J. Phys. Oceanogr. 33 (2), 366–389. https://doi.org/10.1175/1520-0485(2003)033<0366:IOWGAD>2.0.CO.

Sapiega, P., Zalewska, T., Struzik, P., 2023. Application of SWAN model for wave forecasting in the southern Baltic Sea supplemented with measurement and satellite data. Environ. Model. Software 163, 105624. https://doi.org/10.1016/j.envsoft.2023.105624.

Siewert, M., Schlamkow, C., Saathoff, F., 2015. Spatial analyses of 52 years of modelled sea state data for the Western Baltic Sea and their potential applicability for offshore and nearshore construction purposes. Ocean Eng. 96, 284–294. https://doi.org/10.1016/j.oceaneng.2014.12.029.

Smedman, A., Högström, U., Bergström, H., Rutgersson, A., Kahma, K.K., Pettersson, H., 1999. A case study of air-sea interaction during swell conditions. J. Geophys. Res.-Oceans 104 (C11), 25833–25851. https://doi.org/10.1029/1999JC900213.

SMHI, 1982. Climatological ice atlas. Swedish Meteorological and Hydrological Institute, Norrköping, and Institute of Marine Research, Finland.

Soomere, T., 2003. Anisotropy of wind and wave regimes in the Baltic Proper. J. Sea Res. 49 (4), 305–316. https://doi.org/10.1016/S1385-1101(03)00034-0.

Soomere, T., 2005. Wind wave statistics in Tallinn Bay. Boreal Environ. Res. 10 (2), 103–118.

Soomere, T., 2023. Numerical simulations of wave climate in the Baltic Sea: a review. Oceanologia 65 (1), 117–140. https://doi.org/10.1016/j.oceano.2022.01.004.

Soomere, T., Räämet, A., 2011. Spatial patterns of the wave climate in the Baltic proper and the gulf of Finland. Oceanologia 53 (1–TI), 335–371. https://doi.org/10.5697/oc.53-1-TI.335.

Soomere, T., Behrens, A., Tuomi, L., Nielsen, J.W., 2008a. Wave conditions in the Baltic proper and in the gulf of Finland during windstorm Gudrun. Nat. Hazards Earth Syst. Sci. 8 (1), 37–46. https://doi.org/10.5194/nhess-8-37-2008.

Soomere, T., Eelsalu, M., 2014. On the wave energy potential along the eastern Baltic Sea coast. Renew. Energy 71, 221–233. https://doi.org/10.1016/j.renene.2014.05.025.

Soomere, T., Myrberg, K., Lepparanta, M., Nekrasov, A., 2008b. The progress in knowledge of physical oceanography of the Gulf of Finland: a review for 1997–2007. Oceanologia 50 (3), 287–362.

Suursaar, Ü., 2013. Locally calibrated wave hindcasts in the Estonian coastal sea in 1966–2011. Est. J. Earth Sci. 62 (1), 42–56. https://doi.org/10.3176/earth.2013.05.

Suursaar, Ü., 2015. Analysis of wave time series in the Estonian coastal sea in 2003–2014. Est. J. Earth Sci. 64 (4), 289–304. https://doi.org/10.3176/earth.2015.35.

Suursaar, Ü., Kullas, T., 2009. Decadal variations in wave heights off Cape Kelba, Saaremaa Island, and their relationships with changes in wind climate. Oceanologia 51 (1), 39–61. https://doi.org/10.5697/oc.51-1.039.

Zijlema, M., van Vledder, G.P., Holthuijsen, L.H., 2012. Bottom friction and wind drag for wave models. Coast. Eng. 65, 19–26. https://doi.org/10.1016/j.coastaleng.2012.03.002.

The SWAN team, 2019. SWAN Scientific and Technical Documentation. Delft University of Technology version 41.31. Technical Report. http://swanmodel.sourceforge.net/download/zip/. swantech.pdf. downloaded on 10.10.2019.

Tuomi, L., Kahma, K.K., Pettersson, H., 2011. Wave hindcast statistics in the seasonally ice-covered Baltic Sea. Boreal Environ. Res. 16 (6), 451–472.

Tuomi, L., Pettersson, H., Fortelius, C., Tikka, K., Björkqvist, J.-V., Kahma, K.K., 2014. Wave modelling in archipelagos. Coast. Eng. 83, 205–220. https://doi.org/10.1016/j.coastaleng.2013.10.011.

Tuomi, L., Kanarik, H., Björkqvist, J.V., Marjamaa, R., Vainio, J., Hordoir, R., Höglund, A., Kahma, K.K., 2019. Impact of ice data quality and treatment on wave hindcast statistics in seasonally ice-covered seas. Front. Earth Sci. 7, 166. https://doi.org/10.3389/feart.2019.00166.

Unden, P., Rontu, L., Jarvinen, H., Lynch, P., Calvo, J., Cats, G., Cuxart, J., Eerola, K., Fortelius, C., Garcia-Moya, J.A., Jones, C., Lenderlink, G., McDonald, A., McGrath, R., Navascues, B., Nielsen, N.W., deGaard, V., Rodriguez, E., Rummukainen, M., Rõõm, R., Sattler, K., Sass, B.H., Savijärvi, H., Schreur, B.W., Sigg, R., The, H., Tijm, A., 2002. HIRLAM-5 Scientific Documentation.

Wiegel, R.L., 1964. Oceanographical Engineering. Prentice-Hall.

Wiese, A., Staneva, J., Schulz-Stellenfleth, J., Behrens, A., Fenoglio-Marc, L., Bidlot, J.R., 2018. Synergy of wind wave model simulations and satellite observations during extreme events. Ocean Sci. 14 (6), 1503–1521. https://doi.org/10.5194/os-14-1503-2018.

Wu, J., 2012. Wind-stress coefficients over sea surface from breeze to hurricane. J. Geophys. Res. 87 (C12), 9704–9706. https://doi.org/10.1029/JC087iC12p09704.

Publication II

Najafzadeh, F., Jankowski, M.Z., Giudici, A., Männikus, R., Suursaar, Ü., Viška, M., Soomere, T. 2024. Spatiotemporal variability of wave climate in the Gulf of Riga. Oceanologia, 66, 56–77. https://doi.org/10.1016/j.oceano.2023.11.001

OCEANOLOGIA
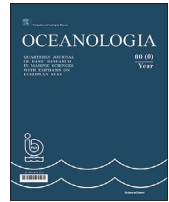
ORIGINAL RESEARCH ARTICLE

Spatiotemporal variability of wave climate in the Gulf of Riga

Fatemeh Najafzadeh [a],*, Mikolaj Z. Jankowski [a], Andrea Giudici [a],
Rain Männikus [a], Ülo Suursaar [c], Maija Viška [d], Tarmo Soomere [a],[b]

[a] School of Science, Tallinn University of Technology, Tallinn, Estonia
[b] Estonian Academy of Sciences, Tallinn, Estonia
[c] Estonian Marine Institute, University of Tartu, Estonia
[d] Latvian Institute of Aquatic Ecology, Riga, Latvia

Abstract Basic properties of wind wave climate in the Gulf of Riga, the Baltic Sea, are evaluated based on modelled wave fields, instrumentally measured and historical visually observed wave properties. Third-generation spectral wave model SWAN is applied to the entire Baltic Sea for 1990—2021 with a spatial resolution of 3 nautical miles (nmi, about 5.5 km) forced by the wind field of ERA5, to the Gulf of Riga and its entrance area with a resolution of 1 nmi (about 1.85 km), and to nearshore areas of this gulf with a resolution of 0.32 nmi (about 600 m). The calculations are performed for an idealised ice-free climate. Wave properties are represented by 36 directional and 32 frequency bins. The simulations are complemented by five sessions of instrumental measurements in the 2000s and two sets of historical visual wave observations from the island of Ruhnu and the Sõrve Peninsula for 1954—2011. Predominantly representing fetch-limited windseas, the wave climate in the gulf is milder and more intermittent than in the open Baltic Sea. The average significant wave height is mostly in the range of 0.6—0.8 m and

peaks at 0.82 m inside the gulf. Typical wave periods are shorter than in the Baltic proper. The spatial pattern of wave heights, with higher wave intensity in the northern and eastern parts of the basin, follows anisotropy in wind conditions. Interannual variations are highly synchronised in different parts of the gulf. Their magnitude is less than 10% of the long-term average wave height. No long-term trend has been found in significant wave height and no distinct decadal variation exists inside the gulf.

1. Introduction

Wave activity may play a particularly important role in driving coastal processes (e.g., erosion, sediment transport) in semi-enclosed marine regions, such as the Baltic Sea (Figure 1) with a total area of 435,000 km^2 (Leppäranta and Myrberg, 2009). Better knowledge of wave properties is needed in many fields, be it port construction, navigation, implementation of offshore electricity generation facilities, or arrangement of insurance (Christensen et al., 2013; Dean et al., 2008; Naulin et al., 2016; Tavakoli et al., 2023).

Several recent studies have produced a fairly good understanding of the main properties of the wave climate and its spatial variations in the Baltic Sea proper (Björkqvist et al., 2018a; Kudryavtseva and Soomere, 2017; Najafzadeh et al., 2021, 2022; Nilsson et al., 2019). During the last decade, this comprehension has been extended to cover the largest sub-basins of this water body, such as the Sea of Bothnia (Björkqvist et al., 2020), Bay of Bothnia (Dvornikov et al., 2017), Arkona Basin (Soomere et al., 2012), and the Gulf of Finland (Björkqvist et al., 2017; Giudici et al., 2023). However, the wave properties in several eastern and southeastern parts of the sea have received less attention and information about the wave climate is scarce in these regions. Therefore, here our focus is on the wave climate of the third largest semi-sheltered sub-basin of the Baltic Sea, the Gulf of Riga (Figure 1).

Figure 1 Map of the study area and the location scheme of visual wave observation sites in the open Baltic Sea and in the Gulf of Riga analysed in the previous research (green circles) (Hünicke et al., 2015) and the sites in the Gulf of Riga (blue pentagons). Red triangles indicate the points where short-term instrumental wave measurements are available. Green pentagram GoR1 is located in an open area of the Gulf of Riga at 23.87°E, 57.7°S. The boxes indicated nested grid areas used in the model. The numbers below the names of the grids show resolution in degrees and the number of grid cells in the East-West and North-South directions.

The water surface area of this gulf is 17,913 km². It has an oval-like shape with a relatively smooth geometry and covers an area of approximately 130 × 140 km (Suursaar et al., 2002). The estimated average depth from the "iowtopo2" version 3 bathymetry (Seifert et al., 2001) is 21 m and the maximum depth reaches 52 m. The 10 m isobath is located approximately 2 km from shore and the 20 m isobath is about 3.5–8 km from the shore along almost the entire Latvian part of the gulf. The northern and northeastern segment of the gulf is even shallower and contains numerous islands and islets. These regions have extensive shallow areas with depths less than 5 m. Also, there is an underwater feature called Gretagrund to the south of the island of Ruhnu. As waves in the Gulf of Riga are relatively short (Eelsalu et al., 2014), the impact of refraction on the wave propagation is comparatively small, except in the north and north-east of this waterbody and in the vicinity of Ruhnu (Männikus et al., 2022), and it is likely that in most occasions waves approach the shoreline at a relatively large angle between the wave propagation direction and the shore normal.

A first-order perception of the predominant winds in the Gulf of Riga can be retrieved from the wind recordings at the neighbouring sites that are open to the Baltic proper. Wind recordings from the island of Vilsandi (Männikus et al., 2020; Soomere and Keevallik, 2001) indicate that moderate and strong winds most frequently blow either from south-west (SW) or north-north-west (NNW). NNW winds are less frequent than SW winds but they may be the strongest (Soomere, 2001). This peculiarity is to some extent supported by an anecdotal observation of extremely high waves near the Daugava River mouth (Davidan et al., 1985). Eastern and south-eastern winds are infrequent and relatively weak (usually below 15 m/s) in the Gulf of Riga.

As the shape of the gulf is comparatively regular, the directional distribution of the local wind properties governs the main features of the wave climate in this gulf. The strongly anisotropic wind climate likely gives rise to a similar anisotropic wave climate: high waves may often occur in its eastern and southern parts and the wave regime along its western coasts is relatively mild.

Due to the semi-enclosed configuration of the gulf and the presence of shallow bays that face the direction of the strongest winds, the water level variability in this gulf is one of the largest in the entire Baltic Sea. The total historical range of water level variations can reach up to 4 m in the narrow and shallow Pärnu Bay (Jaagus and Suursaar, 2013; Männikus et al., 2019). Substantial variations in water depth may lead to notable modifications of wave properties in the relatively shallow northern part of the bay and also impact refraction, shoaling and energy dissipation in the nearshore of the rest of the bay.

The Gulf of Riga is connected to the Baltic proper via Irbe Strait. This strait, with a width of 27 km, provides a channel for waves approaching from the SW into the northern part of the gulf. The sill area between the Kurzeme Peninsula and Sõrve Peninsula is generally less than 10 m deep, except for a narrow 20–22 m deep canyon in its northwestern part. The geometry of Irbe Strait suggests that wave activity in the rest of the Baltic Sea provides a limited contribution to wave fields in the Gulf of Riga. Another outlet, Suur

Strait, connects the gulf with the Väinameri (Moonsund) to the north of the Gulf of Riga. It is relatively narrow (about 4–5 km) and shallow (depths generally less than 5 m). There is very limited wave energy in the shallow Moonsund and thus waves approaching via this strait provide an insignificant contribution to the wave fields in the Gulf of Riga.

Therefore, it is likely that waves (and the parameters of the wave climate) in this basin are usually governed by the local winds and are mostly locally excited. In particular, long-period swell systems are even more infrequent and lower than the ones in the Baltic proper (Björkqvist et al., 2021). This feature provides, inter alia, a unique possibility to identify climatic changes to the meteorological forcing patterns in the gulf by analysing wave patterns or tracking wave-driven alongshore transport (Soomere et al., 2015). Such changes are usually masked by the impact of remote swell on the open ocean coasts.

Current sources of wave data, such as numerical simulations, remote sensing, and in situ measurements have been scarce in the south-eastern and eastern part of the Baltic Sea. Most of the information about wave properties and their temporal changes is extracted from a few simulations with a duration of up to 44 years (Chubarenko et al., 2012; Cieślikiewicz and Paplińska-Swerpel, 2008; Sokolov and Chubarenko, 2020), satellite altimetry and airborne laser scanning (Jahanmard et al., 2022; Kudryavtseva and Soomere, 2016), visual wave observations (Kelpšaitė et al., 2011; Pindsoo et al., 2012; Soomere, 2013) and instrumental wave measurements in the nearshore (Suursaar, 2013; 2015).

All these sources have drawbacks. The wave measurements in the Gulf of Riga are confined to short time series recorded during isolated experiments and long-term hindcasts at those point-measurement locations (Suursaar et al., 2012; Suursaar, 2015). These measurements (Figure 1) are also used to calibrate and verify the SWAN model in this study as described in more detail in Section 2.3. Wave heights retrieved from satellite altimetry are only reliable at a distance of about 0.2° from the shore in the Baltic Sea conditions (Kudryavtseva and Soomere, 2016), that is, restricted to a small area in the central part of the Gulf of Riga.

Being historically an important source of knowledge, visual wave observations inevitably contain an element of subjectivity and uncertainty (Guedes Soares, 1986; Gulev et al., 2003). They have been used to estimate the main properties of wave climate in many areas of the World Ocean in the past (Davidan et al., 1985; Hogben et al., 1986; Hogben and Lumb, 1967). Still, they often fail to properly represent complicated wave fields such as crossing seas or combinations of seas and swells (Badulin and Grigorieva, 2012; Gulev and Hasse, 1999; Orlenko et al., 1984). Observations from ships have poor spatial and temporal resolution, highly variable coverage and extensive gaps (Gulev and Grigorieva, 2006). While observations from the shore characterise only wave properties in the immediate vicinity of the site (Massel, 2013; Soomere, 2013), there have been attempts to establish a connection between visually observed wave height and instrumentally measured ones (Guedes Soares, 1986). Visual observations tend to severely underestimate wave heights compared

to offshore wave properties (Kudryavtseva et al., 2019; Plant and Griggs, 1992).

Methodical visual observations of several storm wave properties in many locations (so-called signal stations) of the Baltic Sea have existed for almost one and a half century (Rosenhagen and Tinz, 2013). Such observations have been performed systematically from the mid-1940s at numerous locations on the shores of the former USSR (Soomere, 2013) using the same routine over almost 70 years (Figure 1). Details of this routine can be found in Soomere and Zaitseva (2007) and Eelsalu et al. (2014). Their results are still the only source for the qualitative representation of the course of wave properties in many segments of the Baltic Sea (Kudryavtseva and Soomere, 2016).

The available visual wave observations in the Gulf of Riga have been critically analysed by Eelsalu et al. (2014) based on two observation sites in Estonian waters. The site on the shore of the island of Ruhnu close to the centre of gulf (Figure 1) represents the waves in this basin well except for a few situations when the island itself shelters the site. Another observation site on the eastern shore of the southern part of Sõrve Peninsula (Figure 1) is sheltered from waves approaching from the SW and NNW, which are the predominant wind directions. Thus, the Sõrve station mostly represents waves that are generated by southern and eastern winds.

The described scarcity both in time and space of in situ and visual wave measurements makes numerical models the most important and useful tool to gather insight about long-term wave information in the Gulf of Riga. Most numerical simulations performed for the Baltic Sea until about 2015 have so far had a spatial resolution of 3—4 nautical miles (nmi) (about 5.5—7 km) (Cieślikiewicz and Paplińska-Swerpel, 2008; Tuomi et al., 2011, 2014). This resolution is insufficient for resolving wave properties in in the Gulf of Riga. Some of these simulations, such as (Räämet and Soomere, 2010) have clearly insufficient spatial and temporal resolution of forcing wind data. Simulations with 3 nmi resolution have indicated that wave-driven transport of coastal sediment in the Gulf of Riga is unusually strong, may contain several convergence and divergence areas (Viška and Soomere, 2013a) and may have a different temporal course compared to that on the shores of the Baltic proper (Viška and Soomere, 2013b).

The wave regime in the Gulf of Riga has been studied numerically by Randmeri (2006) using the third-generation spectral wave model WAM with a resolution of 1 nmi and one-point winds. However, the results have not been published and are not available electronically. The newest simulations of the Baltic Sea wave fields with a spatial resolution of 1 nmi (Björkqvist et al., 2017) or even about 1 km (Nilsson et al., 2019) are focused on other aspects of the Baltic Sea wave climate.

This study attempts to evaluate the main features of the wave climate of the Gulf of Riga, first of all in terms of spatial distributions of significant wave height, its higher quantiles, and extreme wave heights. Further, the frequency of occurrence and joint distribution of wave properties are discussed. We also aim at establishing, to a first approximation, major changes in the wave climate in terms of trends in the wave height in different regions of the gulf. The analysis mostly relies on simulations of time series of wave prop-

erties with a spatial resolution of 1 nmi (about 1.85 km) for 32 years. Simulations with higher resolution have been used to validate the model against local wave data. This is done by using an updated SWAN model setup, which makes use of a nested, high-resolution (~600 m) computational grid, to produce a new, long-term (32 years, 1990—2021) wave hindcast for the Gulf of Riga. We use all available (albeit short-term) wave measurements in this basin to evaluate the performance of the model. In addition, the outcome of simulations is compared with the historical visual wave observations.

The simulations are performed for an idealised ice-free situation. This approach does not affect comparisons of the measured and modelled data sets as measurements have been performed in ice-free time. It may lead to severe overestimation of cumulative wave properties. However, the analysis of Najafzadeh et al. (2022) in the context of the wave climate to the north of the Gulf of Riga suggests that the ignoring of seasonal sea ice insignificantly changes the classic average properties of the wave climate in the Baltic Sea. A comparison of this version of a (future) wave climate with a hindcast that takes into account seasonal ice cover in the gulf will be presented elsewhere.

2. Data and methods

2.1. Wave climate of the Gulf of Riga from visual observations

Procedures of observations of hydrometeorological parameters were unified and described in detail for the observation posts of the former Soviet Union (Guidelines, 1985). Even though the quality of observations (in terms of suitability of the location and accuracy of following the guidelines) was checked regularly, the procedures were apparently not always strictly adhered (Keevallik, 2003). A compact insight into the routine of wave observations, options of the conversion of observed properties into contemporary quantities, and shortages of the relevant procedures and data sets are presented, e.g., in Zaitseva-Pärnaste et al. (2009), Eelsalu et al. (2014), and Kudryavtseva et al. (2019).

Visual observations of wave properties tend to overestimate the wave heights (Massel, 2013) but often realistically represent the temporal course of wave intensity. The visually estimated periods of relatively long waves from oceangoing ships are slightly shorter than the instrumentally measured peak periods (Gulev and Hasse, 1998, 1999). For wave periods <7 s the observations provide estimates that almost exactly match the zero-crossing average wave periods (Davidan et al., 1985). The typical wave periods in the coastal zone of the Baltic Sea are 2—4 s (Broman et al., 2006; Soomere et al., 2012) and thus their visually observed estimates are apparently reliable.

Visual observations of the basic wave properties, such as wave direction, (optionally maximum and mean) wave height and wave period, were performed during 40 years from 1954 until 1995 at Sõrve and during about 50 years (1947—2011, with some gaps) at Ruhnu (Eelsalu et al., 2014). Gaps in observations were frequent during the entire winter and beginning of spring (December—April), and more frequently in January—March. They were associated either
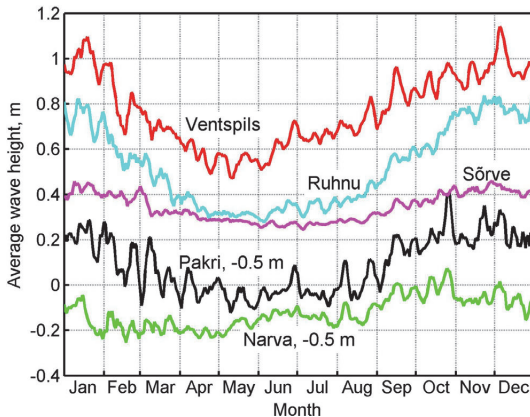
Figure 2 Seasonal variation in the average of visually observed mean wave heights for single calendar days over the period covered by the observations at Ventspils, Ruhnu, Sõrve, Pakri and Narva-Jõesuu. The records from 29 February are merged with the data from 01 March. For better visibility, the Pakri and Narva-Jõesuu data are shifted by −0.5 m concerning the other data sets. From Eelsalu et al. (2014).

with darkness or fog, or with the presence of ice cover. Sea ice is often present in the Gulf of Riga from mid-December until the end of April (Sooäär and Jaagus, 2007). Major gaps eventually because of other reasons exist in 1993—1994 in the Sõrve data set.

The long-term average wave height at the relatively open visual observation site of Ruhnu (0.52 m) is much larger than at Sõrve (0.36 m) (Eelsalu et al., 2014). The reason is that the site at Sõrve is largely sheltered from waves excited by the predominant strong winds and apparently reflects the milder wave regime characteristic to the western part of the Gulf of Riga. The wave climate in the Gulf of Riga is substantially milder than at the eastern coast of the Baltic proper but is similar to that in Narva Bay in the relatively sheltered eastern Gulf of Finland (Zaitseva-Pärnaste et al., 2011). Visually observed wave heights over 2 m are already extreme at the Sõrve station whereas at Ruhnu wave heights exceeding 4 m are not uncommon.

Visually observed wave periods at both sites are concentrated in the range of 2—4 s that are typical for coastal areas of the Baltic Sea (Broman et al., 2006; Soomere et al., 2012). Such short waves are characteristic of relatively small water bodies that are sheltered from long-period swells. Storm conditions with wave height over 2 m at Ruhnu usually have wave periods of 6—7 s. This range of wave periods is characteristic for low swells at Sõrve. Extreme wave storms at Ruhnu may have visually observed wave heights up to 4.8 m and periods 8—9 s (Eelsalu et al., 2014). This wave height represents the average of the five highest waves (not necessarily in a sequence) observed during a 5-min time in the fixed location for wave observations. According to (Guedes Soares, 1986), visually observed values exceed the significant wave height by 15—20%. Therefore, visually recorded waves of this height apparently correspond to significant wave heights about 4 m. Given also that shoaling

may have contributed to the development of the wave field in the observation location, such values are not unrealistic even though wave storms of such intensity have not been instrumentally recorded yet. The directional distribution of visually observed waves has two (at Ruhnu) or three peaks (Sõrve has a tertiary peak for waves approaching from the east) and generally mirrors the two-peak directional structure of moderate and strong winds (Soomere, 2001).

The visually observed wave heights expressed on daily and weekly scales reveal considerable seasonal variation (Figure 2), characteristic to the Baltic Sea. The largest wave intensity is observed in November—January and the lowest in April—July (Eelsalu et al., 2014). This variation is much larger at Ruhnu than in the eastern more sheltered part of the gulf. The wave regime at Sõrve is much similar to the one at Narva-Jõesuu which is also sheltered from part of predominant winds and has a long sea ice season. Interestingly, weekly variations in Figure 2 at Sõrve and Ruhnu are in counter phase on a few occasions (e.g., during the last week of January and February). These occasions reflect differences in the openness of the two sites to different directions. Also, these variations at Ruhnu are sometimes out of phase with similar variations observed at Ventspils (for instance, at the very end of October and clearly in the middle of November). Therefore, the temporal course of wave fields in the Gulf of Riga may reveal several features that do not match those in the Baltic proper.

The variations in the visually observed annual mean wave height at Ruhnu (Figure 3) have only a limited similarity with the similar course on the open coast of the Baltic proper (Liepaja) or at the entrance of the Gulf of Finland (Pakri). Ruhnu and Liepaja data sets reveal a gradual increase in wave activity from the beginning of the 1960s until the mid-1980s. However, short-term interannual variations at these locations are often not synchronised. In particular, in years with relatively low wave intensity at Liepaja and Pakri (1960, 1966 or 1976) the Ruhnu data set shows higher wave activity. The wave height at Ruhnu dropped considerably at the end of the 1980s. A possible reason for this feature is an increase in the frequency of SW winds in the region (Jaagus, 2009; Jaagus and Kull, 2011). However, problems with decreasing quality of observations during the collapse of the Soviet Union may play a role. The wave intensity at Sõrve does not show any substantial changes over the entire time of observation. This feature reflects the sheltered location of the observation site.

Despite suffering from several quality issues, visual wave observations often provide valuable information about wave properties and changes in the wave fields (Gulev and Grigorieva, 2004). Based on this information, it is safe to say that the wave climate in the Gulf of Riga is less severe than the wave regime in the eastern Baltic proper. Waves are generally lower and shorter. While wave properties in the central part of the gulf (at Ruhnu) reveal extensive interannual and decadal variations, wave observations from Sõrve show no substantial variations.

2.2. Instrumental wave measurements

In this study, we use hourly values of significant wave height H_s and peak period T_p of wave fields to validate the SWAN wave hindcast. These properties were measured
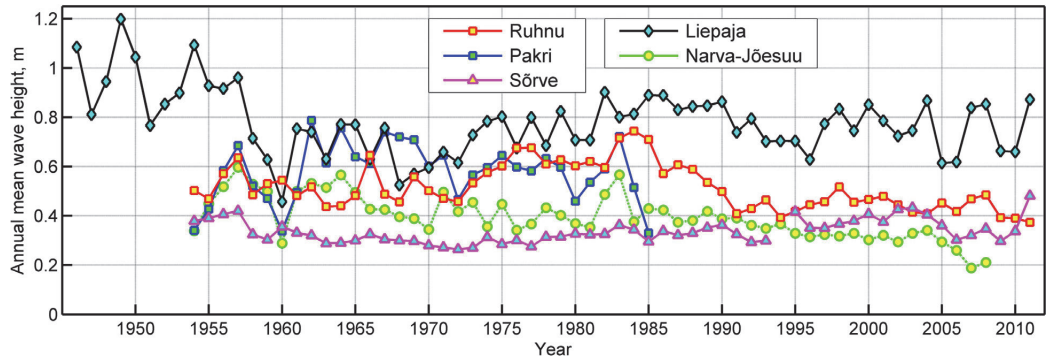
Figure 3   Annual mean visually observed wave height at visual observation sites in the Gulf of Riga (Ruhnu, Sõrve) and Liepaja, Pakri and Narva-Jõesuu. From Eelsalu et al. (2014).

Table 1   The geographical coordinates, water depth of stations, and time intervals of wave measurements in different areas of the Gulf of Riga and at Harilaid. Water depth in the corresponding grid cells of the wave model was estimated using the "iowtopo2" version 3 bathymetry (Seifert et al., 2001) and was in the range of 6—23 m.

Station	Data source	Lon. °E	Lat. °N	Depth (m)	Period of measurements (days)	Number of recordings
Kihnu	EMI	23.95	58.05	11.5	10 Sept 2012—14 May 2013 (247)	5897
Matsi	EMI	23.72	58.33	9.9	13 June—2 Sept 2011 (82)	1941
Kõiguste	EMI	23.02	58.32	12.1	2 Oct 2010—16 May 2011 (227)	5427
Harilaid	EMI	21.82	58.47	13.7	20 Dec 2006—23 May 2007 (155)	3691
					29 July 2013—3 Nov 2013 (98)	2322
Skulte	LHEI	24.36	57.32	15.9	27 July 2020—21 Apr 2021 (269)	6736

using a bottom mounted Recording Doppler Current Profiler (RDCP, RDCP-600 by Aanderaa Data Instruments) operated by Estonian Marine Institute (EMI) in four locations (Suursaar, 2015). A wave buoy (Smartbuoy) was operated at Skulte by the Latvian Institute of Aquatic Ecology (LHEI) (Figure 1, Table 1).

We do not consider recorded wave data during the ice season. For example, at Kihnu data measurements from the beginning of 2013 until April, and from 13 December 2010 at Kõiguste (Suursaar et al., 2012) included near-zero values due to ice cover. As sea ice information is not included in our simulations, we employ only the recordings that are made during the ice-free time for the model validation in the Gulf of Riga.

We also use instrumentally recorded wave data from Harilaid in winter 2006/2007 and autumn 2013 for the validation of SWAN model in the neighbourhood of the study area in the Baltic proper and to compare the properties of waves in the Baltic proper and Gulf of Riga. This site (Figure 1) is in a region where ice is formed much later than in the Gulf of Riga. As will be seen below, the presence of ice in some parts of the sea (Matsi and Skulte) did not distort the match of the modelled and measured wave properties. All time series in Table 1 provide 100% temporal coverage in the sense that the number of recorded wave properties (H_S or T_p) equals the total number of hours during the time interval covered by measurements. Skulte has

the largest number of single recordings (6,736) that cover almost 9 months.

2.3. Wave model setup

Wave properties used in this study were calculated for the time frame 1990—2021 using the SWAN wave model (Booij et al., 1999), cycle III, version 41.31A. It is a third-generation phase-averaged spectral wave model developed and maintained by Delft University of Technology. We employed a three-level nested grid system in spherical coordinates (Giudici et al., 2023). It starts from the (coarse) one that covers the entire Baltic Sea between 9.3° and 30.3° E, and between 53.5° and 65.95° N with 211 × 250 cells (Figure 1). It has a resolution of 0.1° (6') in the east-west direction and 0.05° (3') in the north-south direction, equivalently, about 3 nmi. This grid is used to validate the model against measured wave data in the Baltic proper and to generate boundary conditions for the inner grid. The second (medium-resolution) grid (Figure 1) covers the Gulf of Riga and its vicinity with 113 × 150 grid cells from 21.2° to 24.59° E, and from 56.95° to 59.2° N with a resolution of 0.03° in the east-west direction and 0.015° in the North-South direction. The third level (fine) grids were constructed along the coastline of the gulf. Their resolutions follow the appearance of the geometry and bathymetry of the gulf. The southern side of the Gulf of Riga has a more

or less straight coastline where the resolution of approximately 600 m is enough to replicate spatial variations in the wave properties. The northern side of the gulf and the entire Moonsund have a complicated shape and irregular bathymetry. Hence, grids with a resolution of approximately 300 m were employed (Figure 1).

Extensive calibration of the model was performed using instrumentally measured wave time series from several subbasins of the Baltic Sea (Giudici et al., 2023). The following parameters were addressed: whitecapping coefficient, bottom friction-induced energy dissipation, depth-induced wave breaking, nonlinear transfer of wave energy through three-wave interactions, and the wind drag coefficient. The aim was to reach a model version that would provide acceptable results for the entire Baltic Sea, Gulf of Finland, Gulf of Riga, and for high-resolution nearshore grids along the eastern shore of the Baltic Sea in moderate and strong wind conditions. These parameters were iteratively adjusted in order to maximize the accuracy of the model in selected storms.

The resulting model was used with the following options: the whitecapping coefficient $\delta = 1$ (Pallares et al., 2014; Rogers et al., 2003), the bottom friction coefficient 0.038 m^2/s^3 (Zijlema et al., 2012); the parameters for the depth-induced wave breaking source term $\alpha = 1$ and $\gamma = 0.73$. Wind drag parameterisation was taken from (Wu, 2012), as suggested by Björkqvist et al. (2018a). The default parameters for whitecapping from (Komen et al., 1984) led to the most acceptable results. The presence of currents, varying water levels and seasonal ice-cover was ignored. Further discussion of model details and the rationale behind the configuration choices is detailed in (Giudici et al., 2023) and verification of the model is provided in Section 3.1.

The information about water depths in the Baltic proper was taken from Baltic Sea Bathymetry Database (Baltic Sea Hydrographic Commission, 2013) (http://data.bshc.pro/legal/). The bathymetry data for the Gulf of Riga was

received from Estonian Transport Administration and Latvian Institute of Aquatic Ecology. The resolution of input bathymetry data varied between 50 and 200 m in Estonian waters. In the Latvian waters the input data was coarser: the resolution was 500...1000 m in deeper areas and about 300 m along the coastline. The constructed fine grids thus make full use of the bathymetry data in the Latvian waters and further increase in the resolution of the wave model is not practical.

The wave model was run on this nested grid system in non-stationary mode. For wind forcing, we utilized ERA5 reanalysis, which is a state-of-the-art global atmospheric reanalysis developed by the European Centre for Medium-Range Weather Forecasts (ECMWF). The fifth-generation data set produced by ECMWF from 1979 onwards undergoes trimestral updates. In our study, we employed data that slightly extend beyond the latest WMO climatological standard normals of 1991−2020. Compared to its precursors, ERA5 incorporates a more recent version of the ECMWF Integrated Forecast System model (IFS 41r2, ECMWF, 2006) with increased temporal output, horizontal and vertical resolutions (1 h, 0.25°, and 137 vertical levels, respectively). Additionally, it includes various improvements to different parameterisations (e.g., convection and microphysics) and to the data assimilation scheme (Hersbach et al., 2018).

3. Results

3.1. Comparison of significant wave heights

We have validated the modelled H_S and T_p against all available instrumental wave measurements in and near the study area (Figure 1; Table 2). Since the model hindcast does not include the ice cover, the in situ measurements during the ice season that started from 13 December 2010 at Kõiguste, are eliminated from the validation. Therefore, 1658 single

Table 2 Measured wave properties, bias (measurement minus model), root mean square deviation (RMSD), and correlation coefficient of the wave model at measurement sites at Harilaid and in the Gulf of Riga. The upper row presents estimates for the entire duration of recordings while the lower row represents situations with measured $H_S > 0.5$ m.

Site	H_S (m)					T_p (s)			
	Grid (Figure 1)	ρ	Bias (m)	RMSD (m)	Measured mean H_S (m)	ρ	Bias (s)	RMSD (s)	Measured mean T_p (s)
Kihnu (2012/2013)	Pärnu	0.92	−0.23	0.30	0.67	0.40	0.51	1.21	4.88
		0.83	−0.19	0.28	1.00				
Matsi (2011)	Pärnu	0.92	−0.19	0.24	0.31	0.31	0.83	1.43	4.44
		0.71	−0.12	0.23	0.82				
Kõiguste (2010)	Laim	0.89	−0.29	0.35	0.42	0.20	1.04	1.75	4.99
		0.80	−0.18	0.25	0.94				
Harilaid (2006/2007)	GoR	0.93	−0.35	0.41	0.57	0.62	0.18	1.42	5.55
		0.86	−0.39	0.48	1.03				
Harilaid (2013)	GoR	0.91	−0.16	0.27	0.56	0.56	−0.41	1.46	4.30
		0.89	−0.12	0.27	0.99				
Skulte (2020/2021)	GoR	0.91	0.02	0.19	0.49	0.21	0.36	2.49	3.91
		0.88	0.47	0.62	1.16				
Skulte (2020/2021)	Salac	0.92	0.03	0.20	0.49	0.20	0.38	2.51	3.91
		0.89	0.52	0.67	1.16				
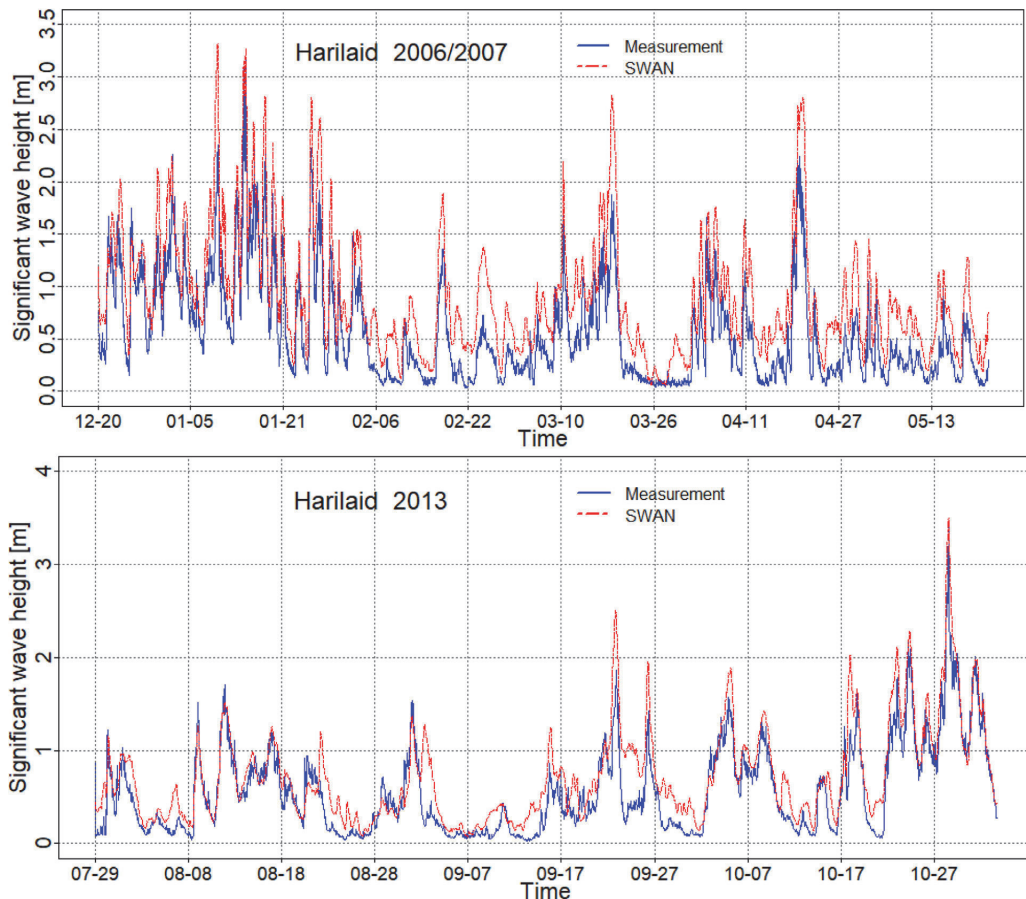
Figure 4 Time series of measured (blue) and modelled (red) significant wave height at Harilaid (Figure 1) in the north-eastern Baltic proper from December 2006 to May 2007 (upper panel) and in July—October 2013 (lower panel).

measurements were used for this purpose. At Kihnu, the wave data after 10 January 2013 include zeros due to the presence of ice cover. These recordings are also omitted from the validation. Thus, 2869 single measurements were employed. The whole data sets at Harilaid, Matsi, and Skulte are recorded during the ice-free period.

The performance of the model in the Baltic proper (equivalently, the quality of information about waves that propagate into the Gulf of Riga from the open Baltic Sea) is estimated using RDCP data at a location in the eastern Baltic proper to the north of the entrance to this gulf (Harilaid, Figure 4).

This location is fully open to the predominant winds and represents well the wave properties in the area for most wind conditions (Suursaar, 2013, 2015). The hindcast for this location is retrieved from a relatively coarse 1 nmi Gulf of Riga grid that also covers the neighbouring areas of the Baltic proper. The match of measured and modelled data is generally good with a correlation coefficient of 0.91—0.93. The modelled wave height almost always follows the

course of measured wave heights. Relative large discrepancies occur between 28 August and 07 September 2013 (Figure 4). The main source of mismatch is probably the influence of complicated bathymetry (including indented coastline, presence of islets, rocks and shallows), which are not ideally captured in the model bathymetry.

The model tends to overestimate wave heights. The average bias (measurement minus model) over the entire period of measurements is −0.35 m in 2006—2007 and −0.16 m in 2013. The root mean square difference (RMSD) varied from 0.41 m to 0.27 m in these years, respectively. The fairly good match at this measurement site in the light of similar estimates of Björkqvist et al. (2018a) suggests that the employed model configuration and wind information are suitable for reconstructing the wave properties at the entrance to the Gulf of Riga.

The wave data in three measurement locations in the northern Gulf of Riga (Figure 5) were retrieved using an RDCP over a range from a few to several months (Table 1). The match of modelled and measured data is better for a
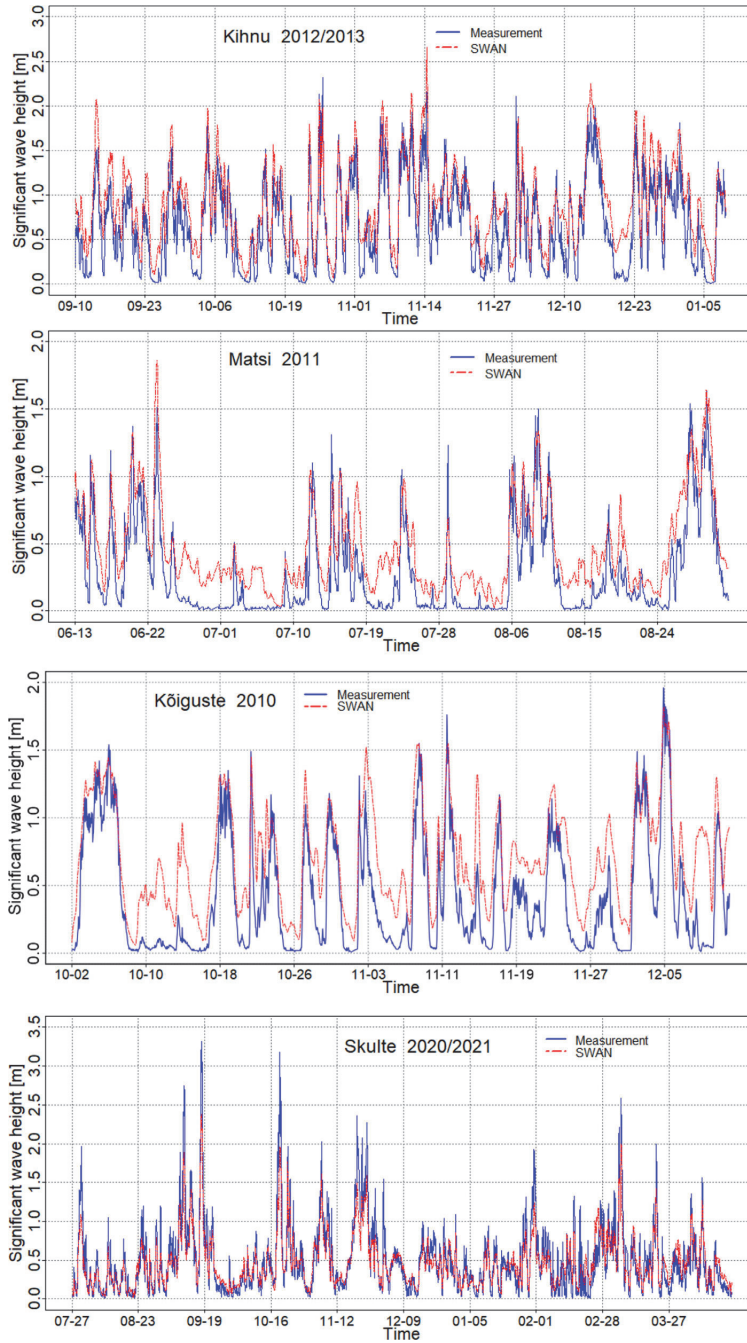
Figure 5 Comparison of the measured (blue) and modelled (red) significant wave height at Kihnu in 2012, Matsi in 2011, Kõiguste in 2010, and Skulte in 2020/2021.

finer-resolution wave model at Kihnu and Matsi. The correlation coefficients for these stations from the grid size of 0.32 nmi (∼600 m, grid called Pärnu) are about 0.92. The bias is lower, in the range of −0.19 to −0.23 m. The RMSD is in the range of 0.24—0.30 m, which is almost the same as for simulations of Björkqvist et al. (2017) for the Gulf of Finland.

The match is less satisfactory for the relatively sheltered area at the south-eastern coast of Saaremaa. The hindcast with the fine spatial resolution (grid called Laim, ∼0.32 nmi, Figure 1) at Kõiguste had a variable match, with the correlation coefficient, bias and rsmd 0.89, −0.29 and 0.35 cm, respectively. The typical mismatch of peaks of wave heights is 10—20 cm at these locations. Higher wave conditions ($H_S >$ about 0.5 m) are reproduced more satisfactorily. Similar to the situation at Harilaid, it is likely that the established differences mainly stem from the complicated bathymetry and geometry of the vicinity of measurement locations. The indented coastline and the presence of islets are accompanied here by numerous rocks and shallows that are not reflected in the existing seabed maps. They are thus often overlooked by the model bathymetry but may sill lead to local variations in wave properties depending on the wave periods and directions.

The situation is different in the southern part of the gulf where in situ wave data are derived from buoy measurements. On average, the hindcast slightly underestimates wave heights (the measurement-model bias is positive) in this part of the Gulf of Riga, at Skulte. The overall course of wave heights is reproduced adequately but the model does not always follow the peak wave heights. The latter feature becomes evident from the comparison of modelled and measured wave situations with $H_S > 0.5$ m. Interestingly, the quality of reproduction of higher waves is better or the same as the replication of all wave conditions at Harilaid, Matsi and Kõiguste while higher waves are reproduced poorly at Skulte. This kind of discrepancy calls for further research and analysis. A comparison of results for the 1 nmi and 0.32 nmi grids at Skulte (Table 2) suggests that the inability of reproduction of relatively severe wave conditions at Skulte does not stem from the insufficient spatial resolution of the inner grid in the area with complicated geometry and bathymetry apparently for the same reasons as discussed above. There is also relatively large bias of reconstructed and measured peak periods (Table 2). These properties have a satisfactory match at Harilaid in the Baltic proper but are poorly correlated in the Gulf of Riga.

3.2. Statistical properties of significant wave heights

The shape of scatter plots of measured and modelled wave heights in the interior of the Gulf of Riga (Figure 6: Kõiguste, Matsi, Kihnu, and Skulte) signals that even though the overall bias between the data sets is fairly small, single values of wave heights can still differ considerably. The correlation coefficients for the two data sets are around 0.92 (Table 2). The relevant Theil-Sen regression coefficients are slightly lower, on the order of 0.91. In four locations the modelled wave heights are slightly overestimated and at Kõiguste several measured wave conditions are much lower

than the associated modelled values. On the contrary, modelled wave heights starting from H_S about 0.5 m are systematically larger than the associated measured values at Skulte. The average bias for such waves is also about 0.5 m (Table 2). The difference between these values increases with the increase in the wave height.

The overall shape of the empirical probability distributions of measured wave heights at all sites in the Gulf of Riga (Figure 7) are characteristic of similar distributions in sheltered coastal areas of the eastern Baltic Sea (Soomere, 2005). About half of the measured wave heights are very low, below 0.25 m, at relatively sheltered Matsi and Kõiguste. This is a typical feature of very sheltered sea areas, such as bays deeply cut into mainland. This part of the distribution is wider at Skulte and Harilaid where more than half of wave events have H_S below 0.5 m. Accordingly, the median H_S is below 0.5 m at Matsi and Kõiguste while it reaches about 0.7 m at Kihnu. Somewhat surprisingly, the median H_S is below 0.5 m also at Skulte even though this area is open to the predominant wind and waves in the Gulf of Riga. The situation is greatly different at Kihnu. The record in this site has a much larger proportion of situations with $H_S > 1$ m whereas the frequency of occurrence of wave heights from 0.25 to 1.25 m varies insignificantly.

The similar distributions for modelled waves are greatly different and resemble analogous distributions in smaller but more open sub-basins of the Baltic Sea such as the Arkona Basin (Soomere et al., 2012). They all qualitatively follow a 2-parameter Weibull distribution with a narrow peak at wave heights 0.25—0.5 m at Matsi and Skulte, at 0.5—0.75 m at Harilaid, and a much wider distribution at Kihnu and Kõiguste. While systematic mismatch of these distributions at the relatively sheltered Matsi and Kõiguste locations may be associated with the complexity of geometry and bathymetry in their neighbourhood, the reasons for the described differences at Kihnu and Harilaid remain unclear. The relevant distributions for Harilaid show also a certain mismatch: the measured data contain a much larger amount of very low waves than the modelled data. As a similar difference is also evident at Skulte, it could be a specific feature of the Gulf of Riga wave climate that is not resolved by the used combination of the SWAN model and its forcing. To understand what exactly causes the described mismatch of modelled and measured wave regimes, wave measurements with better temporal resolution and possibly resolving single waves with periods down to a few tenths of seconds are apparently necessary.

A comparison of visually observed wave heights with their modelled counterparts is not straightforward for several reasons (see Soomere, 2013 and Kudryavtseva et al., 2019 for the relevant discussion). Still, it is natural to expect a qualitative match of statistical properties of observed wave heights and periods with modelled ones as well as some similarity in the course of average wave properties.

The distributions of visually observed wave heights at Ruhnu and Sõrve in the past (Eelsalu et al., 2014) resemble this distribution for measured wave heights at Skulte. Both historical distributions contain about 40% of very low waves (wave height below 0.5 m) and 35% of waves in the range of 0.5—1 m (Eelsalu et al., 2014). These differences more likely stem from the features of visual observations rather than from ignoring the ice cover in simulations.
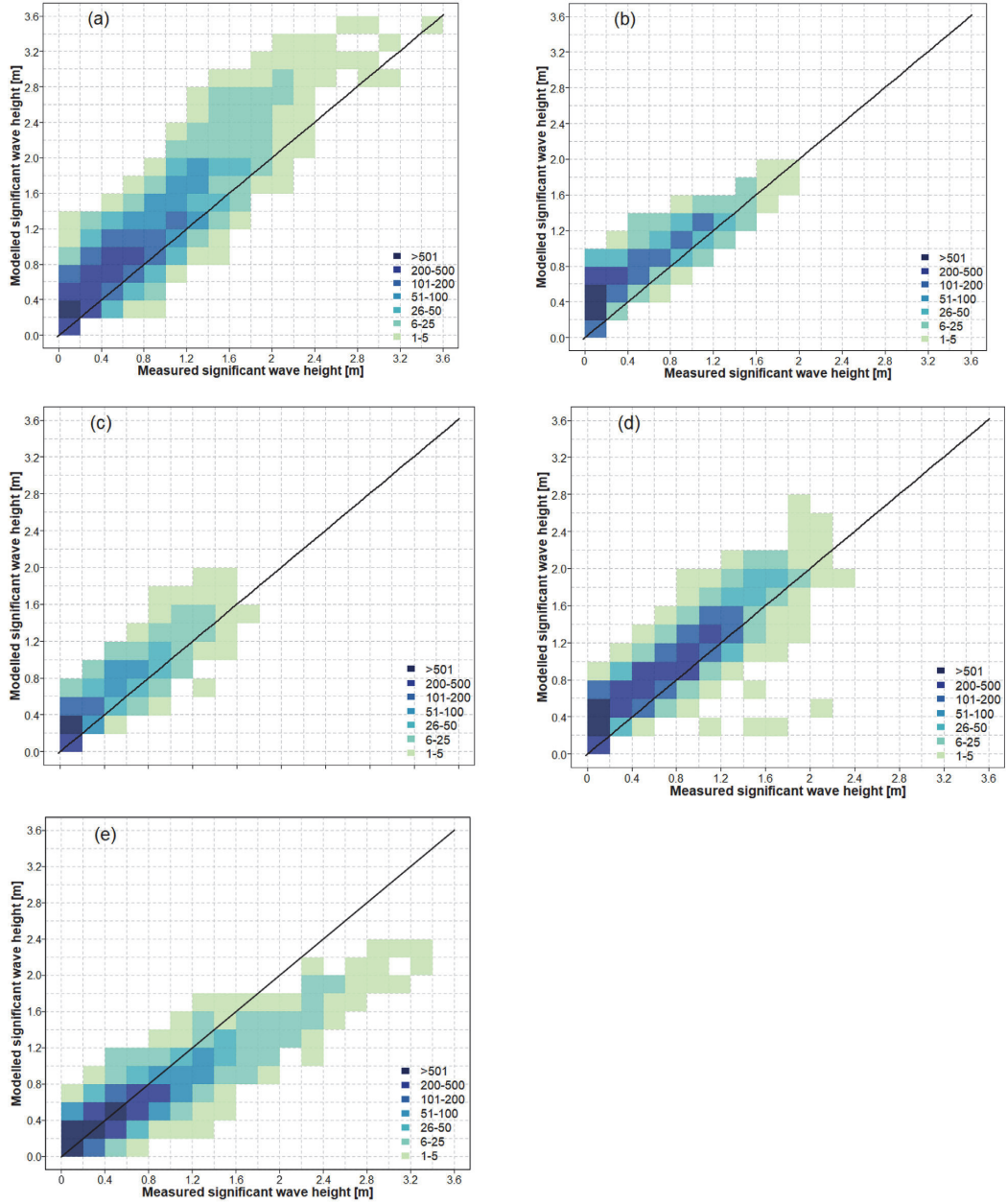
Figure 6 Comparison of the measured and modelled significant wave heights for Harilaid (a), and four measurement sites located in the interior part of the Gulf of Riga; Kõiguste (b), Matsi (c), Kihnu (d), and Skulte (e).

Direct comparisons of visually observed wave properties with similar instrumental records are complicated on the latitudes of the Gulf of Riga. During relatively calm spring and autumn often three observations per day is possible. Therefore, the calmer part of the wave climate is properly reproduced in the observations. However, most wave storms occur during the autumn and winter seasons with relatively limited daylight time when often only one observation per day is possible. It is thus highly likely that a large part of heavy wave conditions are missing from observation records. This perception is supported by the outcome of a comparison of visually observed wave heights
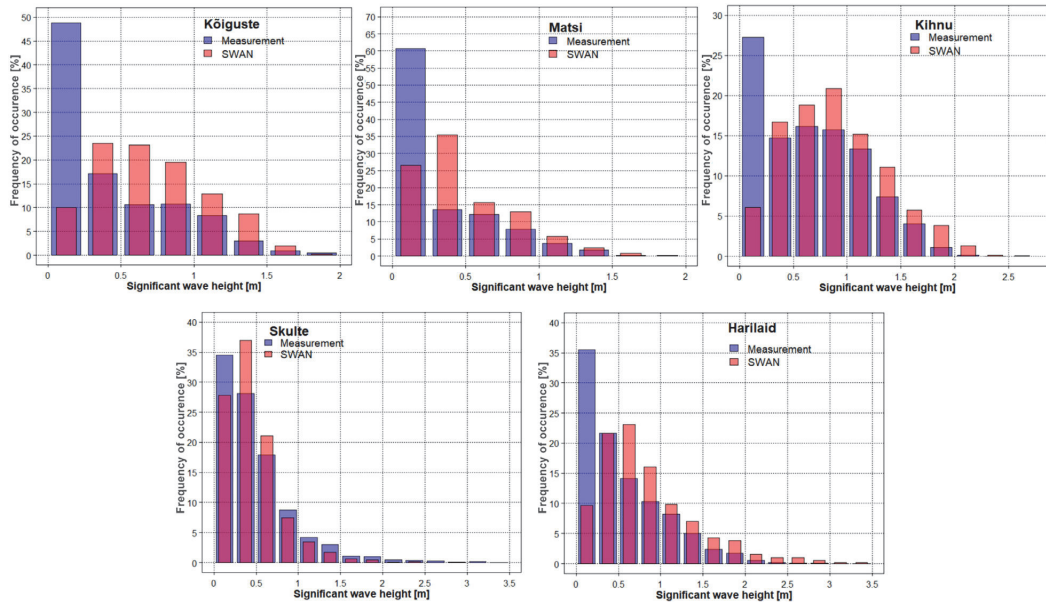
Figure 7 The empirical probability of occurrence of measured (blue) and modelled (red) wave situations at Harilaid and in four locations in the Gulf of Riga. The modelled data sets only represent the time interval covered by observations.
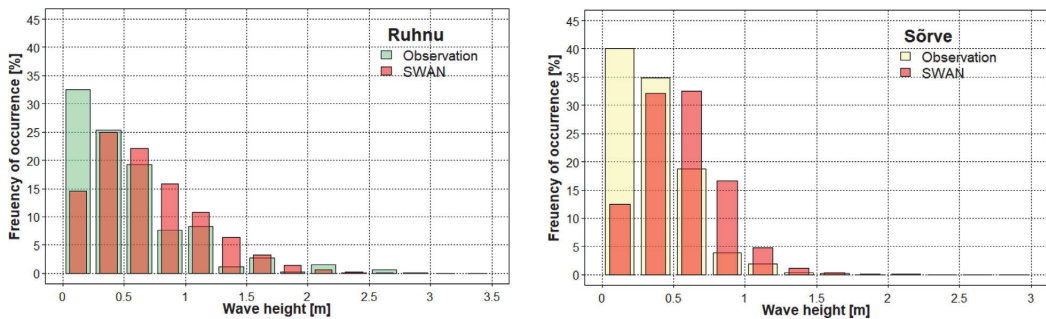
Figure 8 Comparison of the frequency of occurrence of all modelled significant wave heights and visually observed wave heights at Ruhnu (green) and Sõrve (yellow). Bars in the distributions of visually observed wave properties show the simple arithmetic mean of all observations in a single day (Eelsalu et al., 2014). As diurnal variations of wave parameters are almost negligible in the Baltic Sea (Soomere et al., 2012), it is likely that the daily average wave heights adequately represent the wave regime at the sites in question.

from the Caspian Sea shores with satellite-derived wave heights. A direct comparison of the visually observed and satellite-derived wave height records is almost meaningless as it reveals a discrepancy that is larger than the typical wave height. The RMSD between the two sets of records ranges from 0.8 m to 1.1 m in the Caspian Sea conditions (Kudryavtseva et al., 2019) where the average wave height is around 1 m (Lebedev and Kostianoy, 2008). The situation could be a little bit better in comparisons of visually observed and numerically modelled wave heights.

However, Kudryavtseva et al. (2019) demonstrate that already monthly averages of visually observed wave heights may reasonably correlate with the outcome of satellite-

derived information. This feature suggests that a comparison of visually observed wave properties averaged over longer periods with the outcome of numerical simulations may provide reliable additional information about wave climate and its changes.

It is expected that visual observations from the shore provide systematically lower wave heights compared to various estimates of offshore or even nearshore wave heights (unless waves exert strong shoaling). This feature is likely more pronounced for our simulations that ignore the presence of sea ice. This difference is about 50% of the modelled wave heights (Figure 9). Even though there is some similarity in the course of the annual average of visually observed
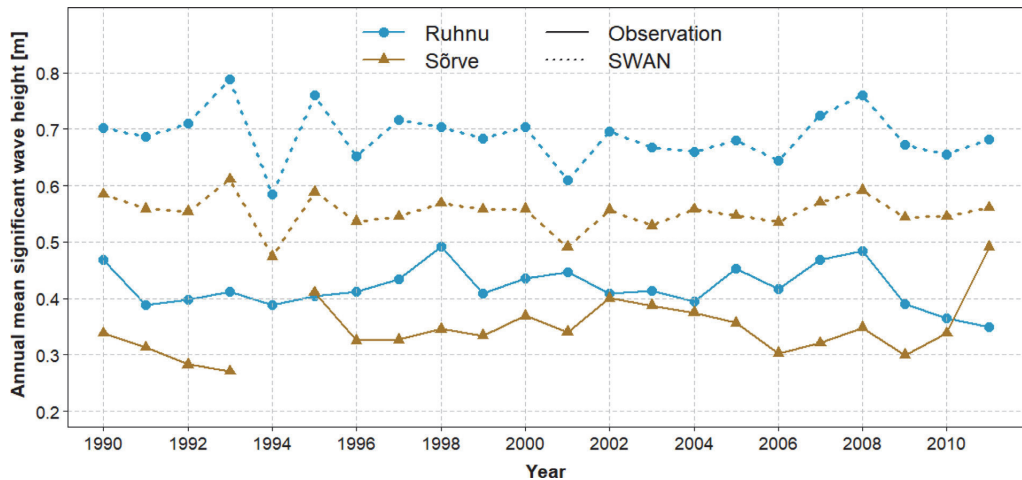
Figure 9   Annual average of visually observed and modelled wave height at Ruhnu and Sõrve.

and modelled wave heights at Ruhnu and Sõrve, the match of these two data sets is poor. Similar to the above, it is likely that the mismatch largely stems from the shortages of visual wave observations.

3.3. Peak periods

The empirical probability distributions of wave periods in the Gulf of Riga exhibits a bell-shape curve around the modal value, resembling a more or less symmetric, Gaussian-like pattern around its maximum (which is also typical for the ocean waves; e.g., Massel, 2013). The most frequent recorded periods are 3–4 s at Skulte, 3–5 s at Matsi and 4–5 s at Kihnu and Kõiguste. The modelled distributions are skewed towards shorter periods at all locations in the interior of the gulf and also considerably underestimate wave periods, especially at Kõiguste. Wave data at Skulte contain numerous estimates of peak periods >10 s. The relevant wave heights are very small. The average wave height of wave fields with peak periods ≥10 s is about 11 cm. For an observer, this is an almost perfectly calm sea surface. As even higher periods are unrealistic, wave fields with periods ≥12 s have been omitted in the analysis.

The distributions of measured and modelled periods match each other well at Harilaid in the Baltic proper. Both distributions resemble the typical shape of such distributions in the Baltic proper. It is therefore likely that the model used in this study appropriately reconstructs the statistics of wave periods in the open part of the gulf and that the mismatch of the modelled and measured periods stems from the inability of this model to replicate wave properties in the northern part of the gulf that has complicated bathymetry and geometry.

The distribution of modelled wave periods in the interior of the Gulf of Riga, first of all at Skulte (Figure 10) matches well the distributions extracted from visual observations (Figure 11). The visually observed wave periods are concentrated between 2 and 4 s both in Sõrve and Ruhnu (Eelsalu et al., 2014). This distribution is narrow and neg-

atively skewed at Sõrve but wider and positively skewed at Ruhnu (Eelsalu et al., 2014). It is likely that the latter feature reflects local wave conditions in the vicinity of the Sõrve observation site. Wave periods longer than 6 s are very rare in the visually observed and modelled data but abundant in the RDCP data. Likely, such occasions are very low-wave situations that originate from the Baltic proper. As such wave conditions are not easy to recognise by the naked eye, they have not been recorded in visual observations.

The performed analysis signals that even though there may be considerable differences in average properties and in the shape of statistical distributions that reflect the wave climate, the performed simulations satisfactorily replicate the course of wave heights in single locations and provide reasonable estimates of average wave heights throughout measurement campaigns. The match of simulated and recorded wave periods is poor; however, the typical values of periods and the shape of distributions of wave periods are replicated adequately.

3.4. Spatial variations in the wave climate

We start the description of the simulated idealised wave climate in the Gulf of Riga from the patterns of long-term average significant wave height (H_S) in its different regions. The wave climate in this water body is milder than in the neighbouring areas of the Baltic proper (Figure 12). As expected based on the properties of predominant winds in the region, waves are systematically higher in the central and eastern parts of the gulf. While the East-West asymmetry is fairly modest, the South-North asymmetry is much more pronounced. Most of the interior of the gulf has long-term average H_S between 0.7 and 0.8 m while the neighbouring Baltic proper regions have it in the range of 1.1–1.2 m (that matches the estimates of Björkqvist et al., 2018a). The area with highest waves, with the average H_S slightly over 0.8 m and a maximum of 0.82 m, is located between islands of Ruhnu and Kihnu and is centered at 30°E, 58°N. The mean
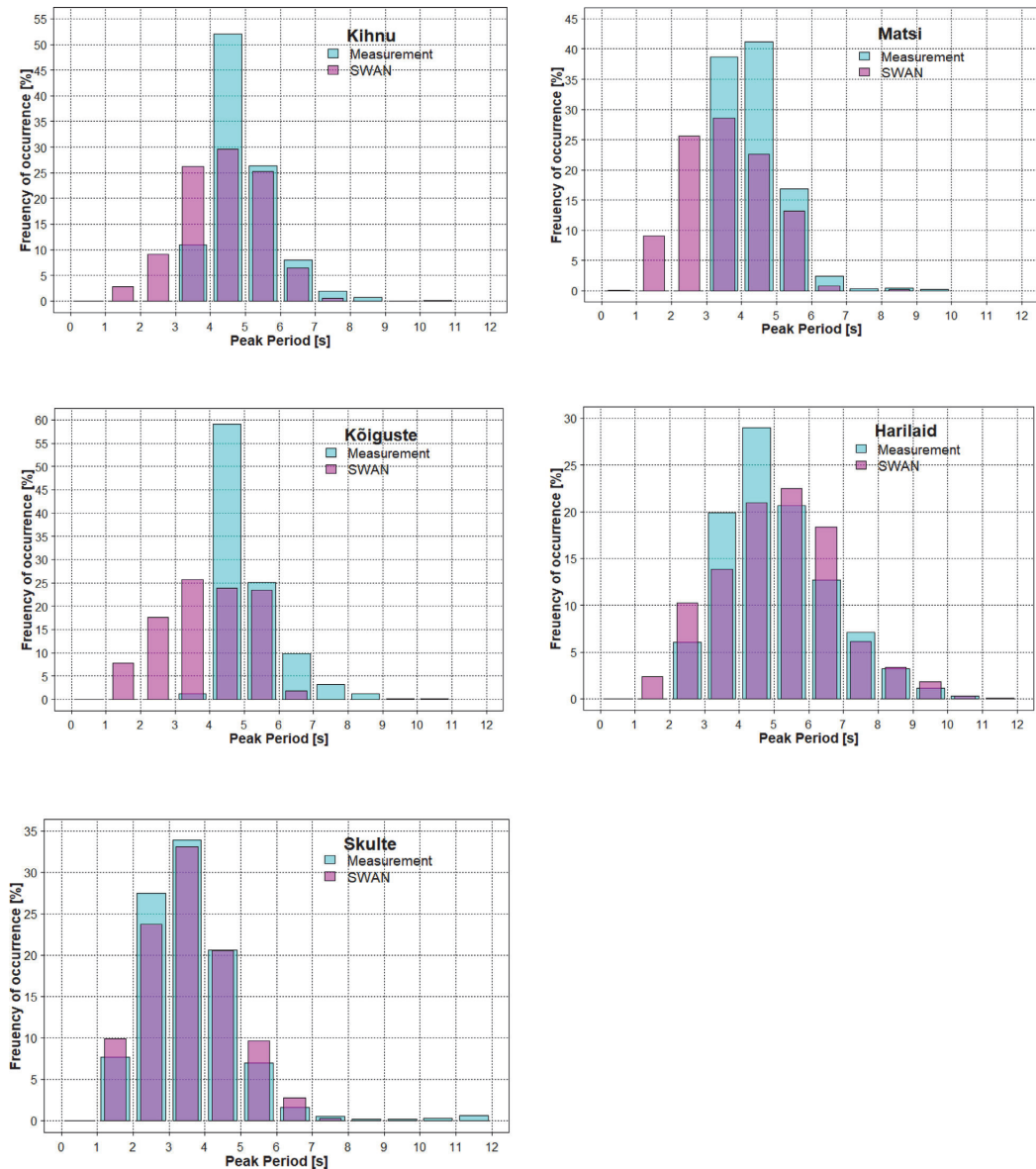
Figure 10 Empirical probability distributions of measured (blue) and observed (red) peak periods in five measurement locations. As the RDCP pressure sensor does not recognise wave periods of shorter waves when deployed to larger depths, wave periods below 2—3 s (depending on deployment depth) are not directly represented in the instrument output at Kihnu, Matsi, Kõiguste, and Harilaid.

H_S is below 0.7 m in the southern part of the gulf to the south of latitude 57°30′N.

The appearance of this map (Figure 12) suggests that moderate and strong SW winds are clearly more frequent than north-western or NNW winds. The calmest region is located near Jurmala at the southern bayhead of the Gulf of Riga. The mean H_S is smaller near the south-western shore compared to the situation near the eastern shore of the gulf. A relatively low average H_S in Pärnu Bay apparently reflects two features. First of all, it mirrors wave attenuation over a relatively shallow seabed in the entrance region of the bay. Secondly, Pärnu Bay is geometrically sheltered for most wave directions. It is likely that high waves penetrate into this bay only for a few wind directions that create the largest water levels in the bay (Suursaar et al., 2002).
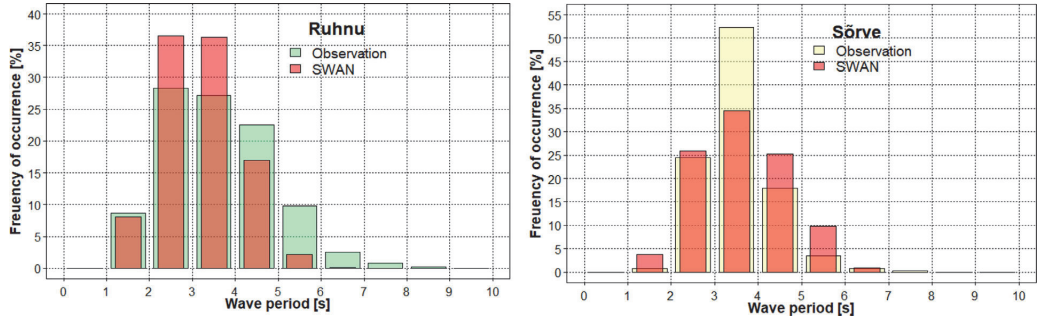
Figure 11 Empirical probability distributions of the frequency of occurrence of observed wave periods at Ruhnu (green) and Sõrve (yellow) (Eelsalu et al., 2014). The colour code is the same as for Figure 8.
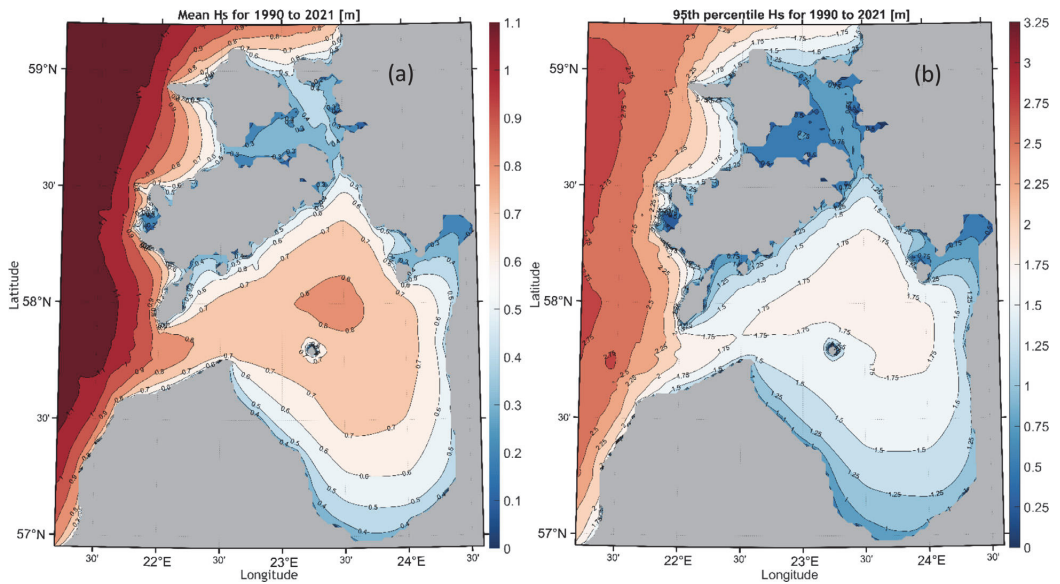
Figure 12 Spatial distribution of the long-term mean H_S (a) and the 95 percentile of H_S (b) in 1990—2021 evaluated using the GoR grid with a resolution of about 1 nmi (Figure 1).

The spatial distribution of higher quantiles of wave heights is slightly more asymmetric in the East-West direction than the above distribution of average wave heights. The area with 95 percentiles lower than 1.5 m (Figure 12) is much wider near Kurzeme Peninsula near the eastern shore of the gulf and extends to the shore of the island of Kihnu. The North-South asymmetry is also more pronounced and high waves are common in the entire northern segment of the gulf. The relevant thresholds (1.75—1.9 m, with a maximum of 1.91 m) are lower than in the neighbouring regions of the Baltic proper where they extend above 2.75 m. The estimates of Björqkvist et al. (2018a) for 1965—2005 led to a similar spatial distribution of 95 percentiles, with values over 2 m between Ruhnu and Kihnu.

The similar distribution for 99 percentiles is similar to the one for 95 percentiles. Typical values of this threshold exceed 2.2 m in the northern and northeastern parts of the gulf and reach over 2.4 m in the northeast, with a maximum of 2.48, while they are close to 4 m in the neighbouring Baltic proper. The estimates of Björqkvist et al. (2018a) again led to a similar spatial distribution of 99 percentiles but with values over 2.5 m in the area where our simulations indicated 2.25—2.5 m.

Wave conditions during extreme storms may be even more severe. It is likely that the January 2005 storm Erwin/Gudrun (Soomere et al., 2008) that created exceptional water levels in the Gulf of Riga (Suursaar et al., 2006) excited wave fields with significant wave heights well over 4
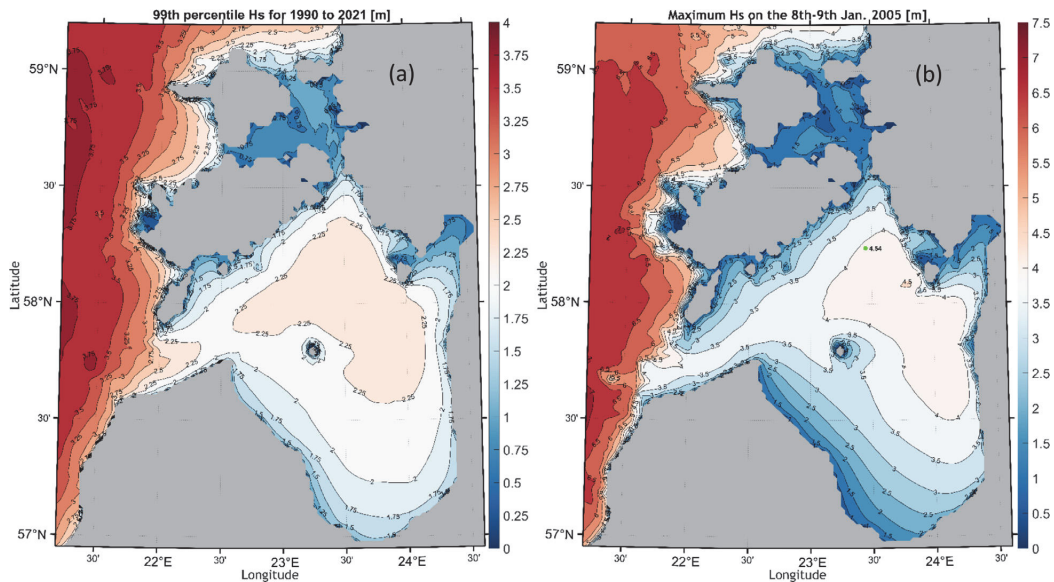
Figure 13 Spatial distribution of the 99 percentile of wave heights in 1990—2021 (a) and maximum wave heights on January 08—09, 2005 wave storm (b).
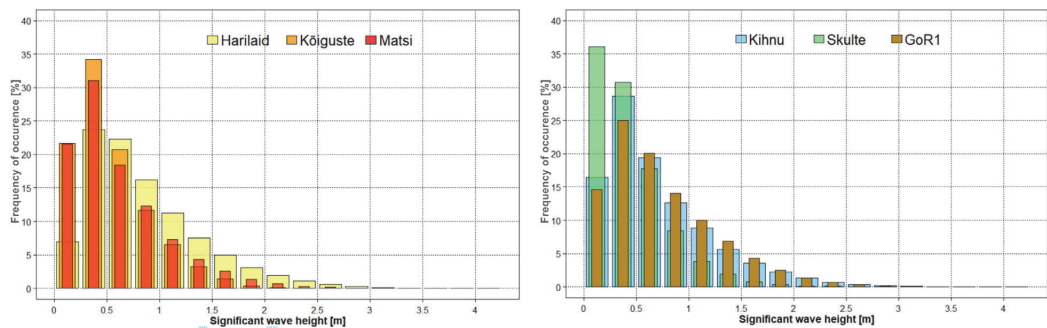
Figure 14 Frequency distributions of modelled H_S at six locations in 1990—2021.

m in the entire eastern part of the gulf, with a maximum of slightly over 4.5 m near the island of Kihnu and in the north of the gulf (Figure 13). These values are clearly smaller than the maximum H_S 6.2 m that was estimated to occur in the Gulf of Riga on 2 November 1969 within the modelled time period of 1965—2006 (Björqkvist et al., 2018b).

3.5. Frequency of occurrence of wave heights and periods

Long-term distributions of the frequency of occurrence of wave fields with different H_S (Figure 14) have the same overall shape in all locations of measurements, except at Skulte where the proportion of wave fields with H_S <0.25 m is clearly higher than in other locations. These locations ev-

idently reflect well wave properties in different parts of the gulf. They all follow a 2-dimensional Weibull distribution. The overall shape of the realisations of this distribution is narrower than similar distributions in the Baltic proper (incl. Harilaid) but still clearly wider than similar ones in sheltered nearshore regions (Soomere, 2005). The median H_S is below 0.5 m, and is closest to 0.5 m at the most open location Skulte. Calm situations, with H_S not exceeding 0.25 m cover about 17—30% of the time in the Gulf of Riga against 7% at Harilaid. The probability of having waves with $H_S > 1$ m varies from 23% at Kihnu down to 7% at Skulte. Wave fields with $H_S > 2$ m occur with a probability of about 1% and $H_S > 3$ m are very rare.

The majority of wave fields have peak periods in the range of 2—5 s, with periods 3—4 s being the most frequent (Figure 15). Waves are thus systematically shorter in
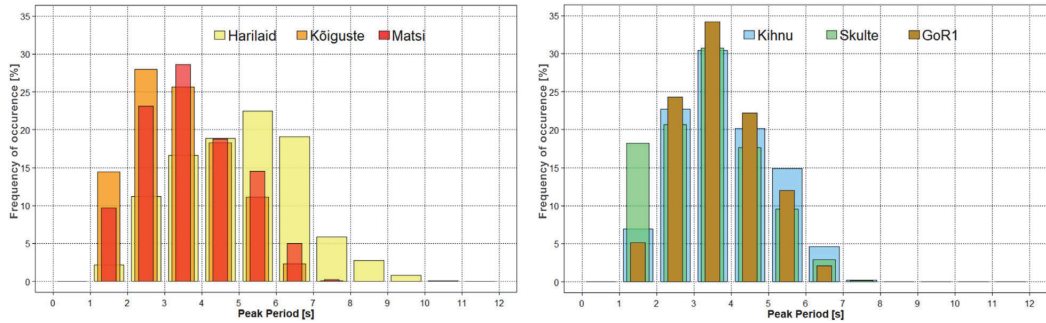
Figure 15   The frequency distribution of modelled wave periods at six in situ measurement sites.

the Gulf of Riga compared to the neighbouring segments of the Baltic proper where the predominant wave periods are 4—7 s.

3.6. Joint distribution of significant wave height and mean period

The joint distribution of visually observed wave heights and periods roughly matches the fully developed wave conditions at Ruhnu but to some extent reflects such distributions for swell-dominated regions at Sõrve (Eelsalu et al., 2014). The simulated data sets provide additional details to this feature. Wave conditions at all sites reveal the presence of two different sets of wave conditions (Figure 16). The properties of the majority of wave fields almost exactly follow the properties of fully developed wave fields with a Pierson-Moskowitz spectrum. The highest waves of this set have slightly longer periods than the corresponding fully developed seas (except for GoR1). The other set of wave conditions has periods much longer than the waves with the same height but with a Pierson-Moskowitz spectrum. As the wave height is mostly below 0.5 m in such situations, they likely reflect waves created in a remote area; possibly in the Baltic proper.

These distributions provide a simple estimate of the combinations of wave heights and periods in the most extreme storms. These combinations likely match the ones for fully developed wave systems with a Pierson-Moskowitz spectrum. For example, at Kihnu extreme wave conditions with a H_S close to 4 m are likely to have a period of 6.5 s.

3.7. Long-term variations

The simulations shed some light on the interannual variability in wave properties. The addressed time interval 1990—2021 contains several implications of rapid climate change in the region. In particular, systematic changes have been observed in the parameters of the generalised extreme value distribution for water level extremes (Kudryavtseva et al., 2021). Such shifts are likely associated with similar shifts in the drivers of water level, including wind properties. However, the simulations were presented for the hypothetical ice-free case, even if the ice was actually present on the sea. In reality, some of the variability would come from actual variations in ice cover.

The course of annual average modelled H_S is qualitatively similar in all addressed locations (Figure 17). The magnitude of interannual variations in the H_S is about 20% ($\pm$10%) from the long-term mean at all sites. The level of such variations was larger in 1990—1997 and 2007—2020. Interannual variations are highly synchronised in different parts of the gulf and near the entrance of the gulf (Harilaid). Importantly, there exists no systematic decrease or increase in the annual average H_S over the considered time interval. On the one hand, this conjecture is consistent with the perception that (scalar) wind properties in the Baltic Sea region have not massively changed during many decades (BACC, 2015). On the other hand, this feature also signals that some wave properties of the Gulf of Riga, at least the average H_S in this basin, may be disconnected from changes to these parameters in the Baltic proper, as noted in (Viška and Soomere, 2013a).

4. Discussion

In general, the simulations of wave time series in the Gulf of Riga clearly expressed some heterogeneity in the wave conditions (Figures 12—13). Wave intensity is relatively large in its central, northeastern and eastern regions. This is consistent with the perception that the majority of moderate and strong winds blow from the southwest in this region (Soomere and Keevallik, 2001). It is however somewhat unexpected that the wave climate of the southern part of this water body is milder than in the north-east also in terms of higher quantiles of wave heights. NNW winds are less frequent but they have the longest fetch and thus have the potential to generate severe waves in the south of this water body. Spatial distributions of wave properties (Figures 12—13) suggest that this potential has not been systematically realized in 1990—2021. Instead, westerly winds have become more frequent (Bierstedt et al., 2015).

The used wave model has been first of all tuned for neighbouring water bodies, such as the Baltic proper or the Gulf of Finland. It tends to show poorer performance than, e.g., in the Gulf of Finland (Giudici et al., 2023) even if applied in a much finer resolution. This feature partially reflects difficulties with a representation of wave properties in regions with highly variable bathymetry, similar to gaps in the performance of wave models in archipelagos
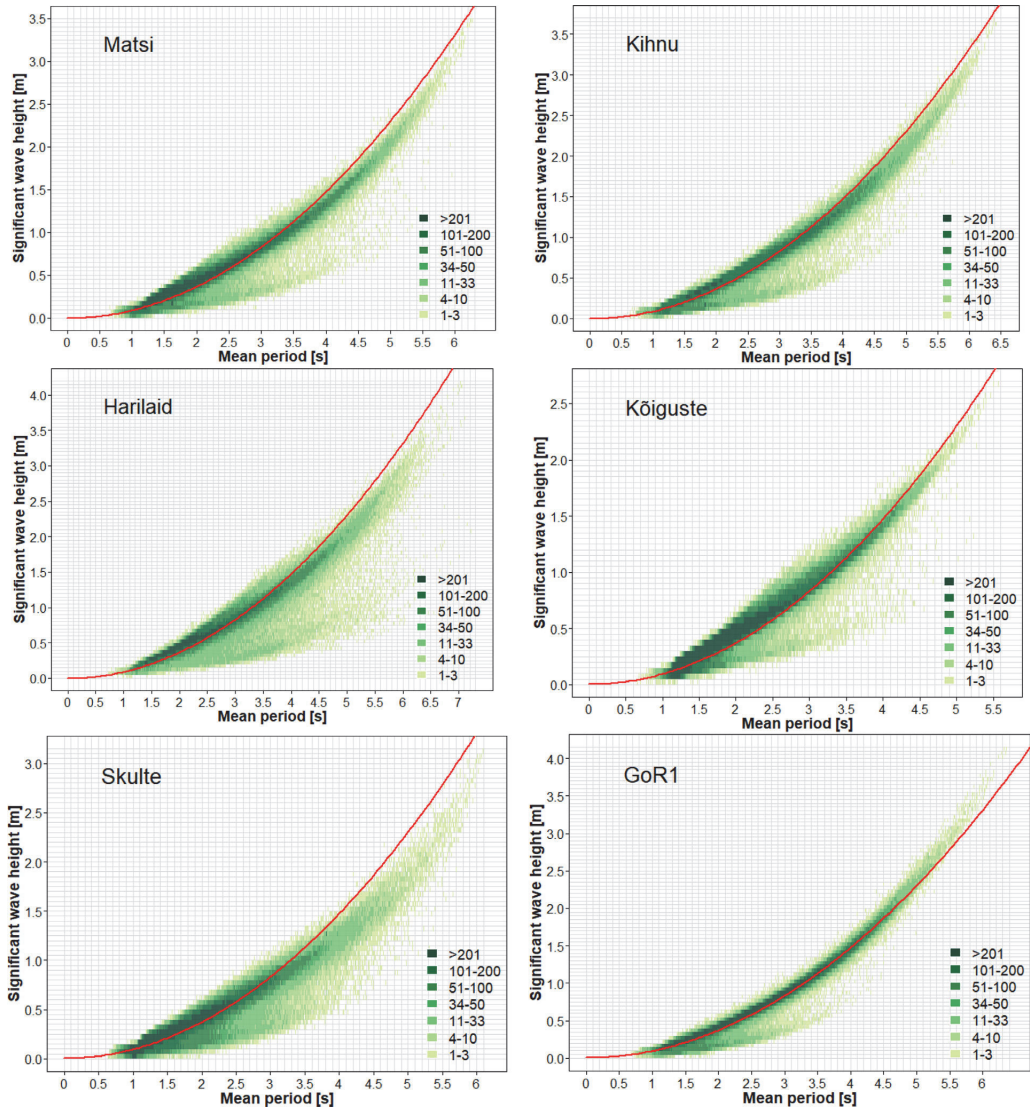
Figure 16 Joint distribution of modelled H_S and mean period. The width of classes of the mean period (T_{02}) is 0.01 s and 0.05 m for H_S. The red line shows the SWH of the fully developed wave systems with the Pierson-Moskowitz spectrum for the given mean period.

(Björkqvist et al., 2018b) where the performance of the wave model depends on the wind direction and apparently on the openness of the particular location towards specific directions. It is particularly evident at Kõiguste where the duration of measured wave storms often differed from the hindcast one. Part of this difference may result from the properties of the device (RDCP), and some from generalisation of the irregular bathymetry in the shallow, archipelago-like sea area. The match is much better in the fully open lo-

cation of Skulte where a waverider buoy was used for wave measurements.

Historical visual observations considerably underestimate the long-term average wave height and provide a distorted estimate of the probability of occurrence of waves of different heights. This distribution overestimates the proportion of almost calm seas, especially in the relatively sheltered location of Sõrve. The match of the interannual course of the measured and modelled data sets is also poor.
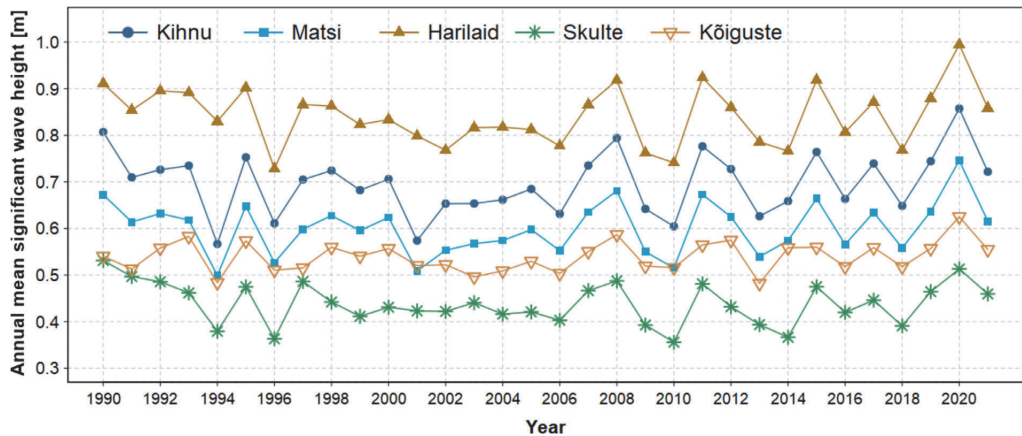
Figure 17 Time series of annual mean modelled H_S at five sites in the Gulf of Riga.

In contrast, the distribution of the observed wave periods matches well the similar distributions generated from modelled data.

Changing properties of wind wave fields are one of the markers of manifestations of climate change over seas and oceans (Charles et al., 2012; Dodet et al., 2010). Time series of common climatic variables (such as wind speed or sea surface temperature) extend back over substantial time intervals (BACC, 2008). Water level time series extend back over almost two and a half centuries in the Baltic Sea (Ekman, 1999). The longest instrumentally measured wave time series only covers a few decades. In this context, visually observed data serve as one of a few options to identify climate changes in the past even though the quality of such records is low. The sets of visually observed wave data are consistent with the hindcast in terms of the magnitude of interannual variations in wave intensity and the absence of any long-term trend in the wave height in the 1990s and 2000s.

A major limitation of the performed numerical simulations and the relevant discussion is the use of an idealised ice-free approach. The Gulf of Riga is at least partially ice-covered each winter in the contemporary climate. Ignoring ice leads to systematic overestimation of cumulative wave energy and its flux on the latitudes of the Gulf of Riga (Najafzadeh et al., 2022). This approach may also lead to major differences in spatial distributions of wave properties in strong storms in partially ice-covered seas (Tuomi et al., 2019) and thus to distortions of spatial distributions of higher quantiles of wave heights. This assumption, however, does not erode the validity of comparison of wave reconstructions with in situ measurements in ice-free times.

Another limitation is the use of constant water level in wave simulations. The Gulf of Riga often experienced large variations in the water level. Both preconditioning (filling first the entire Baltic Sea and then the Gulf of Riga with excess water during some storms) (Männikus et al., 2019) and local changes in water level in the nearshore may impact wave heights. As the Gulf of Riga has a fairly regular shape, with relatively narrow and shallow nearshore, it is likely that changes to the overall water level in the gulf do not add any detectable variation to the wave properties in most of the gulf area.

The situation is more complicated in the nearshore and, in particular, in the narrow and shallow Pärnu Bay. The historic total range of water level variations has reached 4 m (+2.75, −1.25 m) in this bay (Jaagus and Suursaar, 2013) and has apparently exceeded 3 m along most of the eastern shore of the gulf (Männikus et al., 2019). However, extreme events are rare. The water level usually stays within ±50 cm in the entire gulf (Männikus et al., 2019) and the impacts are mostly confined to specific sections of the shore. For example, it has been argued that somewhat higher waves could have been reached Pärnu Bay during extreme storm Gudrun in 2005 (Suursaar et al., 2006).

The relevant effects may to some extent affect the properties of waves in the nearshore, mostly via alterations of refraction, shoaling and bottom-driven loss of energy. These effects first become evident in terms of changes to the wave impact on the shore and wave-driven sediment transport. It is likely, similar to the eastern shore of the Baltic proper, that high waves often approach part of the shores of the Gulf of Riga at large angles between the wave approach direction and shore normal. A decrease in the intensity of refraction in deeper water may amplify this feature. Therefore, the development of local instabilities of the coastline (Ashton et al., 2001) is likely in some segments of this water body. For this reason, it is important to describe not only the general properties of the wave climate of the Gulf of Riga in more detail but also adequately evaluate the directional distribution of severe wave conditions in future research.

5. Conclusions

Wave climate in the Gulf of Riga is considerably milder than in the Baltic proper, Gulf of Bothnia or Gulf of Finland and comparable to that of the Arkona Basin. The long-term average modelled significant wave height is mostly in the range

of 0.7—0.8 m. Wave periods are predominantly 2—5 s and thus systematically shorter than in the Baltic proper. Wave fields are usually fully saturated wind seas or (in the northern part) contain low swells generated in the Baltic proper.

The modelling exercise suggests that the threshold of significant wave height that occurs with a probability of 5% (95 percentiles) is lower than 1.5 m near the Kurzeme peninsula but reaches 1.75—1.9 m in the central, northern and eastern parts of the gulf. The typical values of the threshold for waves that occur with a probability of 1% exceed 2.2 m in the northern and northeastern parts of the gulf and reach over 2.4 m in the northeast. The modelled significant wave height reached well over 4 m in the entire eastern part of the during the January 2005 storm Erwin/Gudrun.

The wave climate varies spatially; the waves are higher and longer in the eastern part of the gulf. Modelled extreme wave heights may reach 4—5 m, with periods up to 7—8 s.

Although historical visual wave observations from the shore underestimate wave heights, they still have a reasonable correlation with simulations in terms of wave periods and interannual variability in wave heights.

There was a substantial interannual variability in the mean wave height without any systematic trend or distinct decadal-scale variation in the wave heights in 1990—2021.

Declaration of competing interests

The authors declare that they have no known competing financial interests or personal relationships that could have appeared to influence the work reported in this paper.

Acknowledgements

References

Ashton, A., Murray, A.B., Arnault, O., 2001. Formation of coastline features by large—scale instabilities induced by high-angle waves. Nature 414 (6861), 296—300. https://doi.org/10.1038/35104541

Badulin, S.I., Grigorieva, V.G., 2012. On discriminating swell and wind-driven seas in Voluntary Observing Ship data. J. Geophys. Res.-Oceans 117 (C11), C00J29. https://doi.org/10.1029/2012JC007937

Baltic Sea Hydrographic Commission, 2013. Baltic Sea Bathymetry Database Version 0.9.3. (Downloaded on 15.02.2020 from http://data.bshc.pro/on).

Bierstedt, S.E., Hünicke, B., Zorita, E., 2015. Variability of wind direction statistics of mean and extreme wind events over the Baltic Sea region. Tellus A 67, 29073. https://doi.org/10.3402/tellusa.v67.29073

Björkqvist, J.V., Kanarik, H., Johansson, M.M., Tuomi, L., 2018b. A wave forecast for the Helsinki archipelago in the Gulf of Finland. 2018 IEEE/OES Baltic International Symposium (BALTIC), June 12—15. Klaipeda, Lithuania. https://doi.org/10.1109/BALTIC.2018.8634863

Björkqvist, J.V., Lukas, I., Alari, V., van Vledder, P.G., Hulst, S., Pettersson, H., Behrens, A., Männik, A., 2018a. Comparing a 41-year model hindcast with decades of wave measurements from the Baltic Sea. Ocean Eng. 152, 57—71. https://doi.org/10.1016/j.oceaneng.2018.01.048

Björkqvist, J.-V., Pärt, S., Alari, V., Rikka, S., Lindgren, E., Tuomi, L., 2021. Swell hindcast statistics for the Baltic Sea. Ocean Sci. 17, 1815—1829. https://doi.org/10.5194/os-17-1815-2021

Björkqvist, J.V., Rikka, S., Alari, V., Männik, A., Tuomi, L., Pettersson, H., 2020. Wave height return periods from combined measurement-model data: a Baltic Sea case study. Nat. Hazards Earth Syst. Sci. 20 (12), 3593—3609. https://doi.org/10.5194/nhess-20-3593-2020

Björkqvist, J.V., Tuomi, L., Fortelius, C., Pettersson, H., Tikka, K., Kahma, K.K., 2017. Improved estimates of nearshore wave conditions in the Gulf of Finland. J. Marine Syst. 171, 43—53. https://doi.org/10.1016/j.jmarsys.2016.07.005

Booij, N., Ris, R.C., Holthuijsen, L.H., 1999. A third-generation wave model for coastal regions: 1. Model description and validation. J. Geophys. Res.-Oceans 104 (C4), 7649—7666. https://doi.org/10.1029/98JC02622

Broman, B., Hammarklint, T., Rannat, K., Soomere, T., Valdmann, A., 2006. Trends and extremes of wave fields in the north-eastern part of the Baltic Proper. Oceanologia 48 (S), 165—184.

Charles, E., Idier, D., Delecluse, P., Deque, M., Le Cozannet, G., 2012. Climate change impact on waves in the Bay of Biscay. France. Ocean Dynam. 62 (6), 831—848. https://doi.org/10.1007/s10236-012-0534-8

Christensen, E.D., Johnson, M., Sørensen, O.R., Hasager, C.B., Badger, M., Larsen, S.E., 2013. Transmission of wave energy through an offshore wind turbine farm. Coast. Eng. 82, 25—46. https://doi.org/10.1016/j.coastaleng.2013.08.004

Chubarenko, B.V., Leitsina, L.V., Esiukova, E.E., Kurennoy, D.N., 2012. Model analysis of the currents and wind waves in the Vistula Lagoon of the Baltic Sea. Oceanology 52 (6), 748—753. https://doi.org/10.1134/S000143701206001X

Cieślikiewicz, W., Paplińska-Swerpel, B., 2008. A 44-year hindcast of wind wave fields over the Baltic Sea. Coast. Eng. 55, 894—905. https://doi.org/10.1016/j.coastaleng.2008.02.017

Davidan, I.N., Lopatoukhin, L.I., Rozhkov, V.A., 1985. Wind Waves in the World Oceans. Gidrometeoizdat, Leningrad (in Russian).

Dean, R.G., Walton, T.L., Hatheway, D., 2008. Wave setup in U.S. flood insurance studies. Coast. Eng. 5, 926—974. https://doi.org/10.1142/9789814277426_0081

Dodet, G., Bertin, X., Taborda, R., 2010. Wave climate variability in the North-East Atlantic Ocean over the last six decades. Ocean Model. 31 (3—4), 120—131. https://doi.org/10.1016/j.ocemod.2009.10.010

Dvornikov, A.Y., Martyanov, S.D., Ryabchenko, V.A., Eremina, T.R., Isaev, A.V., Sein, D.V., 2017. Assessment of extreme hydrological conditions in the Bothnian Bay, Baltic Sea, and the impact of the nuclear power plant "Hanhikivi-1" on the local thermal regime. Earth Syst. Dynam. 8 (2), 265—282. https://doi.org/10.5194/esd-8-265-2017

ECMWF, 2006. IFS Documentation — Cy41r2. Operational Implementation 8 March 2016. Part IV: Physical Processes. Accessed on February 7th, 2023, https://www.ecmwf.int/en/elibrary/79697-ifs-documentation-cy41r2-part-iv-physical-processes.

Eelsalu, M., Org, M., Soomere, T., 2014. Visually observed wave climate in the Gulf of Riga. The 6th IEEE/OES Baltic Symposium Measuring and Modeling of Multi-Scale Interactions in the Marine Environment, May 26—29, 6887829. IEEE Conference Publications, 10. https://doi.org/10.1109/BALTIC.2014.6887829

Ekman, M., 1999. Climate changes detected through the world's longest sea level series. Glob. Planet. Change 21 (4), 215—224. https://doi.org/10.1016/S0921-8181(99)00045-4

Giudici, A., Jankowski, M.Z., Männikus, R., Najafzadeh, F., Suursaar, Ü., Soomere, T., 2023. A comparison of Baltic Sea wave

properties simulated using two modelled wind data sets. Estuar. Coast. Shelf Sci. 290, 108401. https://doi.org/10.1016/j.ecss.2023.108401

Guedes Soares, C., 1986. Assessment of the uncertainty in visual observations of wave height. Ocean Eng. 13 (1), 37—56. https://doi.org/10.1016/0029-8018(86)90003-X

Guidelines, 1985. Guidelines for Hydrometeorological Stations and Posts. Meteorological observations at stations. Leningrad: Gidrometeoizdat 3 (1), 300 pp. (in Russian).

Gulev, S.K., Grigorieva, V., 2004. Last century changes in ocean wind wave height from global visual wave data. Geophys. Res. Lett. 31 (24), L24302. https://doi.org/10.1029/2004GL021040

Gulev, S.K., Grigorieva, V., 2006. Variability of the winter wind waves and swell in the North Atlantic and North Pacific as revealed by the Voluntary Observing Ship data. J. Clim. 19 (21), 5667—5685. https://doi.org/10.1175/JCLI3936.1

Gulev, S.K., Grigorieva, V., Sterl, A., Woolf, D., 2003. Assessment of the reliability of wave observations from voluntary observing ships: insights from the validation of a global wind wave climatology based on voluntary observing ship data. J. Geophys. Res.-Oceans 108 (C7), 3236.

Gulev, S.K., Hasse, L., 1998. North Atlantic wind waves and wind stress fields from voluntary observing ship data. J. Phys. Oceanogr. 28, 1107—1130. https://doi.org/10.1175/1520-0485(1998)028⟨1107:NAWWAW⟩2.0.CO;2

Gulev, S.K., Hasse, L., 1999. Changes of wind waves in the North Atlantic over the last 30 years. Int. J. Climatol. 19 (10), 1091—1117. https://doi.org/10.1002/(SICI)1097-0088(199908)19:10⟨1091::AID-JOC403⟩3.0.CO;2-U

Hersbach, H., Bell, B., Berrisford, P., Biavati, G., Horányi, A., Muñoz Sabater, J., Nicolas, J., Peubey, C., Radu, R., Rozum, I., Schepers, D., Simmons, A., Soci, C., Dee, D., Thépaut, J.-N., 1979 to present. Copernicus Climate Change Service (C3S). Climate Data Store (CDS). https://doi.org/10.24381/cds.bd0915c6

Hogben, N., Dacunka, N.M.C., Olliver, G.F., 1986. Global Wave Statistics. Unvin Brothers, London.

Hogben, N., Lumb, F.E., 1967. Ocean Wave Statistics; a statistical survey of wave characteristics estimated usually from Voluntary Observing Ships sailing along the shipping routes of the world. H.M.S.O, Ministry of Technology, National Physical Laboratory, London, 263 pp.

Hünicke, B., Zorita, E., Soomere, T., Skovgaard Madsen, K., Johansson, M., Suursaar, Ü., 2015. Recent change — sea level and wind waves. In: The BACC II Author Team, Second Assessment of Climate Change for the Baltic Sea Basin. Regional Climate Studies. Springer, 155—185. https://doi.org/10.1007/978-3-319-16006-1_9

Jaagus, J., 2009. Long-term changes in frequencies of wind directions on the western coast of Estonia. In: Kont, A., Tõnisson, H. (Eds.), Climate Change Impact on Estonian Coasts. Publication 11/2009. Tallinn: Institute of Ecology, Tallinn University, 11—24 (in Estonian).

Jaagus, J., Kull, A., 2011. Changes in surface wind directions in Estonia during 1966—2008 and their relationships with large-scale atmospheric circulation. Est. J. Earth Sci. 60, 220—231. https://doi.org/10.3176/earth.2011.4.03

Jaagus, J., Suursaar, Ü., 2013. Long-term storminess and sea level variations on the Estonian coast of the Baltic Sea in relation to large-scale atmospheric circulation. Est. J. Earth Sci. 62 (2), 73—92. https://doi.org/10.3176/earth.2013.07

Jahanmard, V., Varbla, S., Delpeche-Ellmann, N., Ellmann, A., 2022. Retrieval of directional power spectral density and wave parameters from airborne LiDAR point cloud. Ocean Eng. 266, 112694. https://doi.org/10.1016/j.oceaneng.2022.112694

Keevallik, S., 2003. Possibilities of reconstruction of the wind regime over Tallinn Bay. Proc. Estonian Acad. Sci. Eng. 9 (3), 209—219. https://doi.org/10.3176/eng.2003.3.04

Kelpšaitė, L., Dailidienė, I., Soomere, T., 2011. Changes in wave dynamics at the south-eastern coast of the Baltic Proper during 1993—2008. Boreal Environ. Res. 16 (Supplement A), 220—232.

Komen, G.J., Hasselmann, S., Hasselmann, K., 1984. On the existence of a fully developed wind-sea spectrum. J. Phys. Oceanogr. 14 (8), 1271—1285. https://doi.org/10.1175/1520-0485(1984)014⟨1271:OTEOAF⟩2.0.CO;2

Kudryavtseva, N., Kussembayeva, K., Rakisheva, Z.B., Soomere, T., 2019. Spatial variations in the Caspian Sea wave climate in 2002—2013. Est. J. Earth Sci. 68 (4), 225—240. https://doi.org/10.3176/earth.2019.16

Kudryavtseva, N., Soomere, T., 2017. Satellite altimetry reveals spatial patterns of variations in the Baltic Sea wave climate. Earth Syst. Dynam. 8 (3), 697—706. https://doi.org/10.5194/esd-8-697-2017

Kudryavtseva, N., Soomere, T., Männikus, R., 2021. Non-stationary analysis of water level extremes in Latvian waters, Baltic Sea, during 1961—2018. Nat. Hazards Earth Syst. Sci. 21 (4), 1279—1296. https://doi.org/10.5194/nhess-21-1279-2021

Kudryavtseva, N.A., Soomere, T., 2016. Validation of the multi-mission altimeter wave height data for the Baltic Sea region. Est. J. Earth Sci. 65 (3), 161—175. https://doi.org/10.3176/earth.2016.13

Lebedev, S.A., Kostianoy, A.G., 2008. Integrated use of satellite altimetry in the investigation of the meteorological, hydrological, and hydrodynamic regime of the Caspian Sea. Terr. Atmos. Ocean. Sci. 19 (1—2), 71—82. https://doi.org/10.3319/TAO.2008.19.1-2.71(SA)

Leppäranta, M., Myrberg, K., 2009. Physical Oceanography of the Baltic Sea. Springer Science & Business Media, Praxis, Berlin, Heidelberg. https://doi.org/10.1007/978-3-540-79703-6

Männikus, R., Soomere, T., Kudryavtseva, N., 2019. Identification of mechanisms that drive water level extremes from in situ measurements in the Gulf of Riga during 1961—2017. Cont. Shelf Res. 182, 22—36. https://doi.org/10.1016/j.csr.2019.05.014

Männikus, R., Soomere, T., Najafzadeh, F., 2022. Refraction may redirect waves from multiple directions into a harbour: a case study in the Gulf of Riga, eastern Baltic Sea. Est. J. Earth Sci. 71 (2), 80—88. https://doi.org/10.3176/earth.2022.06

Männikus, R., Soomere, T., Viška, M., 2020. Variations in the mean, seasonal and extreme water level on the Latvian coast, the eastern Baltic Sea, during 1961—2018. Estuar. Coast. Shelf Sci. 245, 106827. https://doi.org/10.1016/j.ecss.2020.106827

Massel, S.R., 2013. Ocean Surface Waves: Their Physics and Prediction, 2nd edn. World Scientific, New Jersey, London, Singapore, 692 pp.

Najafzadeh, F., Kudryavtseva, N., Soomere, T., 2021. Effects of large-scale atmospheric circulation on the Baltic Sea wave climate: application of the EOF method on multi-mission satellite altimetry data. Clim. Dynam. 57 (11), 3465—3478. https://doi.org/10.1007/s00382-021-05874-x

Najafzadeh, F., Kudryavtseva, N., Soomere, T., Giudici, A., 2022. Effect of ice cover on wave statistics and wave-driven processes in the northern Baltic Sea. Boreal Environ. Res. 27, 97—116. http://www.borenv.net/BER/archive/pdfs/ber27/ber27-097-116.pdf.

Naulin, J.P., Moncoulon, D., Le Roy, S., Pedreros, R., Idier, D., Oliveros, C., 2016. Estimation of insurance-related losses resulting from coastal flooding in France. Nat. Hazards Earth Syst. Sci. 16, 195—207. https://doi.org/10.5194/nhess-16-195-2016

Nilsson, E., Rutgersson, A., Dingwell, A., Björkqvist, J.-V., Pettersson, H., Axell, L., Nyberg, J., Stromstedt, E., 2019. Characterization of wave energy potential for the Baltic Sea with focus on the Swedish Exclusive Economic Zone. Energies 12 (5), 793. https://doi.org/10.3390/en12050793

Orlenko, L.R., Lopatukhin, L.I., Portnova, G.L. (Eds.), 1984, Studies of the Hydrometeorological Regime of Tallinn Bay. Gidrometeoizdat, Leningrad, 152 pp. (in Russian).

Pallares, E., Sánchez-Arcilla, A., Espino, M., 2014. Wave energy balance in wave models (SWAN) for semi-enclosed domains—Application to the Catalan coast. Cont. Shelf Res. 87, 41—53. https://doi.org/10.1016/j.csr.2014.03.008

Pindsoo, K., Soomere, T., Zujev, M., 2012. Decadal and long-term variations in the wave climate at the Latvian coast of the Baltic Proper. In: Proceedings of the IEEE/OES Baltic 2012 International Symposium "Ocean: Past, Present and Future. Climate Change Research, Ocean Observation & Advanced Technologies for Regional Sustainability,". May 8—11, Klaipėda, Lithuania. IEEE https://doi.org/10.1109/BALTIC.2012.6249160

Plant, N.G., Griggs, G.B., 1992. Comparison of visual observations of wave height and period to measurements made by an offshore slope array. J. Coast. Res. 8 (4), 957—965.

Räämet, A., Soomere, T., 2010. The wave climate and its seasonal variability in the northeastern Baltic Sea. Est. J. Earth Sci. 59 (1), 100—113. https://doi.org/10.3176/earth.2010.1.08

Randmeri, R., 2006. Description of the wave climate of the Gulf of Riga using the WAM wave model. MSc Thesis. Tallinn University.

Rogers, W.E., Hwang, P.A., Wang, D.W., 2003. Investigation of wave growth and decay in the SWAN model: Three regional-scale applications. J. Phys. Oceanogr. 33 (2), 366—389. https://doi.org/10.1175/1520-0485(2003)033⟨0366:IOWGAD⟩2.0.CO;2

Rosenhagen, G., Tinz, B., 2013. New historical data of the southern Baltic Sea coasts. In: Reckermann, M., Köppen, S. (Eds.), 7th Study Conference on BALTEX, 10—14 June 2013, Borgholm, Island of Öland, Sweden, 84 Conference Proceedings, International BALTEX Secretariat, Publication No. 53.

Seifert, T., Tauber, F., Kayser, B., 2001. A high-resolution spherical grid topography of the Baltic Sea—revised edition. Baltic Sea Science Congress 2001, Nov. 25—29.

Sokolov, A.N., Chubarenko, B.V., 2020. Temporal variability of the wind wave parameters in the Baltic Sea in 1979—2018 based on the numerical modeling results. Phys. Oceanogr. 27 (4), 352—363. https://doi.org/10.22449/1573-160X-2020-4-352-363

Sooäär, J., Jaagus, J., 2007. Long-term changes in the sea ice regime in the Baltic Sea near the Estonian coast. Proc. Estonian Acad. Sci. Eng. 13 (3), 189—200.

Soomere, T., 2001. Extreme wind speeds and spatially uniform wind events in the Baltic Proper. Proc. Estonian Acad. Sci. Eng. 7 (3), 195—211. https://doi.org/10.3176/eng.2001.3.01

Soomere, T., 2005. Wind wave statistics in Tallinn Bay. Boreal Environ. Res. 10 (2), 103—118. http://www.borenv.net/BER/archive/pdfs/ber10/ber10-103.pdf

Soomere, T., 2013. Extending the observed Baltic Sea wave climate back to the 1940s. J. Coast. Res. Special Issue 65, 1969—1974. https://doi.org/10.2112/SI65-333

Soomere, T., Behrens, A., Tuomi, L., Nielsen, J.W., 2008. Wave conditions in the Baltic Proper and in the Gulf of Finland during windstorm Gudrun. Nat. Hazards Earth Syst. Sci. 8 (1), 37—46. https://doi.org/10.5194/nhess-8-37-2008

Soomere, T., Bishop, S.R., Viška, M., Räämet, A., 2015. An abrupt change in winds that may radically affect the coasts and deep sections of the Baltic Sea. Clim. Res. 62, 163—171. https://doi.org/10.3354/cr0126

Soomere, T., Keevallik, S., 2001. Anisotropy of moderate and strong winds in the Baltic Proper. Proc. Estonian Acad. Sci. Eng. 7 (1), 35—49. https://doi.org/10.3176/eng.2001.1.04

Soomere, T., Weisse, R., Behrens, A., 2012. Wave climate in the Arkona Basin, the Baltic Sea. Ocean Sci. 8 (2), 287—300. https://doi.org/10.5194/os-8-287-2012

Soomere, T., Zaitseva, I., 2007. Estimates of wave climate in the northern Baltic Proper derived from visual wave observations at Vilsandi. Proc. Estonian Acad. Sci. Eng. 13 (1), 48—64. https://doi.org/10.3176/eng.2007.1.02

Suursaar, Ü., 2013. Locally calibrated wave hindcasts in the Estonian coastal sea in 1966—2011. Est. J. Earth Sci. 62 (1), 42—56. https://doi.org/10.3176/earth.2013.05

Suursaar, Ü., 2015. Analysis of wave time series in the Estonian coastal sea in 2003—2014. Est. J. Earth Sci. 64 (4), 289—304. https://doi.org/10.3176/earth.2015.35

Suursaar, Ü., Kullas, T., Aps, R., 2012. Currents and waves in the northern Gulf of Riga: measurement and long-term hindcast. Oceanologia 54 (3), 421—447. https://doi.org/10.5697/oc.54-3.421

Suursaar, Ü., Kullas, T., Otsmann, M., 2002. A model study of the sea level variations in the Gulf of Riga and the Väinameri Sea. Cont. Shelf Res. 22 (14), 2001—2019. https://doi.org/10.1016/S0278-4343(02)00046-8

Suursaar, Ü., Kullas, T., Otsmann, M., Saaremäe, I., Kuik, J., Merilain, M., 2006. Cyclone Gudrun in January 2005 and modelling its hydrodynamic consequences in the Estonian coastal waters. Boreal Environ. Res. 11 (2), 143—159. https://www.borenv.net/BER/archive/pdfs/ber11/ber11-143.pdf

Tavakoli, S., Khojasteh, D., Haghani, M., Hirdaris, S., 2023. A review on the progress and research directions of ocean engineering. Ocean Eng. 272, 113617. https://doi.org/10.1016/j.oceaneng.2023.113617

The BACC Author Team, 2008. Assessment of climate change for the Baltic Sea basin. Springer Science & Business Media, Berlin, Heidelberg, 473 pp.

The BACC II Author Team, 2015. Second Assessment of Climate Change for the Baltic Sea Basin. Regional Climate Studies. Springer, Cham, Heidelberg, New York, Dordrecht, London. https://doi.org/10.1007/978-3-319-16006-1

Tuomi, L., Kahma, K.K., Pettersson, H., 2011. Wave hindcast statistics in the seasonally ice-covered Baltic Sea. Boreal Environ. Res. 16 (6), 451—472. http://www.borenv.net/BER/archive/pdfs/ber16/ber16-451.pdf

Tuomi, L., Kanarik, H., Björkqvist, J.V., Marjamaa, R., Vainio, J., Hordoir, R., Höglund, A., Kahma, K.K., 2019. Impact of ice data quality and treatment on wave hindcast statistics in seasonally ice-covered seas. Front. Earth Sci. 7, 166. https://doi.org/10.3389/feart.2019.00166

Tuomi, L., Pettersson, H., Fortelius, C., Tikka, K., Björkqvist, J.-V., Kahma, K.K., 2014. Wave modelling in archipelagos. Coast. Eng. 83, 205—220. https://doi.org/10.1016/j.coastaleng.2013.10.011

Viška, M., Soomere, T., 2013a. Long-term variations of simulated sediment transport along the eastern Baltic Sea coast as a possible indicator of climate change. In: Reckermann, M., Köppen, S. (Eds.), 7th Study Conference on BALTEX, 10—14 June 2013, Borgholm, Island of Öland, Sweden. International BALTEX Secretariat, Publication No. 53, 99—100.

Viška, M., Soomere, T., 2013b. Simulated and observed reversals of wave-driven alongshore sediment transport at the eastern Baltic Sea coast. Baltica 26 (2), 145—156. https://doi.org/10.5200/baltica.2013.26.15

Wu, J., 2012. Wind-stress coefficients over sea surface from breeze to hurricane. J. Geophys. Res.-Oceans 87 (C12), 9704—9706. https://doi.org/10.1029/JC087iC12p09704

Zaitseva-Pärnaste, I., Soomere, T., Tribštok, O., 2011. Spatial variations in the wave climate change in the eastern part of the Baltic Sea. J. Coast. Res. Special Issue 64, 195—199. https://www.jstor.org/stable/26482160

Zaitseva-Pärnaste, I., Suursaar, Ü., Kullas, T., Lapimaa, S., Soomere, T., 2009. Seasonal and long-term variations of wave conditions in the northern Baltic Sea. J. Coast. Res. Special Issue 56, 277—281. https://www.jstor.org/stable/25737581

Zijlema, M., van Vledder, G.P., Holthuijsen, L.H., 2012. Bottom friction and wind drag for wave models. Coast. Eng. 65, 19—26. https://doi.org/10.1016/j.coastaleng.2012.03.002

Publication III

Jankowski, M.Z., Soomere, T., Parnell, K.E., Eelsalu, M., 2024. Alongshore sediment transport in the eastern Baltic Sea. Journal of Coastal Research, Special Issue 113, 261–265. https://doi.org/10.2112/JCR-SI113-052.1

Alongshore Sediment Transport in the Eastern Baltic Sea

Mikolaj Z. Jankowski[†*], Tarmo Soomere[†§], Kevin E. Parnell[†], and Maris Eelsalu[†]

[†]Wave Engineering Laboratory
Department of Cybernetics, School of Science
Tallinn University of Technology
Tallinn, Estonia

[§]Estonian Academy of Sciences
Tallinn, Estonia

www.cerf-jcr.org

ABSTRACT

Jankowski, M.Z.; Soomere, T.; Parnell, K.E., and Eelsalu, M., 2024. Alongshore sediment transport in the eastern Baltic Sea. *In:* Phillips, M.R.; Al-Naemi, S., and Duarte, C.M. (eds.), *Coastlines under Global Change: Proceedings from the International Coastal Symposium (ICS) 2024 (Doha, Qatar). Journal of Coastal Research*, Special Issue No. 113, pp. 261-265. Charlotte (North Carolina), ISSN 0749-0208.

The shores of the almost tideless Baltic Sea evolve under the joint impact of surface waves and water level. We identify the basic transport patterns and zones of sediment accumulation and erosion in the eastern Baltic Sea based on the analysis of alongshore and temporal variations in the potential bulk and net alongshore sediment transport. The area covered extends from Cape Taran on the Sambian Peninsula to Cape Kolka at the entrance to the Gulf of Riga. ERA-5 model winds for the period 1996–2022 are employed to produce time series of significant wave height, wave direction and periods using the SWAN model, at a coastal grid resolution of 560 m and a time resolution of 1 h. Sediment transport rates are subsequently calculated with the CERC formula. The basic counterclockwise pattern and most probable areas of accumulation and loss of sediment correspond well with previous findings. The use of much higher spatial resolution makes it possible to add further details to the locations of convergence and divergence zones of sediment transport, such as the divergence zones north of Klaipėda and to the south of Cape Akmenrags. The calculations confirm the surprisingly high rates of net sediment transport that have been reported for some areas, particularly to the southwest of Cape Kolka (up to 700,000 m³/yr). This transport continues towards the south-eastern bayhead of the Gulf of Riga that serve as an end station for most of sand.

ADDITIONAL INDEX WORDS: *Wave modeling, CERC approach, potential transport, sediment compartments.*

www.JCRonline.org

INTRODUCTION

Wave-driven alongshore sediment transport is a fundamental coastal process that shapes the coastline and nearshore of all water bodies. The shores of medium-size microtidal water bodies, such as the Baltic Sea (Leppäranta and Myrberg, 2009), develop mostly under joint impact of surface waves and water level. The wave climate of semi-enclosed water bodies of this type is usually extremely intermittent (that is, short time periods of severe wave conditions are interspersed by longer time intervals with low wave intensity, see, e.g., Soomere and Eelsalu, 2014), mostly contains fetch-limited wave systems (Broman *et al*., 2006) and includes very limited amounts of low-period restoring swells (Björkqvist *et al*., 2021).

As wave periods of the most common high wave systems are relatively short (Broman *et al*., 2006; Soomere *et al*., 2012), waves experience fairly limited impact of refraction in the nearshore and often approach the shore at a large angle with respect to shore normal. The latter feature is most common on sedimentary shores of the eastern Baltic Sea where a large part of the most energy-carrying waves are created by a bi-directional system of predominant winds from the (west-)south-west (W/SW) or (north-)north-west (N/NW) (Soomere, 2003).

The presence of a specific balance of this wind and wave climate, and coastal processes, is seen in many well-known coastal landforms, such as the Curonian Spit.

This specific interplay of the predominant wind and wave direction with the shoreline orientation gives rise to exceptionally intense wave-driven alongshore transport, up to 1,000,000 m³/yr, on the Baltic proper shores of Latvia and Lithuania (Viška and Soomere, 2013; Soomere and Viška, 2014) in the context of the generally mild wave climate of the Baltic Sea, with long-term average significant height only about 1 m near these shores (Björkqvist *et al*., 2018; Sokolov and Chubarenko, 2024).

This interplay also creates a delicate balance of clockwise and counterclockwise wave-driven transport (Viška and Soomere, 2012) that apparently stabilizes even the major landforms, such as the Curonian Spit. The magnitude and even sign of this transport considerably varies in different years (Viška and Soomere, 2012) and decades (Soomere *et al*., 2015). This variability combined with varying orientation of the shoreline gives rise to one major almost persistent divergence point of wave-driven sediment flux near Cape Akmenrags in Latvia and to several temporary divergence points in other segments of this shore (Viška and Soomere, 2013).

Such features divide the seemingly fully interconnected sedimentary system of the eastern Baltic Sea shores from Sambian Peninsula to Cape Kolka into several almost separated units, with major consequences in terms of coastal management,

limiting, e.g., the potential impact distance of adverse impacts carried with coastal sediment.
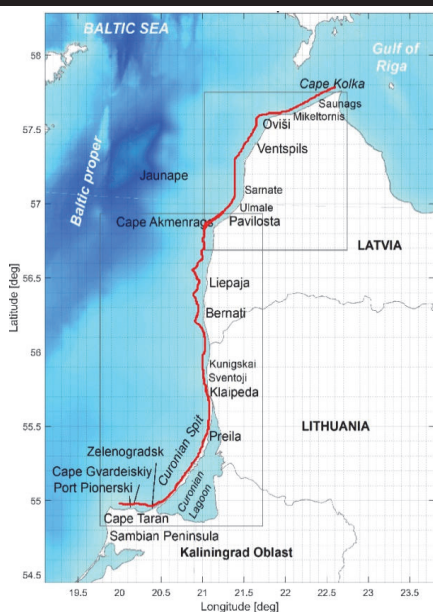

Figure 1. Schematic of the study area in the eastern Baltic Sea. The red line indicates the locations of 672 wave model grid points. The two squares showcase the areas of the SWAN model subgrid nesting.

Even though the earlier simulations (Viška and Soomere, 2013; Soomere and Viška, 2014) seem to catch the most important alongshore changes in the wave-driven sediment flux, their resolution is not sufficient to recognize the impact of less prominent features of the shoreline that apparently become evident as temporary divergence points of sediment flux. Also, several ports, harbors and/or jetties may partially or wholly block wave-driven sediment flux in this coastal stretch.

This paper provides results of detailed evaluation of wave-driven potential sediment flux on the Baltic proper shores of Latvia and Lithuania, and on the northern shore of Kaliningrad District, Russia. This coastal stretch with a total length of about 380 km evidently functions as an almost isolated sedimentary system, with very limited input of sediment from the western shore of Sambian Peninsula in the south (Harff *et al*., 2017) and from the eastern shore of Cape Kolka in the north (Jankowski *et al*., 2024). It is evidently divided into almost disconnected sedimentary compartments by jetties surrounding the Klaipèda Strait and major harbor constructions at Liepaja and Ventspils. It is likely that these compartments may contain smaller weakly connected cells that are separated from each other by smaller coastal engineering structures and/or less prominent headlands.

Such cells become evident in high-resolution simulations (Eelsalu *et al*., 2023).

METHODS
Wave Model

We employ the Coastal Engineering Research Council (CERC) approach (USACE, 2002), according to which wave-driven sediment transport primarily depends on the properties of waves, sediment, and coastline orientation. An application of this approach requires time series of (significant) wave height, (average) wave propagation direction and (peak) period. These properties are reconstructed using a nested version of the third-generation wave model SWAN (Booij *et al*., 1999) and extracted for the use in the CERC formula in a sequence of 672 nearshore grid cells with a typical depth of 8 m. The cycle III, v. 41.31A of this model was forced by ERA5 winds (Hersbach *et al*., 2020) for the time period of 1990–2022.

The presence of sea ice (which is infrequent even in the north of the study area, Najafzadeh and Soomere, 2024), currents and varying water levels were ignored. A detailed validation of this model run for the Baltic proper and Gulf of Riga is provided in Giudici *et al*. (2023) and Najafzadeh *et al*. (2024).

The resolution of the model in the study area is 0.3 nmi (nautical mile), approximately 560 m, or 0.01° in the East-West direction and 0.005° in the North-South direction. As the shoreline and nearshore isobaths are mostly regular in the study area, this resolution is sufficient to resolve the main features of sediment transport.

Wave properties in the wave model grid cell are translated to the associated properties at the breaker line by taking into account both shoaling and refraction in the framework of linear wave theory as described in (Soomere and Viška, 2014). The orientation of the coastline is associated with the orientation of coastal isobaths at appropriate depths.

CERC Approach

The classic Coastal Engineering Research Council (CERC) approach (USACE, 2002) provides instantaneous rates of wave-driven potential alongshore sediment transport [m³/s] based on wave height, period and approach direction at the breaker line, sediment properties, and coastline orientation. The positive direction is to the right for a person looking to the sea.

The potential immersed weight transport rate $I_t = (\rho_s - \rho)(1 - p)Q_t = KEc_{gb} \sin\theta_b \cos\theta_b$ is assumed to be proportional to potential alongshore sediment transport rate Q_t and the arriving wave energy flux Ec_g (E is the wave energy, c_{gb} is the group speed and θ_b is the angle between the wave vector and shore normal at breaking) (USACE, 2002).

The particular values of porosity coefficient ($p = 0.4$), water density ($\rho = 1004$ kg/m³) and density of sediment ($\rho_s = 2650$ kg/m³) are immaterial for our purposes unless they vary substantially. We employ the direction-depending expression $K = 0.05 + 2.6\sin^2 2\theta_b + 0.007u_{mb}/w_f$ for the CERC coefficient K (USACE, 2002). Here $u_{mb} = (H_b/2)\sqrt{g/d_b}$ is the maximum orbital velocity in linear waves with a height of H_b, g is gravity acceleration, d_b is breaking depth, $w_f = 1.6\sqrt{gd_{50}(\rho_s - \rho)/\rho}$ is the fall velocity, with the typical grain

size $d_{50} = 0.17$ mm. The hourly, daily, monthly, annual, and long-term properties of potential transport are calcuted from the values of Q_t [m³/s] in a straightforward manner.

RESULTS

The Baltic Proper Nearshore of Latvia

Consistent with earlier estimates (Viška and Soomere, 2013), both bulk and net alongshore sediment transport are massive, usually in the range of 1–2 million m³/yr in the coastal segment from the Port of Ventspils to Cape Kolka (Figure 2). This transport is unidirectional (counterclockwise to the north-east) in most years at the annual level, with a few exceptions immediately to the south of a point near Oviši where the orientation of the coastline gently changes.

Figure 2. Annual wave-driven potential bulk transport (upper panel), ratio of annual net and bulk transport (middle panel), and annual net transport (lower panel) along the northwestern shore of Latvia from Cape Akmenrags to Cape Kolka. The positive transport direction is counterclockwise to the north-east.

The massive breakwaters of the Port of Ventspils block the entire wave-driven transport. The situation is different to the south of this port. The transport is also almost unidirectional (to the north) between this port and another location with gently turning coastline about 15 km to the south of the port. The bulk transport is also massive between Ventspils and Pavilosta but the net transport has variable direction. The jetty at Pavilosta apparently blocks wave-driven transport and divides the coastal

segment to the north of Cape Akmenrags into two more almost separated sedimentary compartments.

This coastal segment contains several zero-crossings of net transport. The upcrossings indicate divergence points of sediment flux and thus serve as most likely erosion areas (Figure 3). If they occur systematically, they serve as natural barriers separating sediment cells. The downcrossings serve as convergence points of sediment flux and usually as accumulation regions. In a similar manner, areas of increase in alongshore net transport are associated with sediment deficit and areas of decrease in this flux are likely accumulation regions (Figure 3).

This interpretation of alongshore variations of net sediment transport signals that a small headland at grid cell 90 about 15 km to the south of the Port of Ventspils serves a major barrier for sediment flux. This invisible barrier splits the sedimentary system in Figure 3 into two almost separated sedimentary units.
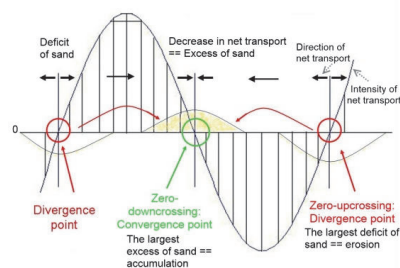
Figure 3. The relationship between the intensity (sinusoidal line) and direction (horizontal arrows) of alongshore net transport and likely accumulation/erosion areas (Soomere and Viška, 2014).

The Nearshore of Lithuania and Kaliningrad District

The situation is largely different in the coastal stretch from Cape Taran to Cape Akmenrags (Figure 4). The magnitude of potential bulk transport is still massive, mostly in the range of 0.5–1 million m³/yr, with peaks up to 2–2.5 million m³/yr between Bernati and Cape Akmenrags. Different from the above, the net transport direction is highly variable both in time and along the shore but with no clear and persistent natural zero-upcrossings. Therefore, waves can move the sediment over large distances along this coastal stretch. Only man-made structures split this stretch into different units. It is expected that the Klaipėda Strait (more specifically, coastal engineering structures at this strait) serves as a major obstacle for wave-driven sediment transport. It is likely that a long jetty that protects the entrance to the Port of Šventoji does the same.

This coastal stretch contains three parts with a different nature of wave-driven sediment transport. The northern shore of the Sambian Peninsula (Kaliningrad District, Russia) hosts predominantly counterclockwise sediment transport to the east. This transport is highly variable along the shore owing to the presence of numerous gently curved headlands. It is likely that breakwaters of Port Pionerski actually block sediment transport

even though this feature does not become clear at the scale of our simulations. Also, Cape Gvardeiskiy almost totally stops wave-driven transport. It is still likely that waves systematically carry sediment towards Zelenogradsk and further towards the Curonian Spit in spite of numerous small-scale coastal protection measures on this part of the coastline.

The nearshore of the Curonian Spit has the lowest level of both bulk and net transport in the entire study area as well as very limited alongshore variation of these quantities (Figure 4). This feature is consistent with the perception that this landform is in an equilibrium stage even though sediment transport along its shores may be fairly strong in single years (Viška and Soomere, 2012). Particularly low alongshore transport rates are characteristic of the northern part of the spit, from the latitude of Preila to the Klaipėda Strait.
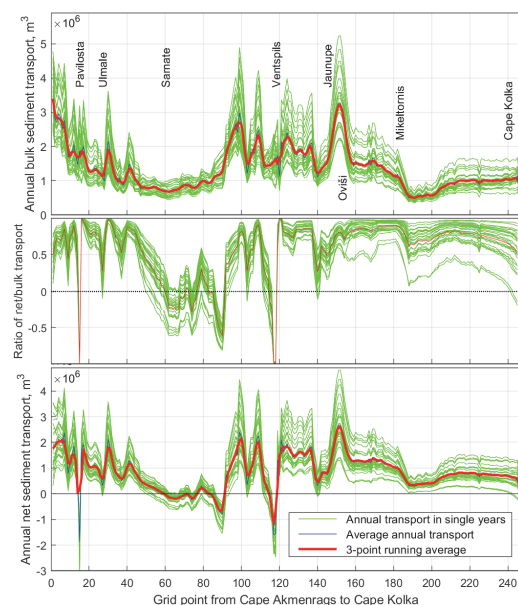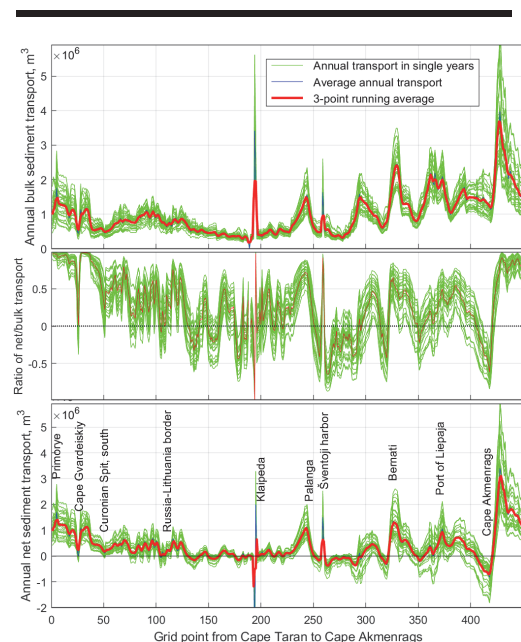

Figure 4. Annual wave-driven potential bulk transport (upper panel), ratio of annual net and bulk transport (middle panel), and annual net transport (lower panel) along the coastal stretch from Cape Taran in Kaliningrad District, Russia, to Cape Akmenrags in Latvia. The positive transport direction is counterclockwise to the east, north-east, and north.

Consistently with the outcome of historical observations and earlier simulations, the coastal segment from the Klaipėda Strait to Cape Akmenrags has a highly variable regime of wave-driven sediment transport. The net transport is very low immediately to the north of Klaipėda. Further to the north, it becomes stronger and direction-variable. The coastal segment from Šventoji to Cape Akmenrags is naturally divided into four weakly

connected compartments. Interestingly, the presence of the Port of Liepaja does not introduce any additional fragmentation of this sedimentary system at the scale of our simulations.

DISCUSSION

Our simulations confirm the general perception that the natural sedimentary system of the nearshore of the eastern Baltic Sea from Cape Taran to Cape Kolka experiences predominantly counterclockwise transport, to the east on the northern shore of Sambian Peninsula, to the north-east along the Curonian Spit and further to the north and finally to the north-east along the shore of Lithuania and Latvia, with one major natural barrier at Cape Akmenrags and two partially transparent barriers at Bernati and to the south of Ventspils. The two latter barriers become evident as temporary reversals of counterclockwise transport (Viška and Soomere, 2013).

The use of higher resolution calculations signals that this sedimentary system consists of several almost totally separated sedimentary compartments with substantially different properties whereas only a small number of separating obstacles are man-made. The transport along the northern shore of Sambian Peninsula is highly variable and not particularly intense but still mostly unidirectional. The western shore of the Curonian Spit is close to an equilibrium stage, with much lower rates and variation in the net transport. The shore segment from Klaipėda to Cape Akmenrags hosts a medium-level intensity of variable-direction transport and contains several naturally separated sedimentary units. The transport rates decrease to the north of Cape Akmenrags suggesting that sediment accumulation dominates in this segment. The Latvian nearshore further north serves as massive transit area that discharges sand to the vicinity of Cape Kolka.

CONCLUSIONS

This study offers valuable insights into sediment transport patterns in the eastern Baltic Sea, which is crucial for effective coastal management in the region. The study area contains segments with greatly different transport intensities. On the one hand, the provided estimates signal that transport rates are unusually high along the entire north-western shore of Latvia from Cape Akmenrags to Cape Kolka. This feature mostly reflects the specific feature of semi-enclosed water bodies like the Baltic Sea where high waves often approach the shore at a large angle. On the other hand, the Curonian Spit and most of the mainland shores of Lithuania are close to equilibrium.

Together with new knowledge about the role of smaller features of the shoreline and man-made structures, these estimates allow for future combined assessments of the vulnerability of the coastal system with coastal erosion studies and studies of accumulation rates or the overall redistribution of sediments (Kelpšaitė-Rimkienė *et al.*, 2021; Šakurova *et al.*, 2023).

The presented results have a direct use in detailed estimates of impacts on human activities, including dredging and shipping as well as harbor and coast management.

ACKNOWLEDGMENTS

LITERATURE CITED

Booij, N.; Ris, R.C., and Holthuijsen, L.H., 1999. A third-generation wave model for coastal regions: 1. Model description and validation. *Journal of Geophysical Research – Oceans*, 104(C4), 7649–7666. https://doi.org/10.1029/98JC02622

Björkqvist, J.-V.; Pärt, S.; Alari, V.; Rikka, S.; Lindgren, E., and Tuomi, L., 2021. Swell hindcast statistics for the Baltic Sea, *Ocean Science*, 17(6), 1815–1829, https://doi.org/10.5194/os-17-1815-2021

Björkqvist, J.V.; Lukas, I.; Alari, V.; van Vledder, G.P.; Hulst, S.; Pettersson, H.; Behrens, A., and Männik, A., 2018. Comparing a 41-year model hindcast with decades of wave measurements from the Baltic Sea. *Ocean Engineering*, 152, 57–71. https://doi.org/10.1016/j.oceaneng.2018.01.048

Broman, T.; Hammarklint, K.; Rannat, Soomere, T., and Valdmann, A., 2006. Trends and extremes of wave fields in the north–eastern part of the Baltic Proper, *Oceanologia*, 48(S), 165–184.

Eelsalu, M.; Viigand, K., and Soomere T., 2023. Quantification of longshore sediment transport and compartments in urban areas: A case study of shores of Tallinn, the Baltic Sea. *Regional Studies in Marine Science*, 67, 103199. https://doi.org/10.1016/j.rsma.2023.103199

Giudici, A.; Jankowski, M.Z.; Männikus, R.; Najafzadeh, F.; Suursaar, Ü., and Soomere, T., 2023. A comparison of Baltic Sea wave properties simulated using two modelled wind data sets. *Estuarine, Coastal and Shelf Science*, 290, 108401. https://doi.org/10.1016/j.ecss.2023.108401.

Harff, J.; Deng, J.J.; Dudzinska-Nowak, J.; Fröhle, P.; Groh, A.; Hünicke, B.; Soomere, T., and Zhang, W.Y., 2017. What determines the change of coastlines in the Baltic Sea? In: Harff, J., Furmańczyk, K., von Storch, H. (Eds), *Coastline Changes of the Baltic Sea from South to East: Past and Future Projection. Coastal Research Library* 19, 15–35. https://doi.org/10.1007/978-3-319-49894-2_2

Hersbach, H.; Bell, B.; Berrisford, P.; Hirahara, S.; Horanyi, A.; Munoz-Sabater, J.; Nicolas, J.; Peubey, C.; Radu, R.; Schepers, D.; Simmons, A.; Soci, C.; Abdalla, S.; Abellan, X.; Balsamo, G.; Bechtold, P.; Biavati, G.; Bidlot, J.; Bonavita, M.; De Chiara, G.; Dahlgren, P.; Dee, D.; Diamantakis, M.; Dragani, R.; Flemming, J.; Forbes, R.; Fuentes, M.; Geer, A.; Haimberger, L.; Healy, S.; Hogan, R.J.; Holm, E.; Janiskova, M.; Keeley, S.; Laloyaux, P.; Lopez, P.; Lupu, C.; Radnoti, G.; de Rosnay, P.; Rozum, I.; Vamborg, F.; Villaume, S., and Thepaut, J.N., 2020. The ERA5 global reanalysis. *Quarterly Journal of the Royal Meteorological Society*, 146(730), 730, 1999–2049. https://doi.org/10.1002/qj.3803

Jankowski, M.Z.; Eelsalu, M.; Parnell, K.E.; Viška, M., and Soomere, T., 2024. Longshore sediment transport analysis for a semi-enclosed basin: a case study of the Gulf of Riga, the Baltic Sea, *Estuarine, Coastal and Shelf Science*.

Kelpšaitė-Rimkienė, L.; Parnell, K.E.; Žaromskis, R., and Kondrat, V., 2021. Cross shore profile evolution after an extreme erosion event—Palanga, Lithuania. *Journal of Marine Science and Engineering*, 9, 38. https://doi.org/10.3390/jmse9010038

Leppäranta, M. and Myrberg, K., 2009. *Physical Oceanography of the Baltic Sea*. Springer Science & Business Media, Praxis, Berlin, Heidelberg. https://doi.org/10.1007/978-3-540-79703-6

Najafzadeh, F. and Soomere, T., 2024. Impact of changes in sea ice cover on wave climate of semi-enclosed seasonally ice-covered water bodies on temperate latitudes: a case study in the Gulf of Riga. *Estonian Journal of Earth Sciences*, 73(1), 26–36. https://doi.org/10.3176/earth.2024.03

Najafzadeh, F.; Jankowski, M.Z.; Giudici, A.; Männikus, R.; Suursaar, Ü.; Viška, M., and Soomere, T., 2024. Spatio-temporal variability of wave climate in the Gulf of Riga, *Oceanologia*, 66(1), 56-77. https://doi.org/10.1016/j.oceano.2023.11.00

Šakurova, I.; Kondrat, V., Baltranaitė, E., Vasiliauskienė, E. and Kelpšaitė-Rimkienė, L., 2023. Assessment of coastal morphology on the south-eastern Baltic Sea coast: The case of Lithuania. *Water*, 15(1), 79. https://doi.org/10.3390/w15010079

Sokolov, A. and Chubarenko, B., 2024. Baltic Sea wave climate in 1979–2018: Numerical modelling results. *Ocean Engineering*, 297, 117088. https://doi.org/10.1016/j.oceaneng.2024.117088

Soomere, T., 2003. Anisotropy of wind and wave regimes in the Baltic proper. *Journal of Sea Research*, 49(4), 305–316, https://doi.org/10.1016/S1385-1101(03)00034-0

Soomere, T. and Eelsalu, M., 2014. On the wave energy potential along the eastern Baltic Sea coast. *Renewable Energy*, 71, 221−233. https://doi.org/10.1016/j.renene.2014.05.025

Soomere, T. and Viška, M., 2014. Simulated wave-driven sediment transport along the eastern coast of the Baltic Sea. *Journal of Marine Systems*, 129, 96–105. https://doi.org/10.1016/j.jmarsys.2013.02.001

Soomere T.; Weisse R., and Behrens, A., 2012. Wave climate in the Arkona Basin, the Baltic Sea, *Ocean Science*, 8(2), 287–300, https://doi.org/10.5194/os-8-287-2012

Soomere, T.; Bishop, S.R.; Viška, M., and Räämet, A., 2015. An abrupt change in winds that may radically affect the coasts and deep sections of the Baltic Sea. *Climate Research*, 62(2), 163–171. https://doi.org/10.3354/cr01269.

Viška, M. and Soomere, T., 2012. Hindcast of sediment flow along the Curonian Spit under different wave climates. In: *Proceedings of the IEEE/OES Baltic 2012 International Symposium "Ocean: Past, Present and Future. Climate Change Research, Ocean Observation & Advanced Technologies for Regional Sustainability," May 8–11, Klaipėda, Lithuania*. IEEE Conference Publications. https://doi.org/10.1109/BALTIC.2012.6249195

Viška, M. and Soomere, T., 2013. Simulated and observed reversals of wave-driven alongshore sediment transport at the eastern Baltic Sea coast. *Baltica*, 26(2), 145–156. https://doi.org/10.5200/baltica.2013.26.15

Publication IV

Ocean Science

Alongshore sediment transport analysis for a semi-enclosed basin: a case study of the Gulf of Riga, the Baltic Sea

Tarmo Soomere[1,2], Mikołaj Zbigniew Jankowski[1], Maris Eelsalu[1], Kevin Ellis Parnell[1], and Maija Viška[3]

[1]Department of Cybernetics, School of Science, Tallinn University of Technology, 19086 Tallinn, Estonia
[2]Estonian Academy of Sciences, Kohtu 6, 10130 Tallinn, Estonia
[3]Department of Marine Monitoring, Latvian Institute of Aquatic Ecology, 1007 Riga, Latvia

Correspondence: Tarmo Soomere (tarmo.soomere@taltech.ee)

Abstract. The properties of wave-driven sediment transport and the dimensions of single sedimentary compartments are often radically different in different parts of semi-enclosed waterbodies with an anisotropic wind climate. The western, southern and eastern shores of the Gulf of Riga are a remote part of the more than 700 km long interconnected sedimentary coastal system of the eastern Baltic Sea from Samland in Kaliningrad District, Russia, to Pärnu Bay, Estonia. Even though shores of the gulf are generally straight or gently curved, the presence of small headlands and variations in the orientation of the coastline give rise to numerous fully or partially separated sedimentary compartments. We decompose sedimentary shores of this gulf into single compartments and cells based on the analysis of wave-driven potential sediment transport using high-resolution wave time series and the Coastal Engineering Research Centre (CERC) approach. The western shore of the Gulf of Riga forms a large interconnected sedimentary system with intense sediment transport that is largely fed by sand transported from the Baltic proper. The southern shore has much less intense sediment transport and is mostly an accumulation area. The south-eastern sector of the gulf is an end-station of counter-clockwise sand transport. The eastern shore consists of several almost isolated sedimentary cells and contains a longer segment where clockwise transport predominates. The transport rates along different shore segments show extensive interannual variations but no explicit trends in the period 1990–2022.

1 Introduction

Wave-driven sediment transport in the surf zone is a core process that shapes the shores of seas and oceans, including the key drivers of beach profile change, functioning of the cut and fill cycle, and loss of sediment to the offshore area via driving surf zone turbulence (Aagaard et al., 2021). It is also the principal agent of coastal erosion, alongshore sediment transport and sediment accumulation in the vicinity of the shoreline. These processes can be unidirectional or circulatory on comparatively straight open-ocean shores where waves usually approach the shore from a specific direction or at a small angle and where major headlands commonly divide the sedimentary system into large cells and extensive compartments (Thom et al., 2018).

The situation is complicated in waterbodies of complex shape, such as the Baltic Sea (Fig. 1) where waves often approach the shore at large angles (Soomere and Viška, 2014; Eelsalu et al., 2024b; Soomere et al., 2024). The interplay of a high angle of approach and wind patterns with a multi-peak directional structure gives rise to exceptionally powerful alongshore sediment flux (Viška and Soomere, 2013b) under a fairly modest wave climate (Björkqvist et al., 2018; Giudici et al., 2023), specific mechanisms that stabilise beaches that are almost at equilibrium (Eelsalu et al., 2022) and persistent sediment flux divergence areas which are most likely erosion hotspots at certain locations with small changes in the orientation of the coastline (Soomere and Viška, 2014; Eelsalu et al., 2023). To better characterise such situations, we use the term "cell" to denote relatively small coastal segments, elementary sedimentary units that either are mostly separated
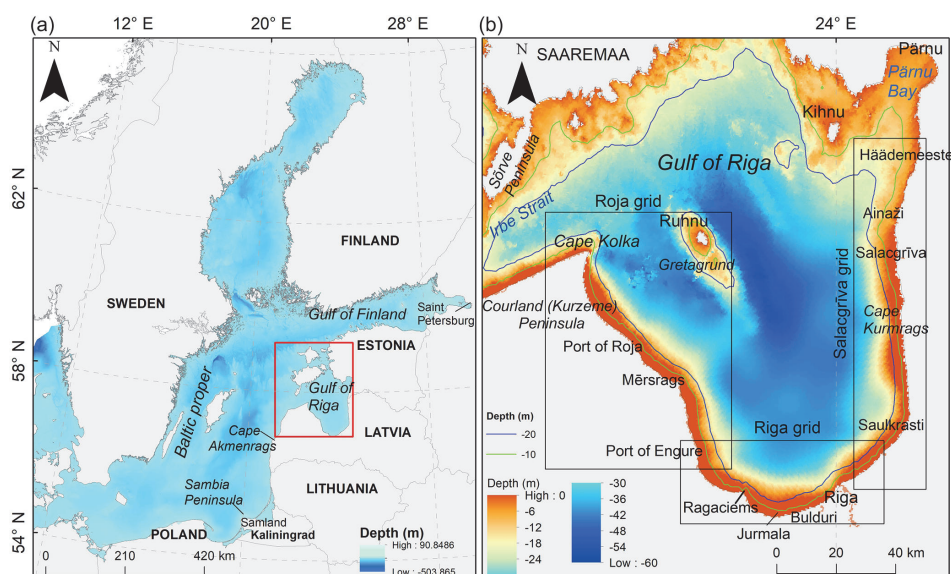
Figure 1. Map of the study area **(a)**, showcasing the three subgrids of the wave model used in the analysis of wave-driven alongshore sediment transport **(b)**. The entire left panel **(a)** represents the area covered by the outermost grid. The area covered by the second-level grid **(a**, red box) is chosen to properly represent the wave fields entering the Gulf of Riga directly from the Baltic proper and via the straits connecting this gulf with the West Estonian Archipelago. See detailed bathymetric maps of the Gulf of Riga in, for example, Tsyrulnikov et al. (2008, 2012).

from the neighbouring segments or exhibit other clearly identifiable features (e.g. cells of predominantly one-directional sediment transit versus cells with almost no net sediment transport). In a similar manner, we use the term "compartment" to denote clusters of cells that usually exchange sediment within the cluster but have either very limited sediment exchange with other compartments (e.g. because of the presence of a major divergence area of sediment flux) or only one-way sediment exchange with a neighbour.

Massive alongshore sediment transport is one of the main reasons for extensive coastal erosion (Eberhards et al., 2009) and the formation of large accumulation features that sometimes occur at a large distance from the erosion areas in the eastern Baltic Sea (Tõnisson et al., 2016). This transport may amplify the impact of coastal defence structures on sediment deficit (Bernatchez and Fraser, 2012). It can also be a major problem from the viewpoint of coastal infrastructure design and maintenance (Bulleri and Chapman, 2010), the management of the urban coastal landscape, and the increasing resilience of coastal socio-ecological systems (Villasante et al., 2023). Persistent sediment flux divergence areas may serve not only as erosion locations but also as invisible barriers to alongshore sediment transport. Such locations may thus split large seemingly connected sedimentary systems into smaller cells and compartments. The separation of large sedimentary systems into smaller cells makes it possible to greatly simplify the analysis of properties of the entire system (Kinsela et al., 2017), better understand the functioning and resilience of single compartments, and reach optimum solutions for the design of various structures or beach management and nourishment actions, as demonstrated, for example, in Cappucci et al. (2020) and Susilowati et al. (2022). Moreover, such divergence areas are natural limits for the propagation of pollution that is carried along the shore with sediment parcels.

Wave-driven sediment transport plays a particularly large role in shaping sedimentary and/or easily erodible shores of relatively young waterbodies, such as the Baltic Sea (Fig. 1). Wave impact is almost negligible for the development of its western, northern and north-eastern bedrock coasts that have very little sandy coast. The other shores of this sea, from southern Sweden counter-clockwise to the vicinity of Saint Petersburg, is predominantly sedimentary, most of which is still rapidly developing (Harff et al., 2017). The coastal stretch from Sambia Peninsula (Samland) to Pärnu Bay in the Gulf of Riga is a $> 700\,\mathrm{km}$ long interconnected sedimentary coastal system, with an almost continuous strip of sand and mostly counter-clockwise sediment transport (Knaps, 1966; see Viška and Soomere, 2013b, for references). This transport is particularly massive along the north-western shore of Latvia where it reaches $1\,000\,000\,\mathrm{m^3\,yr^{-1}}$ (Knaps, 1966).

Wave-driven transport along this stretch of coast was estimated at a relatively low spatial resolution of about 5.5 km

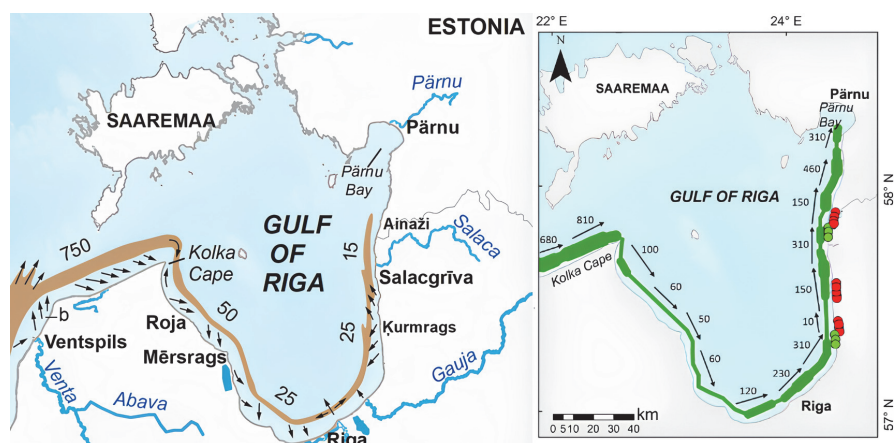**Figure 2.** Left: sediment transport into the Gulf of Riga and along its western, southern and eastern shores in thousands of cubic metres per year evaluated from in situ observations (Knaps, 1966; Ulsts, 1998). Erosion and accumulation areas are indicated with small arrows. Adjusted from graphics created by Kaspar Ehlvest. Right: numerically estimated wave-driven potential net sediment transport in thousands of cubic metres per year for 1970–2007 (Viška and Soomere, 2013b). Numbers indicate the magnitude of transport; arrows its direction; and red and green circles sediment flux divergence and convergence areas in single years, respectively.

for 1970–2007 (Viška and Soomere, 2013b; Soomere and Viška, 2014). There is one major accumulation area near Cape Kolka (north-western Latvia) and one almost permanent sediment flux divergence area near Cape Akmenrags on the western coast of Latvia. Both these features are a result of the interplay between the shape and orientation of this stretch of coast and the two predominant wind directions (south-west and north-west or north-north-west) in the area (Soomere, 2003).

These features divide this sedimentary system into three major compartments. Two of them are weakly interconnected with potential annual net sediment flux across Cape Akmenrags occurring approximately once in 40 years (Soomere and Viška, 2014). Sediment transport from the shores of the Baltic proper to the interior of the Gulf of Riga is apparently an almost entirely one-way process. The spatial resolution of the transport model used in Soomere and Viška (2014), however, is too low to identify smaller-scale features of alongshore sediment transport and partially or totally separated sedimentary cells. Some indication of their presence can be inferred from the existence of temporary divergence areas and reversals (clockwise transport) of alongshore sediment flux (Viška and Soomere, 2013b) at many locations. These simulations have ignored the presence of human-made structures that may partially or totally block wave-driven sediment transport and thus create additional fragmentation of sedimentary systems.

The focus of our study is the Gulf of Riga where observations of Knaps (1966) signal a complicated pattern of erosion, transit and accumulation areas (Fig. 2). Erosion was observed near Roja, south of Mersrags, and between Cape

Kurmrags and Salacgriva, while accumulation was noted to the north of Mersrags, near Jūrmala (Bulduri; Fig. 1b) and Riga, and near Ainaži. These observations, apparently stemming from the 1960s and updated in the 1990s (Ulsts, 1998), suggest that the actual pattern of sediment transport along the shores of this waterbody may be quite complicated.

This conjecture is supported by the analysis of Viška and Soomere (2013b) and Soomere and Viška (2014). They were not able to reproduce minor headlands and smaller changes in the orientation of the coast because of low spatial resolution, and thus they may have overlooked many local features of transport. Their study suggests that sediment transport along the southern and eastern shores of the Gulf of Riga (Fig. 2) could be much more substantial than that estimated in Knaps (1966) and Ulsts (1998). Some of the difference may stem from the limited availability of fine sediment in this part of the study area. More importantly, they highlighted several frequently occurring divergence points of sediment flux and spatially varying temporary reversals of the overall counter-clockwise sediment transport in terms of annual potential net transport between Cape Kurmrags and Saulkrasti (Figs. 1 and 2).

These observations match the conclusions of earlier studies (Knaps, 1966; Ulsts, 1998) suggesting that sediment transport may have a discontinuity (a persistent location of divergence of net sediment flux) in the vicinity of Cape Kurmrags. This kind of discontinuity would be impossible in a wave climate where winds from one particular direction (e.g. south-west, SW) dominate. The transport pattern along any almost-straight coastal stretch would then be one-directional. The presence of such a discontinuity is, how-

ever, a natural feature of shores that evolve under a two-peak directional distribution of predominant winds (Eelsalu et al., 2023, 2024a). This is the case in the study area where SW and north-western or north-north-western (denoted as (N)NW below) winds are dominant (see Sect. 2.2 for details). Waves generated by (N)NW winds predominate in sediment transport to the south of a certain location in the eastern shore of the Gulf of Riga and waves driven by SW winds predominate to the north of it. A natural conjecture deriving from the large alongshore variation in this location (the divergence area of sediment flux) over > 20 km (four grid points of Viška and Soomere, 2013b) between Cape Kurmrags (Fig. 2) and Saulkrasti (Fig. 1b) is that several partially isolated sedimentary compartments may exist in this area.

The main objective of this study is to decompose the sedimentary system along a semi-isolated coast in the interior of the Gulf of Riga (Fig. 1) into partially or totally separated sedimentary cells and compartments based on simulations of wave-driven alongshore transport at a considerably increased spatial resolution that matches the typical spatial scale of coastal formations in this region and allows for the identification of human-made features blocking sediment transport. The improved resolution makes it possible to correlate more exactly the directional structure of incoming wave forcing with the bathymetry and geometry in the study area and sheds more light on the associated structure of alongshore sediment transport. Along with a straightforward update of the earlier estimates of potential sediment transport, we aim to more exactly specify sediment flux divergence and convergence areas and the associated configurations of sedimentary compartments and cells on the sedimentary shores of the Gulf of Riga. This analysis is followed by quantification of trends and interannual variations in the sediment transport in this area. Finally, we question why an interesting signal of wave climate change, namely a permanent increase in bulk transport for 1970–2007 from Cape Taran to Pärnu Bay, combined with an increase in net transport for 1970–1990 and decrease for 1990–2007 (Soomere et al., 2015), was not detected in the Gulf of Riga (Viška and Soomere, 2013a).

As the seabed of the northern and north-eastern parts of this waterbody from the Sõrve Peninsula to Pärnu Bay (Fig. 1b) is rocky or muddy, mostly with a low availability of mobile sediment; the shoreline is heavily indented; and the shallow area contains numerous islets and underwater features (Tsyrulnikov et al., 2008), we focus on the eastern, southern and western shores of the gulf that comprise an almost continuous sandy strip. These coastal stretches are represented by the Salacgriva grid, the Riga grid and the Roja grid, respectively, in Fig. 1b. The northern and north-eastern parts of the gulf are however naturally included in the wave model that covers the entire Gulf of Riga.

We use a set of time series of wave properties derived from a three-level nested SWAN (Simulating WAves Nearshore) wave model with a spatial resolution of the innermost grids of about 600 m. Wave-driven bulk and net potential sedi-

ment transport is evaluated using the Coastal Engineering Research Centre (CERC) approach (USACE, 2002). The results of the analysis are interpreted in terms of annual values of bulk and net potential transport. Section 2 gives an overview of the study area and its wind and wave climate, an insight into how the wave data are obtained and validated, how alongshore sediment flux is evaluated, and how the presence of human-made structures is interpreted. Section 3 presents the analysis of the core properties of sediment flux in different parts of the Gulf of Riga and depicts the division of these shores into sedimentary cells and compartments. Section 4 highlights similarities and differences in sediment transport on the western, southern and eastern shores of the gulf and discusses the implications of the established features for coastal processes.

2 Method and data

2.1 Study area

The Gulf of Riga (Fig. 1) is the third largest semi-enclosed subbasin of the Baltic Sea, with a surface area of $17\,913\,\mathrm{km}^2$ and an average and maximum depth of 21 and 52 m, respectively. A detailed overview of the basic geographical, geological, climatic and oceanographic features of the Baltic Sea and its larger subbasins are provided in Feistel et al. (2005) and Leppäranta and Myrberg (2009). It has an oval-like shape with dimensions of approximately $130\,\mathrm{km} \times 140\,\mathrm{km}$ (Suursaar et al., 2002). As mentioned above, its northern and north-eastern parts have irregular bathymetry and geometry and are not addressed in this study. The bathymetry in the central part of the gulf and in the study area is regular (except for the island of Ruhnu and shallow Gretagrund to the south of this island). The width of the shallow nearshore varies insignificantly. The 10 and 20 m isobaths are located approximately 2 and 3.5–8 km from the shore, respectively, along the Latvian shores (see e.g. Fig. 1 in Tsyrulnikov et al., 2012). The main sedimentological properties of the nearshore of the study area are presented in Viška and Soomere (2013b).

Similar to the entire Baltic Sea, the coasts of the Gulf of Riga are relatively young and develop comparatively rapidly (Harff et al., 2017; Eelsalu et al., 2025b). They have shown only slow coastal retreat or advance for 1935–1990 (Ulsts and Bulgakova, 1998; Eberhards and Lapinskis, 2008). The extent of the eroding areas and the rate of erosion seem to have increased for 1992–2007 (Tõnisson et al., 2013), with the fastest erosion seen near Roja, Engure, Ragaciems and Jūrmala in the western and southern parts of the gulf and near Saulkrasti and Cape Kurmrags in the eastern part (Eberhards and Lapinskis, 2008). See also Luijendijk et al. (2018) for the latest estimates.

According to Bertina et al. (2015), "[the] Gulf of Riga is an area in which combined sea erosion and accumulation processes, as well as alluvial processes, play significant roles

Figure 3. Eroding eastern shore of Cape Kolka. Photo by T. Soomere, 24 August 2013.

in the coastal development." They reported relatively rapid coastline retreat immediately to the south-east of the western jetty of the Daugava River mouth and equally rapid coastline advancement further south-west until the Lielupe River mouth. Coastal processes are fastest during strong (wave) storms when accompanied by a high water level, such as in Hurricane Erwin/Gudrun in 2005 (Eberhards et al., 2006; Lapinskis, 2017), during which the maximum shoreline retreat was 15–27 m. This storm most strongly affected southern and eastern coasts of the Gulf of Riga (Eberhards et al., 2006), and an estimated $0.8 \times 10^6 \, \text{m}^3$ of sediment was lost from the subaerial part of the coastal slope (Lapinskis, 2017).

The described processes are obviously related to unusually massive wave-driven alongshore sediment transport in the eastern Baltic Sea under relatively mild wave conditions (see Sect. 2.2 for more details). About $700\,000$–$800\,000\,\text{m}^3$ of sand is transported per year towards Cape Kolka along the north-western shore of Courland (Kurzeme) Peninsula (Knaps, 1966; Viška and Soomere, 2013b; Jankowski et al., 2024) (Fig. 2). About 90 % of this mass is deposited in the vicinity of Cape Kolka, and only about $50\,000\,\text{m}^3\,\text{yr}^{-1}$ is further transported into the sedimentary system of the Gulf of Riga (Knaps, 1966). This transport is almost entirely one way. The accumulation area is to the north of Cape Kolka as the eastern shore of the cape is rapidly eroding (Fig. 3). The magnitude of sediment transport evaluated from observations is from $15\,000$ to $50\,000\,\text{m}^3\,\text{yr}^{-1}$ in different segments of the study area (Knaps, 1966; Ulsts, 1998). It is much smaller near Riga and remained undefined for the coastal segment to the north of Ainaži in older estimates (Knaps, 1966; Ulsts, 1998), while lower-resolution simulations (Viška and Soomere, 2013b) suggested that potential net transport flux continued almost unidirectionally towards Pärnu.

2.2   Wind and wave climate in the study area

The study area is located at the southern margin of the North Atlantic storm track. It is characterised by the frequent passage of low-pressure systems from the North Atlantic that often produce high winds that are favourable for both severe wave generation (Björkqvist et al., 2017, 2020) and wind energy generation (Barzehkar et al., 2024). The area of relatively persistent high winds (in terms of the capacity factor, Barzehkar et al., 2024) extends from the SW part of the Baltic Sea to the nearshore of Latvia and Estonia and also embraces the Gulf of Riga.

This situation gives rise to a highly anisotropic wind climate that is much more complicated than simply a dominant airflow from the west. While the directional distribution of weaker winds is almost isotropic, moderate and strong winds mostly blow from two directions in the north-eastern Baltic proper (Soomere and Keevallik, 2001; Soomere, 2003). The majority of such winds blow from the SW, while winds from the (N)NW directions are less frequent but may have even larger speeds than the south-west winds (Soomere, 2001). This two-peak pattern of predominant moderate and strong winds is characteristic for the study area. It is less evident at the latitudes of the Gulf of Finland and to the south of Lithuania (Soomere et al., 2024). This strongly anisotropic pattern, with relatively weak and infrequent easterly winds, is evidently responsible for very high water levels in two locations of the Gulf of Riga: Pärnu in the north-east and Riga in the south-east of the gulf (Hünicke et al., 2015; Männikus and Soomere, 2023).

Similar to the entire Baltic Sea, wave fields in the Gulf of Riga are almost entirely driven by local storms and contain a small proportion of long-period swell (Björkqvist et al., 2021; Najafzadeh et al., 2024). This feature means that long-term average significant wave heights are fairly low, well below 1 m in the Gulf of Riga, and even the higher percentiles remain moderate (Fig. 4), but unexpectedly severe wave conditions may occur in this basin (Björkqvist et al., 2017; Najafzadeh et al., 2024). In other words, the wave climate is highly intermittent (Soomere and Eelsalu, 2014) in the sense that most of the annual wave energy arrives at the coast in a few days. Consequently, the propagation direction of waves during these storms plays the most important role in coastal evolution.

As the wave fields of substantial height are fetch-limited (i.e. their properties and most importantly wave propagation direction largely follow the local wind properties) in the Gulf of Riga (Najafzadeh et al., 2024), waves excited by predominant strong winds from the SW or (N)NW play a key role in coastal processes and alongshore sediment transport in this waterbody. More specifically, waves from these narrow ranges of direction often provide up to 80 %–90 % of the total net and bulk transport. In other words, what happens in a particular coastal location largely depends on the delicate
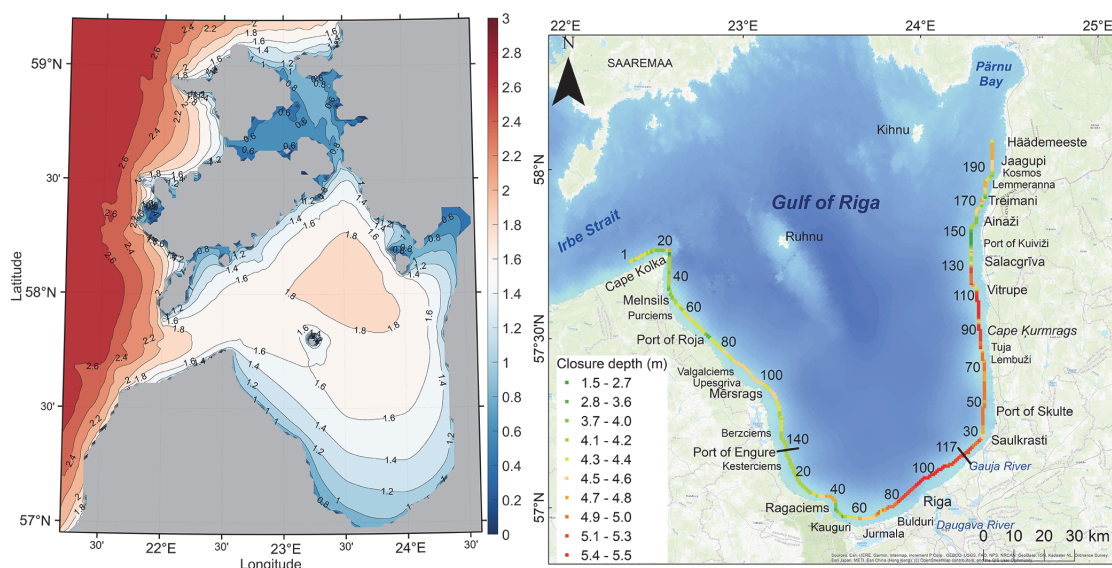
Figure 4. Left: 95th percentile of significant wave height in the Gulf of Riga and its vicinity based on the SWAN model simulations for 1990–2022 with a resolution of 1 nmi (Fig. 1). Right: closure depth (colour code) at wave model grid points and sequential numbers of grid cells selected for the study from three model grids (Roja, Riga and Salacgriva grids; Fig. 1b) based on wave data from Giudici et al. (2023) and Najafzadeh et al. (2024). Short black lines in the right panel are the separation of the model grids with 600 m resolution.

balance of alongshore transport under the impact of these two wave systems (Eelsalu et al., 2024a).

2.3 The SWAN model data for the nearshore of the study area

The instantaneous rate of wave-driven potential alongshore sediment transport is evaluated using the classic Coastal Engineering Research Council (CERC) approach (USACE, 2002). This model relates sediment transport in the nearshore, from the breaker line to the shoreline, with the arriving wave energy flux at the breaker line, water and sediment density, and sediment porosity under the assumption of unlimited availability of non-cohesive sediment. For this purpose we employ a high-resolution time series of significant wave height, average wave propagation direction and peak period reconstructed for the time period 1990–2022 using a triple-nested version of the third-generation phase-averaged spectral wave model SWAN (Booij et al., 1999). The model cycle III, version 41.31A, was forced by ERA5 wind information (Hersbach et al., 2020) in an idealised ice-free set-up. The presence of currents and varying water levels was ignored. Varying water levels do not affect our results because we only consider the idealised case of potential transport that is independent of the particular water level. The main limiter of the accuracy of calculations is the quality of wind and bathymetry information. The presence of currents may mod-

ify wave properties to some extent, but there is currently no way to reliably replicate the current system of the Gulf of Riga. Ignoring ice cover apparently leads to an overestimation of transport of up to 20 % (Najafzadeh and Soomere, 2024).

A detailed overview of the particular wave model implementation and its validation for the Baltic proper and Gulf of Finland against instrumentally recorded wave data is provided in Giudici et al. (2023). The quality of the reconstruction of wave properties in simulations using ERA5 winds in this basin of fairly complicated shape was generally better than in simulations using local high-quality open sea winds (Männikus et al., 2024). An additional verification of the output of the model in the Gulf of Riga and near its entrance in the eastern Baltic proper as well as a thorough description of the Gulf of Riga wave climate 1990–2021 is provided in Najafzadeh et al. (2024) and briefly summarised in Sect. 2.2.

This model is applied to the entire Baltic Sea at a 3 nautical mile (nmi; 1 nmi = 1852 m) resolution and to the Gulf of Riga and its vicinity (Fig. 1) at a 1 nmi resolution (0.03° in the east–west direction and 0.015° in the north–south direction). The eastern, southern and western coastal areas of the gulf, with a mostly straight shoreline, are covered with three realisations of a regular rectangular grid with a resolution of 0.32 nmi (about 600 m) called the Roja, Riga and Salacgriva grids, respectively (Fig. 1b). The extent of the sets of relevant grid points along the shoreline, from which input information

for transport calculations is retrieved, is indicated in Fig. 4. Accordingly, the shoreline of the study area is divided into about 600–800 m long sectors depending on the mutual orientation of the shoreline and grid cells. The grid system employs a one-way information flow of wave properties from the 3 nmi grid to the 1 nmi grid and then separately to each of the three 0.32 nmi grids (Najafzadeh et al., 2024). Simulations of wave properties on the innermost 0.32 nmi grids are performed independently.

An adequate application of the CERC approach presumes that wave properties are known somewhere offshore from the breaker line (USACE, 2002). This is a challenge for high-resolution wave models that extend almost to the shoreline. Several grid points of the wave model close to the shore have a water depth of only 1–2 m. Small waves that are adequately described by the model at such depths may serve as an important constituent of the sediment transport system in this area (Eelsalu et al., 2022). However, most sediment motion is usually generated by a few of the strongest storms in the year (Różyński, 2023). As mentioned above, the wave climate of the eastern Baltic Sea is extremely intermittent: some 30 % of the annual wave energy flux arrives within a few days with very severe waves (Soomere and Eelsalu, 2014). Wave properties for the evaluation of wave-driven transport using the CERC model should be taken from those model grid cells that adequately reflect the most severe wave conditions. Such grid cells are normally located offshore of the breaker line that exists in the strongest storms.

A natural limit for water depth at which the breaker line is located is the closure depth, down to which strong waves systematically relocate sediment. The closure depth, evaluated using wave data at 5.5 km resolution for 1970–2007 (Räämet and Soomere, 2010; Soomere and Räämet, 2011, 2014), varies between 3 and 5 m (Soomere et al., 2017), being the largest near Pärnu and in the Irbe Strait. This resolution obviously does not resolve many important features of nearshore bathymetry and shore geometry in the study area.

To more adequately represent the properties of severe wave storms for the CERC model, we selected wave model grid cells for calculations of wave-driven sediment transport based on the 95th percentile wave heights, bathymetry data and re-estimated closure depths (Fig. 4). More specifically, we employed a four-step procedure for this selection. Firstly, we identified the closest cells along the shoreline that had water depth of at least twice the 95th percentile of simulated significant wave height for each coastal segment. Secondly, we re-evaluated closure depth for these cells (Fig. 4). Thirdly, wave simulations with a resolution of ∼ 600 m for 1990–2022 used in this paper add several nuances to this pattern. They stressed the severity of waves in the south of the gulf near Riga and also showed that the values of closure depth at this resolution do not necessarily match similar values estimated using a lower resolution (Soomere et al., 2017). As the SWAN model adequately resolves the loss and redistribution of wave energy in relatively shallow water, the closure depth

estimated at this resolution may considerably depend on the water depth in a particular grid cell. For this reason, closure depth was re-evaluated for the selected cells. Based on this estimate (Fig. 4), the initially selected cell was replaced by the adjacent cell closer to or further from the coast, keeping in mind that the water depth in the cell finally selected should generally exceed the closure depth evaluated for each particular location. As the fourth step, this selection was on some occasions adjusted to mirror the overall coastline shape with the set of selected grid cells and, where applicable, to maintain a more or less constant distance from the coastline.

The set of selected wave model grid cells (Fig. 4) contains 159 cells along the western shore of the Gulf of Riga (Roja grid; Fig. 1b), 117 cells along the southern shore (Riga grid) and 201 cells along the eastern shore (Salacgriva grid). Each such cell was associated with the average orientation of the coastline and isobaths down to the closure depth. In essence, the coastline of the study area was approximated with a piecewise straight line consisting of lines with this orientation (Fig. 5). The length of such pieces usually varies between 560–800 m depending on the orientation of the coastline with respect to coordinate lines. Some cells were in the overlapping parts of the grids. The natural boundaries of grids were at the port of Engure and at the Gauja River mouth (Fig. 4). These locations are major obstacles for wave-driven alongshore sediment transport. The analysis below includes 22 cells and associated coastal sectors to the west of Cape Kolka (to provide an indication of transport along the shore of the Baltic proper) and 123 cells from Cape Kolka to the port of Engure in the Roja grid, 110 cells from the port of Engure to the Gauja River mouth along the southern shore of the Gulf of Riga, and 190 cells from the Gauja River mouth to the Estonian township of Häädemeeste along the eastern shore of the gulf.

2.4 Wave properties at the breaker line

In situations where waves usually approach the shore at a small angle between the wave propagation direction and shore normal, it is reasonable to evaluate changes in wave properties from the selected wave model grid cells to the breaker line by means of the evaluation of wave shoaling and loss of wave energy due to whitecapping and wave–bottom interaction using simplified formulas (e.g. Larson et al., 2010). The situation is more complicated in the Baltic Sea where waves often approach the shore at large angles (Eelsalu et al., 2024b). Waves in the Gulf of Riga are usually shorter than in the Baltic proper (Eelsalu et al., 2014; Najafzadeh et al., 2024). This feature together with the narrowness of the relatively shallow nearshore (see above, Fig. 1b) implies that the impact of refraction on wave propagation is usually comparatively small and wave fields frequently approach the breaker line in the Gulf of Riga at a relatively large angle.
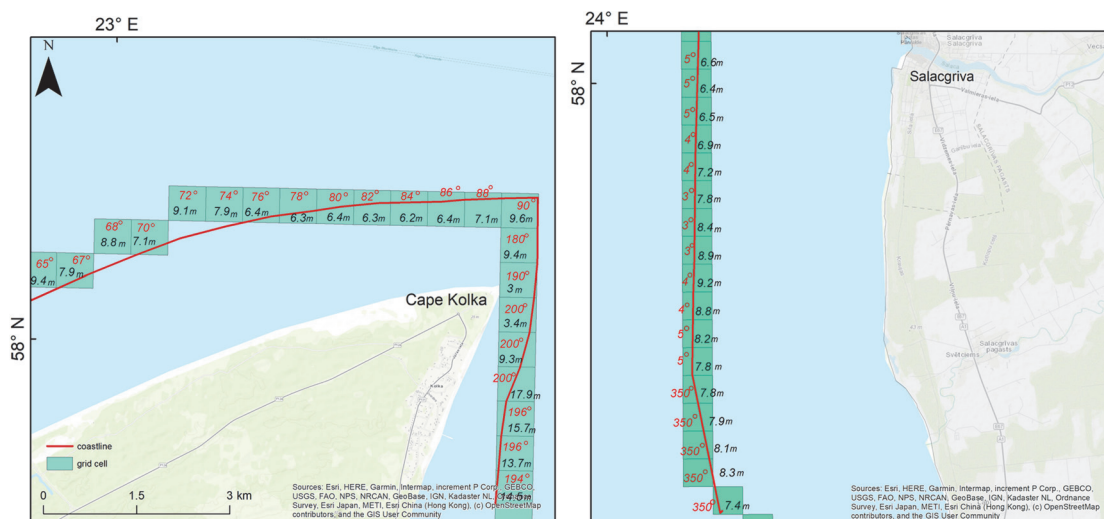
Figure 5. Examples of wave model grid cells used in the analysis, water depth in these cells and the associated orientation of the coastline (bold line in the cells) near Cape Kolka (left) and Salacgriva (right).

In this case it is necessary to evaluate the joint impact of shoaling and refraction to wave properties along the path of the waves from the model grid cell to the breaker line. This can be done, to a first approximation, by assuming that the seabed height increases smoothly shoreward from the wave model grid cell to the breaker line, with isobaths parallel to the shoreline. This assumption, even though not perfect, makes it possible to analytically evaluate the joint effect of shoaling and refraction on the properties of the waves that approach the shore at a relatively large angle during their propagation from the nearshore model grid cells to the breaker line. In the idealised case of a monochromatic wave field with a height H_0 that propagates towards the shore with a phase and group speed c_{f0} and c_{g0}, respectively, and at an angle θ_0 between the wave vector and shore normal, an application of linear wave theory leads to the following algebraic equation of sixth degree for the wave height H_b at the breaker line (Soomere et al., 2013; Soomere and Viška, 2014):

$$H_b^5 g \left(1 - \frac{H_b g}{\gamma_b} \frac{\sin^2 \theta_0}{c_{f0}^2} \right) = H_0^4 \gamma_b c_{g0}^2 (1 - \sin^2 \theta_0). \quad (1)$$

The subscript "b" denotes the wave properties at the breaker line. A simple way to close Eq. (1) is to assume that (a) the breaking index $\gamma_b = H_b / d_b = 0.8$ is constant (where d_b is the water depth at the breaker line) and (b) breaking waves are long waves, which means that $c_{gb} = c_{fb} = \sqrt{g d_b}$ at the breaker line. These approximations are not perfect: the breaking index may substantially vary (Lentz and Raubenheimer, 1999; Power et al., 2010; Raubenheimer et al., 1996, 2001; Sallenger and Holman, 1985), and breaking waves are

often not ideal long waves. An advantage of these assumptions is that they make it possible, to first approximation, to systematically take into account specific features of wave fields that approach the shore at a large angle. The smaller of the two real solutions of Eq. (1) indicates the breaking wave height. The angle between the wave propagation direction and shore normal at breaking is evaluated using Snell's law.

2.5 Evaluation and interpretation of sediment transport

The hourly values of instantaneous potential sediment transport are evaluated for each coastal sector associated with the relevant selected wave model grid cell using the CERC approach (USACE, 2002) based on hourly time series of wave properties at the breaker line. The core approximation in the CERC formula $I_t = K P_t = K E c_{gb} \sin \theta_b \cos \theta_b$ is that the wave-driven transport rate is proportional to the rate of beaching of the wave energy flux $E c_g$ (E is the wave energy at the breaker line) in the given coastal sector. The quantity $I_t = (\rho_s - \rho)(1 - p) Q_t$ has the meaning of the potential immersed weight transport rate that is proportional to the potential alongshore sediment transport rate Q_t (USACE, 2002), ρ_s is the density of non-cohesive sand, p is the porosity coefficient, and ρ is water density. The transport was interpreted as positive (counter-clockwise drift) if it was directed to the right with respect to the observer looking to the sea. The net transport for a coastal sector and a specific time period was evaluated as the sum of directional values of hourly transport, i.e. taking into account the sign of Q_t. This quantity mirrors the amount of sand that would be actually transported along

the shore during a certain time interval under ideal conditions. The bulk transport was calculated as the sum of absolute values of Q_t, equivalently, as an integral of the absolute value of instantaneous transport over the period of interest, from single months to the entire simulation period. This quantity provides an estimate of the total amount of sand that was moved in the sector in any direction, including "back-and-forth" transport under ideal conditions.

We use constant values of the porosity coefficient $p = 0.4$ and water density $\rho = 1004 \, \mathrm{kg \, m^{-3}}$ that roughly correspond to the typical material of sand (quartz) and the average salinity of 4.90–$5.38 \, \mathrm{g \, kg^{-1}}$ of the upper mixed layer of the Gulf of Riga (Skudra and Lips, 2017). We employ the direction-dependent expression $K = 0.05 + 2.6 \sin^2 2\theta_b + 0.007 u_{mb}/w_f$ for the CERC coefficient K (USACE, 2002). Here $u_{mb} = (H_b/2)\sqrt{g/d_b}$ is the maximum orbital velocity in linear waves, and $w_f = 1.6\sqrt{g d_{50}(\rho_s - \rho)/\rho}$ is the fall velocity. We assume that the typical grain size $d_{50} = 0.17 \, \mathrm{mm}$ is constant and apply the density of sand $\rho_s = 2650 \, \mathrm{kg \, m^{-3}}$.

While the modelled wave time series were carefully validated against several sets of recorded wave properties (Giudici et al., 2023; Najafzadeh et al., 2024), a similar validation of evaluated transport rates against direct observations of transport was not possible because of the absence of contemporary field data. For this reason, the validation was performed implicitly by means of a comparison of the results with earlier observations (Knaps, 1966; Ulsts, 1998), the output of lower-resolution simulations (Soomere and Viška, 2014), and otherwise known areas of erosion or accretion. However, as the simulated potential transport reflects the wave impact on coastal sediment under ideal conditions of unlimited availability, actual transport is usually much less intense.

The most interesting coastal segments are the locations of the zero-crossings of net transport. The upcrossings in this projection (positive transport direction to the right with respect to the observer looking to the sea) indicate divergence points of sediment flux and thus serve as the most likely erosion areas (Fig. 6) and natural barriers separating sediment cells. The downcrossings are convergence points of sediment flux that usually mirror accumulation areas. In a similar manner, an increase in alongshore net transport from the left to the right usually reflects locations with sediment deficit, and a decrease in this transport in this direction reflects accumulation regions (Fig. 6).

The resolution of wave and sediment transport models is such that the presence of breakwaters at major river mouths and several smaller harbours is reflected in the location of the grid cells that are used to evaluate wave properties at the breaker line as well as in the local orientation of the breaker line (Fig. 6). Breakwaters of such harbours usually extend to 300–500 m or even more offshore from the coastline into water depths that exceed the closure depth. This is the situation at Roja, Mersrags, Engure, the Daugava River mouth, Skulte, Salacgriva, Kuiviži, Ainaži, Treimani and the Kos-

mos establishment in Estonia. On the one hand, such structures almost totally block wave-driven alongshore sediment transport, most of which occurs in the surf and swash zone. On the other hand, sediment accumulation at the downstream (or outer) side of such structures leads to a rapid variation in the orientation of shoreline and isobaths near the structure. The piecewise linear approximation of the shoreline and isobaths described in Sect. 2.4 largely follows the orientation of the breakwaters or jetties in the relevant cells and thus has substantially different orientation than its neighbouring sections (Fig. 6). The formal application of the CERC approach usually leads to completely unrealistic estimates of sediment transport in such cells. It is therefore natural to remove such locations from calculations of alongshore transport. Moreover, it is also natural to conclude that structures that extend deeper than closure depth serve as almost complete barriers to sediment flux in the sense that waves and associated currents may transport some sediment around them under extreme conditions, but no through-transport occurs under the usual conditions.

A direct consequence of the use of the CERC approach is that we only evaluate alongshore transport. This approximation is partially justified in the light of the presence of unusually strong alongshore transport in the study area under the relatively mild wave climate. The main reason for such intense transport is that waves often approach the shore at a large angle. A natural consequence of this feature is that cross-shore transport usually plays a much smaller role than might be expected in most of the eastern Baltic Sea shores, except for a few locations (e.g. Šakurova et al., 2025). An implication of neglecting cross-shore transport is that shoreline relocation does not necessarily follow the accumulation or erosion rates. However, our conclusions only concern alongshore variations in wave-driven transport and the impact of human-made structures on this transport, and thus they are invariant with respect to the impact of cross-shore transport.

3 Alongshore sediment transport patterns

3.1 Almost unidirectional transport along the western shore

We start the analysis from the western shore of the Gulf of Riga that is represented by the Roja grid in Fig. 1b and is defined to extend from the area of Cape Kolka to the port of Engure (Fig. 4). An extension of the study area to the north-western shore of Cape Kolka over about 15 km (22 wave model grid points; Fig. 5) provides an option to compare the results with in situ observations and earlier simulations. As expected, the intensity of potential wave-driven bulk (independent of direction) sediment transport in the interior of the Gulf of Riga is several times smaller than along the shore of the Baltic proper of Latvia (Fig. 7). While the typical bulk transport is about $1\,000\,000 \, \mathrm{m^3 \, yr^{-1}}$ to the
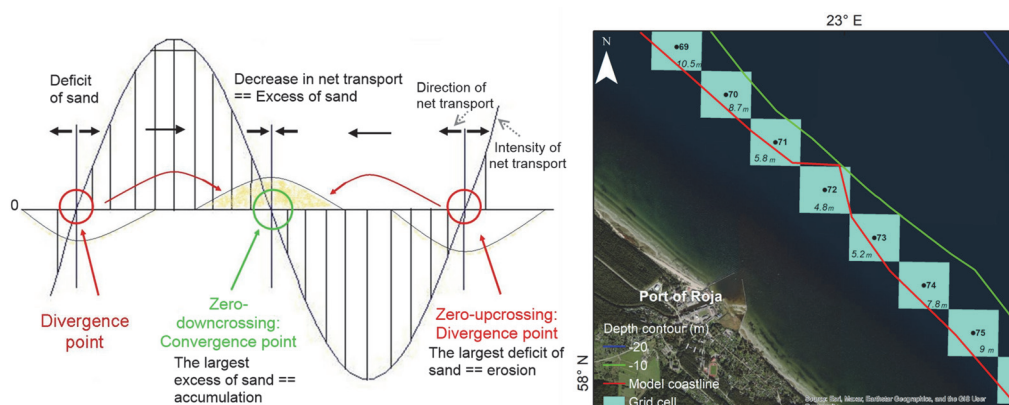
Figure 6. Left: a schematic for the interpretation of alongshore changes in the intensity and direction of wave-driven alongshore net transport areas (Soomere and Viška, 2014). Reprinted with permission from Elsevier, Licence 5850280172485. Right: location of wave model grid cells and orientation of the model coastline in the vicinity of the port of Roja.

west of Cape Kolka (Viška and Soomere, 2013b; Jankowski et al., 2024), it drops to $200\,000 \pm 100\,000\,\mathrm{m^3\,yr^{-1}}$ to the east of the cape, with only one short segment of transport of $300\,000 \pm 200\,000\,\mathrm{m^3\,yr^{-1}}$ around a headland near Mersrags. These quantities are also typical of the southern shore of the gulf, as will be discussed below.

The sediment transport direction is predominantly counter-clockwise (positive in our framework; Fig. 7b), i.e. to the south-east along the western shore of the gulf. Different from many locations on the shores of the Baltic proper (Viška and Soomere, 2013b; Eelsalu et al., 2024b) or in the vicinity of Tallinn Bay on the northern shore of Estonia (Eelsalu et al., 2023), transport in the opposite (clockwise) direction (a reversal) has a considerable role between Purciems (Fig. 4) and the port of Roja, also between Upesgriva and Mersrags, and in some years on the eastern shore of Cape Kolka (Fig. 7c). The latter feature is consistent with historic in situ observations (Knaps, 1966; Ulsts, 1998). The former features are not indicated in historic observations. All three reversals evidently have been smoothed out in earlier lower-resolution simulations (Viška and Soomere, 2013b).

While the shoreline between the eastern side of Cape Kolka and Roja is locally almost straight and gently curving, the water depth in the nearshore of this shoreline contains extensive alongshore variations in selected wave model grid cells. The most significant feature is an up to 40 m deep area a few kilometres to the east of Cape Kolka (Fig. 1b; see also a higher-resolution map in Tsyrulnikov et al., 2008). This deep area becomes evident as a water depth of 14–18 m in several wave model grid cells located less than 1 km from the shoreline (Fig. 5, left panel). The 5 and 10 m isobaths meander noticeably between Cape

Figure 7. Simulated wave-driven potential bulk sediment transport (**a**), ratio of net to bulk transport (**b**) and net potential sediment transport (**c**) along the western shore of the Gulf of Riga. The blue line (average transport for 1990–2022) is almost wholly masked by the red line (three-grid-point running mean of the average transport for 1990–2022) in the upper and lower panels (**a, c**). The data for grid points that follow the orientation of breakwaters of the port of Engure are omitted. See locations in Fig. 4 and a map of the transport scheme in Fig. 13 below.

Kolka and Roja (see, for example, https://fishing-app. gpsnauticalcharts.com/i-boating-fishing-web-app/ fishing-marine-charts-navigation.html, last access: 16 January 2025). This bottom structure apparently reflects streamlined topographical features in the area stemming from Late Weichselian glacial dynamics (Tsyrulnikov et al., 2008) and possibly a different orientation of ice-shaped features at a large angle with respect to the contemporary shoreline in this region during certain stages of the presence of the Fennoscandian ice sheet (Karpin et al., 2023). This leads to considerable variations in the water depth in grid cells selected for the analysis at a scale of 1–2 km. These dissimilarities translate into local differences in the transport rates and the ratio of net and bulk transport (Fig. 7b) because of reasons explained in Sect. 2.3. However, the properties of net transport are less affected, and the "impact" of the described feature is almost lost when averaging over three adjacent grid points.

A discontinuity in the ratio of net and bulk transport to the west of Mersrags mirrors the presence of a headland with abruptly changing orientation of the shoreline. Still, it is likely that, at least in some years, the overall counter-clockwise sediment transport carries sand around this headland to the south-east as the values of net transport are positive along the entire shore of this headland in some years (Fig. 7c).

The pattern of the magnitude of annual net sediment transport reinforces and provides detail about these conjectures. The typical rate of counter-clockwise net transport on the shore of the Baltic proper of Cape Kolka varies from 300 000 to 900 000 $\mathrm{m^3\,yr^{-1}}$, depending on the particular coastal section, with an average of about 600 000 $\mathrm{m^3\,yr^{-1}}$ over a 10 km long stretch to the west of the cape (Fig. 7a). This projection matches the outcome of earlier in situ observations (Knaps, 1966; Ulsts, 1998) and simulations (Soomere and Viška, 2014).

The properties of bulk and net transport vary significantly in different years. The years characterised by very intense (e.g. 1993) or very low (e.g. 2014) bulk transport along the north-western shore of Cape Kolka are not mirrored along the coastal stretch to the east of Cape Kolka. The correlation coefficient of bulk transport in single years over all 22 grid points to the west of this cape and 22 points to the east of this cape is -0.14 ($p = 0.43$). The same feature is evident for the ratio of net and bulk transport (years 2010 and 2015 in Fig. 7b) and for the net transport. The characteristic feature of the net transport is that years with strong counter-clockwise transport to the west of Cape Kolka (e.g. 2011) correspond to almost zero counter-clockwise transport in the western Gulf of Riga. The similar correlation coefficient for net transport in single years is -0.68, with $p < 0.0001$, indicating statistically significant negative correlation between these values.

Interestingly, if the net transport and the net / bulk transport ratio have a maximum in some years west of the cape, these quantities have a minimum to the east, and vice versa (Fig. 7). The change in the sign of the net transport at Cape Kolka in years with strong clockwise transport along the western shore of the cape (e.g. 2010) evidently reflects the changing role of the predominant northerly (N)NW and SW winds in such years. For example, (N)NW winds move sand to the south along both shores of the cape. This transport is negative (clockwise) on its western shore and positive (counter-clockwise) on its eastern shore. Therefore, a major jump and sign change in some annual values of the net transport and the ratio of net and bulk transport at Cape Kolka (highlighted for the year 2011 in Fig. 7b and c) naturally reflect years with predominant northerly (N)NW winds. In contrast, counter-clockwise transport (positive to the north-east) along the western shore of Cape Kolka is driven by westerly winds. These winds create similar transport to the north (clockwise, negative) along the eastern shore of this cape. As waves created by SW winds have short fetch for the eastern shore of Cape Kolka, clockwise transport created by such waves is fairly weak as exemplified by the year 2010 in Fig. 7c. Interestingly, there is no jump or discontinuity in the average bulk transport at this location. Another interesting feature is that the ratio of the net and bulk transport may considerably vary with respect to the average value of this ratio in single years (e.g. 2010 and 2015 in Fig. 7b).

The intensity of potential net transport varies considerably along the western shore of the Gulf of Riga. Its average magnitude from Cape Kolka to Engure is about 50 000 $\mathrm{m^3\,yr^{-1}}$, and this is consistent with previous findings (Knaps, 1966; Ulsts, 1998; Viška and Soomere, 2013b; Soomere and Viška, 2014). The presence of a zero-downcrossing of net transport in some years immediately to the east of Cape Kolka (around cell no. 25) mirrors the presence of an erosion area in this location (Fig. 3). Even though there are several locations of relatively frequently occurring pairs of zero-downcrossings between Cape Kolka and the headland near Mersrags, this coastal segment most likely forms a continuous sedimentary system in which sand can move along the entire segment in different years. The shoreline of this area is slightly curved, and several sand bars exist in the nearshore along the entire section. Small-scale fluctuations in the numerically evaluated bulk sediment transport and reversals of net transport between Cape Kolka and Roja apparently stem from the choice of particular locations of selected wave model grid cells.

Sharp variations in the ratio of net and bulk transport near Roja reflect the presence of the port and breakwaters. They extend to about 5 m water depth (https://www.gpsnauticalcharts.com/main/latvia/ lv613340-port-of-roja-nautical-chart.html, last access: 26 December 2024), whereas closure depth is below 4 m in this location. It is thus likely that these breakwaters and the > 6 m deep entrance channel largely stop alongshore sediment flux. Technically, this feature is reflected by a local reversal of net sediment transport and unrealistic values of net transport and the ratio of net and bulk transport in coastal

Figure 8. Left: western breakwater at the Daugava River mouth. Photo by T. Soomere, 2019. Right: schematic of the location of wave model grid cells and the approximation of the orientation of the shoreline (red and yellow) in the transport model.
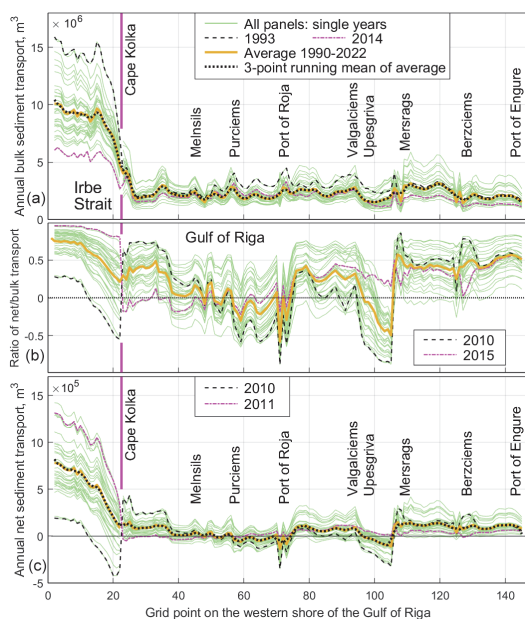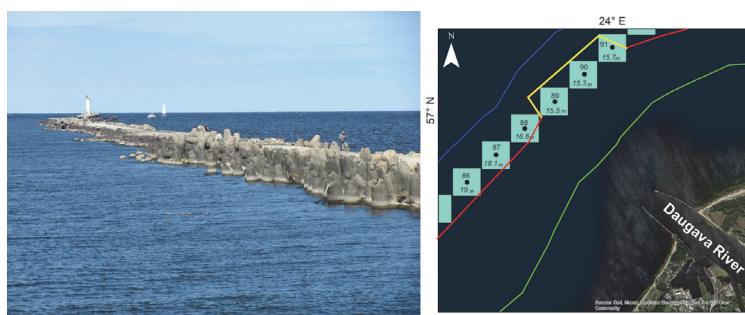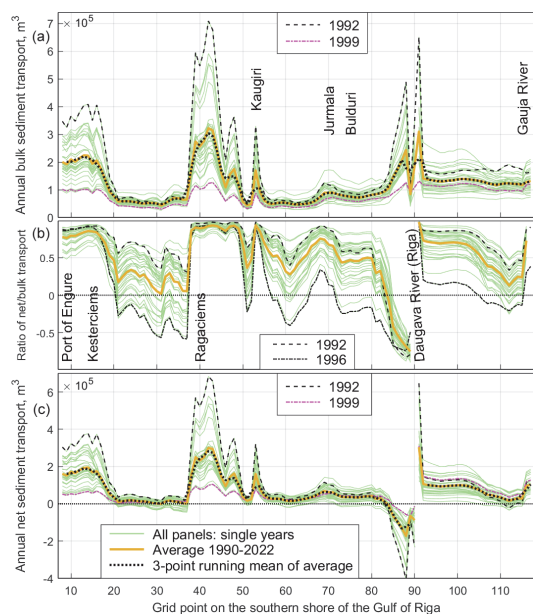

Figure 9. Simulated wave-driven potential bulk sediment transport **(a)**, ratio of net to bulk transport **(b)** and net transport **(c)** along the southern shore of the Gulf of Riga from the port of Engure to the Gauja River mouth. Note the different vertical scales of the upper and lower panels **(a, c)** compared to Fig. 7. The data for grid points that follow the orientation of breakwaters of the port of Engure and jetties at the Daugava River mouth are omitted (Sect. 2.5, Fig. 6). See locations in Fig. 4 and a map of the transport scheme in Fig. 13 below.

sectors corresponding to wave model grid cells no. 71 and no. 72 (Fig. 7b and c) where the presence of breakwaters affects the orientation of the shoreline approximation in these grid cells (Fig. 6). This rapidly changing orientation actually means that the resolution of the model is not sufficient to replicate sediment transport properties near such structures (see Sect. 2.5). Similar effects occur in the vicinity of other harbours in the study area and usually also in the estimates of bulk transport. For this reason the estimates of transport in the vicinity of such structures are ignored in the analysis below and are mostly not represented in Figs. 7, 9 and 10.

Relatively intense net sediment transport evidently takes place between Roja and a headland to the west of Mersrags. The impact of a few small-scale headlands and jetties at grid cells no. 74 and no. 79 interrupts the continuous sand beach and partially stops sediment transport. Their presence is not reflected in the model. A major headland to the north of Mersrags almost completely stops the counter-clockwise transport. The orientation of the coastline changes by about 80°. This feature is visible in Fig. 7c as a reversal of net sediment transport in most years. It is therefore safe to say that even in the absence of harbours and breakwaters the coastal segment from Cape Kolka to the headland at Mersrags formed an almost isolated sedimentary compartment in the past that was to some extent fed by sand from the vicinity of Cape Kolka.

A direct consequence is that there is almost no sand on the eastern side of this headland and also in the vicinity of the port of Mersrags. The water depth of the entrance channel of the port of Mersrags is > 5 m (https://fishing-app.gpsnauticalcharts.com/i-boating-fishing-web-app/fishing-marine-charts-navigation.html?title=Port+of+Mersrags+boating+app#15/57.3345/23.1406, last access: 16 January 2025), and the north mole of this port extends to an area about 4 m deep. It is thus likely that this port almost fully stops sediment transport for the same reasons as discussed for the port of Roja even though this feature is not resolved in our simulations. The sandy beach becomes
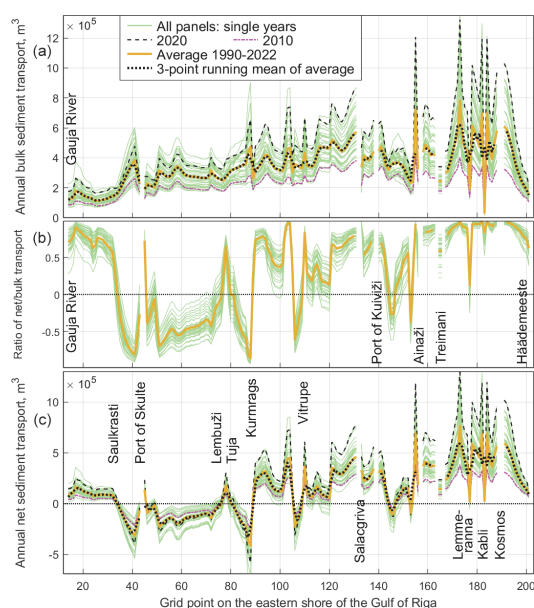
Figure 10. Simulated wave-driven potential bulk sediment transport (**a**), ratio of net to bulk transport (**b**) and net transport (**c**) along the eastern shore of the Gulf of Riga. Note the different vertical scales of the upper and lower panels (**a, c**) compared to Figs. 7 and 9. The data for grid points that follow the orientation of breakwaters of the port of Skulte, Salacgriva, Kuiviži, Treimani and Kosmos are omitted as explained in Sect. 2.5. See locations in Fig. 4 and a map of the transport scheme in Fig. 13 below.

evident again about 10 km to the south of Mersrags, as visible, for example, from Google Earth.

The coastal stretch between Mersrags and Engure also contains a few minor headlands that to some extent modulate the intensity of both bulk and net transport and their ratio. Different from the above, this stretch has almost entirely (in terms of annual means) counter-clockwise sediment transport. Reversals occur only in a couple of years. The water depth of the entrance channel to the port of Engure is > 4 m (https://www.eastbaltic.eu/engure-marina/, last access: 16 January 2025). Breakwaters of this port extend even further from the shoreline than those of the port of Roja and port of Mersrags into clearly deeper water than closure depth (> 3.5 m in this location). It is therefore likely that breakwaters of the port of Engure (not shown in Fig. 7) and accretional features at these breakwaters almost fully stop the wave-driven sediment transport. Together with the headland at Mersrags they separate this coastal stretch into an almost isolated sedimentary compartment.

3.2 Variable transport and accumulation along the southern shore

The southern coast of the Gulf of Riga, represented by the Riga grid in Fig. 1b and defined to extend from the port of Engure to the Gauja River (Fig. 4), changes its orientation from the north–south direction at Engure (Fig. 4) to the west–east direction near Jūrmala and to the south-west–north-east alignment near the Gauja River mouth (Fig. 1b). This pattern of changes means that the largest driver of sediment transport between Engure and Jūrmala are waves generated by (N)NW winds, while the predominant driver near Riga (Daugava River mouth) and further to the east are SW winds, the fetch length of which increases from the west to the east. The coastline is smoothly curved from Engure to Ragaciems (Fig. 4), with a gentle headland at Ragaciems, and is again gently curved from Ragaciems to the Daugava River mouth and to the north-east of the Daugava River mouth. The massive breakwaters at the river mouth (Fig. 8) almost completely stop wave-driven alongshore transport and divide the coastal stretch into two almost totally separated sedimentary compartments. Their presence is represented by abrupt changes in the orientation of the shoreline approximation in the model. As these changes led to unrealistic values of potential transport, model grid cells no. 89, no. 90 and no. 91 (Fig. 8) are omitted in the further analysis.

The local variations in transport are much larger than on the western shore of the Gulf of Riga. The situation between the port of Engure and Kesterciems (Fig. 9) resembles the situation between Mersrags and Engure (Fig. 7). Both coastal segments contain a few minor headlands that to some extent modulate the intensity of both bulk and net transport and their ratio. As the orientation of the coastline changes from the north–south alignment at Kesterciems to the almost west–east arrangement at Ragaciems, it is natural that bulk sediment transport slows from about 200 000 to about 50 000 m^3 yr^{-1} in the section between Kesterciems and Ragaciems where waves from the (N)NW approach the shore at a gradually smaller angle. This transport increases again at Ragaciems where both predominant wave systems, one from the SW and another from the (N)NW (Sect. 2.2), result in transport in the same direction. It slows down in the vicinity of Jūrmala where northerly waves approach the shore at a small angle and provide only a small contribution to the transport, and waves created by SW winds are weak. The scale of calculations resolves the impact of a small headland at Kauguri (Fig. 4) and the presence of depositional features on both sides of jetties of the Daugava River mouth. The typical bulk sediment transport is from 50 000 m^3 yr^{-1} in gently curved coastal segments to 300 000 m^3 yr^{-1} near headlands. It is much larger on both sides of the Daugava River mouth and relatively intense (about 150 000 m^3 yr^{-1}) to the north-east of the Daugava River mouth.

The long-term average transport is predominantly to the south-east and east in the western part of this area, except

for single years, such as 2002. Interannual variations in this transport are analysed in Sect. 3.4. The transport is almost unidirectional (counter-clockwise) in coastal segments to the south of Engure, to the south-east of Ragaciems, and in most of the area between the mouths of the Daugava River and Gauja River (Fig. 9c). It is also almost unidirectional along the coast of Jūrmala. The transport direction varies considerably in single years in the area to the north of Ragaciems. The average net transport in single years in coastal segments corresponding to grid cells 21–37 varies from $-23\,600\,\mathrm{m}^3\,\mathrm{yr}^{-1}$ per cell in 2000 to $35\,700\,\mathrm{m}^3\,\mathrm{yr}^{-1}$ in 1992, with a still-positive average over all years of $10\,430\,\mathrm{m}^3\,\mathrm{yr}^{-1}$ per cell and 50 % of annual values in the range from $-13\,340$ to $8300\,\mathrm{m}^3\,\mathrm{yr}^{-1}$. A clear reversal is present near the Daugava River mouth because of a large depositional feature in this area that modifies the orientation of the coastline, the eastern part of which is being eroded (Bertina et al., 2015).

The average annual net transport is much smaller in this segment, well below $50\,000\,\mathrm{m}^3\,\mathrm{yr}^{-1}$, with an exception near Engure and around Ragaciems where the simulated average values are almost $200\,000\,\mathrm{m}^3\,\mathrm{yr}^{-1}$ and up to $600\,000\,\mathrm{m}^3\,\mathrm{yr}^{-1}$ in single years in a small segment. These estimates match well the historical in situ estimates (Knaps, 1966; Ulsts, 1998); however, earlier lower-resolution simulations for 1970–2007 (Viška and Soomere, 2013b) suggest much more powerful alongshore sediment flux in the vicinity of the Daugava River mouth. Consistent with the above-discussed features, alongshore net transport is almost zero along the gently curved coastal stretch from Kesterciems to Ragaciems and in the vicinity of Jūrmala. The alongshore variations in transport indicate that the areas in the vicinity of Klapkalnciems (where the alongshore net transport decreases; see Fig. 6) and Jūrmala (the eastern part of which serves as a zero-downcrossing region of net transport; see Fig. 6) are sediment accumulation areas. A clear reversal of sediment transport at the Daugava River mouth most probably represents the impact of long-term riverine sediment transport into this area since 1567 when the river established a new entrance into the sea and started to build a new delta (Bertina et al., 2015). This flux of sediment is ignored in the model, and only the current geometry of the delta is taken into account. This simplification is appropriate unless the riverine flux is so intense that the added sediment changes the geometry of the shoreline within the study interval. The spatial pattern of net sediment transport signals that wave impact works against the formation of a river delta, consistently with the presence of net sediment flux downcrossing (reflecting a convergence or accumulation area) near the Daugava River mouth in Fig. 9c and the map of coastline changes from 1938–2007: erosion near the southern jetty of the Daugava River and accumulation further to the south until the Lielupe River mouth (Bertina et al., 2015).

Different from the situation on the western coast of the gulf, sediment transport is high along the entire southern coastal stretch in years of intense transport (e.g. 1992) and low along the entire stretch in years of less intense transport (e.g. 1999). The typical correlation coefficients between pointwise values in different years are 0.88 and 0.895 for bulk and net transport, respectively, with the typical p values < 0.0001. The years with intense bulk transport also have strong net transport (e.g. 1992) and vice versa (e.g. 1999). The relevant correlation coefficients between pointwise values of bulk and net transport in single years vary from 0.58 to 0.75, while all p values are < 10^{-11}. In a similar manner, years with predominantly unidirectional transport have this property along the entire coastal segment (e.g. 1996), except for an approximately 6 km long stretch between the Lielupe River mouth and the western breakwater of the Daugava River mouth, while in years with frequent reversals of this transport reversals occur in about half of this segment. This structure of net transport suggests that the segment in question contains three sedimentary compartments, separated by the headland at Ragaciems and breakwaters of the Daugava River mouth. While sediment from the easternmost system can be transported across the headland at Ragaciems, reverse transport is unusual at an annual scale as the net transport has a zero-upcrossing (and thus a clear divergence point) at this location only in 13 years out of 33 (Fig. 9c). The compartment from Kauguri to the western breakwater of the Daugava River mouth may be considered a combination of two cells with almost unidirectional sediment exchange between them.

3.3 Fragmented eastern shore

The eastern shore of the Gulf of Riga (Figs. 1 and 2) from the Gauja River mouth to the Estonian township of Häädemeeste (Fig. 4), even though generally almost straight, contains one larger (Cape Kurmrags) and several smaller variations in the coastline orientation. Historical in situ observations (Knaps, 1966; Ulsts, 1998) suggest that this area may have several erosion and accumulation areas (Fig. 2) and possibly also several sedimentary cells that are more or less isolated from each other in terms of annual sediment transport.

Different from the western and southern shores of the Gulf of Riga, the sandy shore is not continuous in this area. Some coastal segments have cobble and boulder pavement and consist of material that is not easily erodible, or they are rocky (e.g. at Kuiviži). Several coastal segments in the vicinity of the Latvian–Estonian border and Häädemeeste are almost completely devoid of sand, and wave-driven sediment transport is very limited. Therefore, the actual transport, evaluated in Knaps (1966) and Ulsts (1998), may well be just a small fraction of the simulated potential transport.

This coastal segment is evolving, similar to the shores of the Latvian and Lithuanian Baltic proper, under a delicate balance of two predominant wind and wave systems ((N)NW and SW; Eelsalu et al., 2024a) that in this case work exactly against each other. This is the natural reason why the potential bulk transport (Fig. 10a) increases from about $150\,000\,\mathrm{m}^3\,\mathrm{yr}^{-1}$ in the south to about $400\,000\,\mathrm{m}^3\,\mathrm{yr}^{-1}$ in the

north: while the heights of waves generated by the (N)NW winds slowly decrease in this direction because of a shorter fetch, the impact of waves excited by SW winds (that is weak in the south of this stretch) considerably increases with the increase in fetch length for these winds.

The transport direction along this stretch is highly variable (Fig. 10b and c), with typical lengths of stretches of unidirectional transport of only a few kilometres. The transport in the region immediately to the north-east of the Gauja River mouth is almost fully counter-clockwise to the north-east. The transport is predominantly clockwise from Saulkrasti to Cape Kurmrags, has a variable direction from Cape Kurmrags to Ainaži at the Latvian–Estonian border, and is predominantly to the north (counter-clockwise) in the Estonian part of the study area. This variation apparently mimics changes in the orientation of the shoreline and the changing balance of the fetch lengths of the predominant south-west and north-north-west winds. These lengths are more or less equal in the middle of this coastal stretch. The nearshore of its northern part is to some extent sheltered against waves from the north, north-north-west and north-west by the island of Kihnu and the Estonian mainland.

Consistent with Viška and Soomere (2013b), the average potential net transport along this stretch varies considerably, between about 15 000 and 590 000 $m^3 yr^{-1}$ (in terms of three-point running average; Fig. 10c). Its intensity generally increases from the south to the north similar to the bulk transport. There are several persistent zero-upcrossings in the net sediment transport, together with alongshore variations in the sign of the ratio of net and bulk transport (Fig. 10b and c). These features signal that the sedimentary system of the eastern coast of the Gulf of Riga is highly fragmented. This aspect was not resolved by earlier simulations (Viška and Soomere, 2013b; Soomere and Viška, 2014) that provided a highly generalised picture of the system. Consequently, long-range transport of sediment along this coastal section is unlikely, and there are several natural reversals of the overall counter-clockwise sediment transport pattern along with associated sediment erosion and accumulation regions.

The presence of several human-made structures, such as the port of Skulte; jetties at Salacgriva, Kuiviži, Ainaži and Treimani; and the historical recreation centre for USSR astronauts (Kosmos in Fig. 10), augments the fragmentation. Together with headlands such as Cape Kurmrags and other smaller headlands that serve as invisible barriers to sediment transport, they separate the coastal stretch into numerous almost isolated sedimentary cells with a typical length of 5–25 km. The longest interconnected coastal segments are near Saulkrasti (ca. 21 km), from the port of Skulte to Cape Kurmrags (ca. 25 km), from Vitrupe to Salacgriva (ca. 16 km), and from Treimani to Kosmos (ca. 14 km).

The breakwaters of the port of Skulte extend to the water depth of about 4 m, and the entrance channel to this port is 8–9 m deep (https://www.gpsnauticalcharts.com/main/latvia/lv613310-port-of-skulte-nautical-chart.html, last ac-

cess: 16 January 2025). This structure is thus a major obstacle to sediment transport and delineates the northern end of the sedimentary compartment between the port and the Gauja River mouth. The region to the SW of these jetties apparently is an accumulation area, and the area to the north is likely subject to erosion. The accumulation feature at the Gauja River mouth and the associated change in the orientation of the coastline give rise to a local net sediment transport reversal in single years but still allow counter-clockwise sediment flow to the north in most years. A clear sediment flux convergence area at Saulkrasti (Fig. 10c) matches the presence of a long and wide sandy beach. Together with an extensive sediment transport reversal that apparently extends to Lembuži and possibly even to Kurmrags, its presence signals that the Saulkrasti region has been the end location of counter-clockwise sand motion along the rest of the shores of the Gulf of Riga. This conjecture is supported by the absence of any notable accumulation feature adjacent to the southern breakwater of the port of Skulte about 6 km to the north of Saulkrasti.

Figure 10c indicates the presence of a persistent reversal area (that is, transport to the south) of net sediment transport to the north of Saulkrasti. This reversal signals that waves from the northern directions dominate the wave-driven transport over this more than 30 km long segment (that is split into two parts by the port of Skulte). It is not clear whether a minor headland near Lembuži serves as a major barrier of net transport. Even though it creates a zero-upcrossing of annual net sediment transport, the location of this upcrossing varies by several kilometres in single years (Fig. 10c). It is thus likely that wave-driven sediment flux passes this headland on many occasions and that the coastal segment from the port of Skulte to Cape Kurmrags is a connected compartment.

The most significant net sediment flux divergence area is located at Cape Kurmrags, essentially a very minor headland that insignificantly extends into the sea. Together with a sister headland about 3 km to the north, they are an almost impermeable barrier for wave-driven sediment motion in our model in terms of annual average sediment transport. As single storms still apparently can move sediment around these capes, the sedimentary systems to the north and south of these capes are not totally isolated from each other.

While bulk transport gradually increases from the south to the north between Cape Kurmrags and Salacgriva, net transport greatly varies in this segment. It has a short but clear reversal in terms of annual values near Vitrupe. Similar to the above, it is likely that waves in single storms carry sediment across this location and thus the coastal segment from Cape Kurmrags to Salacgriva is a connected sedimentary compartment. Extensive variations in the intensity of potential net transport indicate areas prone to erosion (if this transport increases from the left to the right; Fig. 6) or accumulation (segments in which the net transport accordingly decreases) in this compartment.

Sediment transport at and to the north of Salacgriva is fragmented. Several minor headlands to the south of Salacgriva modulate the transport properties but do not serve as barriers. Jetties on both sides of the Salaca River and Kuivižu River mouths and especially the > 5 m deep entrance channel to Salacgriva almost totally block alongshore sediment transport. The same applies to jetties at Ainaži, Treimani and Kosmos. As the coast to the north of Cape Kurmrags contains very limited fine sediment, the simulated (potential) sediment transport by at least an order of magnitude exceeds the actual wave-driven transport. The nature of the coast and the location and size of accumulation features at different obstacles confirm that the transport is predominantly to the north.

The properties of transport in single years have many particular features in this coastal segment. The years with intense bulk transport generate large transport throughout the segment. In a similar manner, in years with low bulk transport the intensity of bulk transport is low over the entire segment (Fig. 10a). Interestingly, this feature is not true for the net transport. While its intensity in the northern part of the segment matches the intensity of bulk transport, the situation is different in the south, especially between the port of Skulte and Cape Kurmrags, where net transport in these years is at the average level.

3.4 Potential bulk and net alongshore sediment transport over the entire area

Estimates of interannual and decadal variations in the bulk and wave-driven potential sediment transport integrated along the eastern Baltic Sea, from Cape Taran to Pärnu Bay, including the western, southern and eastern coasts of the Gulf of Riga (Soomere et al., 2015), have revealed a major regime shift in transport properties around the year 1990. While potential bulk transport integrated from Samland to Pärnu continued to grow from 1970–2007, net transport increased only until about 1990 and decreased from 1990–2007. Major changes in the bulk and net transport were clearly visible on the shore of the Baltic proper of the Kaliningrad District (of Russia), Lithuania and Latvia but not on the shores of the Gulf of Riga. The bulk potential transport decreased to some extent from 1990–2007 on the shores of this gulf, while the net transport was at an almost constant level (Viška and Soomere, 2013a).

A possible reason for the absence of this probable signal of climate change in the Gulf of Riga (Viška and Soomere, 2013a) may be the use of values of potential transport integrated over the entire set of its western, southern and eastern shores. As these shores are oriented very differently with respect to predominant wind directions from the SW and (N)NW (Sect. 2.2), it is likely that such a signal is present on some of these shores only.

The average intensity of potential alongshore sediment transport per grid cell is largest (bulk and net transport of about 352 000 and 100 000 $\mathrm{m^3\,yr^{-1}}$) on the eastern shore of
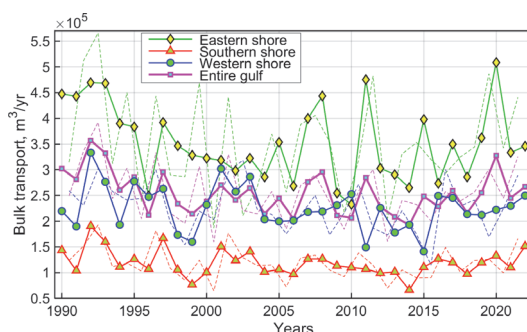

Figure 11. Average annual (solid lines with markers) and storm season (thin dashed lines) potential bulk sediment transport per wave model grid cell along western, southern and eastern shores of the Gulf of Riga from 1990–2022. The annual bulk transport decreases in 1990–2005 in the entire study area ($-5590\,\mathrm{m^3\,yr^{-1}}$) and on the eastern shore ($-10\,600\,\mathrm{m^3\,yr^{-1}}$), and this decrease is statistically significant ($p = 0.018$ and $p = 0.0008$, respectively). A similar decrease is not statistically significant on the southern and western shore ($-920\,\mathrm{m^3\,yr^{-1}}$, $p = 0.75$ and $-2160\,\mathrm{m^3\,yr^{-1}}$, $p = 0.20$, respectively). This transport increases slowly (with the relevant slope from 1020 to 1760 $\mathrm{m^3\,yr^{-1}}$) in all addressed coastal segments, but this increase is far from being statistically significant as the quantity p is in the range of 0.23 to 0.64.

the Gulf of Riga (Figs. 2 and 11). The location and orientation of this segment are such that high waves generated by predominant strong SW and (N)NW winds commonly arrive at the coast at a large angle and thus generate strong alongshore transport. This does not automatically mean massive net or actual sediment transport. Almost the entire eastern shore of the Gulf of Riga (except for an accumulation area at Saulkrasti) suffers from a deficit of sediment (Knaps, 1966; Ulsts, 1998). Consequently, the magnitude of actual sediment transport along this shore is only a small fraction of the potential transport.

The potential sediment transport is considerably weaker on the other shores of the Gulf of Riga. Its magnitude on the western shore (bulk and net transport of about 226 000 and 54 000 $\mathrm{m^3\,yr^{-1}}$) is, on average, about 64 % and 54 % of that on the eastern shore and only about 34 % and 67 % (bulk and net transport of about 119 000 and 67 000 $\mathrm{m^3\,yr^{-1}}$) on the southern shore (Fig. 11). These differences evidently reflect the combination of the direction of predominant SW and (N)NW winds (Sect. 2.2) and orientation of the coastal segments. While (N)NW winds apparently generate the same magnitude of potential transport on the eastern and western shores, the contribution of waves driven by westerly winds is almost missing on the western shore. This explains the difference in transport by a factor of 2. Similarly, waves created by westerly winds are still low on the southern shore even though they arrive at this shore segment at a large angle. Waves driven by (N)NW winds are commonly much

stronger, but they arrive at a small angle and usually do not generate massive alongshore transport.

The intensity of bulk transport does not increase in the study area (Fig. 11). Different from the properties of this transport integrated over the longer coastal stretch from Samland to Pärnu from 1970–2007 (Soomere et al., 2015), this transport decreases by up to 30 % on the eastern shore and in the entire gulf from 1990–2005, and it exhibits no obvious trend for 2005–2022 (Fig. 11). This pattern is, however, consistent with the course of bulk sediment transport integrated from Cape Kolka to Pärnu Bay in earlier lower-resolution simulations (Viška and Soomere, 2013a). Interestingly, Viška and Soomere (2013a) also indicated maxima in this quantity around the years 2004 and 2007.

It is therefore likely that the intensity of wave-driven sediment transport and thus also coastal processes in the interior of the Gulf of Riga develop independently from (or even in counter-phase to) the transport on the shores of the eastern Baltic proper. The probable reason is the presence of long coastal segments in the gulf that are differently oriented with respect to the predominant wind directions from SW and (N)NW.

Another implication of this feature that becomes evident is the difference in the pattern of interannual variations in bulk transport on different shore segments. Namely, transport on the eastern and western shores of the gulf contains extensive interannual variations (standard deviation (SD) 79 000 and 32 000 m^3 yr^{-1}, respectively) but has no obvious trend (less than 1800 m^3 yr^{-1}, $p > 0.37$) for 2005–2022. The situation was different on the southern shore where transport had large interannual variations (SD 30 000 m^3 yr^{-1}) in 1990–2005 but has been almost steady (SD 18 200 m^3 yr^{-1}, slow increase by 1025 m^3 yr^{-1}, $p = 0.23$) since then. It is likely that this difference reflects different temporal patterns of changes to winds from the two predominant directions from SW and (N)NW (Eelsalu et al., 2024a) that become evident differently, in differently oriented segments.

Additional information about the structure of the temporal course of transport is provided by analysis of transport during so-called storm seasons, specifically the 12-month time periods from July to June of the subsequent year (Männikus et al., 2019; Eelsalu et al., 2022). The use of such time periods (Figs. 11 and 12) often better characterises the severity of winds in the relatively windy autumn and winter seasons and thus also of interannual variability in sediment transport intensity. The differences between this quantity and annual bulk transport are relatively large on the eastern shore and fairly small on the southern shore. Consistent with the above, storm season bulk transport has not exhibited any significant trend since 2005. The relevant slopes of the trend lines for the entire gulf and for the western, southern and eastern shores vary from 1550 to 4300 m^3 yr^{-1}, with p in the range 0.25 to 0.41.

Different from above but consistent with Viška and Soomere (2013a), average potential net sediment transport
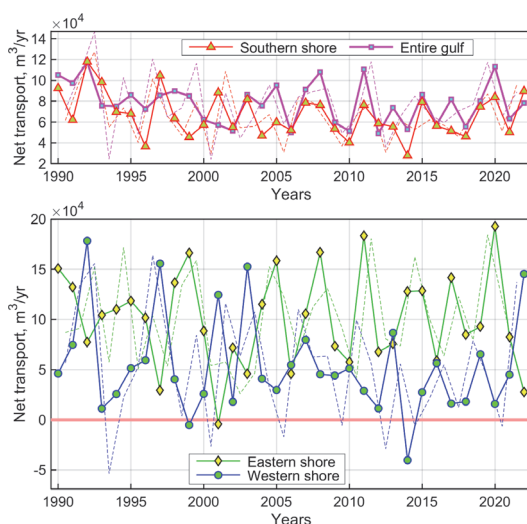

Figure 12. Average annual (solid lines) and storm season (thin dashed lines) potential net sediment transport per wave model grid cell along western, southern and eastern shores of the Gulf of Riga in single years 1990–2022.

integrated over the entire study area (Fig. 12) displays almost no long-term (less than 530 m^3 yr^{-1}, $p = 0.15$) and decadal changes. It also exhibits much smaller interannual variations than bulk transport in single segments (Fig. 11). Interannual variations in the net transport are, however, significantly different in the three coastal segments. While these variations are fairly limited on the southern shore (SD 20 700 m^3 yr^{-1}), they are much larger on the western and eastern shores (49 000 and 47 330 m^3 yr^{-1}, respectively). While interannual variations in bulk transport are weakly correlated (correlation coefficient 0.19 for annual values and −0.09 for storm season values), interestingly, most of these large variations in net transport are exactly in counter-phase on the western and eastern shores. This feature is less evident in annual values of net transport that have a correlation coefficient −0.16 and $p = 0.39$ but impressive and statistically significant at a > 99 % level in terms of net transport during storm seasons, with a correlation coefficient −0.59 and $p = 0.0003$.

The described feature explains why temporal variations in the bulk and net transport integrated over the western, southern and eastern coasts of the Gulf of Riga are different from those highlighted in Soomere et al. (2015), who identified a gradual increase in the bulk transport over a longer coastal stretch from Cape Taran to Pärnu Bay and a change in the slope of trend in the net transport around the year 1990. The main reason is the presence of the differently oriented eastern shore of the Gulf of Riga. The predominant wind and wave directions from SW and (N)NW act in the same manner in all segments of the stretch from Cape Taran to Pärnu

Bay, except for the western shore of the Gulf of Riga. The winds and waves that produce counter-clockwise transport in all other parts of this longer stretch generate clockwise transport on the western shore of the Gulf of Riga (and vice versa) because of its different orientation. When the net transport is integrated over the western and eastern segments of this gulf, these variations cancel each other and lead to limited interannual variations in the total net transport in the entire gulf.

4 Discussion and conclusions

The new high-resolution wave data from the SWAN model allowed for a vital update of the earlier estimates of wave-driven potential sediment transport rates, their interannual and decadal variations, the location of divergence and convergence areas of sediment flux, and associated patterns of sedimentary compartments and cells on the sedimentary shores of the Gulf of Riga, as well as a further understanding of the difference between some implications of climate change on the shores of the Baltic proper and in the interior of the Gulf of Riga.

4.1 Limitations of simulations

The reliability of estimates of this kind is basically determined by (i) the quality of input wave information and (ii) limitations of the sediment transport model. The set of wave properties used in our study has been extracted from recent high-resolution simulations of wave fields in the study area using the most contemporary wind information (Sect. 2.3). The model output has been verified against recorded wave data in many locations of the Baltic Sea (Giudici et al., 2023; Männikus et al., 2024) and the Gulf of Riga (Najafzadeh et al., 2024). Even though the match between reconstructed and recorded wave properties is not always perfect (Eelsalu et al., 2025a), the quality of input wave data is definitely not the main limitation for the quality of the output simulations.

Significantly larger uncertainties are introduced because of the poor resolution of nearshore bathymetry as it affects the wave data. This affects the choice of wave model grid cells (Sect. 2.4) that are relatively distant from the shoreline in areas where wave–bottom interaction is relatively weak. The conversion of wave properties in these cells into breaking wave properties (Sect. 2.4) assumes that the seabed is plane and thus ignores all local features of bathymetry.

The largest differences between simulated and observed transport are introduced by well-known limitations of the CERC model (see Sect. 2.5). This model only takes into account instantaneous wave properties, assumes unlimited availability of non-cohesive sediment with constant properties in each coastal segment and ignores cross-shore transport (USACE, 2002). This means inter alia that the result is independent of the actual sequence of storms. Moreover, the

Figure 13. Transport directions (arrow widths correspond to the rate of potential net transport), major interconnected sedimentary compartments separated by major natural divergence points of net sediment transport (green rectangles), and large harbours and jetties (black rectangles) that split the sedimentary compartments into almost separated cells. Blue arrows indicate counter-clockwise transport, and red arrows show clockwise transport. Parallel narrow blue and red arrows denote the variable transport regime in different years.

CERC model only provides an estimate of potential sediment transport under idealised conditions.

Some other assumptions may contribute to the uncertainties of the model output, as mentioned in Sect. 2.3. The wave model has been run with an idealised ice-free set-up, the use of which leads to an overestimation of the annual cumulative wave energy flux (Najafzadeh and Soomere, 2024) and thus also bulk transport. Ignoring currents and varying water levels most likely does not substantially affect the results.

4.2 General sediment transport patterns

The simulations reinforced the well-known predominant counter-clockwise pattern of wave-driven sediment transport along the western, southern and eastern shores of the Gulf of Riga. The main advance from the material presented here is a more detailed and substantiated pattern of transport, identification of major sediment transit regions, and divergence (erosion) and convergence (accumulation) areas on these shores. Together with the locations of harbours these areas define the extent and location of the major sedimentary compartments and cells (Fig. 13). The simulations have highlighted different structural properties of sediment transport on the western, southern and eastern shores of the gulf.

The short coastal section immediately to the south-east of Cape Kolka has a clearly visible erosion point associated

with a frequent divergence of sediment flux. The western shore from Cape Kolka to a headland to the north of Mersrags has relatively intense counter-clockwise transport that is reversed in some years. It apparently formed a large interconnected sedimentary compartment in the past that is now split into almost isolated cells by breakwaters and jetties. The shore segment to the south of Mersrags to the port of Engure forms another interconnected sedimentary compartment.

The southern shore has much less intense and more unidirectional counter-clockwise sediment transport that encompasses the entire segment and weakens to the east towards some extensive accumulation areas. The vicinity of the Daugava River mouth became a major endpoint of this transport after the construction of jetties. Part of this transport may have passed the river mouth in the past and reached the ultimate end location at Saulkrasti.

The potential sediment transport is much larger along the eastern shore than along the southern shore and increases from the south to the north. This shore contains a longer segment of predominantly clockwise transport and is split into two almost separated sedimentary compartments by an area of divergence of sediment flux near Cape Kurmrags. The compartment to the north of Cape Kurmrags is split into several smaller almost isolated sedimentary cells by breakwaters and jetties. The deficit of fine sediment severely limits the actual transport.

4.3 Interannual and decadal variations in sediment transport

The simulations explained the reason for a mismatch of temporal variations in the wave-driven sediment transport in the interior of the Gulf of Riga in earlier lower-resolution simulations (Viška and Soomere, 2013a) from those identified for longer segments of the eastern Baltic Sea proper (Soomere et al., 2015) as discussed in Sect. 3.4. The reason is a specific orientation of some shore segments of the gulf with respect to the predominant moderate and strong winds (usually southwestern and north-north-western; Sect. 2.2; Soomere, 2003) that create the majority of waves responsible for sediment transport.

These winds generate radically different transport properties on the differently oriented western, southern and eastern shores of the gulf. The western shore is mostly affected by northerly winds. Waves generated by these winds approach the shore at a large angle with respect to the shore normal and thus, if present, drive intense counter-clockwise transport over long distances. Winds from the south-west blow to the offshore over this coastal segment and only occasionally contribute to the clockwise transport. Thus, counter-clockwise transport usually prevails, and its magnitude is mostly governed by the properties of the northerly winds.

The southern shore is jointly affected by frequent but relatively weak and short waves created by south-western winds and occasionally waves excited by strong but less frequent

northerly winds. The latter waves usually approach the shore at a small angle and thus do not generate strong alongshore transport. As a result, the intensity of both bulk and net transport is low, and accumulation predominates over long sections of the southern shore.

The eastern shore experiences strong waves generated by both south-western and northerly winds. Both wave systems can be strong and often arrive at the shore at a large angle. Therefore, the direction of transport is jointly covered by these two wave systems. The instantaneous transport direction is thus variable, and the annual average reflects the balance of the wave systems in a particular year. The only exception is the southernmost part of the shore at Saulkrasti that is an endpoint of transport from the west and from the north.

It is therefore natural that the balance of the two components of the local bi-directional structure of moderate and strong winds together with the different orientation of the shoreline in the three coastal segments translates into an interesting mismatch of wave-driven transport properties on the western and eastern shores of the gulf (Fig. 12).

The intensity of bulk transport combines the joint impact of both wave systems and thus largely follows variations in wind speed. The intensity of net transport additionally expresses the changing role of these wave systems. Stronger than average waves from the northerly directions result in stronger than average transport to the south on both eastern and western shores. This means more intense than usual counter-clockwise transport on the western shore and more intense than usual clockwise transport on the eastern shore.

This property naturally translates into a mirrored pattern of time periods of high and low net potential transport on the western and eastern shores of the Gulf of Riga (Sect. 3.4, Fig. 12). This pattern underscores a highly interesting feature of the dynamics of the Gulf of Riga: almost regular fluctuations in the system with almost constant amplitude and with a timescale of 3–4 years (Fig. 12) that most likely represent the changing role of northerly winds (Eelsalu et al., 2024a).

4.4 Implications for coastal processes

The presented features also translate into several observations with respect to the difference in structural properties of sediment transport and connectivity in the three coastal segments. It is likely that the synchronisation of water levels and wave approach (and sediment transport) directions supports the stability of relatively small beaches or sedimentary cells (Eelsalu et al., 2022). This mechanism apparently is not applicable on the western and southern shores of the gulf where large excursions of sediment parcels and long sections of transit are typical. Both these segments contain only one major divergence area that may serve as a barrier for sediment transport and a couple of human-made structures that limit the transport range. This mechanism may, however, become apparent on the eastern shore that is divided into sev-

eral smaller cells by one major divergence area and several jetties or moles.

The presence of long interconnected sedimentary compartments signals that strong storms may bring large amounts of sediment into motion. A typical consequence of this feature is the rapid straightening of parts of the coast, a process that has already created numerous coastal lakes near the eastern shore and turned the river mouths downdrift on the southern shore of the Gulf of Riga. Another possible consequence is siltation of harbour entrance channels. These processes are much less intense on the eastern shore in spite of the even larger intensity of wave-driven potential transport. A concealed feature is the potential large spread of hazardous materials in the event of sediment contamination along the western and southern shores.

In this context, the presented high-resolution simulations provide valuable insights into sediment transport patterns along the Gulf of Riga coastlines compared to older, essentially basic estimates from in situ observations (Knaps, 1966; Ulsts, 1998) and earlier low-resolution simulations (Soomere and Viška, 2014). These findings aid in the planning of harbour and coastal infrastructure as well as in the assessment of several kinds of environmental impacts. It is however not straightforward to link the outcome of our simulations with actual areas of erosion and accumulation (e.g. Luijendijk et al., 2018) because our analysis assumes unlimited availability of fine non-cohesive sediment. Another direct limitation of our study is that it does not take into account cross-shore transport and sediment sources (e.g. from rivers) and sinks.

The decomposition of the sedimentary system of the Gulf of Riga into smaller compartments and cells provides vital information for management solutions and importantly for the identification of potential erosion and accumulation areas. This information is crucial for developing and closing the sediment budget in this microtidal waterbody. It also indicates how far sediment may be transported from a particular location under the current wind and wave climate. The results are largely invariant with respect to grain size and sediment availability (unless the grain size varies strongly over short distances) even if the potential transport greatly exceeds actual transport. A natural extension of this research would be a similar analysis of sediment transport, compartments and cells along the sedimentary shores of the Baltic proper, ideally including the Polish coastline. Another much-needed extension could be developed using variable locations of the nearshore wave model grid cells. These cells are selected in this study in relatively deep water seaward from the breaker line even in the most severe storms. For wave conditions occurring more often than the SWAN model is capable of adequately replicating, wave properties closer to the shoreline and wave–bottom interactions that decrease wave energy without the generation of massive sediment transport are taken into account. Such improvements would clearly increase the value of simulation results for users and managers of the coastal area.

References

Aagaard, T., Brinkkemper, J., Christensen, D. F., Hughes, M. G., and Ruessink, G.: Surf zone turbulence and suspended sediment dynamics – A review, J. Mar. Sci. Eng., 9, 1300, https://doi.org/10.3390/jmse9111300, 2021.

Barzehkar, M., Parnell, K. E., Soomere, T., and Koivisto, M.: Offshore wind power plant site selection in the Baltic Sea, Reg. Stud. Mar. Sci., 73, 103469, https://doi.org/10.1016/j.rsma.2024.103469, 2024.

Bernatchez, P. and Fraser, C.: Evolution of coastal defence structures and consequences for beach width trends, Quebec, Canada, J. Coastal Res., 28, 1550–1566, https://doi.org/10.2112/JCOASTRES-D-10-00189.1, 2012.

Bertina, L., Krievans, M., Burlakovs, J., and Lapinskis, J.: Coastal development of Daugavgriva Island, located near the Gulf of Riga, Proc. Latvian Acad. Sci. B, 69, 290–298, https://doi.org/10.1515/prolas-2015-0045, 2015.

Björkqvist, J.-V., Tuomi, L., Tollman, N., Kangas, A., Pettersson, H., Marjamaa, R., Jokinen, H., and Fortelius, C.: Brief communication: Characteristic properties of extreme wave events observed in the northern Baltic Proper, Baltic Sea, Nat. Hazards Earth Syst. Sci., 17, 1653–1658, https://doi.org/10.5194/nhess-17-1653-2017, 2017.

Björkqvist, J.-V., Lukas, I., Alari, V., van Vledder, G. P., Hulst, S., Pettersson, H., Behrens, A., and Männik, A.: Comparing a 41 year model hindcast with decades of wave measurements from the Baltic Sea, Ocean Eng., 152, 57–71, https://doi.org/10.1016/j.oceaneng.2018.01.048, 2018.

Björkqvist, J.-V., Rikka, S., Alari, V., Männik, A., Tuomi, L., and Pettersson, H.: Wave height return periods from combined measurement–model data: a Baltic Sea case study, Nat. Hazards Earth Syst. Sci., 20, 3593–3609, https://doi.org/10.5194/nhess-20-3593-2020, 2020.

Björkqvist, J.-V., Pärt, S., Alari, V., Rikka, S., Lindgren, E., and Tuomi, L.: Swell hindcast statistics for the Baltic Sea, Ocean Sci., 17, 1815–1829, https://doi.org/10.5194/os-17-1815-2021, 2021.

Booij, N., Ris, R. C., and Holthuijsen, L. H.: A third-generation wave model for coastal regions: 1. model description and validation, J. Geophys. Res.-Oceans, 104, 7649–7666, https://doi.org/10.1029/98JC02622, 1999.

Bulleri, F. and Chapman, M. G.: The introduction of coastal infrastructure as a driver of change in marine environments, J. Appl. Ecol., 47, 26–35, https://doi.org/10.1111/j.1365-2664.2009.01751.x, 2010.

Cappucci, S., Bertoni, D., Cipriani, L. E., Boninsegni, G., and Sarti, G.: Assessment of the anthropogenic sediment budget of a littoral cell system (Northern Tuscany, Italy), Water, 12, 3240, https://doi.org/10.3390/w12113240, 2020.

Eberhards, G. and Lapinskis, J.: Processes on the Latvian coast of the Baltic Sea: atlas, Riga, University of Latvia, Riga, ISBN 9789984450209, 2008.

Eberhards, G., Lapinskis, J., and Saltupe, B.: Hurricane Erwin 2005 coastal erosion in Latvia, Baltica, 19, 10–19, 2006.

Eberhards, G., Grine, I., Lapinskis, J., Purgalis, I., Saltupe, B., and Torklere, A.: Changes in Latvia's seacoast (1935–2007), Baltica, 22, 11–22, 2009.

Eelsalu, M., Org, M., and Soomere, T.: Visually observed wave climate in the Gulf of Riga, in: The 6th IEEE/OES Baltic Symposium Measuring and Modeling of Multi-Scale Interactions in the Marine Environment, IEEE Conference Publications, 26–29 May 2014, Tallinn, Estonia, https://doi.org/10.1109/BALTIC.2014.6887829, 2014.

Eelsalu, M., Parnell, K. E., and Soomere, T.: Sandy beach evolution in the low-energy microtidal Baltic Sea: attribution of changes to hydrometeorological forcing, Geomorphology, 414, 108383, https://doi.org/10.1016/j.geomorph.2022.108383, 2022.

Eelsalu, M., Viigand, K., and Soomere, T.: Quantification of sediment budget in extensively developed urban areas: a case study of Tallinn Bay, the Baltic Sea, Regional Studies in Marine Science, 67, 103199, https://doi.org/10.1016/j.rsma.2023.103199, 2023.

Eelsalu, M., Soomere, T., and Jankowski, M. Z.: Climate change driven alongshore variations of directional forcing of sediment transport on the eastern Baltic Sea coast, J. Coastal Res., 113, 256–260, https://doi.org/10.2112/JCR-SI113-051.1, 2024a.

Eelsalu, M., Viigand, K., Soomere, T., and Parnell, K. E.: Systematic analysis of alongshore sediment transport patterns in varying sea level conditions for evaluating stability of the coastal areas in the microtidal Baltic Sea, J. Coastal Res., 113, 53–57, https://doi.org/10.2112/JCR-SI113-011.1, 2024b.

Eelsalu, M., Piho, L., Aigars, J., Kelpšaitė-Rimkienė, L., Kondrat, V., Kruusmaa, M., Parnell, K. E., Ristolainen, A., Šakurova, I., Skudra, M., Viška, M., and Soomere, T.: Exponential distribution of wave-driven near-bed water speeds under short-crested waves: a case study in the eastern Gulf of Riga, the Baltic Sea, P. Est. Acad. Sci., 74, 23–42, https://doi.org/10.3176/proc.2025.1.03, 2025a.

Eelsalu, M., Soomere, T., Parnell, K. E., and Viška, M.: Attribution of alterations in coastal processes in the southern and eastern Baltic Sea to climate change driven modifications of coastal drivers, Oceanologia, 67, 67103, https://doi.org/10.5697/LXTZ5389, 2025b.

Feistel, R., Nausch, G., and Wasmund, R.: State and evolution of the Baltic Sea, 1952–2005, Wiley, Hoboken, New Jersey, https://doi.org/10.1002/9780470283134, 2005.

Giudici, A., Jankowski, M. Z., Männikus, R., Najafzadeh, F., Suursaar, Ü., and Soomere, T.: A comparison of Baltic Sea wave properties simulated using two modelled wind data sets, Estuar. Coast. Shelf S., 290, 108401, https://doi.org/10.1016/j.ecss.2023.108401, 2023.

Harff, J., Deng, J. J., Dudzinska-Nowak, J., Fröhle, P., Groh, A., Hünicke, B., Soomere, T., and Zhang, W. Y.: What determines the change of coastlines in the Baltic Sea?, in: Coastline Changes of the Baltic Sea from South to East: Past and Future Projection, Coastal Research Library, vol. 19, edited by: Harff, J., Furmańczyk, K., and von Storch, H., Springer, 15–35, https://doi.org/10.1007/978-3-319-49894-2_2, 2017.

Hersbach, H., Bell, B., Berrisford, P., Hirahara, S., Horanyi, A., Munoz-Sabater, J., Nicolas, J., Peubey, C., Radu, R., Schepers, D., Simmons, A., Soci, C., Abdalla, S., Abellan, X., Balsamo, G., Bechtold, P., Biavati, G., Bidlot, J., Bonavita, M., De Chiara, G., Dahlgren, P., Dee, D., Diamantakis, M., Dragani, R., Flemming, J., Forbes, R., Fuentes, M., Geer, A., Haimberger, L., Healy, S., Hogan, R. J., Holm, E., Janiskova, M., Keeley, S., Laloyaux, P., Lopez, P., Lupu, C., Radnoti, G., de Rosnay, P., Rozum, I., Vamborg, F., Villaume, S., and Thepaut, J. N.: The ERA5 global reanalysis, Q. J. Roy. Meteor. Soc., 146, 1999–2049, https://doi.org/10.1002/qj.3803, 2020.

Hünicke, B., Zorita, E., Soomere, T., Madsen, K. S., Johansson, M., and Suursaar, Ü.: Recent change – Sea level and wind waves, in: Second Assessment of Climate Change for the Baltic Sea Basin, Regional Climate Studies, edited by: The BACC II Author Team, Springer, 155–185, https://doi.org/10.1007/978-3-319-16006-1_9, 2015.

Jankowski, M. Z., Soomere, T., Parnell, K. E., and Eelsalu, M.: Alongshore sediment transport in the eastern Baltic Sea, J. Coastal Res., 113, 261–265, https://doi.org/10.2112/JCR-SI113-052.1, 2024.

Karpin, V., Heinsalu, A., Ojala, A. E. K., and Virtasalo, J.: Offshore murtoos indicate warm-based Fennoscandian ice-sheet conditions during the Bølling warming in the northern Gulf of Riga, Baltic Sea, Geomorphology, 430, 108655, https://doi.org/10.1016/j.geomorph.2023.108655, 2023.

Kinsela, M. A., Morris, B. D., Linklater, M., and Hanslow, D. J.: Second-pass assessment of potential exposure to shoreline change in new south Wales, Australia, using sediment compartments framework, J. Mar. Sci. Eng., 5, 61, https://doi.org/10.3390/jmse5040061, 2017.

Knaps, R. J.: Sediment transport near the coasts of the Eastern Baltic, in: Development of sea shores under the conditions of oscillations of the Earth's crust, Valgus, Tallinn, 21–29, 1966.

Lapinskis, J.: Coastal sediment balance in the eastern part of the Gulf of Riga (2005–2016), Baltica, 30, 87–95, https://doi.org/10.5200/baltica.2017.30.10, 2017.

Larson, M., Hoan, L. X., and Hanson, H.: Direct formula to compute wave height and angle at incipient breaking, J. Waterw. Port C. Div., 136, 119–122, https://doi.org/10.1061/(ASCE)WW.1943-5460.0000030, 2010.

Lentz, S. and Raubenheimer, B.: Field observations of wave setup, J. Geophys. Res.-Oceans, 104, 867–875, https://doi.org/10.1029/1999JC900239, 1999.

Leppäranta, M. and Myrberg, K.: Physical Oceanography of the Baltic Sea, Springer Science & Business Media, Praxis, Berlin, Heidelberg, https://doi.org/10.1007/978-3-540-79703-6, 2009.

Luijendijk, A., Hagenaars, G., Ranasinghe, R., Baart, F., Donchyts, G., and Aarninkhof, S.: The state of the world's beaches, Sci. Rep.-UK, 8, 6641, https://doi.org/10.1038/s41598-018-24630-6, 2018.

Männikus, R. and Soomere, T.: Directional variation of return periods of water level extremes in Moonsund and in the Gulf of Riga. Baltic Sea, Reg. Stud. Mar. Sci., 57, 102741, https://doi.org/10.1016/j.rsma.2022.102741, 2023.

Männikus, R., Soomere, T., and Kudryavtseva, N.: Identification of mechanisms that drive water level extremes from in situ measurements in the Gulf of Riga during 1961–2017, Cont. Shelf Res., 182, 22–36, https://doi.org/10.1016/j.csr.2019.05.014, 2019.

Männikus, R., Soomere, T., and Suursaar, Ü.: How do simple wave models perform compared with sophisticated models and measurements in the Gulf of Finland?, Est. J. Earth Sci., 73, 98–111, https://doi.org/10.3176/earth.2024.10, 2024.

Najafzadeh, F. and Soomere, T.: Impact of changes in sea ice cover on wave climate of semi-enclosed seasonally ice-covered water bodies on temperate latitudes: a case study in the Gulf of Riga, Est. J. Earth Sci., 73, 26–36, https://doi.org/10.3176/earth.2024.03, 2024.

Najafzadeh, F., Jankowski, M. Z., Giudici, A., Männikus, A., Suursaar, Ü., Viška, M., and Soomere, T.: Spatiotemporal variability of wave climate in the Gulf of Riga, Oceanologia, 66, 56–77, https://doi.org/10.1016/j.oceano.2023.11.001, 2024.

Power, H. E., Hughes, M. G., Aagaard, T., and Baldock, T. E.: Nearshore wave height variation in unsaturated surf, J. Geophys. Res.-Oceans, 115, C08030, https://doi.org/10.1029/2009JC005758, 2010.

Räämet, A. and Soomere, T.: The wave climate and its seasonal variability in the northeastern Baltic Sea, Est. J. Earth Sci., 59, 100–113, https://doi.org/10.3176/earth.2010.1.08, 2010.

Raubenheimer, B., Guza, R. T., and Elgar, S.: Wave transformation across the inner surf zone, J. Geophys. Res.-Oceans, 101, 25589–25597, https://doi.org/10.1029/96JC02433, 1996.

Raubenheimer, B., Guza, R. T., and Elgar, S.: Field observations of set-down and set-up, J. Geophys. Res.-Oceans, 106, 4629–4638, https://doi.org/10.1029/2000JC000572, 2001.

Różyński, G.: Coastal protection challenges after heavy storms on the Polish coast, Cont. Shelf Res., 266, 105080, https://doi.org/10.1016/j.csr.2023.105080, 2023.

Šakurova, I., Kondrat, V., Baltranaitė, E., Gardauskė, V., Kelpšaitė-Rimkienė, L., Soomere, T., and Parnell, K. E.: Initial adjustment of underwater profiles after nourishment in a mild wave climate: a case study near Klaipėda, the Baltic Sea, Est. J. Earth Sci., 74, 22–33, https://doi.org/10.3176/earth.2025.02, 2025.

Sallenger, A. H. and Holman, R. A.: Wave energy saturation on a natural beach of variable slope, J. Geophys. Res.-Oceans, 90, 11939–11944, https://doi.org/10.1029/JC090iC06p11939, 1985.

Skudra, M. and Lips, U.: Characteristics and inter-annual changes in temperature, salinity and density distribution in the Gulf of Riga, Oceanologia, 59, 37–48, https://doi.org/10.1016/j.oceano.2016.07.001, 2017.

Soomere, T.: Extreme wind speeds and spatially uniform wind events in the Baltic Proper, Proc. Estonian Acad. Sci. Eng., 7, 195–211, https://doi.org/10.3176/eng.2001.3.01, 2001.

Soomere, T.: Anisotropy of wind and wave regimes in the Baltic proper, J. Sea Res., 49, 305–316, https://doi.org/10.1016/S1385-1101(03)00034-0, 2003.

Soomere, T. and Eelsalu, M.: On the wave energy potential along the eastern Baltic Sea coast, Renew. Energ., 71, 221–233, https://doi.org/10.1016/j.renene.2014.05.025, 2014.

Soomere, T. and Keevallik, S.: Anisotropy of moderate and strong winds in the Baltic Proper, Proc. Estonian Acad. Sci. Eng., 7, 35–49, https://doi.org/10.3176/eng.2001.1.04, 2001.

Soomere, T. and Räämet, A.: Spatial patterns of the wave climate in the Baltic Proper and the Gulf of Finland, Oceanologia, 53, 335–371, https://doi.org/10.5697/oc.53-1-TI.335, 2011.

Soomere, T. and Räämet, A.: Decadal changes in the Baltic Sea wave heights, J. Marine Syst., 129, 86–95, https://doi.org/10.1016/j.jmarsys.2013.03.009, 2014.

Soomere, T. and Viška, M.: Simulated sediment transport along the eastern coast of the Baltic Sea, J. Marine Syst., 129, 96–105, https://doi.org/10.1016/j.jmarsys.2013.02.001, 2014.

Soomere, T., Pindsoo, K., Bishop, S. R., Käärd, A., and Valdmann, A.: Mapping wave set-up near a complex geometric urban coastline, Nat. Hazards Earth Syst. Sci., 13, 3049–3061, https://doi.org/10.5194/nhess-13-3049-2013, 2013.

Soomere, T., Bishop, S. R., Viška, M., and Räämet, A.: An abrupt change in winds that may radically affect the coasts

and deep sections of the Baltic Sea, Clim. Res., 62, 163–171, https://doi.org/10.3354/cr01269, 2015.

Soomere, T., Männikus, R., Pindsoo, K., Kudryavtseva, N., and Eelsalu, M.: Modification of closure depths by synchronisation of severe seas and high water levels, Geo-Mar. Lett., 37, 35–46, https://doi.org/10.1007/s00367-016-0471-5, 2017.

Soomere, T., Eelsalu, M., Viigand, K., and Giudici, A.: Linking changes in the directional distribution of moderate and strong winds with changes in wave properties in the eastern Baltic proper, J. Coastal Res., 113, 190–194, https://doi.org/10.2112/JCR-SI113-038.1, 2024.

Susilowati, Y., Nur, W. H., Sulaiman, A., Kumoro, Y., and Yunarto: Study of dynamics of coastal sediment cell boundary in Cirebon coastal area based on integrated shoreline Montecarlo model and remote sensing data, Regional Studies in Marine Science, 52, 102268, https://doi.org/10.1016/j.rsma.2022.102268, 2022.

Suursaar, Ü., Kullas, T., and Otsmann, M.: A model study of the sea level variations in the Gulf of Riga and the Väinameri Sea, Cont. Shelf Res., 22, 2001–2019, https://doi.org/10.1016/S0278-4343(02)00046-8, 2002.

Thom, B. G., Eliot, I., Eliot, M., Harvey, N., Rissik, D., Sharples, C., Short, A. D., and Woodroffe, C. D.: National sediment compartment framework for Australian coastal management, Ocean Coast. Manage., 154, 103–120, https://doi.org/10.1016/j.ocecoaman.2018.01.001, 2018.

Tõnisson, H., Orviku, K., Lapinskis, J., Gulbinskas, S., and Zaromskis, R.: The Baltic States – Estonia, Latvia and Lithuania, in: Coastal Erosion and Protection in Europe, edited by: Pranzini, E. and Williams, A., Routledge, London, 47–80, https://doi.org/10.4324/9780203128558, 2013.

Tõnisson, H., Suursaar, Ü., Alari, V., Muru, M., Rivis, R., Kont, A., and Viitak, M.: Measurement and model simulations of hydrodynamic parameters, observations of coastal changes and experiments with indicator sediments to analyse the impact of storm St. Jude in October, 2013, J. Coastal Res., 75, 1257–1261, https://doi.org/10.2112/SI75-25, 2016.

Tsyrulnikov, A., Tuuling, I., and Hang, T.: Streamlined topographical features in and around the Gulf of Riga as evidence of Late Weichselian glacial dynamics, Geol. Q., 52, 81–89, 2008.

Tsyrulnikov, A., Tuuling, I., Kalm, V., Hang, T., and Flodén, T.: Late Weichselian and Holocene seismostratigraphy and depositional history of the Gulf of Riga, NE Baltic Sea, Boreas, 41, 673–689, https://doi.org/10.1111/j.1502-3885.2012.00257.x, 2012.

Ulsts, V.: Latvian coastal zone of the Baltic Sea, State Geological Survey of Latvia, ISBN 9789984929903, 1998.

Ulsts, V. and Bulgakova, J.: General lithological and geomorphological map of Latvian shore zone – Baltic Sea and Gulf of Riga, State Geological Survey of Latvia, Riga, ISBN 9984929906, 1998.

USACE: Coastal Engineering Manual, Manual No. 1110-2-1100, Department of the Army, US Army Corps of Engineers, https://www.publications.usace.army.mil/USACE-Publications/Engineer-Manuals/u43544q/636F617374616C20656E67696E656572696E67206D616E75616C/ (last access: 16 January 2025), 2002.

Villasante, S., Richter, K., Bailey, J., Blenckner, T., Farrell, E., Mongruel, R., Timmermann, K., Bouma, T., Melaku Canu, D., Chen, M., Lachs, L., Payo, A., and Sousa Pinto, I.: Building Coastal Resilience in Europe, Position Paper 27 of the European Marine Board, edited by: Alexander, B., Muñiz Piniella, A., Kellett, P., Rodriguez Perez, A., Van Elslander, J., Bayo Ruiz, F., and Heymans, J. J., Ostend, Belgium, https://doi.org/10.5281/zenodo.8224055, 2023.

Viška, M. and Soomere, T.: Long-term variations of simulated sediment transport along the eastern Baltic Sea coast as a possible indicator of climate change, in: Publication No. 53, 7th Study Conference on BALTEX, Conference Proceedings, 10–14 June 2013, Borgholm, Island of Öland, Sweden, edited by: Reckermann, M. and Köppen, S., International BALTEX Secretariat, 99–100, https://www.baltex-research.eu/oland2013/material/Proceedings_Final_web.pdf (last access: 16 January 2025), 2013a.

Viška, M. and Soomere, T.: Simulated and observed reversals of wave-driven alongshore sediment transport at the eastern Baltic Sea coast, Baltica, 26, 145–156, https://doi.org/10.5200/baltica.2013.26.15, 2013b.

Publication V

Eelsalu, M., Soomere, T., Jankowski, M.Z., 2024. Climate change driven alongshore variations of directional forcing of sediment transport on the eastern Baltic Sea coast. Journal of Coastal Research, Special Issue 113, 190–194. https://doi.org/10.2112/JCR-SI113-038.1

Climate Change Driven Alongshore Variations of Directional Forcing of Sediment Transport on the Eastern Baltic Sea Coast

Maris Eelsalu[†]*, **Tarmo Soomere[†§]**, and **Mikolaj Zbigniew Jankowski[†]**

[†]Wave Engineering Laboratory
Department of Cybernetics, School of Science
Tallinn University of Technology
Tallinn, Estonia

[§]Estonian Academy of Sciences
Tallinn, Estonia

www.cerf-jcr.org

www.JCRonline.org

ABSTRACT

Eelsalu, M.; Soomere, T., and Jankowski, M.Z., 2024. Climate change driven alongshore variations of directional forcing of sediment transport on the eastern Baltic Sea coast. *In:* Phillips, M.R.; Al-Naemi, S., and Duarte, C.M. (eds.), *Coastlines under Global Change: Proceedings from the International Coastal Symposium (ICS) 2024 (Doha, Qatar)*. *Journal of Coastal Research*, Special Issue No. 113, pp. 256-260. Charlotte (North Carolina), ISSN 0749-0208.

This study addresses the impact of systematic changes in the wind and wave directions to the magnitude and direction of wave-induced sediment transport along the eastern Baltic Sea shores. The analysis is performed using the CERC approach in terms of potential net and bulk transport based on a recent reconstruction of hourly wave time series using the SWAN model with a spatial resolution of 1–3 nautical mile forced for 1990–2021 by ERA5 winds. The majority of alongshore sediment transport is driven by waves approaching from one or two narrow (±15°) ranges of directions. A large part of the study area experiences a delicate balance of alongshore transport under the impact of waves driven by south-western and (north-)north-western (N/NW) winds. These wave systems produce up to 80–90% of the total net and bulk transport. Significant changes have occurred to the directional distribution of this transport owing to a decrease in the contribution of waves from the NW or NNW in many sections of the study area. This change is mostly associated with the magnitude and frequency of such winds and obviously infringes the balance or even direction of sediment transport in sectors affected by bi-directional wave patterns. Climate change driven rotation of wind direction only affects the magnitude of sediment transport in coastal sectors that develop under the impact of a single-peak wind system.

ADDITIONAL INDEX WORDS: *Sediment transport, climate change, Baltic Sea, wave climate.*

INTRODUCTION

Sedimentary shores of the Baltic Sea have experienced significant change over recent decades (Harff *et al.*, 2017). Its southern and eastern sedimentary shores exhibit intensified coastal processes (Orviku *et al.*, 2003; Suursaar *et al.*, 2015) and accelerated coastal erosion in many locations (Ryabchuk *et al.*, 2012, 2020) despite postglacial uplift of a large part of the eastern Baltic Sea coast (Rosentau *et al.*, 2007).

The wave fields in the Baltic Sea primarily follow local winds and are highly intermittent (Soomere and Eelsalu, 2014), with 1/3 of the annual wave energy flux packed within 3–4 stormiest days. Long-period restoring swells are weak and infrequent (Björkqvist *et al.*, 2021). Therefore, the wind (and thus wave) directions during the strongest storms in the year play a key role in the formation of alongshore sediment transport patterns.

Winds from two predominant directions (frequent south-western (SW) and infrequent strong north-north-western (NNW) winds) (Soomere, 2003) provide the majority of annual wave energy flux in the area (Eelsalu *et al.*, 2022). Waves generated by these winds frequently approach the shore at a large angle with respect to the shore normal and thus strongly contribute to alongshore sediment transport (Viška and Soomere, 2013) and

produce a delicate balance of this transport (Soomere and Viška, 2014). While wave intensity has not increased in this region (Sokolov and Chubarenko, 2024), even a small change in the predominant storm wave approach direction, can lead to significant modifications in alongshore sediment transport (Flor-Blanco *et al.*, 2021) and drastic results on the coast. The frequency of winds from different directions during the stormiest months in the Baltic Sea area has experienced significant alterations (Jaagus and Kull, 2011; Bierstedt *et al.*, 2015). An increase in the frequency of SW winds in wintertime (Jaagus and Kull, 2011, Bierstedt *et al.*, 2015) has probably already caused sizable modifications in the sediment transport patterns. The long-term mean rate of coastal retreat has increased almost twice along several coastal segments in Latvia since the 1990s (Eberhards and Lapinskis, 2008). Shoreline changes of some segments of the West Estonian Archipelago are up to 5 times faster than 50 years ago (Suursaar *et al.*, 2015). Changes in the alongshore sediment transport along the coasts of Lithuania and Latvia in 1970–2007 have been attributed to a rotation of wind directions (Soomere *et al.*, 2015). However, the spatial extension, alongshore variations and actual impact of directional changes in wind patterns on sediment transport are yet unknown.

This study focuses on the changes in the wave-driven alongshore sediment transport along the eastern coast of the Baltic Sea (Figure 1). Ultimately, this analysis enables the identification of coastal areas at risk of significant change or threatened by large-scale erosion.
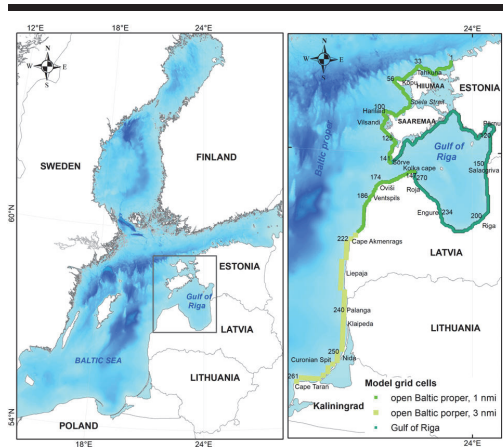
Figure 1. Study area in the Baltic Sea (left panel, grey box indicates the 1 nautical mile (nmi) SWAN wave model grid). Right panel: coastal sections considered in this study. Green squares: coastal sections open to the Baltic proper with a wave model resolution of ~1 nmi. Light green squares: nearshore model grid cells of the Baltic proper with a resolution of ~3 nmi. Dark green: grid cells in the nearshore of the interior of the Gulf of Riga with 1 nmi resolution. The nearshore of southern Saaremaa is not considered for detailed analyses.

METHODS

Wave Data

The analysis covers the entire sedimentary nearshore of the eastern Sea from the northern Hiiumaa, Estonia, to the Cape Taran, Kaliningrad District, Russia (Figure 1). Calculations of alongshore sediment transport rely on a recent reconstruction of the wave climate in the region (Giudici *et al.*, 2023) using a multi-nested version of the SWAN wave model (Booij *et al.*, 1999), cycle III, version 41.31A. A coarse model covers the entire Baltic Sea with a resolution of 3 nautical mile (nmi). A medium-level model extends to the Gulf of Riga and the adjacent coastal areas of the Baltic proper, with a resolution of about 1700 m (~1 nmi, Giudici *et al.*, 2023). The wave spectrum is computed for 36 directions and 32 frequencies, ranging from 0.05 to 1 Hz. The model is forced with wind information from the ERA5 reanalysis (Hersbach *et al.*, 2018). For this study significant wave height, peak period, and wave direction are utilized for alongshore sediment transport calculations in the selected nearshore grid cells during the latest WMO climatological standard normal 1990–2021 with a temporal resolution of 1 h.

Wave-driven Potential Sediment Transport

The time series of wave-driven alongshore sediment transport for selected coastal segments (Figure 1) are estimated using the Coastal Engineering Research Centre (CERC) approach (USACE, 2002). This approach assumes that the wave-driven potential transport rate $I_t = KP_t = KEc_{gb}\sin\theta_b\cos\theta_b$ is proportional to the rate of beaching of the wave energy flux c_g

that makes an angle θ_b with the shore normal. The quantity $I_t = (\rho_s - \rho)(1-p)Q_t$ has the meaning of the potential immersed weight transport rate, Q_t is the potential alongshore sediment transport rate, E is wave energy, c_g is group speed and subscript "b" indicates the relevant values at the breaker line.

We use constant values of porosity coefficient $p = 0.4$ for coastal sediment and water density $\rho = 1004$ kg/m^3 that corresponds to the average salinity of 4.90–5.38 g/kg of the upper layer of the Gulf of Riga (Skudra and Lips, 2017). The water density is somewhat larger in the Baltic proper but this difference does not affect our results. We employ the expression $K = 0.05 + 2.6\sin^2 2\theta_b + 0.007u_{mb}/w_f$ for the CERC coefficient K (USACE, 2002). Here $u_{mb} = (H_b/2)\sqrt{g/d_b}$ is the maximum orbital velocity in linear waves, $w_f = 1.6\sqrt{gd_{50}(\rho_s - \rho)/\rho}$ is the fall velocity, g is gravity acceleration, H_b is wave height at breaking and d_b is breaking depth. We assume that the typical grain size $d_{50} = 0.17$ mm and the density of sand $\rho_s = 2650$ kg/m^3 are constant. Wave properties at the breaker line are evaluated based on the joint impact of refraction and shoaling resolved in the frame of linear wave theory. In the idealised case of monochromatic waves with a height H_0 and a group and phase speed c_{g0} and c_{f0} in a wave model grid cell, the wave height H_b at the breaker line is described by the following algebraic equation of 6th degree (Soomere and Viška, 2014):

$$H_b^5 g\left(1 - \frac{H_b g \sin^2\theta_0}{\gamma_b c_{f0}^2}\right) = H_0^4 \gamma_b c_{g0}^2(1 - \sin^2\theta_0). \quad (1)$$

Estimates of the Changes in Alongshore Sediment Transport

Changes to the alongshore sediment transport caused by alterations of wave approach directions are analysed with a resolution of 30°. This resolution allows to specify the prevailing wave direction(s) that drive(s) the majority of alongshore transport in each coastal section, and subsequently to quantify the contribution of waves from prevailing directions to the annual net transport. These directions are identified for both positive (counterclockwise) and negative (clockwise) directions. Doing so makes it possible to identify coastal areas where a bi-directional sediment transport pattern exists and to evaluate alterations created by changes in these patterns. Statistical significance of changes in net alongshore sediment transport driven by waves from each directional range were estimated utilizing the Mann-Kendall test at a 95% level.

RESULTS

Prevailing Wave Directions of Alongshore Sediment Transport

The majority of annual alongshore sediment transport is driven by waves approaching from a narrow directional range within 30°. The contribution of wave fields from such a range into the transport is up to 80–90% in certain coastal sections (Figure 2). This feature is common along the coast of the West Estonian Archipelago. Its western shores have complicated geometry and are open to the prevailing wave directions. Coastal sections in those locations are characterized by an almost unidirectional alongshore sediment transport (Figure 2a).

The primary driving force of alongshore sediment transport

on the coasts of Hiiumaa and Saaremaa are wave fields from the SW and NW. Their ratio varies according to the coastline orientation (Figure 2a). Sediment transport on the northern shore of Hiiumaa is largely governed by NW-NNW waves from 300°–330° that contribute up to 60% of total transport. Conversely, on the SW side of the Kõpu Peninsula, counterclockwise sediment transport is predominantly driven by SW waves.
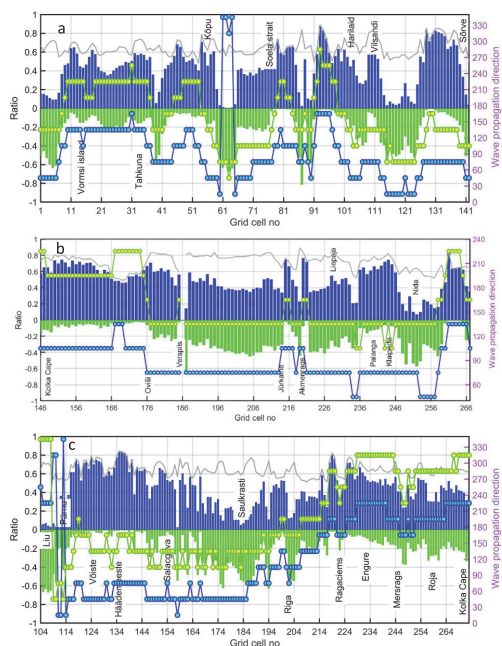

Figure 2. Ratio of annual net transport driven by waves from a narrow directional range to the bulk wave-driven transport: (a) near the West Estonian Archipelago, (b) in the nearshore of Latvia and Lithuania, (c) in the Gulf of Riga. Blue and green bars: counterclockwise/clockwise transport, respectively, driven by waves within a 30° range. Cyan circles on blue line and yellow circles on green line: prevailing counter-clockwise/clockwise clockwise transport wave direction (±15°), respectively. Vertical scale (±15°): wave propagation direction (180° opposite to the approach direction). Horizontal scale: grid cell number in Figure 1. Gray line: total contribution of two prevailing wave directions to the average annual bulk transport. The data reflect the annual average over 12 month long stormy periods (from July to June of subsequent year) in 1990–2021. Spatial resolution of panel (b) starting from Jurkalne is 3 nmi.

Sediment transport along the western coast of Saaremaa, from Harilaid to Sõrve, is primarily driven by waves that alternate between directions 315±15° and 255±15°. Single prevailing wave directional range may contribute up to 80% of the annual transport (Figure 2a, near Sõrve). This feature indicates strong unidirectional sediment transport along this part of the shores of the West Estonian Archipelago. The varying nature of the single prevailing wave direction is likely to generate numerous local convergence and divergence areas.

Along both shores of Cape Kolka the sediment transport is unidirectional and counterclockwise towards the east (Figure 2b). The transport is driven by waves that approach from directions 270°–300°. Waves from all other directions much less contribute to the annual alongshore sediment transport.

Along extensive sections of the coastline between Oviši and Palanga, approximately 80% of the average annual alongshore sediment transport is almost evenly driven by two wave systems, with minor fluctuations in a few coastal sections. Waves from the direction 255°±15° drive sediment to the northeast, while waves from the direction 315°±15° carry sediment clockwise to the southeast. Therefore, alterations in the properties of these wave systems are likely to significantly impact coastal processes.

The balance between two predominant wave systems is different in the coastal segment from Palanga to the latitude of Nida. The prevailing wave directions responsible for most of the annual sediment transport are, as above, 255°±15° and 315°±15°. However, their respective contributions vary along the Curonian Spit. While the coastal section from Palanga to Klaipėda appears to be dominated by WSW waves, the shoreline to the south of Klaipėda is characterized by the dominance of NW waves. In the vicinity of Cape Taran the wave direction is from NW and gives rise counterclockwise prevailing alongshore transport.

The prevailing sediment transport directions vary significantly between the eastern and western coasts of the Gulf of Riga (Figure 2c). The eastern shore from Pärnu to Salacgriva is primarily influenced by waves from the west, leading to counterclockwise sediment transport along most of the sections. The western shore to the south-east (SE) of Cape Kolka is sheltered against waves from the SW and sediment transport is predominantly driven by northerly waves, inducing counterclockwise transport towards Riga. The southern shore is developing under joint impact of waves from the west and north.

Changes in Alongshore Sediment Transport

The analysis reveals several significant changes in the directional distribution of alongshore sediment transport, (Figure 3). Remarkably, a distinct change in sediment transport patterns occurred owing to changes in properties of waves from the (N)NW. Alongshore sediment transport driven by these waves decreased over 31 so-called storm seasons (from June to May of the subsequent year) from 1990 to 2021 (Figure 3, left panel). This feature evidently reflects a certain shift in wind patterns in the Baltic Sea region.

The described changes along the coast of the West Estonian Archipelago occurred because of alterations of waves from the directions 300°–330° (in some short sections from the directions 330°–360°). Along certain coastal segments of Saaremaa and Hiiumaa (e.g., Harilaid, Vilsandi nearshore areas), waves from these directions prevail and drive large part of the alongshore sediment transport. Therefore, a more pronounced change is evident, as illustrated in Figure 3 (left).

The changes in question are particularly notable along the Baltic proper nearshore of Latvia and Lithuania, where the balance of two wave systems creates a bi-directional alongshore sediment transport. These changes, driven by waves ranging from 300° to 330°, become evident in the coastal segment from Oviši to Palanga (Figure 3). Waves within this directional range contribute nearly half of the alongshore sediment transport

(Figure 2b). Changes driven by these waves are particularly rapid (Figure 3, left panel). These alterations may have led to significant shifts in coastal processes, affecting the existing balance of bi-directional sediment transport.
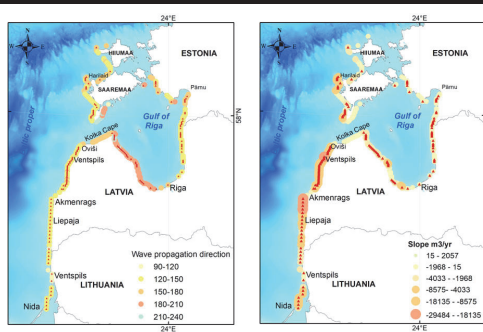

Figure 3. Changes in the alongshore sediment transport driven by waves from a particular direction range (wave propagation direction on the left). The slope of trends of transport rates that has been driven by wave directions is indicated on the left panel. Red markers represent the prevailing directional range that drives the alongshore sediment transport where change has occurred (see Figure 2). Note that only these coastal sections are represented where change has occurred at a ≥95% level of statistical significance.

In the interior of the Gulf of Riga, changes in alongshore sediment transport are, mainly driven by alteration of properties of waves from the north-east (NE) and NW. NE waves have modified sediment transport rates on the western shore of the Gulf of Riga, while NW waves have influenced alongshore sediment transport on the eastern shore (Figure 3).

The significant variation in the slope of trends of transport rates across the study area (Figure 3) reflects different forcing wave directions and the relative importance of these directions in the annual bulk alongshore sediment transport (Figure 2). For example, on the eastern coast of the Gulf of Riga, the slope of the trend in the transport rate driven by NW waves is smaller compared to the similar slope at the Baltic proper coast of Latvia, where the change of transport rates is influenced by waves from the same direction. This difference arises from different relative contributions of these waves to the alongshore sediment transport (see Figure 2b,c).

Trend in the overall net wave-driven potential sediment transport is nonzero at a ≥95% significance level in 38 grid points and in 82 grid points at a ≥90% level out of 551 points in the study area. This trend is nonzero in 124 grid points at a lower (≥80%) level of significance. It is highly likely that in some locations, changes to sediment transport driven by prevailing wind and wave direction(s) affect the overall net transport (Figure 4, points 188 and 197).

Importantly, the prevailing wave directions (±15°) for counterclockwise and clockwise alongshore sediment transport have been stable over the period of 1990–2021 (Figure 4, lower panels). Therefore, most changes identified in various sources are driven by the change in the balance of the frequency and/or magnitude of winds and waves from the predominant directions.

This kind of change eventually more strongly affects the impact of wind and waves from the (N)NW. As the usual frequency of occurrence of NW waves is approximately three times less than SW waves, any missing or weaker NW wave event has stronger relative importance. However, along the Baltic proper in Latvia, their contribution to the total transport remains almost equal. A slight decrease can be noticed in the number of days of waves from NW–NNW directions.
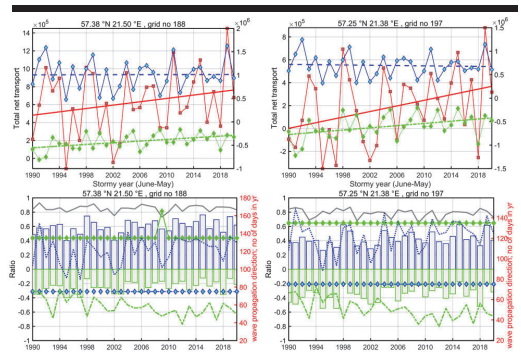

Figure 4. Changes in two selected coastal sectors presented in Figure 1 over storm years in 1990–2021 along the Baltic proper. Upper panels: Blue: counterclockwise (CCW) transport lead by waves from a 30° wave range, green: clockwise (CW) transport from a 30° wave range. Transport rates (m³/yr) correspond to the right vertical scale. Red line: average net transport in 1990–2021, left vertical scale. Lower panels: Bars indicate the annual contribution driven by waves creating CCW (blue) and CW (green) wave systems; gray line: total contribution by two wave systems; blue and green line: total number of days with waves creating CCW and CW transport, respectively. Green and blue markers: wave direction leading to CCW or CW transport direction, respectively, in each storm year. Scale left: ratio; scale right: wave propagation direction and number of days.

DISCUSSION AND CONCLUSIONS

The presented analysis first of all reveals that the majority of wave-driven alongshore sediment transport on sedimentary shores of the eastern Baltic Sea is dominated by waves from one or two narrow (±15°) directional ranges. Such wave systems often contribute about 80% of sediment transport. This means that any changes in their properties may lead to major alterations of sediment transport.

We demonstrate that specifically the contribution of waves from the NW or NNW has significantly decreased in many sections of the study area. This change obviously infringes the balance of sediment transport. Most likely it is already reflected in the current course of coastal processes, including the observed increase in erosion rates (Weisse et al., 2021). As long-period restoring swells are almost absent in the Baltic Sea, this change may affect recovery conditions after storms and change the balance of joint impact of several coastal drivers. This feature apparently will have the strongest impact in locations where wave systems from different directions are synchronized with background sea level variations (Eelsalu et al., 2022).

In conclusion, we have shown that (i) the bi-directional

system of winds and waves drives up to 80–90% of alongshore sediment transport on the eastern shores of the Baltic Sea and (ii) the properties of (the components of) this system have considerably changed in many locations of the study area. This change may have led to substantial alterations in coastal processes in the study area.

LITERATURE CITED

Bierstedt, S.E.; Hünicke, B., and Zorita, E., 2015. Variability of wind direction statistics of mean and extreme wind events over the Baltic Sea region. *Tellus A*, 67, 29073, https://doi.org/10.3402/tellusa.v67.29073

Björkqvist, J.-V.; Pärt, S.; Alari, V.; Rikka, S.; Lindgren, E., and Tuomi, L., 2021. Swell hindcast statistics for the Baltic Sea, *Ocean Science*, 17(6), 1815–1829, https://doi.org/10.5194/os-17-1815-2021

Booij, N.; Ris, R.C., and Holthuijsen, L.H., 1999. A third-generation wave model for coastal regions: 1. Model description and validation. *Journal of Geophysical Research: Oceans*, 104(C4), 7649-7666. https://doi.org/10.1029/98JC02622

Eberhards, G. and Lapinskis, J., 2008. Processes on the Latvian coast of the Baltic Sea: atlas, Riga, University of Latvia, Riga.

Eelsalu, M.; Parnell, K.E., and Soomere, T., 2022. Sandy beach evolution in the low-energy microtidal Baltic Sea: attribution of changes to hydrometeorological forcing. *Geomorphology*, 414, 108383, https://doi.org/10.1016/j.geomorph.2022.108383

Flor-Blanco, G.; Alcántara-Carrió, J.; Jackson, D.W.T.; Flor, G., and Flores-Soriano, C., 2021. Coastal erosion in NW Spain: Recent patterns under extreme storm wave events. *Geomorphology*, 387, 107767, https://doi.org/10.1016/j.geomorph.2021.107767

Giudici, A.; Jankowski, M.Z.; Männikus, R.; Najafzadeh, F.; Suursaar, Ü., and Soomere, T., 2023. A comparison of Baltic Sea wave properties simulated using two modelled wind data sets. *Estuarine, Coastal and Shelf Science*, 290, 108401, https://doi.org/10.1016/j.ecss.2023.108401

Harff, J.; Deng, J.J.; Dudzinska-Nowak, J.; Fröhle, P.; Groh, A.; Hünicke, B.; Soomere, T., and Zhang, W.Y., 2017. What determines the change of coastlines in the Baltic Sea? In: Harff, J.; Furmańczyk, K., von Storch, H. (Eds), *Coastline Changes of the Baltic Sea from South to East: Past and Future Projection. Coastal Research Library*, 19, 15–35, https://doi.org/10.1007/978-3-319-49894-2_2

Hersbach, H.; Bell, B.; Berrisford, P.; Biavati, G.; Horányi, A.; Muñoz Sabater, J., Nicolas, J., Peubey, C., Radu, R., Rozum, I.; Schepers, D.; Simmons, A., Soci, C.; Dee, D., and Thépaut, J.-N.; ERA5 hourly data on pressure levels from 1940 to present. Copernicus Climate Change Service (C3S). Climate Data Store (CDS). https://doi.org/10.24381/cds.bd0915c6

Jaagus, J. and Kull, A., 2011. Changes in surface wind directions in Estonia during 1966–2008 and their relationships with large-scale atmospheric circulation. *Estonian Journal of Earth Sciences*, 60(4), 220–231, https://doi.org/10.3176/earth.2011.4.03

Orviku, K.; Jaagus, J.; Kont, A.; Ratas, U., and Rivis, R., 2003. Increasing activity of coastal processes associated with climate change in Estonia. *Journal of Coastal Research*, 19(2), 364–375.

Rosentau, R.; Meyer, M.; Harff, J.; Dietrich, R., and Richter, A., 2007. Relative sea level change in the Baltic Sea since the Littorina Transgression. *Zeitschrift für Geologische Wissenschaften*, 35(1/2), 3–16.

Ryabchuk, D.; Spiridonov, M.; Zhamoida, V.; Nesterova, E, and Sergeev, A., 2012. Long term and short term coastal line changes of the eastern Gulf of Finland. Problems of coastal erosion. *Journal of Coastal Conservation*, 16(3), 233–242, https://doi: 10.1007/s11852-010-0105-4.

Ryabchuk, D.; Sergeev, A.; Burnashev, E.; Khorikov, V.; Neevin, I.; Kovaleva, O.; Budanov, L.; Zhamoida, V., and Danchenkov, A., 2020. Coastal processes in the Russian Baltic (eastern Gulf of Finland and Kaliningrad area). *Quarterly Journal of Engineering Geology and Hydrogeology*, 54(1), qjegh2020-036, https://doi.org/10.1144/qjegh2020-036

Skudra, M. and Lips, U., 2017. Characteristics and inter-annual changes in temperature, salinity and density distribution in the Gulf of Riga. *Oceanologia*, 59(1), 37–48. https://doi.org/10.1016/j.oceano.2016.07.001

Sokolov, A. and Chubarenko, B., 2024. Baltic Sea wave climate in 1979-2018: Numerical modelling results. *Ocean Engineering*, 297, 117088, https://doi.org/10.1016/j.oceaneng.2024.117088

Soomere, T., 2003. Anisotropy of wind and wave regimes in the Baltic proper. *Journal of Sea Research*, 49(4), 305–316, https://doi.org/10.1016/S1385-1101(03)00034-0

Soomere, T. and Eelsalu, M., 2014. On the wave energy potential along the eastern Baltic Sea coast. *Renewable Energy*, 71, 221–233, https://doi.org/10.1016/j.renene.2014.05.025

Soomere, T. and Viška, M., 2014. Simulated wave-driven sediment transport along the eastern coast of the Baltic Sea. *Journal of Marine Systems.*, 129, 96–105, https://doi.org/10.1016/j.jmarsys.2013.02.001

Soomere, T.; Bishop, S.R.; Viška, M., and Räämet, A., 2015. An abrupt change in winds that may radically affect the coasts and deep sections of the Baltic Sea. *Climate Research*, 62(2), 163–171, https://doi.org/10.3354/cr01269

Suursaar, Ü.; Jaagus, J., and Tõnisson, H., 2015. How to quantify long-term changes in coastal sea storminess? *Estuarine, Coastal and Shelf Science*, 156, 31–41, https://doi.org/10.1016/j.ecss.2014.08.001

USACE, 2002. Coastal Engineering Manual. Department of the Army. U.S. Army Corps of Engineers. Manual No. 1110-2-1100.

Viška, M. and Soomere, T., 2013. Simulated and observed reversals of wave-driven alongshore sediment transport at the eastern Baltic Sea coast. *Baltica*, 26(2), 145–156, https://doi.org/10.5200/baltica.2013.26.15

Curriculum vitae

Personal data

Name:	Mikołaj Zbigniew Jankowski
Date of birth:	28 February 1997
Place of birth:	Szczecin, Poland
Citizenship:	Polish

Contact data

Address:	Ehitajate tee 5, 19086 Tallinn
Phone:	(+372) 57705997
E-mail:	mikolaj.jankowski@taltech.ee

Education

Educational Institution	Graduation year	Education (Field of study/degree)
Bangor University	2016–2020	Physical oceanography (F734) / Master of Science
13th High School in Szczecin	2013–2016	High School

Language competence

Language	Level
English	Fluent
Polish	Native
German	Intermediate (B1)
Spanish	Intermediate (B1)
Estonian	Beginner (A1)

Professional employment

January 2021–to date: early-stage researcher, Tallinn University of Technology

Special courses and further training

Period	Educational or other organisation / type
03.06–03.08 2018	Alfred Wegener Institute (AWI), Bremerhaven / internship
07.05–21.06 2019	Marine Centre Wales, Menai Bridge / internship
27.03–31.03 2023	Baltic Earth Winter School, Warnemünde / winter school
15.05–15.07 2023	Helmholtz Zentrum Hereon, Geesthacht / internship

Research activity

Articles indexed by the Web of Science database (1.1)

Giudici, A., Jankowski, M.Z., Männikus, R., Najafzadeh, F., Suursaar, Ü., Soomere, T., 2023. A comparison of Baltic Sea wave properties simulated using two modelled wind data sets. Estuarine, Coastal and Shelf Science, 290, 108401. https://doi.org/10.1016/j.ecss.2023.108401

Najafzadeh, F., Jankowski, M.Z., Giudici, A., Männikus, R., Suursaar, Ü., Viška, M., Soomere, T., 2024. Spatiotemporal variability of wave climate in the Gulf of Riga. Oceanologia, 66, 56–77. https://doi.org/10.1016/j.oceano.2023.11.001

Soomere, T., Jankowski, M.Z., Eelsalu, M., Parnell, K.E., Viška, M., 2025. Alongshore sediment transport analysis for a semi-enclosed basin: a case study of the Gulf of Riga, the Baltic Sea. Ocean Science, 21(2), 619–641. https://doi.org/10.5194/os-21-619-2025

Articles in other peer-reviewed international journals (1.2)

Jankowski, M.Z., Soomere, T., Parnell, K.E., Eelsalu, M., 2024. Alongshore sediment transport in the eastern Baltic Sea. Journal of Coastal Research, Special Issue 113, 261–265. https://doi.org/10.2112/JCR-SI113-052.1

Eelsalu, M., Soomere, T., Jankowski, M.Z., 2024. Climate change driven alongshore variations of directional forcing of sediment transport on the eastern Baltic Sea coast. Journal of Coastal Research, Special Issue 113, 190–194. https://doi.org/10.2112/JCR-SI113-038.1

Articles published in other conference proceedings (3.4)

Giudici, A., Männikus, R., Najafzadeh, F., Jankowski, M.Z., Soomere, T. Suursaar, Ü., 2022. High-resolution wave model for coastal management and engineering in the eastern Baltic Sea. In: Köppen, S., Reckermann, M. (eds.), 4th Baltic Earth Conference "Assessing the Baltic Sea Earth System", Jastarnia, Hel Peninsula, Poland, 30 May to 3 June 2022. Conference Proceedings. International Baltic Earth Secretariat Publication No. 21, 150–151.

Giudici, A., Männikus, R., Jankowski, M.Z., Soomere, T., 2024. Analysis of wave properties in the Baltic Sea: integrating findings from the Gulf of Finland, Gulf of Riga and Western Baltic Coasts. In: Reckermann, M., Aigars, J., Andrusaitis, A., Meier, H.E.M., Kuliński, K. (eds.), 5th Baltic Earth Conference "New Challenges for Baltic Sea Earth System Research", Jūrmala, Latvia, 13–17 May 2024. Conference Proceedings. Assembled by Silke Köppen. International Baltic Earth Secretariat Publication No. 23, 61–62.

Soomere, T., Jankowski, M.Z., Parnell, K.E., 2024. Intriguing variations of sediment transport in the Gulf of Riga. In: Reckermann, M., Aigars, J., Andrusaitis, A., Meier, H.E.M., Kuliński, K. (eds.), 5th Baltic Earth Conference "New Challenges for Baltic Sea Earth System Research", Jūrmala, Latvia, 13–17 May 2024. Conference Proceedings. Assembled by Silke Köppen. International Baltic Earth Secretariat Publication No. 23, 71–72.

Viška, M., Tõnisson, H., Männikus, R., Jankowski, M.Z., 2024. Coastal dynamics of the Daugavgriva Island beach in the Gulf of Riga, Latvia. In: Reckermann, M., Aigars, J., Andrusaitis, A., Meier, H.E.M., Kuliński, K. (eds.), 5th Baltic Earth Conference "New Challenges for Baltic Sea Earth System Research", Jūrmala, Latvia, 13–17 May 2024. Conference Proceedings. Assembled by Silke Köppen. International Baltic Earth Secretariat Publication No. 23, 80–81.

Abstracts of conference presentations (5.2)

Giudici, A., Männikus, R., Najafzadeh, F., Jankowski, M.Z., Soomere, T., 2023. High-resolution Baltic Sea wave climatology obtained from two modelled wind data sets: a comparison. Baltic Sea Science Congress 2023 (21–25 August 2023, Helsinki, Finland).

Giudici, A., Jankowski, M.Z., Männikus, R., Najafzadeh, F., Soomere, T., 2023. Baltic Sea Wave Climatology Dataset: high-resolution validation and comparison of the wave properties calculated using two input winds for the period 1979–2022. The Gulf of Finland and Eastern Baltic Sea Science Days 2023 (16–17 November 2023, Tallinn, Estonia).

Jankowski, M.Z., Parnell, K.E., Soomere, T., Eelsalu, M., 2023. Longshore sediment transport analysis for the Gulf of Riga based on high-resolution wave model results. 13th International Workshop on Modeling the Ocean (IWMO) (27–30 June 2023, Hamburg, Germany).

Jankowski, M.Z., Parnell, K.P., Soomere, T., Eelsalu, M., Viska, M., 2023. Analysis of longshore sediment transport for the Gulf of Riga using high-resolution wave model results. Baltic Sea Science Congress 2023 (21–25 August 2023, Helsinki, Finland).

Jankowski, M.Z., Eelsalu, M., Parnell, K.E., Soomere, T., Viska, M., 2023. Modelled rates of potential bulk and net sediment transport along the Gulf of Riga coastlines. The Gulf of Finland and Eastern Baltic Sea Science Days 2023 (16–17 November 2023, Tallinn, Estonia).

Jankowski, M.Z. Parnell, K.E., Soomere, T., 2024. Decomposing alongshore sediment transport into cells and compartments: A case study in the Gulf of Riga, the Baltic Sea. 8th IAHR Europe Congress "Water – Across boundaries" (4–7 June 2024, Lisbon, Portugal).

Jankowski, M.Z., Soomere, T., Parnell, K.E., Eelsalu, M., 2024. Sediment transport along the eastern coast of the Baltic Sea. 4th Scientific Conference of Polish Marine Researchers "The State and Trends of Changes in the Marine Environment" (16–18 September 2024, Szczecin, Poland).

Jankowski, M.Z., Soomere, T., Eelsalu, M., Parnell, K.E., 2025. Temporal variability of alongshore sediment transport in the eastern Baltic Sea. Baltic Sea Science Congress 2025 (26–30 May 2025, Sopot, Poland).

Najafzadeh, F., Jankowski, M., Giudici, A., Männikus, R., Suursaar Ü., Soomere, T., Viska, M., 2023. Wave climate and its variability in the Gulf of Riga. Baltic Sea Science Congress 2023 (21–25 August 2023, Helsinki, Finland).

Elulookirjeldus

Isikuandmed

Nimi:	Mikołaj Zbigniew Jankowski
Sünniaeg:	28.02.1997
Sünnikoht:	Szczecin, Poola
Kodakondsus:	Poola

Kontaktandmed

Address:	Küberneetika instituut, Tallinna Tehnikaülikool, Ehitajate tee 5, 19086 Tallinn
Telefon:	(+372) 57705997
E-post:	mikolaj.jankowski@taltech.ee

Hariduskäik

2021–2025	Tallinna Tehnikaülikool, PhD
2016–2020	MSci F734, füüsikaline okeanograafia, Bangori ülikool
2013–2016	Keskharidus: Szczecini 12. keskkool

Keelteoskus

Inglise keel	Kõrgtase

Teenistuskäik

2021–praeguseni:	doktorant-nooremteadur, Tallinna Tehnikaülikool

Teaduslikud publikatsioonid on esitatud ingliskeelses elulookirjelduses